Investigating the Effects of Inositol Depletion Using a Simple Eukaryotic Organism *Dictyostelium discoideum*

Anna Dominika Frej

Research thesis submitted for the degree of Doctor of Philosophy at Royal Holloway University of London in February 2016

Declaration of Authorship

I, Anna Frej, hereby declare that the work presented in this thesis is my own unless otherwise indicated, and that all published work has been acknowledged. Furthermore, I affirm that I have neither fabricated nor falsified the results reported therein.

Signed: …….

Date: ……02.02.2016……..

Abstract

Inositol, produced *in vivo* by the biosynthetic enzyme inositol-3-phosphate synthase (Ino1), is an essential component of inositol phosphates and phosphoinositides that are involved in important cell signalling pathways. Dysregulation of inositol signalling has been implicated in various diseases, including bipolar disorder, Alzheimer's disease, and diabetes. Research relating to inositol regulation in cells has primarily focused on the molecular and cellular effects of inositol depletion without considering the effects of altered Ino1 levels. This PhD study employed a simple eukaryote, *Dictyostelium discoideum,* to investigate the distinct effects of the loss of Ino1 and inositol depletion. Ablation of *ino1* in this model produced an inositol auxotrophy phenotype and affected development, with the former being only partially restored by an exogenous inositol supply. The removal of exogenous inositol from the *ino1*$^{-}$ mutant resulted in a 56% decrease in intracellular inositol levels within 12 hours, a reduction in cytokinesis and substrate adhesion, and an accumulation of autophagosomes. Inositol depletion also triggered a decrease in phosphoinositide levels. Intriguingly, the absence of the Ino1 protein and inositol depletion cause distinct metabolic changes, with the greatest changes seen following Ino1 loss. These data suggest a role for the Ino1 protein beyond inositol biosynthesis. To investigate this role, an immunoprecipitation approach was used, where an Ino1 binding partner, Q54IX5, was identified. Q54IX5 is likely to function as a macromolecular adaptor protein. Thus, this study has identified distinct cellular and metabolic effects for both inositol depletion and loss of Ino1, with implications for our understanding of human diseases.

List of Tables and Figures

Abbreviations

aa	Amino Acid
AC	Adenylate Cyclase
AIP1	ALG-2 Interacting Protein 1
APS	Ammonium Persulfate
Arp 2/3	Actin-Related Proteins ARP2 and ARP3
Ax	Axenic
bp	Base Pairs
BLAST	Basic Local Alignment Search Tool
2,3-BPG	2,3-bisphosphoglycerate
cAMP	cyclic Adenosine Monophosphate
CAR1	cAMP Receptor 1
CBZ	Carbamazepine
CDD	Conserved Domain Database
CDP-DAG	Cytidine Diphosphate-diacylglycerol
cDNA	complementary DNA
CIAP	Calf Alkaline Phosphatase
CRAC	Cytosolic Regulator of Adenylate Cyclase
DAG	Diacylglycerol
DAPI	4’,6’-Diamidino-2-phenylindole
DHAP	Dihydroxyacetone Phosphate
ddH_2O	Double Distilled Water
DGKA	Diacylglycerol Kinase
DH	Dbl-homologous Domain
DIF-1	Differentiation Inducing Factor 1
DMSO	Dimethyl Sulfoxide
dNTPs	Deoxynucleotide Trisphosphatases

DTT	Dithiotreitol
EDTA	Ethylenediaminetetracetic Acid
EGTA	Ethylene-glycol Tetraacetic Acid
FDA	Fluorescein Diacetate
GAP	GTPase Activating Proteins
gDNA	genomic DNA
GDP	Guanosine Diphosphate
GEF	Guanine Nucleotide Exchange Factor
GFP	Green Fluorescent Protein
GPCR	G-protein Coupled Receptors
GpmA	Glycerate PhosphoMutase
GSK-3	Glycogen Synthase Kinase-3
GTP	Guanosine-5'-triphosphate
IMPase	Inositol Monophosphatase
Ino1	Inositol-3-phosphate-synthase
IP3	Inositol Trisphosphate
IPPase	Inositol Polyphosphate 1-phosphatase
IPTG	Isopropyl β-D-1-thiogalactopyranoside
IRdye 800	InfraRed dye 800
Li^+	Lithium
MOPs	3-(*N*-morpholino)propanesulfonic acid
NAD^+/H	Nicotinamide Adenine Dinucleotide (oxidised/reduced)
NCBI	National Centre for Biotechnology Information
NP40	Nonidet P40
PA	Phosphatidic Acid
PBS	Phosphate Buffered Saline
PCR	Polymerase Chain Reaction

PefB	Penta EF-hand Calcium Binding Protein
PFA	Paraformaldehyde
PH	Plekstrin Homology
PhdA	PH-domain Containing Protein
PI3K	Phosphoinositide 3-kinase
PI	Phosphatidylinositol
PIP	Phosphatidylinositol Monophosphate
PIP2	Phosphatidylinositol Bisphophosphate
PIP3	Phosphatidylinositol Trisphophosphate
PKC	Protein Kinase C
PLA2	Phospholipase A2
PLC	Phospholipase C
PMSF	Phenylmethanesulfonyl Fluoride
PTEN	Phosphatidylinositol-3,4,5-trisphosphate 3-phosphatase
SDS	Sodium Dodecyl Sulphate
SDS-PAGE	Sodium Dodecyl Sulphate Polyacrylamide Gel Electrophoresis
SecG	SEC7 Domain-containing Protein
SEL1	Sel-1 Repeat
SEL1L	Protein sel-1 Homolog 1
SUMO	Small Ubiquitin-related Modifier
TEMED	Tetramethylethylenediamine
TORC	Target of Rapamycin Complex
TPR	Tetratricopeptide Repeat
VPA	Valproic Acid
UAS_{INO}	Inositol Sensitive Upstream Activation Sequence
WASP	Wiskott–Aldrich Syndrome Protein

Acknowledgements

I would like to thank my supervisor at Royal Holloway, Professor Robin Williams and my advisor Doctor Alessandra Devoto, for their guidance, advice and support during the time of this PhD. I would also like to thank my second supervisor, Doctor Grant Churchill from University of Oxford for being part of this project, and to all the collaborators from the universities of Glasgow, Cambridge and Reading, who supported this project with their knowledge and resources.

I would also like to acknowledge The Dr Hadwen Trust, the UK's leading non-animal medical research charity, without whose funding this project would not have been possible.

I thank my family, especially my husband and my mother for all their love and encouragement. I would like to express my gratitude to my friends and colleagues with whom I worked in the Williams lab. I thank Nicholl, for her friendship, inspiration and help during the time when I started this work in the Williams lab. I wish to say special thank you to Grant for his invaluable advice and support that I have received in the lab and during thesis write-up; and for all the laughter we had together; you made my time during this PhD a great experience. I would also like to express my deep gratitude to Versha for her constant friendship, encouragement, strength and emotional support; you have been like a sister to me. Finally, thank you to Joanna and to all my friends who I cannot list here. You have all helped me to grow as a person during the time I have spent at Royal Holloway; without you, I would have not made it this far.

Table of Contents

Chapter 1
Introduction

Chapter I

Introduction

1.1 Inositol and its derivatives

Myo-inositol, hereafter referred to as inositol, is the most widely occurring stereoisomer of inositol (Clements and Darnell, 1980) (Figure 1.1). It is a six carbon cyclic polyalcohol, which is present in a variety of cell types, including neurons. Cells can obtain inositol from three major sources. It can be synthesized *de novo* from glucose-6-phosphate by inositol-1-phosphate synthase (Ino1, EC5.5.1.4), recycled in the phosphatidylinositol cycle by a number of enzymes including inositol monophosphatase (IMPase), or transported from extracellular space by inositol specific transporters (Daniel et al., 2009; Deranieh and Greenberg, 2009) (Figure 1.2).

Inositol is synthesised *de novo* from D-glucose-6-phosphate by an isomerase 1-L-myo-Inositol-1-phosphate synthase (Ino1) (Stein and Geiger, 2002). The proposed biochemical process involves oxidation, enolisation, intramolecular aldol cyclisation, and reduction steps, with nicotinamide adenine dinucleotide (NAD^+) used as a cofactor (Stein and Geiger, 2002). Inositol in turn regulates the transcription of the Ino1 encoding gene, where increased levels of inositol inhibit *ino1* transcription (Hirsch and Henry, 1986). The biosynthesis of inositol is an evolutionarily conserved pathway, and the Ino1 protein, together with the gene encoding it, have been regarded as ancient in origin (Majumder et al., 2003). Inositol has also been shown to be necessary for cell survival in a variety of organisms, including *Saccharomyces cerevisiae, Dictyostelium discoideum, Arabidopsis thaliana,* and a parasite *Trypanosoma brucei* (Culbertson and Henry, 1975; Fischbach et al., 2006; Henry et al., 1977; Lester and Gross, 1959; Martin and Smith, 2006; Meng et al., 2009).

Inositol constitutes part of two important families of molecules: phosphoinositides and inositol phosphates (Deranieh and Greenberg, 2009) (Figure 1.1). These molecules are critically involved in a range of cellular functions, including phospholipid synthesis, the unfolded protein response (UPR) and protein secretion (Deranieh and Greenberg, 2009).

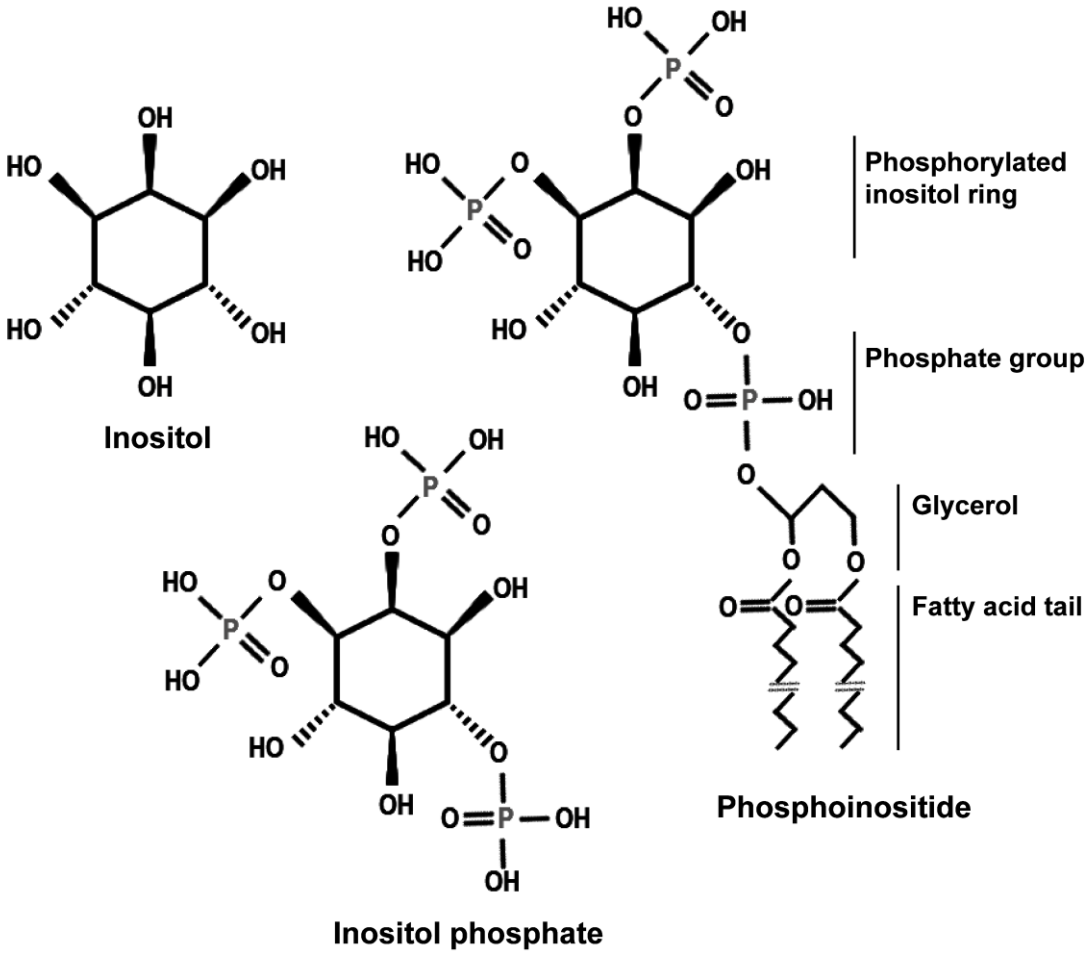

Figure 1.1 The chemical structures of inositol, inositol phosphate and phosphoinositide. Inositol is a cyclic polyalcohol. Inositol phosphate, shown here as 1,4,5-inositol trisphosphate, is a phosphorylated inositol, and phosphoinositide, shown here as phosphatidylinositol 4,5-bisphosphate, is a lipid containing a phosphorylated inositol head group and two fatty acid tails linked by a glycerol backbone.

Phosphoinositides form part of cell membranes and play role in cell motility and intracellular membrane trafficking (Corvera et al., 1999). Phosphoinositides are formed by phosphorylation of an inositol ring in a phosphatidylinositol molecule. Phosphatidylinositol (PI) comprises of a glycerol backbone linked to two fatty acid tails and a phosphate group attached to an inositol ring (Figure 1.1). PI is synthesised from the precursor

cytidine diphosphate diacylglycerol (CDP-DAG) by reaction with inositol, which is catalysed by the enzyme CDP-diacylglycerol inositol phosphatidyltransferase, also known as phosphatidylinositol synthase (PIS EC 2.7.8.11) (Figure 1.2). PIS is located in the endoplasmic reticulum, although it is also present in the plasma membrane in yeast (Tanaka et al., 1996). PI is then transferred to membranes either in vesicles or by specific transfer proteins (Krauss and Haucke, 2007). Phosphoinositides are maintained at steady state levels in the inner leaflet of the plasma membrane by a continuous and sequential series of phosphorylation and dephosphorylation reactions by specific kinases, phosphatases and phospholipase C enzymes (Kurnasov et al., 2013) (Figure 1.2).

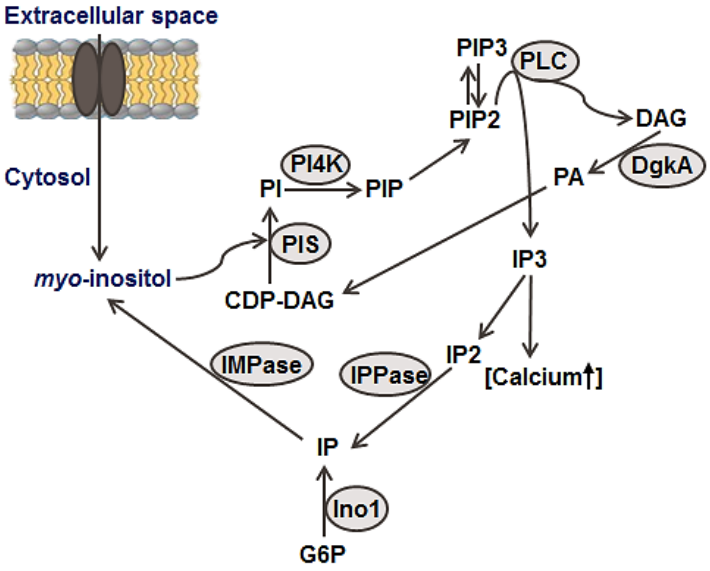

Figure 1.2 Inositol uptake, *de novo* biosynthesis, and recycling. Inositol is produced from glucose 6-phosphate (G6P), which is converted by an isomerase Ino1 to inositol 1-phosphate (IP), which is subsequently dephosphorylated by inositol monophosphatase (IMPase) to inositol. Inositol can be phosphorylated to form phosphoinositides (PI, PIP, PIP2, PIP3), or it can form part of inositol phosphates. Phosphatidic acid (PA) is produced from diacylglycerol (DAG) by diacylglycerol kinase (DGKA), and is a precursor to phosphatidylinositol. Inositol phosphates are produced by the cleavage of PIP2 by phospholipase C (PLC). Inositol 1,4,5-triphosphate (IP3) is an example of a second messenger that initiates separate intracellular signalling cascades, leading to the release of intracellular calcium (Ca^{2+}) that can lead to a modulation in gene transcription. The recycling of inositol is completed by sequential dephosphorylation of inositol phosphates with the help of inositol polyphosphate phosphatase (IPP). Inositol can be also transported from extracellular sources into the cytosol by specialised transporters located at the plasma membrane. Abbreviations: PIS, phosphatidylinositol synthase; IMPase, inositol monophosphatase; Ino1, inositol-1-phosphate synthase; IPPase, inositol polyphosphate phosphatase; IP, inositol phosphate; IP2, inositol bisphosphate; IP3, inositol trisphosphate; CDP-DAG, cytidine diphosphate-diacylglycerol; DAG, diacylglycerol; DgkA, diacylglycerol kinase; PLC, phospholipase C; PI4K, phosphatidylinositol 4-kinase; PI, phosphatidylinositol; PIP, phosphatidylinositol phosphate; PIP2, phosphatidylinositol bisphosphate; PIP3, phosphatidylinositol trisphosphate.

Inositol phosphates consist of another group of inositol-containing molecules. Inositol phosphates originate from the cleavage of phosphatidylinositol 4,5-bisphosphate (PIP2) by phospholipase C (PLC) to produce inositol 1,4,5-triphosphate (IP3) and DAG (Burton et al., 2009) (Figure 1.2). The central role of IP3 is to trigger the release of intracellular calcium but it can also be phosphorylated to form inositol phosphates (IP4, IP5, IP6) or inositol pyrophosphates (IP7 and IP8) (Bennett et al., 2006; Burton et al., 2009), which are involved in the regulation of gene expression and in post-translational protein modifications (Shen et al., 2003; Steger et al., 2003).

1.2 Inositol metabolism in disease

Inositol is naturally present in many fruits, vegetables, grains and meat, and a diet restrictive in inositol reduces its levels in the brain (Shaldubina et al., 2006). Magnetic resonance spectroscopy (MRS) studies showed that inositol is present in the human brain at 3.93 +/- 1.13 mM in young subjects and 4.69 +/- 0.69 mM in older subjects (Kaiser et al., 2005). Altered inositol metabolism has been implicated in various human diseases, including metabolic, cardiovascular, neurodegenerative and neuropsychiatric diseases (Cocco et al., 2004; Croze et al., 2013; Deranieh and Greenberg, 2009; McLaurin et al., 1998; Moore et al., 1999; Scioscia et al., 2007; Shimohama et al., 1998; Teo et al., 2009; Thakkar et al., 1990; Toker and Agam, 2014; Trushina et al., 2012). Inositol has also been shown to prevent the onset of gestational diabetes, and chronic supplementation with inositol has improved insulin sensitivity and reduced fat accretion in mice (Croze and Soulage, 2013; Croze et al., 2015, 2013; Kennington et al., 1990; Murphy et al., 2015; Santamaria et al., 2015; Scioscia et al., 2007; Thakkar et al., 1990; Zheng et al., 2015). Additionally, increased glucose has been demonstrated to competitively inhibit inositol uptake by cells (Coady et al., 2002). Inositol has been also shown to be therapeutic in patients with bulimia and binge eating disorder (Manji et al., 1996), and to increase plasmalogens in serum and decrease low density lipoprotein C (LDL-C) in cardiovascular health (Maeba et al., 2008).

Inositol imbalance has also been linked to neurodegenerative diseases and neuropsychiatric disorders. In Alzheimer's disease, *scyllo*-inositol and *myo*-inositol isomers have been shown *in vitro* to inhibit the formation of Aβ42 fibrils (Fenili et al., 2007; McLaurin et al., 2000, 1998). Furthermore, Ino1 protein activity and levels are higher in the brains of Alzheimer's disease patients, as measured post-mortem (Shimohama et al., 1998). Additionally, inositol is used as a therapeutic in bipolar disorder treatment, a neuropsychiatric condition characterised by recurring mood swings (Chengappa et al., 2000; Nierenberg et al., 2006), and has been tested as a therapy for depression and panic disorders (Palatnik et al., 2001). Inositol has been also found to reduce anxiety in a rat model during the maze behavioural test (Cohen et al., 1997). In humans, clinical studies have shown that 10 out of 15 patients experienced reduced severity in bipolar disorder when inositol intake was reduced (Shaldubina et al., 2006). Furthermore, in humans, diacylglycerol kinase eta (DGKH) has been one of the prominent genes associated with bipolar disorder (Baum et al., 2008). DGKH (*Dictyostelium* DgkA), an enzyme that phosphorylates diacylglycerol (DAG) to generate phosphatidic acid (PA) (Figure 1.2),, is involved in inositol signalling and plays a key role in promoting cell growth (Topham and Epand, 2009).

1.3 Inositol depletion theory and inositol depleting drugs

Inositol imbalance has been implicated in the aetiology of bipolar disorder, where a decrease in inositol levels has been reported in the brains of bipolar disorder patients undergoing drug therapy (Belmaker et al., 2002; Davanzo et al., 2001; Moore et al., 1999). Furthermore, inositol depletion has been demonstrated as a common effect of three structurally different bipolar disorder treatments, valproic acid (VPA) (Figure 1.3), lithium, and carbamazepine, in cultured rat sensory neurons and in the simple biomedical model organism *Dictyostelium discoideum* (Williams et al., 2002). VPA,

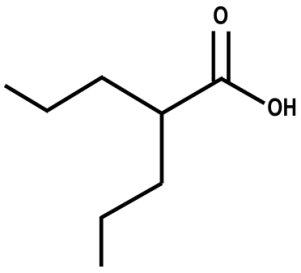

Figure 1.3 The structure of valproic acid (VPA)

lithium, and carbamazepine also prevented the collapse and increased the spread area of the growth cones of rat sensory neurons (Williams et al., 2002). These effects were reversed by the addition of inositol to the culture medium, suggesting that these treatments act via inositol depletion (Williams et al., 2002) and corroborating the inositol depletion theory, which states that mood stabilising drugs such as lithium act via lowering inositol levels (Berridge et al., 1989).

VPA (2-propylpentanoic or 2-propylvaleric acid) is a branched short-chain fatty acid used as a first-choice treatment for acute mania (Terbach et al., 2011). It is also a widely used medication in the treatment of bipolar disorder, epilepsy, migraine, and more recently has been suggested for use in cancer or Alzheimer's disease (Terbach and Williams, 2009). Although VPA has been suggested to target inositol signalling in cells and indirectly inhibit inositol-1-phosphate synthase, the mechanism of VPA action in bipolar disorder therapy remains unknown (Ju et al., 2004; Shaltiel et al., 2004; Vaden et al., 2001).

Lithium is another inositol depleting drug prescribed for bipolar disorder therapy (Ketter et al., 2016). Lithium inhibits inositol polyphosphate 1-phosphatase (IPPase) and inositol monophosphatase (IMPase), which are both involved in inositol recycling (Berridge et al., 1989; Parthasarathy et al., 2003; Serretti et al., 2009). This inhibition causes a depletion of inositol in cells, an increase in inositol monophosphate levels (the substrate of IMPase), and a downregulation of the phosphoinositide cycle. Lithium has been also shown to suppress phosphatidylinositol (3,4,5)-trisphosphate (PIP3) signalling in *Dictyostelium* and in human cells (King et al., 2009). Thus, numerous studies have suggested that both VPA and lithium decrease inositol level through either the inhibition of phosphatidylinositol recycling or via inhibition of *de novo* inositol biosynthesis. Since inositol depletion is a common mechanism of action of bipolar disorder therapies, and inositol levels are lowered in bipolar disorder patients, the effect of inositol depletion may be used as a molecular indicator in identifying improved bipolar disorder treatments.

1.4 Glycolysis and inositol signalling

Research into the pathology of inositol metabolism led to the identification of a number of signalling pathways and molecular targets linked to inositol signalling. Glycolysis is one of the pathways linked to inositol metabolism (Shi et al., 2005). Previous studies have shown that *Saccharomyces cerevisiae* glycolysis mutants (lacking triose phosphate isomerase Tpi1, or phosphoglycerate kinase Pgk1) are inositol-auxotrophs. The *tpi1* and *pgk1* mutants accumulate cellular dihydroxyacetone phosphate (DHAP) 30-fold over the basal level (Shi et al., 2005). DHAP is a product of fructose 1,6-bisphosphate breakdown, and upon its production it is rapidly and reversibly isomerised to glyceraldehyde 3-phosphate (Figure 1.4) (Shi et al., 2005). DHAP was shown to competitively inhibit yeast Ino1 *in vitro* (Shi et al., 2005). In the *tpi1* yeast mutant, the level of *ino1* expression was not changed, suggesting that the inositol auxotrophy phenotype was due to the inhibitory activity of DHAP on Ino1. Similarly, another *S.cerevisiae* glycolysis mutant, *pgk1,* defective in the conversion of 3-phosphoglyceroyl phosphate to 3-phosphoglycerate, also accumulated DHAP and was unable to survive without exogenous inositol supply to the growth media (Shi et al., 2005). Additionally, *in vitro* studies have shown that carbohydrate metabolites, glyceraldehyde 3-phosphate (G3P) in the glycolytic pathway and oxaloacetate (OAA) (fatty acid degradation), inhibit the activity of human and yeast Ino1 proteins (Shi et al., 2005). Finally, in *Dictyostelium,* the ablation of *ino1* led to an accumulation of a glycolytic intermediate, 2,3-bisphosphoglycerate (2,3-BPG) (Fischbach et al., 2006). Overall, these data suggest a cross-talk between glycolysis and inositol signalling.

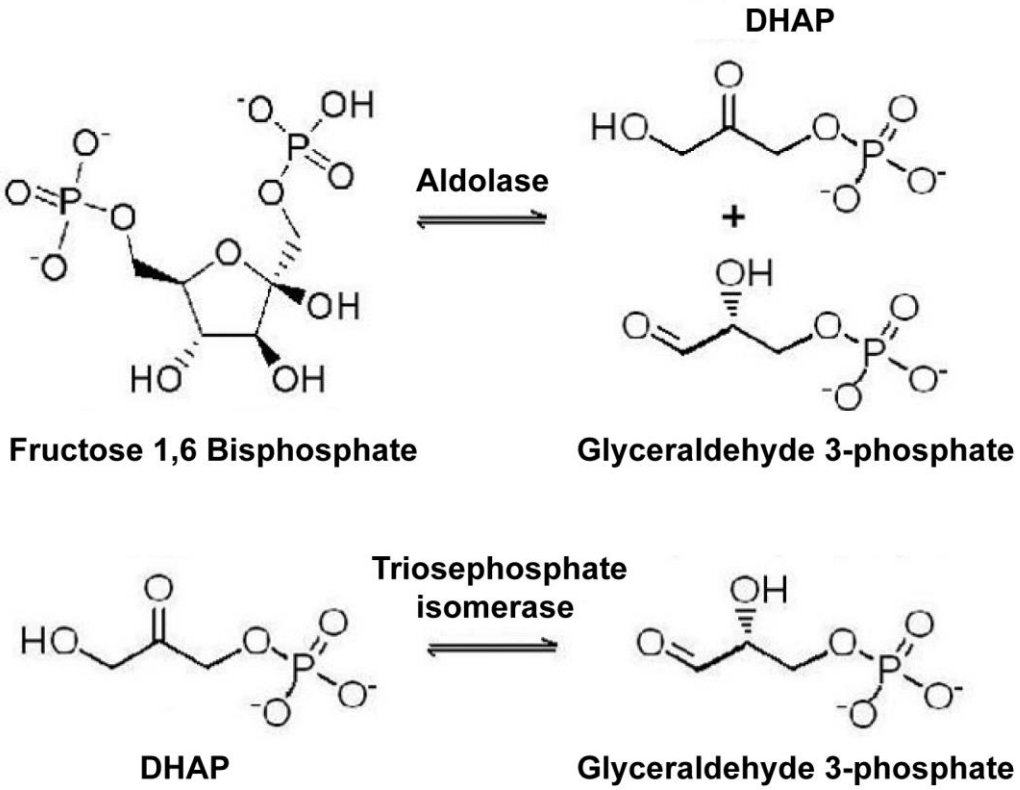

Figure 1.4 Dihydroxyacetone phosphate (DHAP) in the glycolysis pathway. DHAP is produced during the fourth step of glycolysis when aldolase splits fructose 1,6 bisphosphate into DHAP and glyceraldehyde 3-phosphate. In the fifth step of glycolysis DHAP, is rapidly isomerised by triosephosphate isomerase into glyceraldehyde 3-phosphate.

1.5 SUMO regulation of the inositol synthesis pathway

Sumoylation is another cellular process that has been associated with inositol metabolism. Sumoylation is a post-translational protein modification by highly conserved small ubiquitin-related modifier (SUMO) proteins (Henley et al., 2014; Wang and Dasso, 2009). Sumoylation can influence the localisation, stability or interactions of the modified proteins by, for example, directing the assembly and disassembly of dimeric and multimeric protein complexes (Kerscher, 2007) and thus dysregulation of sumoylation has pathological consequences. Indeed, dysfunction of a number of proteins regulated by sumoylation was implicated in human diseases including cancer, Huntington's, Alzheimer's disease (also linked to impaired inositol metabolism), and Parkinson's disease, as well as spinocerebellar ataxia 1 and amyotrophic lateral sclerosis (Cho et al., 2015; Henley et al., 2014; Sarge and Park-Sarge, 2009).

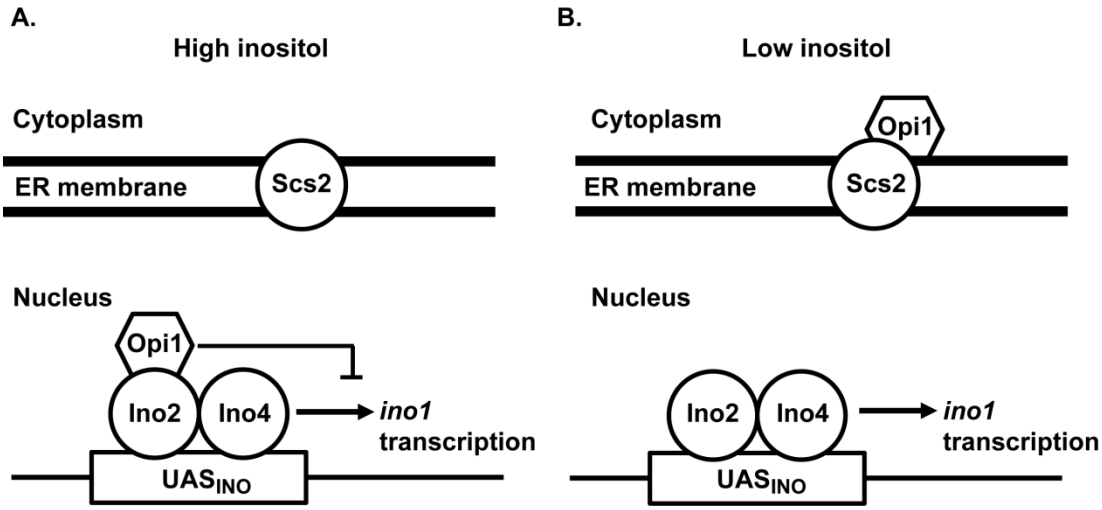

Figure 1.5 SUMO pathway regulation of inositol production. Schematic of the function of the endoplasmic reticulum (ER) type II integral membrane protein Scs2 in inositol synthesis in the yeast *Saccharomyces cerevisiae.* In the presence of inositol, the Scs2 protein remains at the ER membrane and a transcriptional repressor Opi1 is bound to Ino2/Ino4 regulators at the inositol-sensitive upstream activation sequence (UAS_{INO1}) in the promoter site, thus inhibiting the transcription of the *ino1* gene. When inositol levels decrease, Scs2 sequesters the Opi1 repressor, and thus enables Ino2/Ino4 regulators to initiate *ino1* transcription. Adapted from Felberbaum et al. (2012).

Although the mechanism under which sumoylation operates is not yet fully understood, in *S.cerevisiae* it has been linked to inositol regulation. In this model, mutations in the SUMO proteases Ulp1 and Ulp2 decrease *ino1* gene transcription, causing impaired cell growth in the absence of inositol, and leading to an accumulation of the sumoylated proteins *in vivo* (Felberbaum et al., 2012). One of the identified proteins was Scs2, a type II integral membrane protein in the endoplasmic reticulum (ER) and a member of the vesicle-associated (VAP) family proteins, which regulates phosphatidylinositol synthesis and lipid trafficking, and when deleted results in inositol auxotrophy (Felberbaum et al., 2012). Thus, an interdependence between SUMO and inositol has been proposed, where protein sumoylation regulates inositol production and inositol modulates SUMO protein conjugation in cells (Figure 1.5). Furthermore, inositol starvation both increased the global sumoylation level and at the same time led to desumoylation of some specific proteins (Felberbaum et al., 2012). Finally, in the phosphoinositol pathway, sumoylation also regulates the class III phosphatidylinositol 3-kinase (PI3K-III) complex (and its product phosphatidylinositol 3-phosphate, PIP), which is involved in the control of autophagy, endocytosis or cytokinesis (Reidick et al., 2014).

1.6 *Dictyostelium discoideum* as a biomedical model

Investigation into the molecular mechanism of the regulation of inositol signalling has been previously conducted using mammalian tissue culture as well as simple model organisms, such as *Dictyostelium discoideum or S.cerevisiae*. The use of simple model organisms provides some advantages over more complex models such as neuronal culture, due to the challenges in handling mammalian cells for experimental purposes. Simple model organisms offer easy genetic manipulation and maintenance in a laboratory environment. *Dictyostelium* is an established simple biomedical model organism that is used in cell biology and molecular pharmacology research (Annesley and Fisher, 2009; Escalante and Vicente, 2000; Francione et al., 2011; King et al., 2010; Nichols et al., 2015; Stephens et al., 2008; Williams, 2005). Compared to mammalian model organisms, *Dictyostelium* cells are relatively easy to genetically manipulate and observe phenotypic changes (King and Insall, 2009; Manstein et al., 1989; Montagnes et al., 2012; Williams, 2005). The genome of *Dictyostelium* has been fully sequenced and contains a number of human disease-related orthologues (Eichinger et al., 2005). Examples of research related to human diseases where *Dictyostelium* has previously been used as a model organism, include studies to characterise the molecular mechanism of drug action in bipolar disorder and epilepsy treatment (Boeckeler et al., 2006; Eickholt et al., 2005; Ludtmann et al., 2011; Teo et al., 2009; Williams et al., 1999, 2002; Xu et al., 2007), research into the molecular mechanism of Alzheimer's disease (Ludtmann et al., 2014; McMains et al., 2010), research into taste perception and to assess emetic liability (Cocorocchio et al., 2015; Robery et al., 2013, 2011), as a model for human mitochondrial diseases (Francione et al., 2011), and in studies of cell growth and differentiation (Escalante and Vicente, 2000; Maeda, 2005).

Changes in inositol levels can be studied in *Dictyostelium* or yeast (*S.cerevisiae*), where the expression of the *ino1* gene is regulated by the intracellular level of inositol (Shaltiel et al., 2004; Shetty and Lopes, 2010; Steger et al., 2003; Williams et al., 2002). In such experiments, mutagenesis

can also be applied to study inositol depletion. For instance, a library of random mutants can be created in *Dictyostelium* by restriction enzyme mediated mutagenesis (REMI), where an insertional cassette is introduced into cells and is integrated into the genome at frequently occurring restriction enzyme sites, and mutants are selected based on the antibiotic resistance present in the cassette (Kuspa and Loomis, 1994). Genes identified using such techniques can be further examined for their role in inositol signalling and the inositol depleting effects produced by drug treatment. A reduction of cellular inositol in *Dictyostelium* cells can be reversed by the addition of inositol to the growth medium, since cells are able to take up inositol from extracellular sources (Fischbach et al., 2006). Discoveries into the mode of action of inositol depleting drugs have been made using these methods in *Dictyostelium,* thus validating this organism as a suitable biomedical model for the research into inositol depletion effects on a cell (Williams, 2009; Williams et al., 2002).

1.7 *Dictyostelium* development

In addition to a role as a basic biomedical model, *Dictyostelium* is also widely used to study multicellular development. In the wild, *Dictyostelium* undergoes development following starvation (Eichinger et al., 2005) (Figure 1.6). In the presence of a food source, *Dictyostelium* lives as a single-celled amoeba. During an onset of environmentally unfavourable conditions, such as a lack of nutrients, cells start to release pulses of the extracellular chemical cyclic adenosine monophosphate (cAMP), which is sensed by neighbouring cells (Chisholm and Firtel, 2004). The cAMP signal is then propagated by cells and initiates intracellular events that lead to chemotactic cell movement. Cells chemotax towards each other to form aggregates that via a number of developmental stages differentiate into a multicellular structure called a fruiting body. The fruiting body is a multicellular organism that contains spores held aloft by dead, vacuolated stalk cells (Loomis, 2014). When conditions are favourable, spores germinate to release the single–celled amoebae (Eichinger et al., 2005).

This developmental process is completed within 24 hours, and is sensitive to intracellular inositol changes (Fischbach et al., 2006), as well as exposure to inositol-depleting drugs (Williams et al., 2002). This process can be artificially stimulated in the laboratory by plating the cells onto a substrate without nutrients, like agar plates or nitrocellulose filters. Thus, this makes *Dictyostelium* a simple eukaryotic model organism that can be used to study cell and developmental biology (Adley et al., 2006).

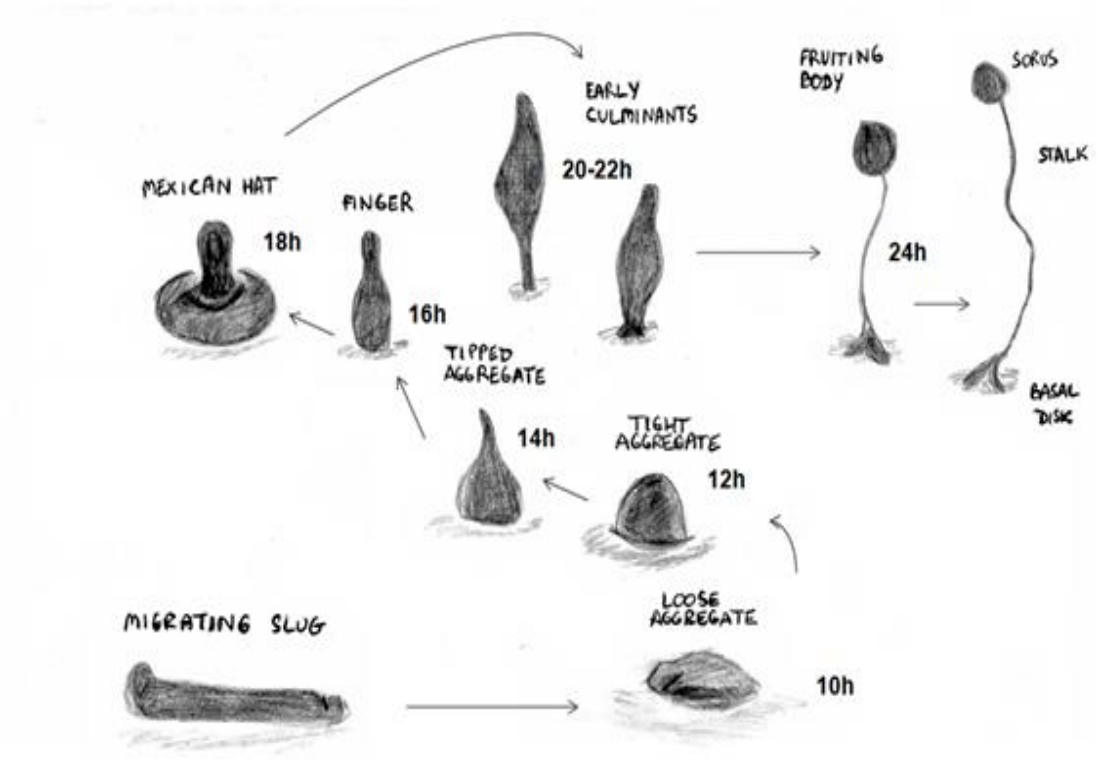

Figure 1.6 Multicellular development of *Dictyostelium discoideum*. Depletion of nutrients triggers the developmental program, where starving *Dictyostelium* cells aggregate to form mounds, and then differentiate into fruiting bodies. In the aggregation stage, cells interact forming streams that migrate toward an aggregation centre to form aggregates (8-10 hours). The aggregates elongate to form structures called first fingers (12-13 hours). At this stage of development, cells differentiate into anterior prestalk and posterior prespore cells in a motile multicellular slug. The slugs further differentiate into structures called culminants and then into a fruiting body (Chisholm and Firtel, 2004). This process takes 24 hours, and the mature fruiting body comprises a basal disk, a stalk and a sorus (the spore head), which contains spores that can be dispersed. Upon germination, amoebae emerge to resume a single-celled existence.

Inositol signalling is involved in a number of cellular processes that can be investigated using *Dictyostelium* as a model organism. The following paragraphs describe an involvement of inositol derivatives, phosphoinositides and inositol phosphates, in cell motility (chemotaxis), cell polarity, cell

adhesion, cytokinesis, and autophagy processes, which can be assayed in *Dictyostelium*.

1.8 Chemotaxis

Chemotaxis is an essential part of the early phase of *Dictyostelium* development, when cells deprived of nutrients release cAMP, thus stimulating surrounding cells to migrate towards the aggregation centre, which is a point source from where this chemical is being released. To efficiently chemotax, cells must be able to sense the chemoattractant and relay the signal within the cell to trigger the events that lead to cytoskeletal rearrangement, allowing for cell orientation and movement towards the source of the chemoattractant. Important aspects of chemotaxis thus include initiating morphological changes to induce cell polarity and the maintenance of the directionality of movement.

Detection of a cAMP signal initiates intracellular signalling via the activation of cyclic AMP receptor 1 (cAR1), a G-protein coupled receptor, which then transmits the signal to downstream effectors initiating forward movement (Stephens et al., 2008). Stimulation of cAR1 activates phosphatidylinositol-3-kinase (PI3K), target of rapamycin complex 2 (TORC2) and phospholipase A2 (PLA2) (Figure 1.7). Activated PI3K phosphorylates PIP2 into PIP3, while phosphatase and tensin homologue (PTEN) dephosphorylates PIP3 back into PIP2. PTEN is located at the rear end of the cell leading to a decrease in the level of PIP3 in the posterior end of the cell to create a PIP3 gradient (Stephens et al., 2008). The accumulation of PIP3 at the leading edge of migrating cells initiates a translocation of a family of pleckstrin homology (PH) domain-containing proteins which act as effectors of PIP3 and play important roles in chemotaxis (Stephens et al., 2008). These proteins include PhdA (PH-domain containing protein A), which is involved in the initiation of F-actin polymerisation, and cytosolic regulator of adenylate cyclase (CRAC) and PkbA (PKB-related) proteins, which propagate the release of intracellular cAMP via the activation of adenylate cyclase (AC) (Huang et al., 2003; Insall et al., 1994; Lilly and Devreotes,

1995). *Dictyostelium* cells also chemotax in the absence of PIP3 gradients (when a strong gradient of chemoattractant was used) suggesting that there are other mechanisms of cell directionality during chemotaxis, which may involve sensing TORC2 and PLA2 (Hoeller and Kay, 2007). TORC2 is involved in F-actin polymerisation at the leading edge of the cell during PKB/RasG signalling (Charest et al., 2010; Kamimura et al., 2008; King and Insall, 2008). PLA2 has been shown to regulate chemotaxis by elevating calcium levels in cells via the conversion of membrane phospholipids to lysophospholipids and arachidonic acid, leading to calcium release (King and Insall, 2009).

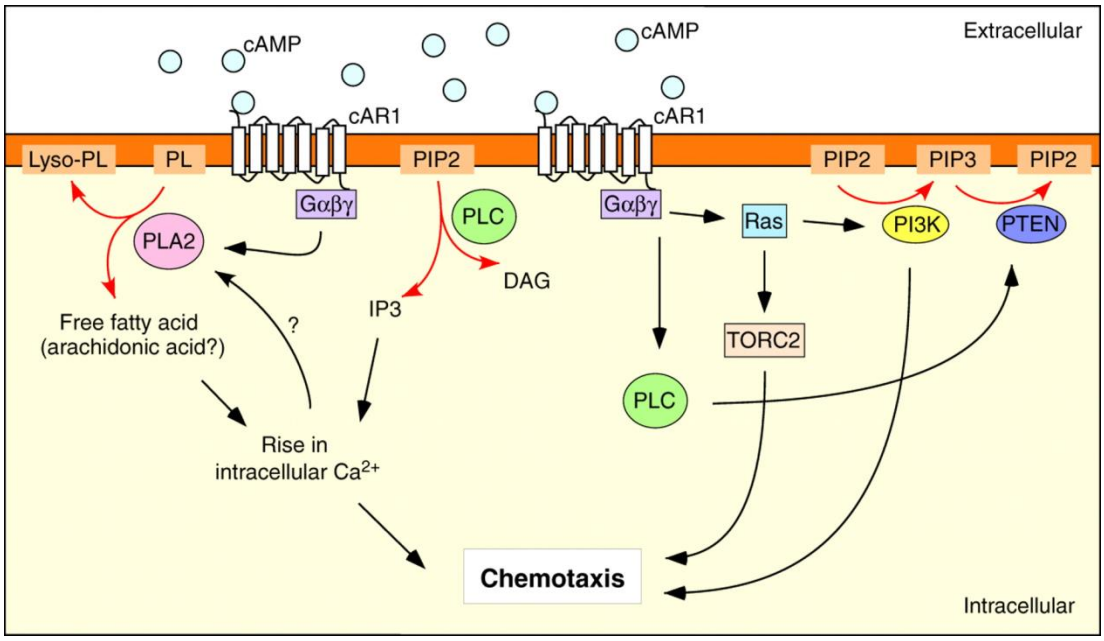

Figure 1.7 Regulation of chemotaxis in *Dictyostelium*. In *Dictyostelium*, chemotaxis is controlled by extracellular cAMP binding to the cAR1 receptor, and the partially redundant pathways involving PI3K, TORC2 and PLA2. The PI3K pathway is regulated by PLC via PIP2 and PTEN. The TORC2 pathway activates F-actin polymerisation via RasG signalling. The PLA2 pathway is dependent on fatty acid release triggering increased calcium levels. In steep chemoattractant gradients, these pathways are dispensable, however, in shallow chemoattractant gradients, the PI3K pathway is crucial for efficient chemotaxis. Red arrows indicate enzymatic reactions. Abbreviations: PL, phospholipids; Lyso-PL, lyso-phospholipids; PLA2, phospholipase A2; Gαβγ, heterotrimeric G protein; cAR1, cAMP receptor 1; PI3K, phosphatidylinositol-3-kinase; TORC2, target of rapamycin complex 2; PTEN, phosphatase and tensin homologue; PLC, phospholipase C; IP3, inositol trisphosphate; PIP2, phosphatidylinositol 4,5-bisphosphate; PIP3, phosphatidylinositol 3,4,5-trisphosphate. After Kölsch et al. (2008).

1.9 Phosphoinositides in cell polarity and cell adhesion

Phosphoinositides are important for cellular processes determining cell polarity and adhesion. Multiple signalling pathways have been proposed to control patterns of cell polarity through a feedback loop mechanism (King and Insall, 2009). In *Dictyostelium,* Ras proteins present at the leading edge of cells can be rapidly activated by cAMP binding to cAR1, driving the polarisation of PIP3 distribution (Sasaki et al., 2004). However, in *Dictyostelium* cells, polarised PI3K signalling and subsequent morphological changes in the absence of G-proteins have also been shown, suggesting that cellular polarity can be maintained independently of cAR1/heterotrimeric G protein signalling (Sasaki et al., 2004). Regardless, PIP3 remains an important molecule in *Dictyostelium* chemotaxis, and although it does not exclusively dictate directionality of movement, it's functional importance highlights the importance of its precursor, inositol, in the events leading to cell movement.

Reorganization of the actin cytoskeleton is crucial for cell motility, chemotaxis, and adhesion. Actin-binding proteins and membrane lipids, especially PIP2 and PIP3, are involved in this process, where some actin-binding proteins interact with, or are regulated by, phosphoinositides (Wu et al., 2014). For example, PIP2 activates Talin, a protein that binds to β-integrins to enhance cell adhesion (Figure 1.8). PIP2 also activates WASp family proteins, which in turn activate the Arp2/3 complex proteins that are involved in actin filament assembly during chemotaxis (Pollitt and Insall, 2009; Wu et al., 2014), and the actin-depolymerizing factor (ADF)/cofilins, which coordinate organization of actin filament assembly and disassembly (Bamburg and Bernstein, 2010). PIP3 activates various guanine nucleotide exchange factor proteins that regulate small GTP-binding proteins such as Rho, Rac, Ras and Cdc42 (Wu et al., 2014). In neutrophils, PIP3 has been associated with actin polymerisation via Rho GTPases (Figure 1.9). PIP3 has been also implicated in determining cell polarity during movement (King and Insall, 2009). Together PIP2 and PIP3 play important roles in actin cytoskeleton organisation, including cell movement, adhesion and

cytokinesis, and alterations of phosphoinositol levels have been linked to diseases related to cell migration, like cancer (Wu et al., 2014).

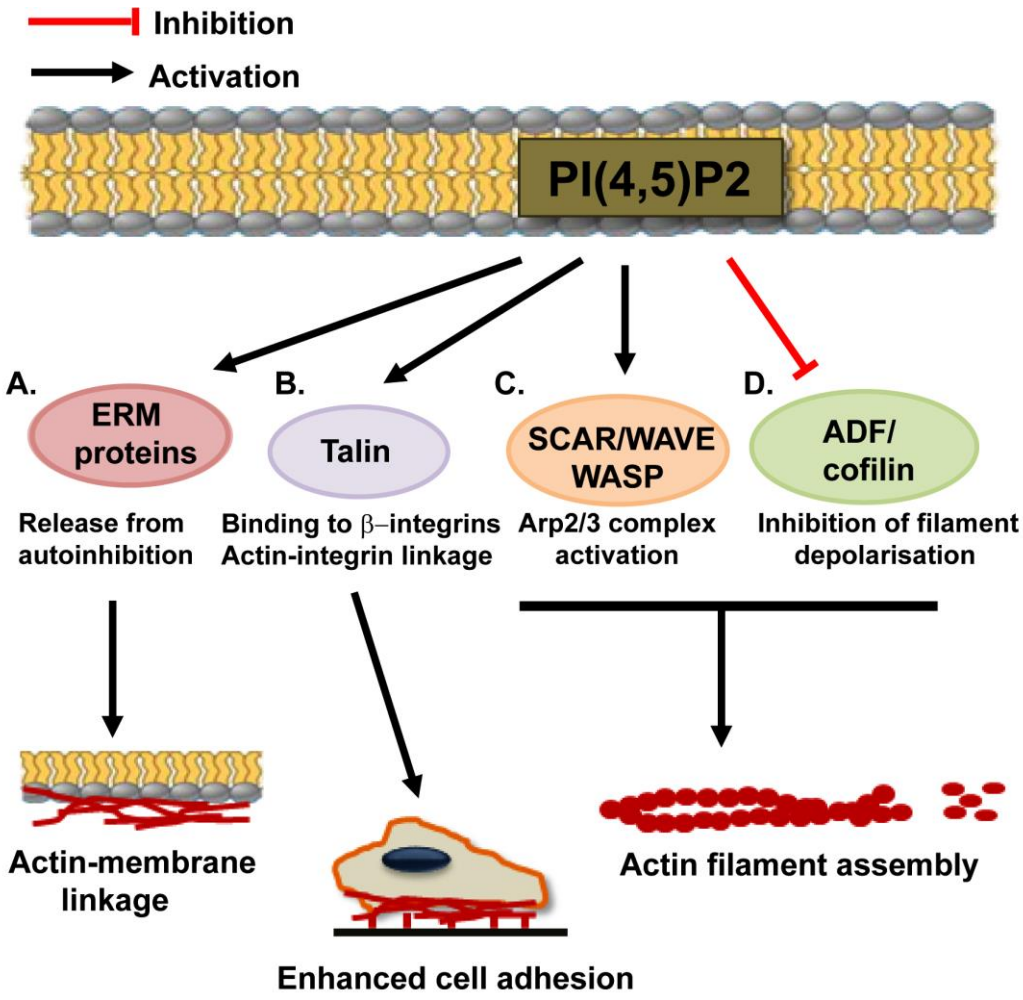

Figure 1.8 Regulation of actin binding proteins by PIP2. PIP2 regulates cell function via actin-binding proteins such as ERM proteins, Talin, SCAR/WAVE/WASP and ADF/cofilin. (A) The presence of PIP2 and phosphorylation of ERM (Ezrin-Radixin-Moesin) membrane–actin-tethering proteins lead to an activation of the ERM complex. The activated ERM proteins bind to F-actin filaments. In *Dictyostelium*, a protein called enlazin, which is a natural fusion of an ERM family protein and the actin cross-linker fimbrin, contributes to cell adhesion and cortical mechanics (Octtaviani et al., 2006). (B) Integrin proteins bind to Talin, which in turn binds to actin, increasing cell adhesion events. (C) PIP2 activates the WASp proteins SCAR/WAVE, leading to Arp2/3 complex activation and actin branch formation on the inside of the cell membrane (Pollitt and Insall, 2009). (D) The actin-depolymerising factor (ADF)/cofilins integrate transmembrane signals to coordinate the spatial and temporal organization of actin filament assembly/disassembly (Bamburg and Bernstein, 2010). Inactive cofilin remains bound to PIP2 at the plasma membrane. Dissociation of cofilin from PIP2 increases severing of actin filaments. Adapted from Wu et al. (2014).

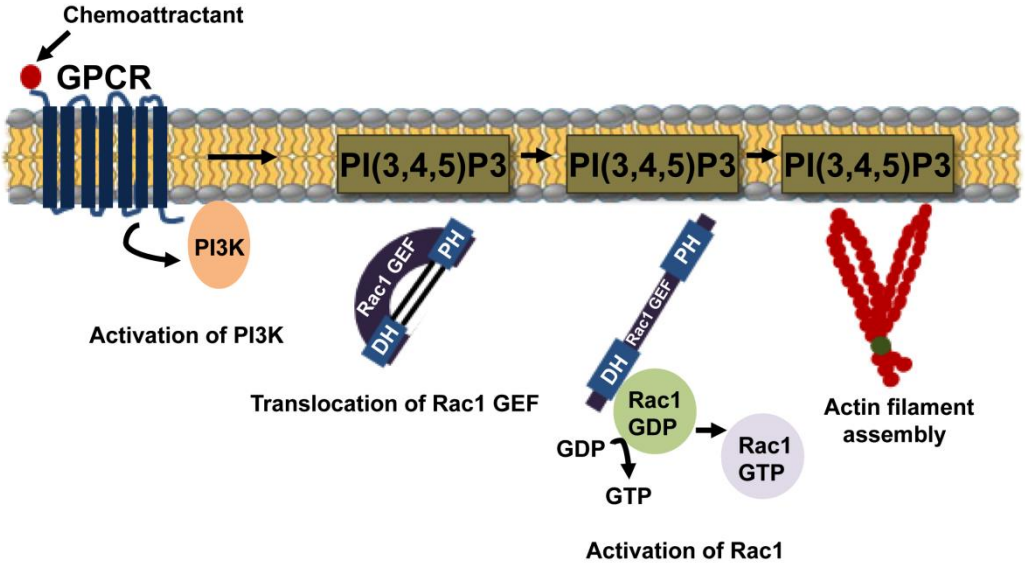

Figure 1.9 Activation of actin filament assembly by PIP3. Activation of actin filament assembly occurs by transient production of PIP3, activating Rho GTPase, a member of the family of guanine nucleotide exchange factors (GEFs). The pathway starts with PI3K activation, which leads to the accumulation of activated Rac (Rac-GTP). Adapted from Wu et al. (2014).

1.10 Cytokinesis

Phosphoinositides also play role in processes leading to cell cytokinesis, an essential cellular function enabling cells to divide into two daughter cells. Cytokinesis is a sequential process occurring in three stages: assembly of the cytokinetic apparatus, furrow progression and fission (scission) of the newly-formed daughter cells (Uyeda and Nagasaki, 2004) (Figure 1.10). In *Dictyostelium,* the first step involves microtubules of the mitotic spindle initiating the position of a division plane where the cleavage furrow will form. The next step involves the ingression and severing of the cleavage furrow. The process of ingression involves accumulation of myosin II in the furrow and the constriction of an equatorial actomyosin ring, where an increased level of PIP2 is necessary for furrow stability (Brill et al., 2011a; D'Avino et al., 2005). *Dictyostelium* also uses other myosin II-independent methods to induce the furrowing of the equatorial ring. These alternative cytokinesis events occur when cells are adhered to a substrate, and one of these is cell-cycle coupled (Knecht and Loomis, 1987; Nagasaki et al., 2002; Uyeda and Nagasaki, 2004; Zang et al., 1997). Mechanistically, these two cytokinesis processes are different. During myosin II-dependent cytokinesis,

cells detach from the substrate and become more round with a V-shaped contractile ring. By contrast, during myosin II-independent cell division, cells are flat and remain attached to a substrate throughout the cleavage furrow separation and have a U-shaped contractile ring. Ingression of the equatorial ring occurs as a result of two opposing traction forces generated by the two polar leading edges of an adherent cell (Uyeda and Nagasaki, 2004). Wild-type cells utilise both methods of cytokinesis during normal growth on a solid substrate, where cells initially detach forming the V-shaped contractile ring, re-spread and attach to a substrate to complete the division (Uyeda and Nagasaki, 2004). The third form of cytokinesis is also linked to a cell-substrate interaction, and relies on an extension of the part of the cell where the leading edge pulls away from the centre of a cell, leaving a long tail of cytoplasm behind that eventually leads to cell separation (Hibi et al., 2004). Thus, myosin and actin contractile ring are required to provide the force necessary for the separation of a dividing cell, and the disruption of either actin or myosin components has a severe impact on cytokinesis. *Dictyostelium* myosin II mutants are however still able to separate when cells are attached to a substrate.

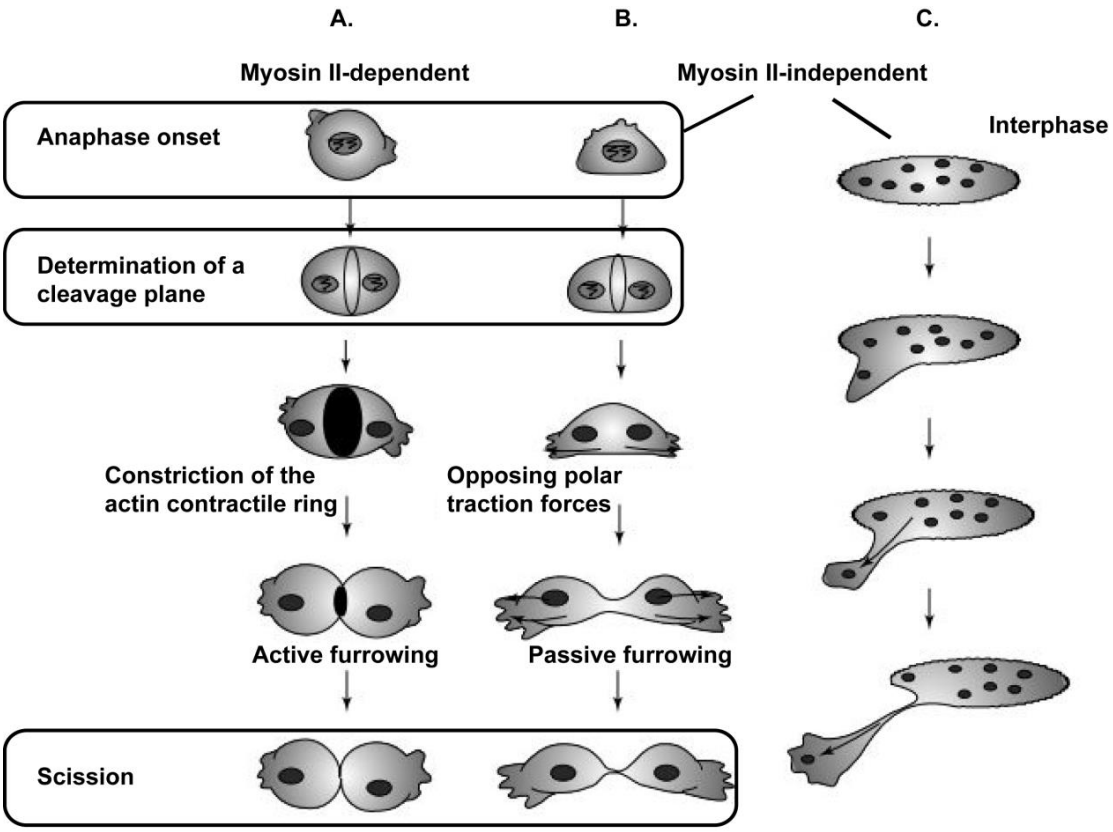

Figure 1.10 Cytokinesis in *Dictyostelium*. Three forms of cell division are presented here. (A) Myosin II-dependent cell division relies on myosin accumulation in the cleavage furrow, initiating the constriction of the actin contractile ring. (B) Myosin II-independent cell division relying on the opposite polar traction forces to separate the cleavage furrow. This type of cell division was observed in myosin II null cells, and can only occur on a substrate but not in suspension. (C) Another form of myosin II-independent cell division where the leading edge of a cell is pull away from the centre of the cell, tearing the cell apart. Adapted from Uyeda and Nagasaki (2004).

1.11 Autophagy

Inositol metabolism has been associated with macroautophagy (Criollo et al., 2007; Sarkar et al., 2005; Toker and Agam, 2014; Vicencio et al., 2009). Macroautophagy (hereafter referred to as autophagy) is a process triggered by stress conditions, for example nutrient starvation, to promote cell survival; however, it can sometimes lead to cell death (Denton et al., 2012). Although autophagy is not usually associated with programmed cell death, it is typically involved in the death of cells during development of an organism (Denton et al., 2012). During autophagy cells digest cellular components via the activity of enzymes that originate in lysosomes. It is a highly regulated catabolic process that comprises a number of steps: induction,

autophagosome nucleation, expansion and completion, lysosome fusion, degradation and recycling (Figure 1.11).

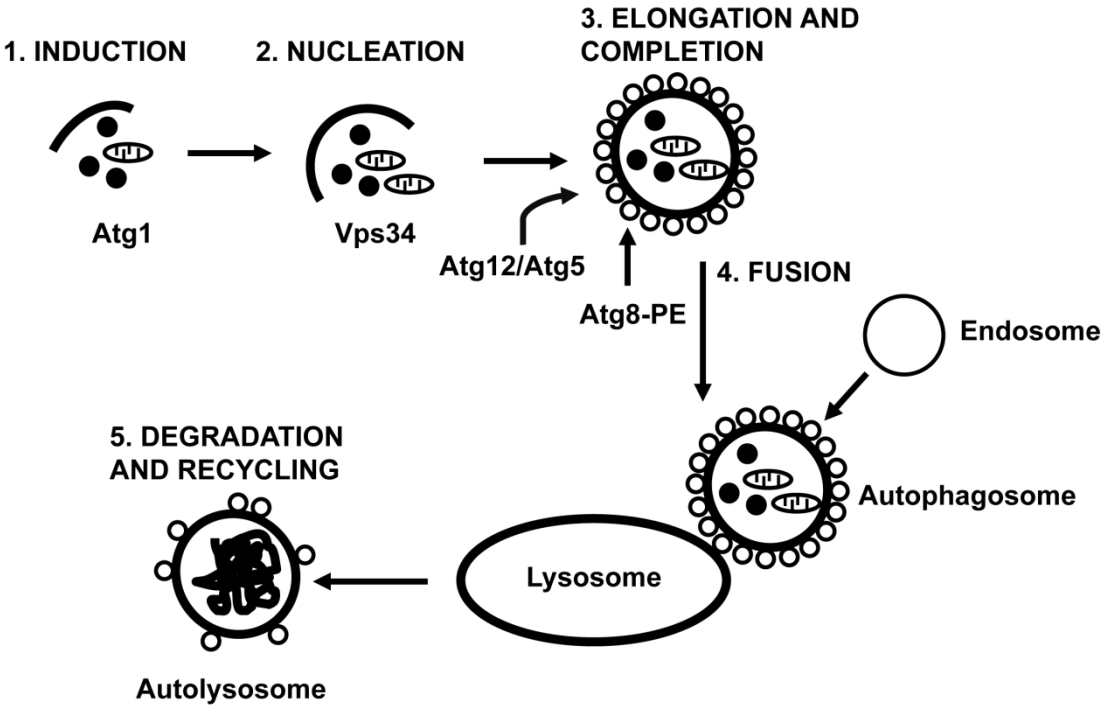

Figure 1.11 Autophagosome formation in eukaryotic cells. The induction of autophagosome formation starts with Atg1 that localises to the membrane sac generated from the pre-autophagosomal structure (isolation membrane). An autophagy-specific Vps34 PI3-kinase complex I assists in the nucleation of the forming autophagosome. The complex is essential for the recruitment of the Atg8-phosphatidylehanolamine (Atg8-PE) conjugate and the Atg12-Atg5 conjugate to the pre-autophagosomal structure. Atg8-PE remains at the autophagosome membrane even after autophagosome maturation. Autophagosome maturation involves elongation, completion and fusion with endosome structures. These steps are essential for the subsequent fusion with lysosomes. The final steps of autophagy involve degradation and recycling of the engulfed cellular material.

The autophagy-related gene-1 (Atg1) complex is responsible for the activation of autophagy. The nucleation of newly-formed vesicles happens upon the activation of class-III phosphatidylinositol-3-kinase (Vps34), Beclin-1/Atg6, and several other proteins, which recruit lipids and proteins for the formation of autophagosomes (Chen and Klionsky, 2011; Denton et al., 2012; Mizushima et al., 2002). Following nucleation, the vesicles are elongated and completed by the ubiquitin-like proteins that modulate conjugation of the Atg8 protein to the lipid phosphatidylethanolamine (PE), and assembly of an Atg12/Atg5 complex, which then assists in the binding of Atg8-PE to the autophagosome membrane (Chang and Neufeld, 2010; Chen and Klionsky, 2011; Yang and Klionsky, 2010). The Atg12/Atg5 complex is highly

conserved among eukaryotes, and the conjugation of Atg12 to Atg5 resembles ubiquitination reactions, where the C-terminal glycine of Atg12 is covalently attached by an isopeptide bond to lysine 130 of Atg5 (Mizushima et al., 2002). Atg8 is present on the elongating vesicle membrane and remains on the autophagosomal membrane after autophagosome formation is completed (Mizushima et al., 2002). The final step of autophagosome formation is the fusion of autophagosomes with lysosomes. Proper function of microtubules, an acidification of autophagosomes, and the fusion with endosomes are essential steps allowing for the fusion with lysosomes (Kovács et al., 1982; Yamamoto et al., 1998). The significance of the endosome fusion events remains unclear; however, it has been shown that a perturbation of endosome function leads to an accumulation of autophagosomes that cannot fuse with lysosomes (Nara et al., 2002).

Dictyostelium cells rely on autophagy during starvation conditions and development (Giusti et al., 2009; Kosta et al., 2004; Luciani et al., 2011; Otto et al., 2004, 2003). Nutrient starvation and cAMP induce autophagy in *Dictyostelium,* while the presence of the differentiation factor DIF-1, acting as a secondary signal, triggers programmed cell death; a process that is essential for proper development of this organism (Luciani et al., 2011).

An increased number of autophagosomes has been found in many human diseases, including degenerative diseases of the muscle and the nervous system like amyotrophic lateral sclerosis (ALS), Alzheimer's disease, Parkinson's disease, and Huntington's disease (Wong and Holzbaur, 2015). These diseases are characterised by an accumulation of misfolded proteins that failed to be degraded via the ubiquitin-proteasome system (Mizushima et al., 2002).

1.12 Aims of this work

Inositol signalling plays vital role in cell homeostasis and its dysregulation has been implicated in various diseases, including neurodegenerative and metabolic diseases. Cellular processes such as development, cell movement, cytokinesis and autophagy relate to inositol

regulation and are the subject of current research. Various yeast mutants impaired in inositol production have been demonstrated to rely on exogenous inositol for survival. In *Dictyostelium,* inositol depletion has been shown to decrease cell growth and to inhibit development (via the action of inositol depleting drugs). Molecular targets affected by a change in inositol levels are however still not fully identified.

This thesis investigates the mechanism and the consequences of inositol depletion in *Dictyostelium* cells with the use of molecular biology, lipid analysis, metabolomic and proteomic approaches. I also examine the characteristics and cellular functions of Ino1 protein and inositol depletion using the following strategies:

- Identification and characterisation of the potential homologue of inositol biosynthetic enzyme, Ino1, in *Dictyostelium*
- Genetic manipulation of the *ino1* gene in *Dictyostelium* and the generation of the *ino1* knock-out mutant
- Analysis of the effects of inositol depletion and the Ino1 loss on cell function in *Dictyostelium*
- Characterisation of cellular roles of the Ino1 protein, including growth effects resulting from a mutation in the enzyme catalytic core, the effects of inositol depleting drugs on the development of *Dictyostelium ino1* mutants, and identification of the Ino1 protein-protein interaction

Chapter 2
Materials and Methods

Chapter II

Materials and Methods

2.1 Materials

2.1.1 Reagents obtained from Sigma-Aldrich Ltd (Poole, England)

2-Propanol, 4′,6-Diamidino-2-phenylindole 4',6-Diamidino-2-Phenylindole, Dihydrochloride (DAPI), acrylamide (30% solution), ammonium persulfate (APS), bacteriological agar, β-mercaptoethanol, caffeine, cyclic adenosine monophosphate (cAMP), dithiothreitol (DTT), ethylenediaminetetraacetic acid (EDTA), ethylene glycol tetraacetic acid (EGTA), Fluorescein Diacetate (FDA), Fluoromount Aqueous Mounting Medium, horse serum, sodium dodecyl sulphate (SDS), Luria-broth (LB) tablets, magnesium chloride, Nonidet-P40 (NP40), Tween 20, phenylmethylsulfonyl fluoride (PMSF), potassium chloride, sucrose, phosphatase inhibitor tablets (PhosStop, Roche), propidium iodide (PI), protease Inhibitor Cocktail Tablets (cOmplete ULTRA Tablets, Mini, Roche), sodium chloride, sodium dihydrogen phosphate (NaH_2PO_4), sodium fluoride, sodium orthovanadate, sodium phosphate dibasic (Na_2HPO_4), N,N,N′,N′-Tetramethylethylenediamine (TEMED), trizma base; Triton-100, TruPAGE Precast Gels, TruPAGE LDS Sample Buffer.

2.1.2 Reagents obtained from other suppliers

Agarose, deoxynucleotide trisphosphates (dNTPs) (Bioline, London, England); Ethidium bromide (Bio-Rad Laboratories, Hemel Hampstead, England); Axenic (Ax) medium, SM medium, LoFlo medium (ForMedium, Hunstanton, England); Imperial Protein Stain with Coomassie dye R-250, 6xLoading dye (Fermentas); NuPage MOPS buffer, NuPage Transfer buffer, NuPage SDS-polyacrylamide gel (Invitrogen), Tris-borate-EDTA (TBE), 10x glycine buffer (ThermoFisher Scientific, Loughborough, England); ethanol, dipotassium hydrogen phosphate (K_2HPO_4), glycerol, acetic acid, acetone,

bromophenol blue, chloroform, dimethyl sulfoxide (DMSO), glucose, hydrochloric acid, isopropyl β-D-1-thiogalactopyranoside (IPTG), methanol, paraformaldehyde (PFA), potassium dihydrogen phosphate (KH_2PO_4), sodium hydroxide (VWR International Ltd., Lutterworth, England).

2.1.3 Antibiotics

Ampicillin (Sigma-Aldrich Co. Ltd., Poole, England); Blasticidin, penicillin/streptomycin (Pen/Strep) solution x100 (PAA Laboratories Ltd. Yeovil); Hygromycin, Geneticin (G418) (Invitrogen, part of ThermoFisher Scientific, Loughborough, England).

2.1.4 Molecular weight standards

GeneRuler 100 bp and 1 kb DNA Ladder (0.1 µg/µl); PageRuler Plus pre-stained protein ladder (ThermoFisher Scientific, Loughborough, England).

2.1.5 Restriction enzymes

All restriction enzymes were obtained from ThermoFisher Scientific (Loughborough, England) and New England Biolabs (UK) Ltd. (Hitchin, England).

2.1.6 Other enzymes

RNase A, DNase (Sigma-Aldrich Co. Ltd., Poole, England); BIOTaq polymerase (Bioline, London, England); Q5 High-Fidelity PCR polymerase (New England Biolabs (UK) Ltd., Hitchin, England); Phusion High-Fidelity PCR polymerase (ThermoFisher Scientific, Loughborough, England); Calf Alkaline Phosphatase (CIAP) (Promega UK, Southampton, England).

2.1.7 Antibodies

GFP rat [3H9] monoclonal antibody, GFP Trap agarose beads, RFP mouse [6G6] monoclonal antibody, RFP rat [5F8] monoclonal antibody, RFP Trap agarose beads (ChromoTek GmbH, Germany); IRDye 800 Goat Anti-Rat, IRDye 800 Goat Anti-Mouse (Licor Bioscience Ltd., Nebraska, USA); mouse monoclonal anti-FLAG M2 antibody (Sigma-Aldrich Ltd., Poole, England).

2.1.8 Kits

QIAfilter Plasmid Maxi Kit and MiniElute PCR purification kit (QIAgen Ltd, Crawley, West Sussex, UK); GenElute HP Plasmid Midiprep and Maxiprep kit, GenElute PCR Clean-Up Kit (Sigma-Aldrich Co. Ltd., Poole, England); High Pure RNA Isolation kit (Roche, West Sussex, England); DNase treated with DNA-free kit (Ambion supplied by Invitrogen, part of ThermoFisher Scientific, Loughborough, England); First Strand cDNA Synthesis kit, Pierce BCA Protein Assay Kit, TOPO® TA Cloning kit (ThermoFisher Scientific, Loughborough, England); β-Galactosidase Enzyme Assay System with Reporter Lysis Buffer (Promega UK, Southampton, England).

2.1.9 Bacterial strains

TOP10 chemically-competent *E.coli*, chemically-competent *JM107 E.coli* (Invitrogen, part of ThermoFisher Scientific, Loughborough, England); 10β-competent cells (New England Biolabs (UK) Ltd., Hitchin, England); *Raoultella planticola* (lab-made stock).

2.1.10 Primers (Table S1, supplementary material)

Custom-made oligonucleotides were purchased from MWG-Biotech AG (Eurofins) (Germany) or Sigma-Aldrich Co. Ltd. (Poole, England).

2.1.11 Equipment

Bio-Rad gel casting system, Bio-Rad wide mini-sub cell electrophoresis system, Gel Doc XR system, GenePulser Xcell electoporator (Bio-Rad Laboratories, Hemel Hempstead, England); GeneFlash gel documentation system (Syngene Bio-Imaging); 505Di peristaltic pump (Watson Marlow); centrifuge (Biofuge 13, Jencons); microcentrifuge (ThermoFisher Scientific, Loughborough, England); PeqSTAR 2x thermocycler, PeqSTAR 96 Universal thermocycler, 4mm EP cuvettes (PEQLAB Ltd. Portsmouth, England); Odyssey Infrared Imaging System (Li-cor Biosciences, Nebraska, USA); Olympus IX71 microscope (U-RFL-T laser, 482nm emission, Olympus UPlanFL 60x oil immersion objective with NA 1.25) with an QImaging RetigaExi Fast1394 digital camera.

2.2 Methods

2.2.1 Bioinformatic analysis

Dictyostelium Ino1 protein homologues were identified in other species by performing the Basic Local Alignment Search Tool (BLAST) using the engine from the National Centre for Biotechnology Information site (NCBI). The BLAST search options were optimised for more dissimilar sequences (discontinuous megablast). The search parameters were as follows: program = BLASTP 2.2.25; matrix = blosum62; threshold = 0.01. The BLAST search was performed within the 'non-redundant' ('nr') database of nucleic acid collection, which allowed for any given sequence within this database to appear only once, thus minimising possible duplications. Discontinuous megablast option allowed for cross-species comparisons.

Phylogenetic analysis and evolutionary history were acquired with the MEGA program, version 5, using the neighbour-joining method with 500 bootstrap replicates (Tamura et al., 2011). The Phyre^2 (Protein Homology/analogY Recognition Engine V 2.0) (Kelley et al., 2015) and the Conserved Domain Database (CDD) (NCBI) (Marchler-Bauer et al., 2014) engines were used to obtain the information regarding the structure and conserved functional domains in the human and *Dictyostelium* Ino1 and the Q54IX5 proteins.

2.2.2 *Dictyostelium discoideum* methods

2.2.2.1 Cell culture

Dictyostelium discoideum cells were stored at -80ºC as spores in 1x sterilised phosphate buffer KK2 (16.2 mM KH_2PO_4, 4 mM K_2HPO_4) or as cells frozen in horse serum containing 7% DMSO. Every four weeks, *Dictyostelium* frozen stock cells were plated onto plates containing SM agar (Sigma) and 300 µl live *Raoutella planticola*, and incubated at 22 °C until visible plaques formed. Liquid plates were prepared with the cells collected from the growth zone of the SM agar plate and incubated in Ax medium (ForMedium), with 100 µg/ml penicillin and 100 µg/ml streptomycin at 22 °C.

The *ino1*$^{-}$ mutant cells were grown in the presence of 10 µg/ml blasticidin S with 500 µM inositol. Cell lines transformed with extrachromosomal plasmids (389-2, pTX, pDdGal) were cultured in the presence of 50 µg/ml hygromycin (Invitrogen) or at least 10 µg/ml geneticin (G418) (Invitrogen). Cells were maintained in tissue culture plates or shaking (120 rpm) at 22 °C and harvested in mid-log phase ($4x10^6$ cells/ml).

2.2.2.2 Growth

Dictyostelium cells that were grown in tissue culture dishes were washed twice with buffer KK2 (16.2 mM KH_2PO_4, 4 mM K_2HPO_4) and counted using haemocytometer. $1x10^5$ cells per sample per repeat were incubated in 10 ml aliquots in a 150 ml conical flask. Cells were shaken at 22 °C for 5 to 7 days and cell density was calculated daily using haemocytometer counts at the same time of the day.

2.2.2.3 Viability

Fluorescein Diacetate (FDA) dye (Sigma) was used to stain live cells. FDA is a non-fluorescent compound that is cleaved by metabolically active cells into a green fluorophore. Adherent cells were washed once in KK2 (16.2 mM KH_2PO_4, 4 mM K_2HPO_4). FDA concentrated stock (10 mg/ml in acetone) was added to cells in KK2 to reach a final concentration of 0.05 mg/ml. Cells were incubated in the dark for 10 minutes at room temperature. Following the incubation, the cells were washed twice in KK2 and viewed under the Olympus IX71 microscope (Zeiss filter set 09: BP 450-490, FT 510, LP 515) to observe green fluorescence.

Propidium iodide (PI) dye (Sigma) was used to stain the nuclei of dead cells. PI dye reaches the nucleus by passing through the damaged plasma membrane of dead cells, and intercalates in the DNA double helix of the cell. Adherent cells were washed once in KK2 (16.2 mM KH_2PO_4, 4 mM K_2HPO_4). PI was added to cells in KK2 to a final concentration of 4 µM. Cells were incubated in the dark for 10 minutes at room temperature. Following the incubation, the cells were washed twice in KK2 and viewed under the

Olympus IX71 microscope (Zeiss filter set 09: BP 450-490, FT 510, LP 515) to observe red fluorescence.

2.2.2.4 Development

Dictyostelium developmental phenotypes were analysed using filter assays (Boeckeler et al., 2006; Williams et al., 2002). Cells growing in shaking suspension (120 rpm) in Ax medium (ForMedium) were counted using a haemocytometer, and $1x10^7$ cells were harvested. Cells were washed twice in KK2 (16.2 mM KH_2PO_4, 4 mM K_2HPO_4) and evenly distributed on a 47 mm nitrocellulose filter soaked in KK2 (Millipore, USA), which was then placed on an absorbent pad saturated with KK2 or KK2 mixed with a drug. The filter was incubated for 24 hours at 22 °C in a moist environment. Development images were captured with the use of a dissection microscope (Leica) and a QImaging RetigaExi Fast1394 digital camera.

2.2.2.5 Chemotaxis

Dictyostelium chemotaxis was analysed using a Dunn chamber (Hawksley, Sussex, UK) assay (Zicha et al., 1991). *Dictyostelium* cells growing in shaking suspension (120 rpm) in Ax media (ForMedium) were counted using a haemocytometer and $1x10^7$ cells were harvested. Cells were washed twice in KK2 (16.2 mM KH_2PO_4, 4 mM K_2HPO_4), centrifuged, re-suspended in 6 ml KK2 and placed in a 100 ml conical flask at 22 ºC to be pulsed for 5 hours with cAMP (90 ml KK2 + 3 µl 200 mM cAMP). Following that, cells were centrifuged, washed twice in KK2, re-suspended in 1 ml KK2 ($1x10^7$ cells/ml), and placed on ice. 25 µl of cells were transferred to a cover slip and allowed to adhere for 5-10 minutes. 22 µl of KK2 was placed to the inner well and 36 µl to the outer well of a cleaned and dried Dunn chamber, ensuring that KK2 surrounded the whole cell. The coverslip with cells was inverted and placed on top of the Dunn chamber, ensuring that no bubbles were present in the inner well of the Dunn chamber. KK2 buffer was drained from the outer well using 3MM absorbent paper cut into small triangles. The Dunn chamber was sealed in place with Vaseline. 70 µl of 5 µM cAMP (1 µl 200 mM stock in a serial 1:40 and 1:1000 dilution) was added to the outer

well of the Dunn chamber, and incubated in a moist chamber for 30 minutes. Following the incubation, images of chemotaxing cells were recorded every 15 seconds over a 12-minute period, using Olympus IX71 microscope (objective 40x) with a QImaging RetigaExi Fast1394 digital camera.

2.2.2.6 Cell adhesion

Dictyostelium cells were grown in culture dish plates in Ax media (ForMedium). Cells were washed twice in KK2 (16.2 mM KH_2PO_4, 4 mM K_2HPO_4), counted using a haemocytometer and $1x10^5$ cells/ml were plated into each well of 6-well plates containing 2 ml of growth medium. After 24 hours the medium was gently removed with an aspirator, cells were re-suspended using a pipette, and an aliquot of cells was immediately taken out and placed on ice. Cells were counted using a haemocytometer. The counting procedure was repeated every 24 hours for 7 days.

2.2.2.7 Cytokinesis

A single round slide (stored in 80% ethanol) was placed into each well of a 12-well tissue culture plate. Each well was washed twice with 1 ml sterile distilled water. Approximately $5x10^6$ cells re-suspended in 0.5 ml of KK2 (16.2 mM KH_2PO_4, 4 mM K_2HPO_4) were placed into each well. Cells were left to adhere for 30 minutes, prior to being washed in KK2 with gentle aspiration to remove the liquid. Cells were fixed with 1 ml of ice cold methanol for 5 minutes in the -20 °C freezer. Each well was washed once with KK2 and DAPI (Sigma) was added (1:250 dilution of 2 µg/ml DAPI in KK2), and incubated for 5 minutes at room temperature in the dark. Following the incubation, DAPI was replaced with ddH_2O and 12.5 µl of mounting medium (Fluoromount Aqueous Mounting Medium, Sigma) was placed onto a microscope slide. The coverslip with cells was placed onto the drop of mounting medium, and dried in the dark overnight at room temperature. DAPI fluorescence was visualised using an Olympus IX71 microscope (oil objective 60x) with a QImaging RetigaExi Fast1394 digital camera. The number of cells having 1, 2, 3, or more nuclei was counted using ImageJ v1.46a software, and the percentage relative to the total number of cells for a given

sample was counted. Three independent experiments were conducted. Over 350 cells were counted per condition.

2.2.2.8 Autophagy

Autophagy was measured in *ino1*$^{-}$ cells transformed with the *atg8-GFP* construct (Otto et al., 2003) (dictybase.org). Cells were grown in Ax medium (ForMedium) with shaking (120 rpm) for 72 hours (- inositol condition had inositol removed for 24 hours prior to the experiment), with 16 hour incubation in LoFlo medium (ForMedium) to reduce the background autofluorescence. The cells were viewed using an Olympus IX71 microscope (60x objective with oil) with a QImaging RetigaExi Fast1394 digital camera to record green fluorescence. The number of autophagosomes was counted and the cell surface area was measured using ImageJ v1.46a software. Three independent experiments were conducted; between 117 and 180 cells were analysed per condition.

2.2.3 Molecular biology methods

2.2.3.1 Polymerase chain reaction (PCR)

DNA was amplified by polymerase chain reaction (PCR) with the following conditions: 2 µl DNA, 2 µl 2 mM dNTPs, 2 µl NH_4 BioTaq reaction buffer, 1 µl $MgCl_2$, 0.5 µl BioTaq DNA polymerase (5 U/µl), 2 µl forward and 2 µl reverse primer (10 pmol). PCR amplification with other DNA polymerases (Q5 and Phusion) was set up according manufacturer's instructions.

The PCR amplification was set up according to the following cycling conditions: initial denaturation at 95 °C for 10 minutes, 30 cycles of denaturation at 95 °C for 30 seconds, annealing at 56 °C (temperature depending on primer melting points) for 45 seconds, extension at 72 °C with the time dependent on the length of the product being amplified (one minute per 1,000 base pairs), followed by the final extension at 72°C for 10 minutes. DNA samples were then stored at 4°C for short-term or -20°C for long-term storage.

2.2.3.2 Agarose gel electrophoresis

Gel electrophoresis was used to separate and visualise DNA using 1% agarose gels containing 30 µg/ml ethidium bromide (Sigma) and TBE buffer (89 mM Tris base / 89 mM Borate/ 2 mM EDTA pH 8.3 ±0.1). 5 µl of DNA were mixed with 1x DNA loading dye. The gel was run for 40 minutes to 1 hour at 100-110 V (depending on the size of the gel) and visualised using the GeneFlash gel documentation system (Syngene Bio Imaging).

2.2.3.3 Bacterial transformation

Chemically-competent cells (*JM107 E.coli*) were used for the transformations during DNA cloning procedures. Agar plates were prepared from sterile LB agar medium (according to Sigma's protocol) with added ampicillin (Sigma) at a concentration 100 µg/µl. 30 ml of the agar media was poured into a 90 mm Petri dish and allowed to set. Bacteria were thawed on ice. 10 µl of DNA ligation reaction was added to 50 µl of competent cells. The cells were incubated with DNA on ice for 30 minutes, and then heat-shocked for 30-second at 42 °C (water bath or heat block), followed by immediate transfer to ice, where the cells remained for 2 minutes. 250 µl of room temperature LB medium was added to the cells and incubated at 37 °C for 1 hour. After incubation, the cells were plated onto the agar plates and incubated at 37 °C overnight.

2.2.3.4 Plasmid preparation

Plasmids that were used for sequencing or cloning procedures were purified from bacterial transformants using the Qiagen QIAfilter or Sigma GenElute plasmid kits, according to manufacturer's instructions.

Plasmid minipreps that were not performed with commercial kits were prepared as follows: 2 ml of an overnight *E.coli* culture was harvested for 3 minutes at 4,000 rpm. The pellet was re-suspended in 200 µl of buffer P1 (50 mM Tris-Cl pH 8.0, 10 mM EDTA, 50 µg/ml RNase A), and lysed with 200 µl of buffer P2 (200 mM NaOH, 1% w/v SDS). Following 5-minute incubation at room temperature, 200 µl of buffer P3 (3M potassium acetate pH 5.5) was added, mixed with the sample by inversion, and incubated on ice for 5

minutes. After the incubation, samples were centrifuged at 17,000 *g* for 10 minutes to pellet the cell debris. The supernatant was transferred to a new 1.5 ml microcentrifuge tube, and the plasmid DNA was precipitated with 0.7 volumes of isopropanol, followed by centrifugation at 17,000 *g* for 10 minutes. The pellet was washed with 600 µl of 70% ethanol, and centrifuged at 17,000 *g* for 5 minutes. The pellet was air dried to remove residual ethanol, and DNA was re-suspended in ddH_2O.

2.2.3.5 Construction of the knock-out vector (Figure 2.1 A)

PCR was used to amplify two gene fragments inside the open reading frame of the *ino1* gene using Ax2 genomic DNA as a template. PCR products were purified using the GenElute PCR Clean-Up Kit (Sigma) or QIAquick spin PCR purification kit (Qiagen) protocol. The pLPBLP vector used to construct the *ino1* knock-out cassette contained the blasticidin-S deaminase gene conferring resistance to the blasticidin antibiotic (Faix et al., 2004). The pLPBLP vector and the gene fragments were double-digested with appropriate restriction enzymes before each fragment was separately cloned into the vector. Double digests were performed with BamHI/PstI for the 5' fragment and NcoI/KpnI for the 3' fragment for 2 hours at 37 °C. Prior to cloning each fragment in, the double-digested pLPBLP vector was treated with 1 µl of Calf Intestinal Alkaline Phosphatase (CIAP) (1 U/µl) and incubated for 1 hour at 37 °C. CIAP was inactivated at 65 °C for 20 minutes. Digested PCR products and pLPBLP vector were purified using GenElute PCR Clean-Up Kit (Sigma) or QIAquick spin PCR purification kit (Qiagen Ltd., UK), and ligated together using 1 µl T4 DNA ligase (1 U/µl) at different ratios of insert:vector (10:1 and 20:1). The ligation reactions were incubated at room temperature for 1 hour, and then the ligase was inactivated at 65 °C for 20 minutes. The constructs were transformed into chemically-competent *JM107 E.coli* cells and the DNA from the resultant colonies tested for the presence of an insert by a double-digest with restriction enzymes that were used in the cloning steps. The second fragment was inserted using the same methodology. Plasmid DNA with confirmed insertion of both gene fragments was processed with QIAfilter Plasmid Maxi prep kit (Qiagen) according to the

manufacturer's protocol. Correct sequence of the knock-out cassette was verified by gene sequencing.

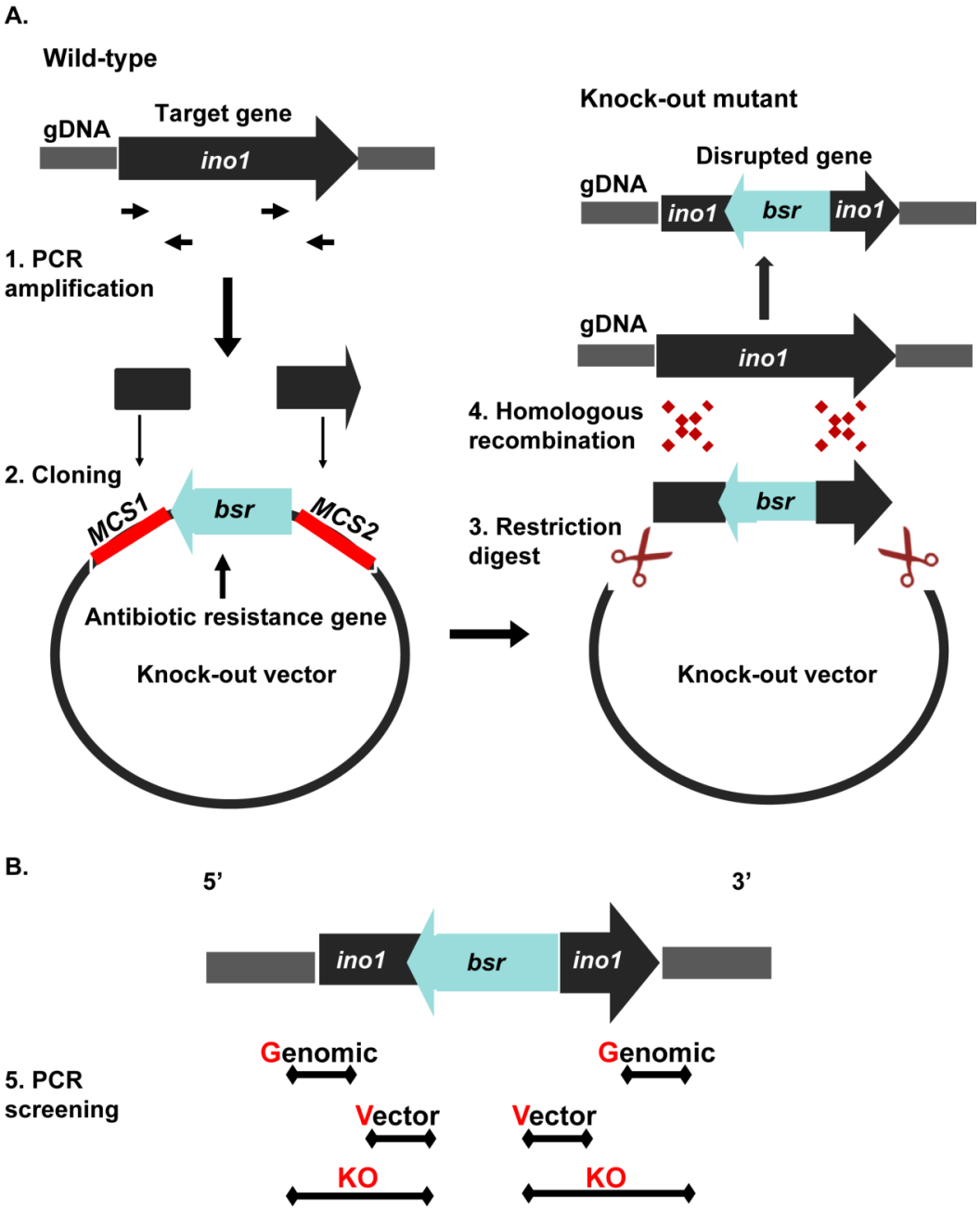

Figure 2.1 Schematic of the *ino1* gene knock-out and screening procedure. (A) 5' and 3' *ino1* gene fragments were amplified from gDNA of wild-type cells (Ax2) using PCR and cloned into the knock-out vector (pLPBLP) at multiple cloning sites (MCS) 1 and 2 to create a knock-out cassette. The blasticidin resistance gene was oriented in the opposite direction to the cloned *ino1* fragments (the orientation of the genes is indicated by the arrows). The knock-out cassette was excised from the knock-out vector and transformed into *Dictyostelium* Ax2 cells. Homologous recombination allowed for the creation of an *ino1* knock-out mutant with a disrupted *ino1* gene. (B) Correct transformants were identified by a PCR screen. The primers used for the screening procedure are shown, where (G)enomic, (V)ector and (K)nock-(O)ut primer combinations were designed for the 5' and 3' sites of the *ino1* gene to confirm the correct integration of the knock-out cassette into the *Dictyostelium* genome.

2.2.3.6 Transformation of *Dictyostelium* by electroporation

The knock-out fragment containing blasticidin resistance cassette was excised from the pLPBLP plasmid using 5 µl of KpnI (10 U/µl) and 5 µl of BamHI (10 U/µl) restriction enzymes. The digested construct (20 µg) was precipitated with isopropanol, and resuspended in sterile water at 1 µg/µl. $1x10^7$ *Dictyostelium* Ax2 cells were chilled on ice for 10 minutes followed by one wash with 10 ml KK2 buffer and two washes with 10 ml electroporation (EP) buffer (10 mM sodium phosphate buffer pH 6.1, 50 mM sucrose). The pellet was re-suspended in 700 µl EP buffer, transferred to a 0.4 cm cuvette together with 20 µl of previously digested DNA (1 µg/µl), and incubated on ice for 10 minutes. The cells were electroporated with a Bio-Rad GenePulser Xcell electroporator using 1 pulse, 850V, 25uF, resistance ∞ and incubated on ice for 10 minutes. After this incubation, 8µl of 100mM $CaCl_2$ and 8µl of 100mM $MgCl_2$ were added to the cuvette, and further incubated at room temperature for 15 minutes, prior to the cells being transferred into 10 ml Ax medium (ForMedium) containing penicillin/streptomycin (100x). 100 µl of the culture was transferred into each well of a 96-well plate. After 24 hours, 100 µl Ax medium (ForMedium) containing blasticidin was added to each well to a final concentration of 10 µg/ml.

2.2.3.7 Overexpression of fluorescently-tagged proteins

Overexpression plasmids containing N-terminal GFP and N-terminal FLAG (pTX) and pDXA-3H-Hyg were obtained from dictybase.org; the plasmid containing C-terminal RFP (389-2) was kindly provided by Dr Annette Müller-Taubenberger. The plasmids were transformed into *JM107 E.coli* competent cells (Sigma) and prepared with QIAfilter Plasmid Maxi prep kit (Qiagen) according to manufacturer's protocol. Ax2 genomic or complementary DNA was used as a template to PCR amplify (with Q5 High-fidelity DNA polymerase, NEB Biolabs) the *ino1*, *gpmA, secG, pefB* and *Q54IX5* genes. PCR products were purified using the GenElute PCR Clean-Up Kit (Sigma) or QIAquick spin PCR purification kit (Qiagen), and digested with the following the restriction enzymes: *ino1:* EcoRI and BamHI to clone into 389-2 plasmid, BamHI and XbaI to clone into pTXGFP, SacI and XbaI to clone into pDXA-3H-Hyg (removing 3H sequence); *gpmA:* SacI and XhoI to

clone into pTXGFP and pTXFLAG; *secG:* SacI and XbaI to clone into pTXGFP and pTXFLAG; *pefB:* BamHI and XbaI to clone into pTXGFP and pTXFLAG; *Q54IX5 :* BamHI and XbaI to clone into pTXGFP and pTXFLAG. Digested products were purified with GenElute PCR Clean-Up Kit (Sigma) or QIAquick spin PCR purification kit (Qiagen) and ligated to a selected plasmid using T4 DNA ligase (Fermentas) according to the supplier's protocol. Correct sequences were verified by gene sequencing. 10-20 µg of the plasmid DNA was transformed by electroporation in *Dictyostelium* Ax2 or *ino1*$^-$ mutant cells. The transformants were selected with 10 µg/ml geneticin or 50 µg/ml hygromycin for approximately two weeks. Correct transformants were analysed using an Olympus IX81 microscope with FV1000 confocal laser (HeNe laser, 543 nm emission, Olympus UPLSAPO 60x oil immersion objective).

2.2.3.8 DNA extraction from transformants

Recombinants growing in 96 well plates in medium containing blasticidin were screened for homologous integration by genomic DNA extraction and PCR amplification. Genomic DNA was extracted as follows: 200 µl of the cell suspension was collected from individual wells and transferred into a 1.2 ml PCR tube, centrifuged for 3 minutes at 1,500 g, and the cell pellet was re-suspended in 48 µl of the lysis buffer (50 mM KCl, 10 mM Tris pH 8.3, 2.5 M $MgCl_2$, 0.45% Nonidet P 40, 0.45% Tween 20) and 2 µl Proteinase K (822 U/ml) (Fermentas). The samples were incubated for 5 minutes at room temperature followed by 1 minute incubation at 95 °C. 5 µl of the extracted DNA was used in the PCR screening protocol.

2.2.3.9 Screening for *ino1*$^-$ homologous recombinants

Screening for *ino1*$^-$ homologous recombinants was performed using PCR with primers (Table S1) designed to detect whether the *ino1* knock-out cassette was inserted correctly into the *ino1* locus in the *Dictyostelium* genome. Three primer sets were used to screen for the knock-out cassette: knock-out construct, vector control and genomic control. The primer set for the knock-out construct included one primer outside the knock-out cassette, in the genomic DNA, and one primer in the blasticidin resistance cassette.

The vector control primer set included one primer within the knock-out DNA fragment and the blasticidin resistance cassette. The genomic control primer set included one primer outside the knock-out cassette, in the genomic DNA, and one primer in the blasticidin resistance cassette (Figure 2.1 B). The correct transformants were serially diluted using 96-well plates to select for an isogenic cell line.

2.2.3.10 RNA extraction and RT-PCR analysis

$1x10^7$ cells were harvested and washed twice with KK2 (16.2 mM KH_2PO_4, 4 mM K_2HPO_4) buffer. RNA was extracted using High Pure RNA Isolation Kit (Roche Applied Science), DNase treated with DNA-free™ Kit (Ambion), and cDNA was synthesised with First Strand cDNA Synthesis Kit (Fermentas) using 1 µg of RNA and Oligo(dT)18 primers according to manufacturer's instructions. 2 µl of the cDNA was used in the subsequent PCR amplification, as described in the polymerase chain reaction section above (2.2.3.1).

2.2.4 Proteomics analysis

2.2.4.1 SDS-PAGE (sodium dodecyl sulfate polyacrylamide gel electrophoresis)

Loading buffer (2X) was made according to the following recipe: 1.6 ml 2 M Tris pH 6.8, 6 ml 80% glycerol, 10 ml 10% SDS, 2.5 ml β-mercaptoethanol, ddH_2O, bromophenol blue. Running buffer (10X) was made according to the following recipe: 75 g Tris base, 360 g glycine, 250 ml of 10% SDS solution, made up to 2.5 l with ddH_2O; 2M Tris pH 8.8; 2 M Tris pH 6.8.

TruPAGE Precast Gels (Sigma) or NuPage SDS-polyacrylamide gel (Invitrogen) were used for SDS-PAGE gel electrophoresis with the supplier's recommended buffers. Gels used that were not from commercially available sources were prepared as follows: resolving gel (7%): 2.25 ml acrylamide, 1.9 ml Tris pH 8.8, 5.65 ml ddH_2O, 200 µl 10% SDS, 100 µl 10% ammonium persulphate (APS) in ddH_2O, 10 µl tetramethylethylenediamine (TEMED);

stacking gel: 2.55 ml acrylamide, 0.94 ml Tris pH 6.8, 11.25 ml ddH_2O, 150 µl 10% SDS, 150 µl 10% APS in ddH_2O; 15 µl TEMED.

Protein samples to analyse by gel electrophoresis were prepared by boiling cell pellets at 95°C (for standard protein detection 1x10^7 cells were used) for 10 minutes in 2X loading buffer. 5 µl of Page Ruler Plus Prestained Protein Ladder (Fermentas) per well was used as a molecular marker. The gel was run at 200 volts in running buffer for 1 -1.5 hours, or as specified by a manufacturer.

2.2.4.2 Western blot analysis

Proteins separated by SDS-PAGE were transferred to PVDF membrane (Immobilon-FL Transfer Membrane). PVDF membrane was activated by saturation in methanol. Blotting paper (3 MM), sponges and the activated membrane were soaked in transfer buffer (1 X ETB made fresh with 100 ml 10 X ETB (75 g Tris base; 360 g glycine; 25 ml 10% SDS), 100 ml methanol and 800 ml ddH_2O). The transfer block was prepared in a tank kept on ice, filled with the transfer buffer, and run at 400 mA for 1 hour.

To visualise the proteins, the membranes were immunostained with appropriate antibodies. The membrane soaked in 5% milk in PBST (1X PBS, 1% Tween 20) buffer was gently rocked for 1 hour at room temperature. Following the incubation, the primary antibody, mouse or rat anti-RFP monoclonal antibody, rat anti-GFP monoclonal antibody (ChromoTek) or anti-FLAG M2 monoclonal antibody (Sigma), was added at a 1:1000 dilution in the milk buffer (5% milk in 1X PBS with 1% Tween 20) and incubated overnight at 4 °C with gentle rocking. The membrane was rinsed in 1X PBS (10X stock: 14.4 g Na_2HPO_4, 80 g NaCl, 2 g KCl, 2.4 g KH_2PO_4, made up to 1l with ddH_2O, pH 7.4) and the excess primary antibody was washed off with 3 x 10 minute washes in PBST (PBS, 1% Tween 20). The secondary antibody, IRDye 800 goat anti-rat or goat anti-mouse (Li-cor Biosciences), was added to the membrane at a 1:2000 dilution in 5% milk in PBST (1X PBS, 1% Tween 20) buffer, and incubated at room temperature for 1 hour with gentle rocking. The membrane was rinsed in PBS followed by with 3 x

10 minute washes in PBST. The immunostaining was visualised with the Odyssey Infrared Imaging System (Li-cor Biosciences).

2.2.4.3 Immunoprecipitation

Aggregation-competent cells were washed with KK2 (16.2 mM KH_2PO_4, 4 mM K_2HPO_4), re-suspended at a density of 3-4 x10^8 cells/ml in KK2, and shaken for 20 minutes at 250 rpm with 2.5 mM caffeine. The cells were then centrifuged and the pellet was lysed (0.5 % NP40, 40 mM Tris-HCl, 20mM NaCl, 5 mM EGTA, 5 mM EDTA, 10 mM DTT, 1 mM PMSF, 2X protease cocktail inhibitor and 2X phosphatase inhibitor (Roche)). Cell lysates were incubated with RFP-Trap or GFP-Trap agarose beads (ChromoTek) for 1 hour at 4°C with gentle agitation. The beads were collected and washed twice with the IP wash buffer (10 mM Tris-HCl, 150 mM NaCl, 0.5 mM EDTA, 1 mM PMSF, 2X protease cocktail inhibitor and 2X phosphatase inhibitor (Roche)). Immunocomplexes were dissociated from the beads by incubating samples at 95 °C for 10 minutes, followed by centrifugation to collect the beads. The immunoprecipitated proteins were separated by SDS-PAGE and analysed by Western blot analysis, or stained with Commassie blue (Pierce) stain and analysed by mass spectrometry (MS). MS analysis was conducted by S. Lilla and Prof R. Insall (Beatson Institute, Glasgow).

2.2.5 Metabolomics analysis

Dictyostelium discoideum Ax2 and *ino1*$^-$ strains were grown at 22 °C in shaking (120 rpm). Additional samples of Ax2 cells that were used as a control were grown in the presence of 500 µM *myo*-inositol. *Ino1*$^-$ cells were cultured in medium containing 500 µM *myo*-inositol and 10 µg/ml blasticidin. Inositol was removed from the growth medium for 12 and 24 hours, and the cells growing in inositol were washed twice in KK2 (16.2 mM KH_2PO_4, 4 mM K_2HPO_4), and re-suspended in medium without inositol. After 24 hours of inositol starvation, 500 µM *myo*-inositol was added to the growth medium. Samples for the nuclear magnetic resonance (NMR) spectroscopy analysis were prepared with 2 x 10^7 cells. The cells were washed twice in KK2 and the pellets were freeze-dried.

NMR spectrometry (conducted by Dr S P Claus and C. Le Roy, University of Reading) was performed as follows: freeze-dried cell pellets were re-suspended in 1 ml of Water/Methanol (1:2) and vortexed for polar metabolite extraction. Samples were centrifuged at 2,400 *g* for 5 minutes and supernatants were dried in a vacuum concentrator for 4.5 hours at 45°C. Dried samples were re-suspended in 80 µl of phosphate buffer (in 90 % D2O and 0.05 % sodium 3-(tri-methylsilyl) propionate-2,2,3,3-d4 (TSP) as a 1H NMR reference). 50 µl of the solution was transferred into 1.7 mm capillary NMR tubes. Spectra were acquired at 300 ºK on a Bruker Avance DRX 700 MHz NMR Spectrometer (Bruker Biopsin, Rheinstetten, Germany) operating at 700.19 MHz and equipped with a CryoProbe from the same manufacturer. All spectra were acquired using a 1-dimensional noesy pulse sequence [recycle delay – 90º - t1 – 90º - tm – 90º - acquire free induction decay (FID)] with water suppression applied during RD of 2 s, a mixing time (tm) of 100 ms and a 90º pulse set at 7.70 µs. For each spectrum, 512 scans were accumulated over a spectral width of 9803.9 Hz, and all FIDs were multiplied by a broadening line function of 0.3 Hz prior to Fourier transformation. All spectra were manually phased, baseline-corrected and calibrated to the TSP standard at δ 0.000 using the software MestReNova (version 10.0.1, Mestrelab Research S.L., Spain).

2.2.6 Lipid analysis

Dictyostelium discoideum Ax2 and *ino1*$^-$ strains were grown at 22 °C in shaking culture (120 rpm). Additional samples of Ax2 cells that were used as a control were grown in the presence of 500 µM *myo*-inositol. *Ino1*$^-$ cells were cultured in medium containing 500 µM *myo*-inositol and 10 µg/ml blasticidin. Inositol was removed from the growth medium for 12 and 24 hours, and the cells growing in inositol were washed twice in KK2 (16.2 mM KH_2PO_4, 4 mM K_2HPO_4), and re-suspended in medium without inositol. After 24 hours of inositol starvation, 500 µM *myo*-inositol was added to the growth medium. Samples for the mass spectroscopy analysis were prepared with 1.7 x 10^6 cells. The cells were washed twice in KK2 and the pellets were freeze-dried.

Glycerophospholipid levels were analysed by mass spectroscopy, as previously described (Clark et al., 2014) (conducted by Dr J. Clark and Dr P. Hawkins, Babraham Institute, Cambridge).

2.2.7 Fluorescence microscopy

To analyse protein localisation, cells producing fluorescently-tagged proteins were cultured in Ax medium (or for *ino1*$^-$ cells in Ax2 medium containing 500 µM inositol and 10 µg/ml blasticidin), washed twice in KK2 (16.2 mM KH_2PO_4, 4 mM K_2HPO_4), and allowed to adhere to a glass coverslip before being visualised with an Olympus IX71 microscope (U-RFL-T laser, 482 nm emission, Olympus UPlanFL 60x oil immersion objective with NA 1.25) with an QImaging RetigaExi Fast1394 digital camera and ImagePro6.3 software.

2.3 Software

Phylogenetic analysis was performed using Mega, version 5 (Tamura et al., 2011). Statistical analysis was performed using Prism 5, version 5.02 (GraphPad Software, Inc.). Microscopy images were captured and chemotaxis data was analysed using ImagePro Plus, version 6.3 (Media Cybernetics, Inc.). Number of nuclei, autophagosomes and cell size was analysed using ImageJ v1.46a (developed by Wayne Rasband, National Institutes of Health). Mass spectrometry data was analysed using Scaffold3 (Proteome Software, Inc.).

2.4 World-wide web references

Dictyostelium gene and protein information: http://dictybase.org/
http://www.uniprot.org/

BLAST: http://www.ncbi.nlm.nih.gov/BLAST/
http://dictybase.org/tools/blast

Protein domain analysis:

Phyre^2: http://www.sbg.bio.ic.ac.uk/phyre2/html/page.cgi?id=index

CDD: http://www.ncbi.nlm.nih.gov/cdd

Chapter 3
Bioinformatic analysis of Ino1

Chapter III

Bioinformatic analysis of Ino1

3.1 Introduction

Inositol-3-phosphate synthase (Ino1) UniProt ID Q54N49 is a key enzyme in the inositol and phosphoinositide synthesis pathway. Ino1 catalyses the first and rate-limiting step in the biosynthesis of all inositol-containing compounds, converting glucose 6-phosphate to inositol 3-phosphate (Seelan et al., 2004) (Figure 3.1). The proposed biochemical process involves an oxidation, enolisation, intramolecular aldol cyclisation, and reduction steps (Jin et al., 2004). Nicotinamide adenine dinucleotide (NAD^+) is used as a cofactor by Ino1.

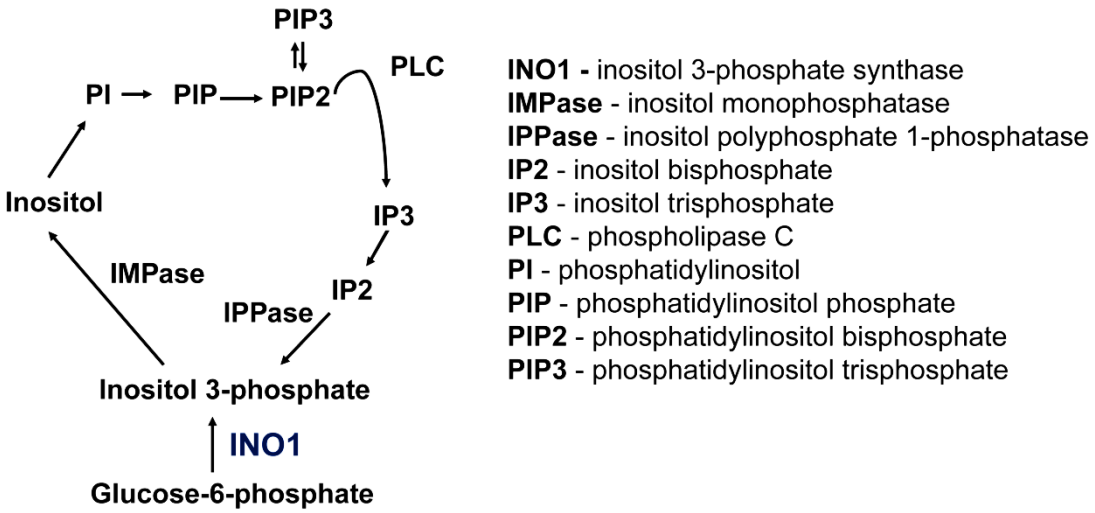

Figure 3.1 Inositol signalling. Ino1 enzyme converts glucose 6-phosphate to inositol 3-phosphate, which is a rate-limiting step in inositol production.

Ino1 has been cloned from and characterised in a variety of evolutionarily distinct organisms including yeast, plants, flies, humans, *Archaebacteria*, and bacteria (Majumder et al., 2003). The structure and catalytic activity of Ino1 was studied in yeast, humans, *C.elegans* and various bacterial species (Abreu and Aragão, 2007; Bachhawat and Mande, 1999; Dean-Johnson and Henry, 1989; Lohia et al., 1999; Majumder et al., 1997;

Norman et al., 2002; Park et al., 2000; RayChaudhuri et al., 1997; Seelan et al., 2009a; Stein and Geiger, 2002). These studies showed that Ino1 forms homotetramers or trimers and its monomer is composed of a NAD-binding domain, a catalytic region, and N- and C-terminal domains (Stein and Geiger, 2002). Amino acids located in the vicinity of the active site in the catalytic region are disordered in the unbound form of the Ino1 enzyme. The folding of this domain is nucleated upon substrate binding, leading to an encapsulation of the bound substrate (Stein and Geiger, 2002).

The Ino1 protein and the gene encoding it are ancient in origin (Majumder et al., 2003). Comparing Ino1 proteins from distinct biological species revealed that prokaryotic and eukaryotic proteins group separately, and that Ino1 proteins from eukaryotes shared a high degree of similarity, with conserved stretches of amino acids (Majumder et al., 2003). Prokaryotic Ino1 proteins diverged from their eukaryotic counterparts early in evolution and became quite divergent, whereas eukaryotic Ino1 proteins remained quite stable during their evolution (Majumder et al., 2003). This study further revealed that plant Ino1 proteins were of monophyletic origin, and that the Ino1 proteins of fungi contained an extra stretch of amino acids at the N-terminus that was specific to this group. Despite the difference between prokaryotic and eukaryotic Ino1 proteins, the Ino1 catalytic core has been remarkably evolutionarily conserved (Majumder et al., 2003).

In this chapter, bioinformatic analysis of the inositol-3-phosphate synthase (Ino1) protein from *Dictyostelium discoideum* is described. To gain a more detailed understanding of the structural characteristics of Ino1 and its evolutionary conservation, BLAST analysis, sequence alignment to infer protein homology, and phylogenetic and domain structure analysis were performed and are discussed here.

3.2 Domain and structure analysis of *Dictyostelium* Ino1

To better understand the function of the *Dictyostelium* Ino1 protein, the identity and evolutionary conservation of its domains were researched. The Phyre2 web portal (Kelley et al., 2015), and the Conserved Domain Database

(CDD) (accessible from NCBI webpage) (Marchler-Bauer et al., 2014, 2002), were used to search for structural information about *Dictyostelium* Ino1 and to identify the conserved functional domains (CDs) within the protein. The CDD is a compilation of multiple sequence alignments representing protein domains that are conserved in molecular evolution (Marchler-Bauer et al., 2002). The CDD tool operates by comparing protein sequences to models of protein families (as opposed to other single sequences) accessed from Pfam or SMART databases to investigate patterns of conservation and divergence in molecular evolution (Marchler-Bauer et al., 2002). A CDD search with the term “Ino1” showed that the protein belonged to a conserved NAD_binding_5 domain superfamily (accession: cl00554; PSSM ID: 260495). Also, using the Conserved Domain Architecture Retrieval Tool (CDART) (Geer et al., 2002) with the query term: Q54N49 (*Dictyostelium* Ino1 UniProt ID), showed that *Dictyostelium* Ino1 belongs to a conserved NAD_binding_5 domain superfamily that is present in 4,553 proteins in cellular organisms. The Phyre2 web portal was used to perform structural analysis of Ino1. This search confirmed the presence of four domains in the Ino1 monomer: an NAD-binding domain, characterised by a Rossman fold typical of an oxidoreductase (Kleiger & Eisenberg, 2002), C-terminal and N-terminal domains, and an inositol synthase (catalytic) site (Figure 3.2).

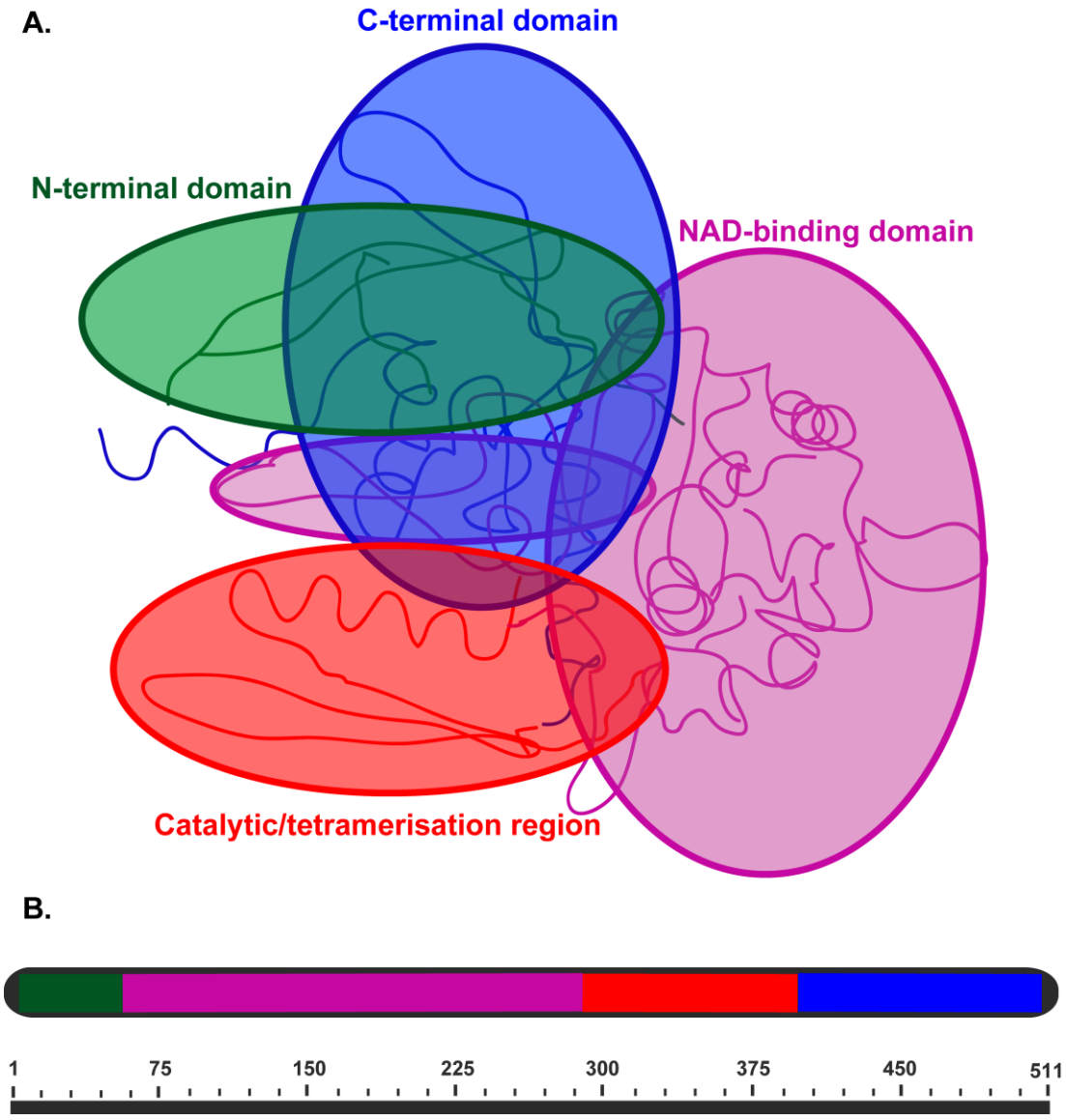

Figure 3.2 Domain positioning in the *Dictyostelium* Ino1 monomer. The structure of *Dictyostelium* Ino1 protein was modelled using Protein Homology/analogy Recognition Engine V2.0 (Phyre[2]), the NCBI protein database, and literature searches. *Dictyostelium* Ino1 (DDB_G0285505) contains 511 amino acids and the presence of the tetramerisation domain suggests that it forms multimers. (A) The structure of the Ino1 monomer with individual regions coloured as follows: green, the N-terminal region; purple, the NAD-binding domain; red, the catalytic or tetramerisation region; blue, the C-terminal region. The N- and C-termini, along with residues from the NAD-binding domain, form a close association. Upon binding of monomers to each other, the catalytic regions would be sequestered in the core of the protein multimer. (B) Domain positioning in *Dictyostelium* Ino1 protein along with approximate amino acid residue numbers.

3.3 BLAST analysis

BLAST analysis of the *Dictyostelium* Ino1 protein (DDB_G0285505) against all sequenced genomes was performed using the NCBI PSI-BLAST

engine. This analysis revealed the presence of potential homologues across various biological kingdoms. The top Ino1 homologues from a range of species are presented (Table 3.1), using a selection of proteins with >50% sequence identity, similar protein length, and an e-value $<10^{-40}$, as previously suggested (Eichinger et al., 2005). BLAST analysis revealed that *Dictyostelium* Ino1 was homologous to Ino1 proteins from a large variety of species, including plants and brown algae (the highest identity was to common tobacco Ino1), vertebrates (the highest identity was to frog and salmon Ino1), insects, fungi, and bacteria (Table 3.1). This remarkable degree of evolutionary conservation illustrates the importance of inositol signalling in a range of organisms including humans.

Accession	Organism	Protein Length	Identity (%)	E-Value
Q54N49	*Dictyostelium discoideum* (Social amoeba)	511	100	0
Q9LW96	*Nicotiana tabacum* (Common tobacco)	510	67	0
D8LQB3	*Ectocarpus siliculosus* (Brown alga)	533	66	0
C4PW34	*Arabidopsis thaliana* (Mouse-ear cress)	511	66	0
Q41107	*Phaseolus vulgaris* (Kidney bean)	511	65	0
P42802	*Citrus paradisi* (Grapefruit)	507	64	0
Q7ZXY0	*Xenopus laevis* (African clawed frog)	563	63	0
B5X3P3	*Salmo salar* (Atlantic salmon)	551	62	0
D6WV33	*Tribolium castaneum* (Red flour beetle)	526	62	0
Q9JHU9	*Mus musculus* (Mouse)	557	59	1.00E-177
O97477	*Drosophila melanogaster* (Fruit fly)	565	59	1.00E-175
Q6AYK3	*Rattus norvegicus* (Rat)	557	59	1.00E-175
Q9NPH2	*Homo sapiens* (Human) (isoform 1)	558	58	1.00E-176
Q2NL29	*Bos taurus* (Bovine)	557	58	1.00E-174
P90626	*Entamoeba histolytica* (Anaerobic parasitic protozoan)	508	56	1.00E-168
P11986	*Saccharomyces cerevisiae* (Baker's yeast)	533	53	1.00E-153
P42800	*Candida albicans* (Ascomycete fungus)	520	52	1.00E-152

Table 3.1 Homology search results (BLAST analysis) identifying proteins related to *Dictyostelium* Ino1 (EC 5.5.1.4) in other species. The UniProt accession numbers are indicated. Protein length refers to the number of amino acid residues. The identity is given as a percentage relative to *Dictyostelium discoideum* Ino1. The E-value indicates statistical significance of a given pairwise alignment and is a reflection of the size of the database and the scoring system used. Lower E-values indicate greater significance of the homology.

3.4 Phylogenetic analysis

A phylogenetic tree to show the evolutionary conservation of the Ino1 proteins was constructed using the Molecular Evolutionary Genetics Analysis (MEGA) 5 software, with a neighbour-joining method and 500 bootstrap (the number of resampling analyses) replications to assess the reliability of the nodes (Tamura et al., 2011) (Figure 3.3). The tree also included human and *A.thaliana* peptidyl-prolyl isomerases as outgroups, to represent proteins that are outside the Ino1 protein family but that are still isomerases. The phylogenetic tree showed that all the Ino1 proteins from the group of species analysed were more closely related to each other than they were to the outgroup (Figure 3.3). The first node on the tree had a bootstrap value of 52, and it separated the Ino1 proteins of bacterial and eukaryotic origins. The second node had a bootstrap value of 100, and it showed that Ino1 proteins of fungal origin formed a distinct group to those of other eukaryotes. *Dictyostelium discoideum* Ino1 protein falls within the same group as that of brown algae, consistent with the close similarity of these proteins. *Dictyostelium* Ino1 was also present on the same node as Ino1 from other eukaryotic species, although it was separate from the higher animals (like human or frog Ino1) or plants (like maize or *A.thaliana*). Overall, this phylogenetic analysis showed that eukaryotic Ino1 proteins are distinct from Ino1 proteins present in prokaryotes, and that *Dictyostelium* Ino1 protein is more closely related to Ino1 proteins from higher organisms than it is to the fungal Ino1 proteins.

Figure 3.3 Phylogenetic analysis of Ino1 proteins from different biological kingdoms. Bootstrap consensus tree showing the evolutionary relationship between the Ino1 proteins of *Dictyostelium* and other species. The tree was generated in the Molecular Evolutionary Genetics Analysis (MEGA) 5 program via the Neighbour-Joining method with 500 bootstrap replications applied to assess the reliability of the nodes. Numbers represent percentage of replicate trees in which the associated taxa clustered together. Human and *A.thaliana* peptidyl-prolyl isomerases (EC 5.2.1.8) denote the root of the tree.

3.5 Homology alignment

A portion of the catalytic region of *Dictyostelium* Ino1 (amino acids 283-454) protein was aligned to the corresponding amino acid sequence of the Ino1 protein from other species (Figure 3.4). The alignment showed a high degree of amino acid conservation in this region, confirming the evolutionary relatedness of *Dictyostelium* Ino1 to other Ino1 proteins. Further homology analysis was performed with a comparison of *Dictyostelium* Ino1 (Q54N49) to the three human Ino1 (Q9NPH2) isoforms, and this analysis again showed a high degree of similarity between the proteins (Figure 3.5). Human Ino1 isoform 3 lacks the N-terminal portion present in the other proteins in this alignment; otherwise, all three human Ino1 isoforms are nearly identical. Aligning human Ino1 isoform1 with *Dictyostelium* Ino1

showed strong sequence homology, with 58% identity and 83% similarity (Figure 3.6).

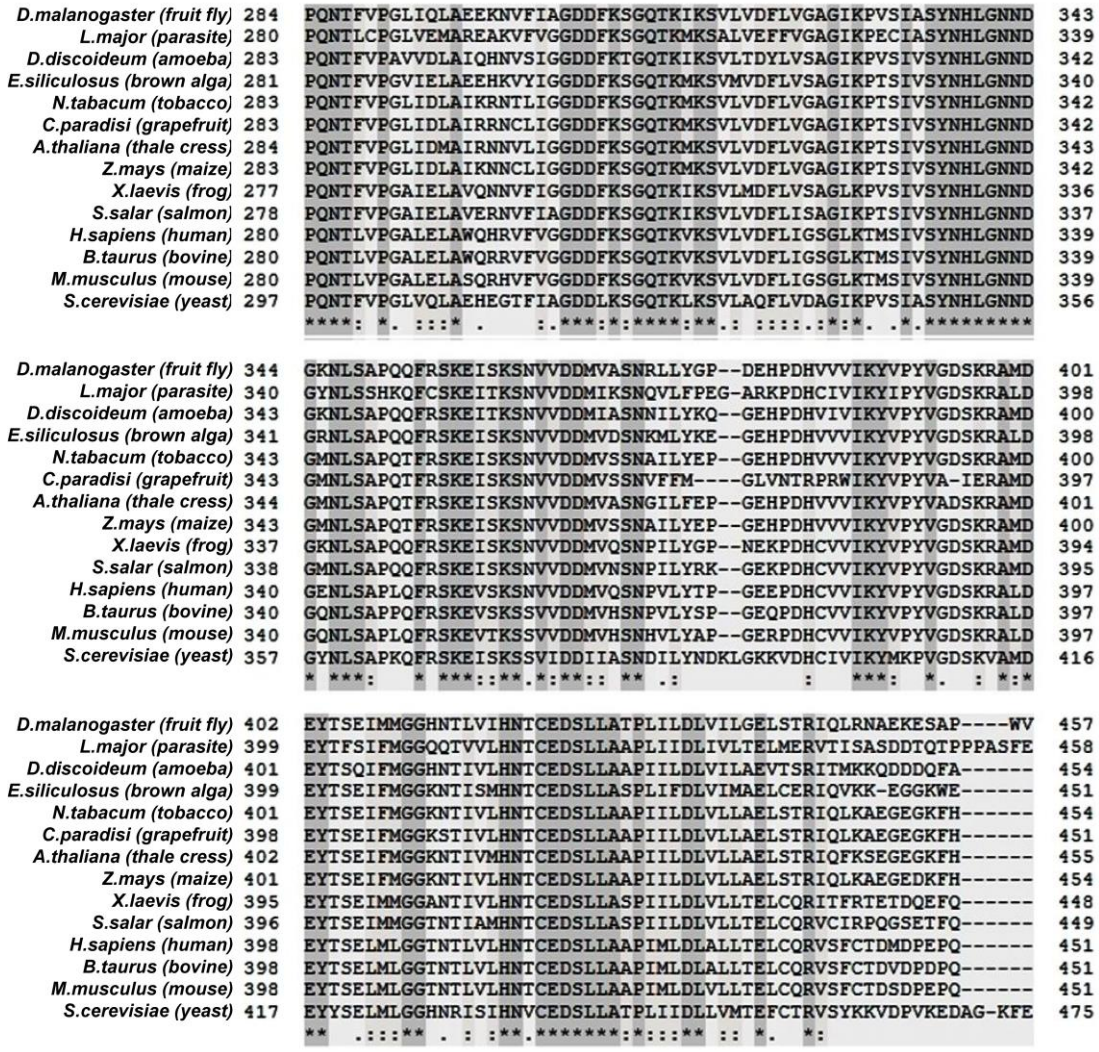

Figure 3.4 Conservation of the Ino1 catalytic region. Multiple sequence alignment of the putative active site regions of Ino1 proteins from different species show highly conserved amino acid residues that were considered to be important for Ino1 activity. The names of the species used in the alignment are indicated on the left, along with the amino acid position numbers. Identical amino acids are marked by an asterisk and highlighted in dark grey. The multiple sequence alignment was conducted using the UniProt website.

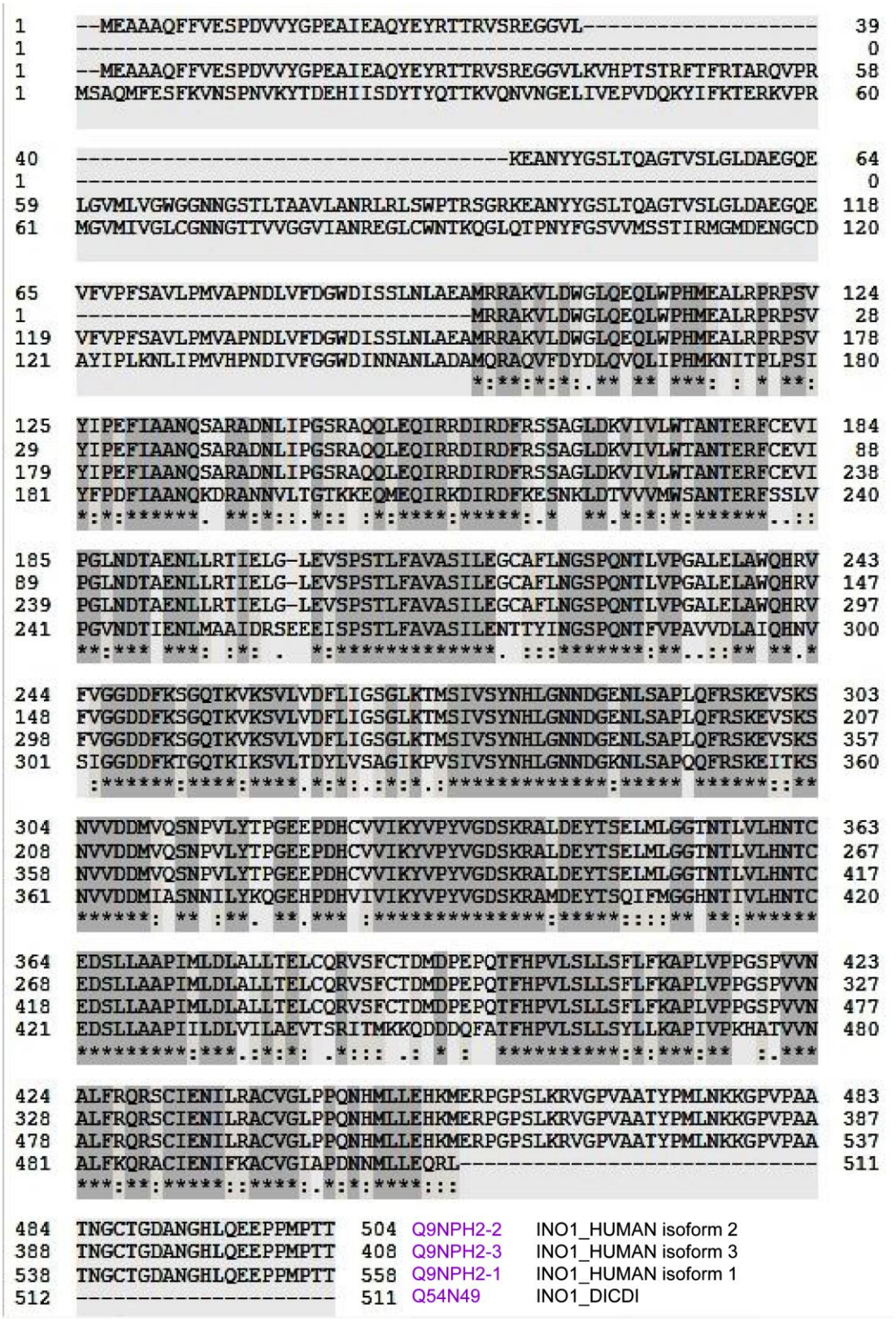

Figure 3.5 Homology between human Ino1 isoforms and *Dictyostelium* Ino1. Multiple sequence alignment of the human and *Dictyostelium* Ino1 proteins showing similarity in the amino acid residues, from the top: human Ino1 isoform 2, isoform 3, isoform 1, *Dictyostelium* Ino1. Identical amino acids are marked by an asterisk and highlighted in dark grey; similar amino acids are marked by a colon. The multiple sequence alignment was conducted using the UniProt website.

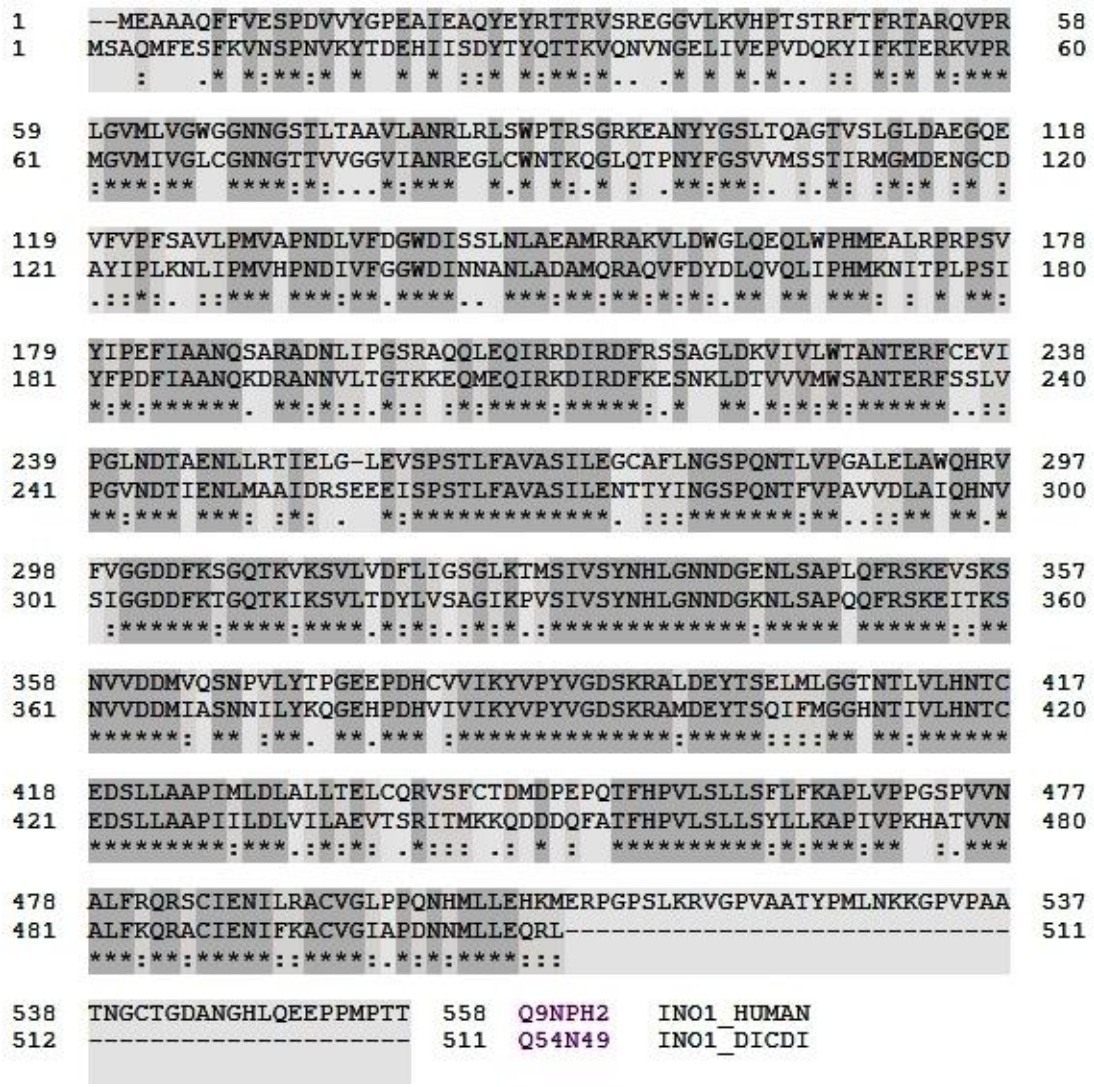

Figure 3.6 Homology between human and *Dictyostelium* Ino1 proteins. Sequence alignment of the human (isoform1) (top sequence) and *Dictyostelium* (bottom sequence) Ino1 proteins, showing similarity in the amino acid residues. Identical amino acids are marked by an asterisk and highlighted in dark grey; similar amino acids are marked by a colon. The proteins were 58% identical and 83% similar. The sequence alignment was conducted using the UniProt website.

The homology between human and *Dictyostelium* Ino1 isoform 1 proteins was analysed in more detail, where *Dictyostelium* (Q54N49) and human (Q9NPH2-1) protein sequences were compared, in view of the amino acid conservation seen in the Ino1 proteins from other species (Figure 3.7). The proteins were of similar size (511 amino acids for *Dictyostelium* Ino1 and 558 amino acids for human Ino1) and showed common conserved domains, including NAD-binding and catalytic domains. These conserved domains were also present in Ino1 proteins from a variety of biological species,

suggesting a highly conserved catalytic role of Ino1 throughout evolution and supporting the use of *Dictyostelium* to analyse Ino1 function.

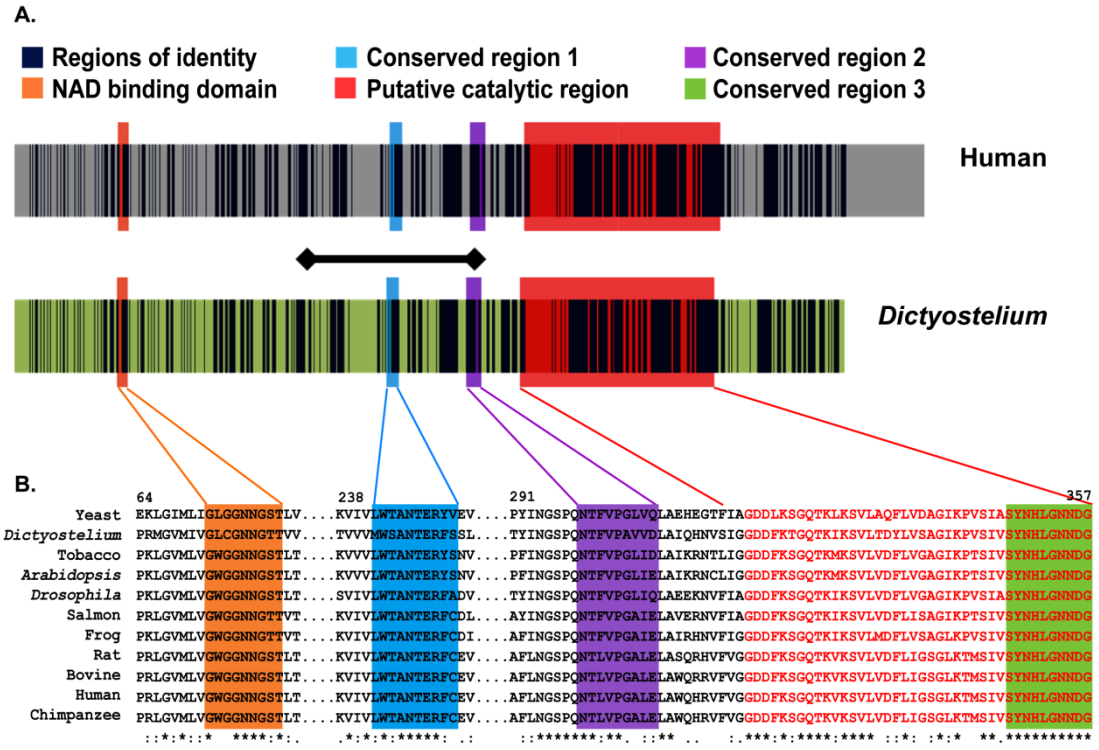

Figure 3.7 Conservation of the Ino1 protein between *Dictyostelium* and humans. (A) Sequence homology between the human isoform 1 (Q9NPH2-1) and *Dictyostelium* (Q54N49) Ino1 is present throughout the proteins. Identical amino acids are represented as dark vertical lines. The NAD-binding (orange) and catalytic (red) domains are among the regions that are highly conserved in eukaryotic Ino1 proteins; the other regions are highlighted in blue, green and purple. The tetramerisation domain containing the putative catalytic region (with the conserved amino acid residues SYNHLGNNDG) is shown in red. The amino acids that were ablated in *Dictyostelium* Ino1 are marked by a dark horizontal bar (◆——◆). (B) Alignment of the conserved regions of Ino1 proteins from various species, where '*' denotes identity, ':' high conservation, '.' low conservation.

3.6 Discussion

Proteins are composed of domains, which are mobile units that define protein function and are subject to genetic modifications throughout molecular evolution. In *Saccharomyces cerevisiae,* the active Ino1 protein is a homotetramer (Stein and Geiger, 2002). The crystal structure of *S.cerevisiae* Ino1 shows that the N- and C-terminal portions of the Ino1 monomer are in close proximity and make most of the contacts between the monomers (Stein and Geiger, 2002). Ino1 uses NAD^+ as a co-factor

(Majumder et al., 1997). The NAD-binding domain, positioned between the N-and C-terminal regions, also protrudes into the cleft between these regions. The active site of the enzyme is formed by substrate binding, which nucleates its own complete encapsulation (Stein and Geiger, 2002). The catalytic region additionally provides a tetramerisation interface during the assembly of multimers (Stein and Geiger, 2002). The presence of these domains in the Ino1 protein was previously reported in a number of distinct biological species (Majumder et al., 2003). Through the domain analysis, *Dictyostelium* Ino1 was shown to contain an evolutionarily conserved catalytic region, an NAD-binding domain, and N- and C-terminal domains that are structurally positioned as previously described (Stein and Geiger, 2002); these features are indicative of the same mechanism of action of the enzyme as in other species.

To establish the relatedness of *Dictyostelium* Ino1 with that of other species, the Basic Local Alignment Search Tool was used. This search identified a number of potential Ino1 homologues from a variety of species, including mammals (human, mouse, bovine), plants (*Arabidopsis thaliana*, maize, tobacco), frog (*Xenopus laevis*), fish (salmon), fly (*Drosophila melanogaster*), protozoa (*Leishmania major*) and yeast (*Saccharomyces cerevisiae*). The expectation value (E) threshold was used as a measure to verify whether the homology match is likely to be significant. The e-value is the number of expected matches in a random database, where the lower the e-value, the more likely is the match to be significant. The top potential *Dictyostelium* Ino1 homologues, with the highest e-value (0), were the proteins from plants (tobacco, *A.thaliana,* kidney bean, and grapefruit), brown alga, frog (*X.laevis)* and salmon. All of these Ino1 homologues were over 60% identical to *Dictyostelium* Ino1. Human Ino1 protein had an e-value of 10^{-176} and was 58% identical to *Dictyostelium* Ino1, supporting the close homology of these two proteins.

The biosynthesis of inositol is an evolutionarily conserved pathway (Majumder et al., 2003), and since Ino1 is responsible for the biosynthesis of inositol, a phylogenetic tree was constructed to better understand the

evolutionary relationship of the *Dictyostelium* Ino1 protein to that of other organisms. A phylogenetic tree shows the evolutionary relationship between groups of organisms called taxa. The ends on the tree branches represent groups of descendent taxa, which are often separate species, and the nodes on the tree are the common ancestors of the descendants. All the Ino1 proteins grouped together, separately from the tree outgroup (peptidyl-prolyl isomerase), which is an enzyme from the same family of proteins (an isomerase), supporting the evolutionary relatedness of the Ino1 protein homologues from prokaryotes and eukaryotes. The grouping of Ino1 proteins separately from the outgroup was validated by the bootstrap value of 98. Bootstrapping is a resampling analysis that involves removing amino acids in the Ino1 protein at random from the analysis, rebuilding the tree, and testing if the same nodes are recovered. *Dictyostelium discoideum* Ino1 protein was found to group with the Ino1 protein homologues from higher organisms, including human. This finding is in agreement with the data obtained during the Ino1 BLAST analysis, validating the evolutionary conservation between *Dictyostelium* and other eukaryotic Ino1 proteins.

The evolutionary relatedness of Ino1 in archaeal (*T.gammatolerans*) and eukaryotic species (including *Dictyostelium*, yeast, plants and mammals) was not well supported by the phylogenetic analysis, as indicated by a low bootstrap value (52) (Hillis and Bull, 1993). Although Ino1 proteins from archaea, eubacteria and cyanobacteria most likely evolved independently from each other, and the Ino1 proteins are quite divergent in the prokaryotic species, a number of archaeal proteins remain similar to the eubacterial proteins (Majumder et al., 2003). Thus, despite the fact that the archaeal and eukaryotic Ino1 proteins are evolutionarily distinct, a higher homology in certain regions of the Ino1 proteins could have affected the poor split on the phylogenetic tree (Majumder et al., 2003). Also, the low homology observed between *Dictyostelium* and yeast Ino1 proteins is reflected in the phylogenetic tree, where the yeast Ino1 protein grouped separately from the Ino1 proteins from other eukaryotes, as previously reported (Majumder et al., 2003).

Sequence homology was studied by aligning amino acids that constitute part of the putative catalytic region of the INO1 proteins. Potential homologues of *Dictyostelium* Ino1 from different taxa showed a remarkable conservation of the amino acids in the catalytic region, corroborating the notion that Ino1 is evolutionarily conserved (GhoshDastidar et al., 2006; Majumder et al., 2003; Stein and Geiger, 2002). Additionally, sequence alignments also showed high similarity between human (all three Ino1 isoforms) and *Dictyostelium* Ino1 proteins. Compared to the *Dictyostelium* protein, human Ino1 contains an additional C-terminal domain that is considered specific to Ino1 proteins of animal origin, the function of which is unknown (Majumder et al., 2003). Further analysis of the domain structure of the human and *Dictyostelium* Ino1 proteins showed that the functional domains occupied the same relative amino acid positions and contained stretches of amino acids that were highly conserved, confirming the homology and indicating a similarity in function between the human and *Dictyostelium* Ino1 proteins.

3.7 Summary

Study of the relatedness of Ino1 amino acid sequences from a variety of species, including the *Dictyostelium* Ino1 homologue, using domain conservation, BLAST, phylogenetic and sequence alignment analyses, showed a high degree of conservation of Ino1 throughout evolution. These data together support the notion that *Dictyostelium* can be used as a model to study the function of the Ino1 protein in relation to other eukaryotic species, and, in particular, human Ino1 protein.

Chapter 4
Ino1 gene deletion and rescue

Chapter IV

Ino1 gene deletion and rescue

4.1 Introduction

This chapter describes the genetic manipulation of the *ino1* gene in *Dictyostelium,* and the analysis of the growth and development of the *ino1*$^-$ mutant strains. Homologous recombination was the strategy used to generate the *ino1* knock-out mutant in *Dictyostelium.* Homologous recombination is a process where nucleotide sequences are exchanged between two similar or identical molecules of DNA (Figure 4.1), and allows for gene alternations by the introduction of cloned sequences at exact locations (De Lozanne and Spudich, 1987). Gene alternations can include introduction of point mutations, addition of extra copies of the gene or the deletion of a gene. Homologous recombination has been previously used successfully in yeast and mammalian cells (Witke et al., 1987), and to generate gene deletions in *Dictyostelium* (De Lozanne and Spudich, 1987; Fischbach et al., 2006; Pakes et al., 2012; Witke et al., 1987). To complement for the loss of *ino1* gene, extrachromosomal plasmids that expressed genes from a constitutive promoter were introduced into *ino1*$^-$ cells.

The *Dictyostelium discoideum ino1* gene (DDB0231710 dictybase.org) is located on chromosome 4, has a length of 1672 base pairs, and includes one intron at position 1389–1528. The gene encodes a protein of 511 amino acids. A single isoform of Ino1 exists in *Dictyostelium*. Similar to mammalian and yeast homologues, *Dictyostelium* Ino1 is responsible for *de novo* inositol biosynthesis (Majumder et al., 1997). A previous study of a *Dictyostelium ino1* deletion mutant reported an inhibition of cell growth in liquid, an inability to phagocytose both on bacterial lawns and bacteria in suspension, developmental defects leading to multi-tipped aggregates with generally delayed development, a reduction in phosphoinositol levels, and an increase

in the level of 2,3-BPG (glycolytic pathway product) (Fischbach et al., 2006). The *ino1* mutant was completely unable to grow without an exogenous supply of inositol (minimum concentration of 100 μM) in the growth media. Cells lost viability when deprived of inositol for 24 hours, and did not resume growth when inositol was supplied. The work presented in this chapter reports a successful deletion of the portion of the *Dictyostelium ino1* gene to allow for an analysis of the effects of inositol depletion and Ino1 loss.

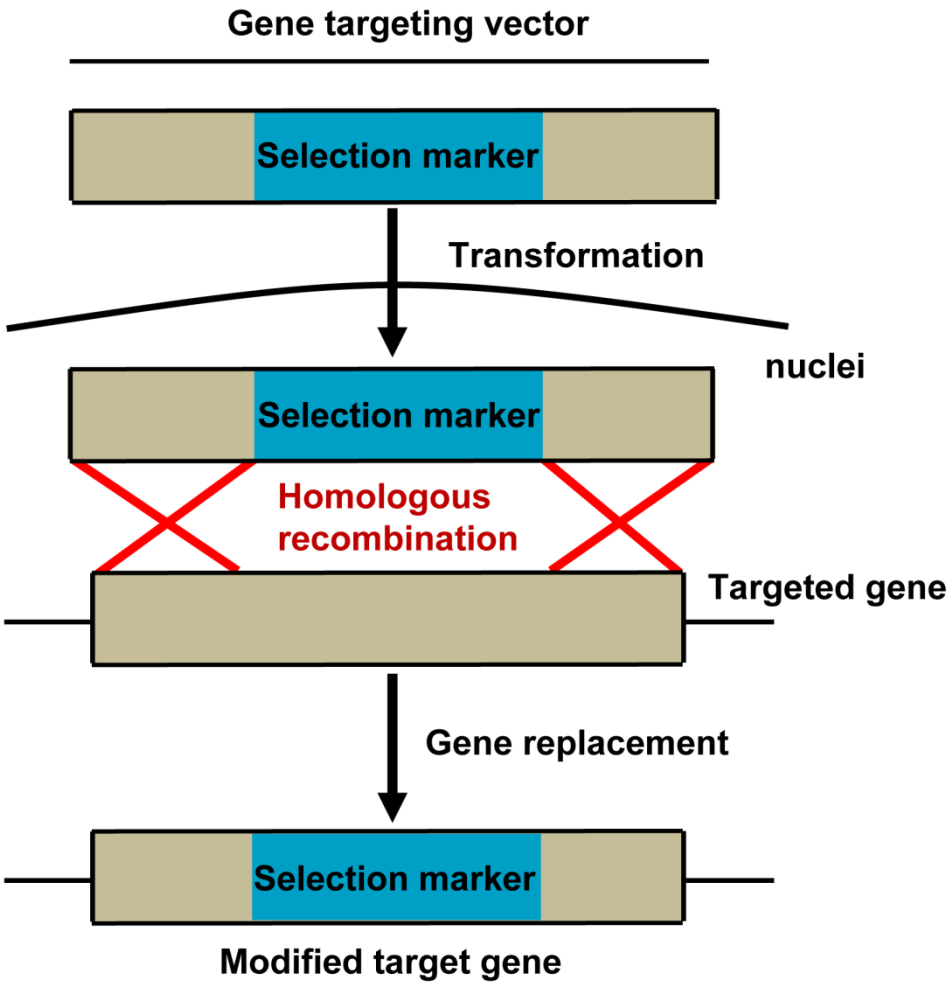

Figure 4.1 Homologous recombination. Schematic represents a process of homologous recombination, where a construct that contains DNA homologous to the targeted gene and a selection marker is introduced into cells. Upon homologous recombination and an exchange of DNA, the targeted gene is modified. The modified gene now contains the desired mutation (substitution or deletion) and a selection marker to allow for selection of transformants.

4.2 Creating an *ino1*$^-$ mutant

To investigate the role of Ino1 in *Dictyostelium*, the *ino1* gene was partially removed through homologous integration of a knock-out cassette into the *Dictyostelium* (Ax2) genome. The cassette was designed with 540 base pairs of the 5' region of the *ino1* gene, including the start codon, and 477 base pairs at the 3' region of the *ino1* gene, excluding the stop codon, with these regions flanking a blasticidin resistance gene used as a selection marker for the transformation (Figure 4.2 A). The 5' and 3' regions of the *ino1* gene were amplified by PCR from *Dictyostelium* genomic DNA, and cloned into the knock-out vector pLPBLP (Faix et al., 2004). Restriction enzyme analysis was performed to verify the presence of the 5' and 3' *ino1* gene fragments in the knock-out vector (Figure 4.2 B) Restriction digests of the knock-out plasmid with single enzymes were used to confirm that the enzymes cut the vector once, while digests with enzyme combinations were used to show the presence of the 5' and 3' *ino1* fragments, as well as the entire knock-out cassette (Figure 4.2 B). Additionally, correct gene sequences present in the *ino1* knock-out vector were confirmed by DNA sequencing.

Wild-type *Dictyostelium* Ax2 was transformed by electroporation of the *ino1* knock-out cassette previously digested with BamHI and KpnI enzymes (Figure 4.2 A). Transformed *Dictyostelium* cells were plated into 96-well dishes with added 500 µM inositol to supplement a possible lethal loss of endogenous inositol (Fischbach et al., 2006). Potential knock-out mutants were selected for cassette integration by survival in the presence of blasticidin (10 µg/ml).

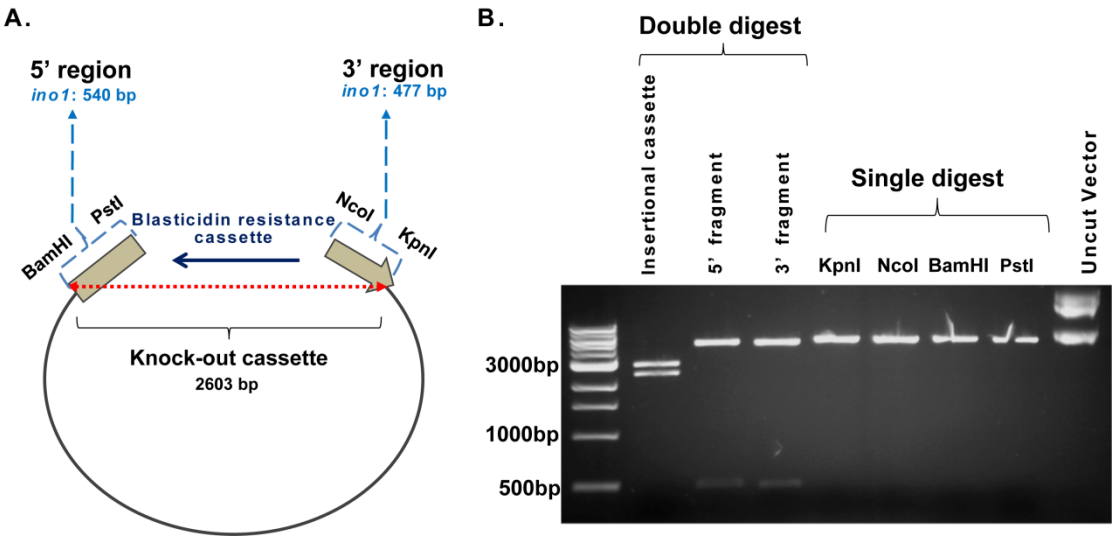

Figure 4.2 Construction and restriction digest analysis of the *ino1* knock-out vector. The *ino1* gene was partially removed using a homologous integration technique. (A) Schematic showing the construction of the *ino1* knock-out cassette. 5' and 3' fragments of the *ino1* gene were cloned into the pLPBLP plasmid that contained the blasticidin resistance cassette with a promoter positioned to ensure the blasticidin gene is transcribed in the opposite direction to the *ino1* gene fragments. The *ino1* 5' and 3' fragments were cloned into the pLPBLP vector using unique restriction enzymes as follows: 5' fragment, BamHI/PstI (540bp) and 3' fragment, NcoI/KpnI (477bp). The whole knock-out cassette (used for transformation of *Dictyostelium*) was released by cutting with BamHI/KpnI (2603bp) restriction enzymes. The enzymes used for cloning, and the sizes of the DNA fragments are indicated on the diagram. The complete knock-out vector contained 5,526 base pairs. (B) Restriction digest analysis of the constructed *ino1* knock-out vector. The undigested (uncut) knock-out vector was used as a control, and the single digest for each restriction enzyme that was used in the cloning was performed as an additional control reaction to confirm that the enzymes cut in a single place.

4.2.1 PCR screening analysis of the *ino1*$^-$ mutant

To isolate potential *ino1* knock-out mutants, cells resistant to blasticidin were screened by PCR to identify strains showing homologous integration of the knock-out cassette, as previously described (Adley et al., 2006) (Figure 4.3). In these screens, three primer combinations were used, providing diagnostic products for genomic (G) DNA, for vector (V) DNA, and to identify colonies showing homologous integration of the knock-out (K) cassette. These three products were screened at both the 5' and 3' regions of the gene. For the genomic controls, the primers were designed so that one primer would anneal to the genomic DNA in the region outside of the knock-out cassette, and the other primer to the genomic DNA that formed part of the knock-out cassette. For the vector controls, the primers were designed to

anneal to the genomic DNA region within the knock-out cassette and to a DNA sequence in the blasticidin resistance gene. A unique knock-out band to diagnose the homologous integration was obtained by amplifying the DNA region with two primers, one located in the genomic DNA region outside of the knock-out cassette and the other in the DNA sequence in the blasticidin resistance gene. These primer combinations were designed for the 5' and 3'-regions (corresponding to the 5' and 3' regions of the *ino1* gene) of the *ino1* knock-out cassette (Figure 4.3). To identify potential *ino1*$^-$ cell lines, ~143 blasticidin resistant colonies transformed with the knock-out construct were screened. From these screens, one positive integrant showed homologous integration at the 5' and 3' regions of the *ino1* gene (Figure 4.3).

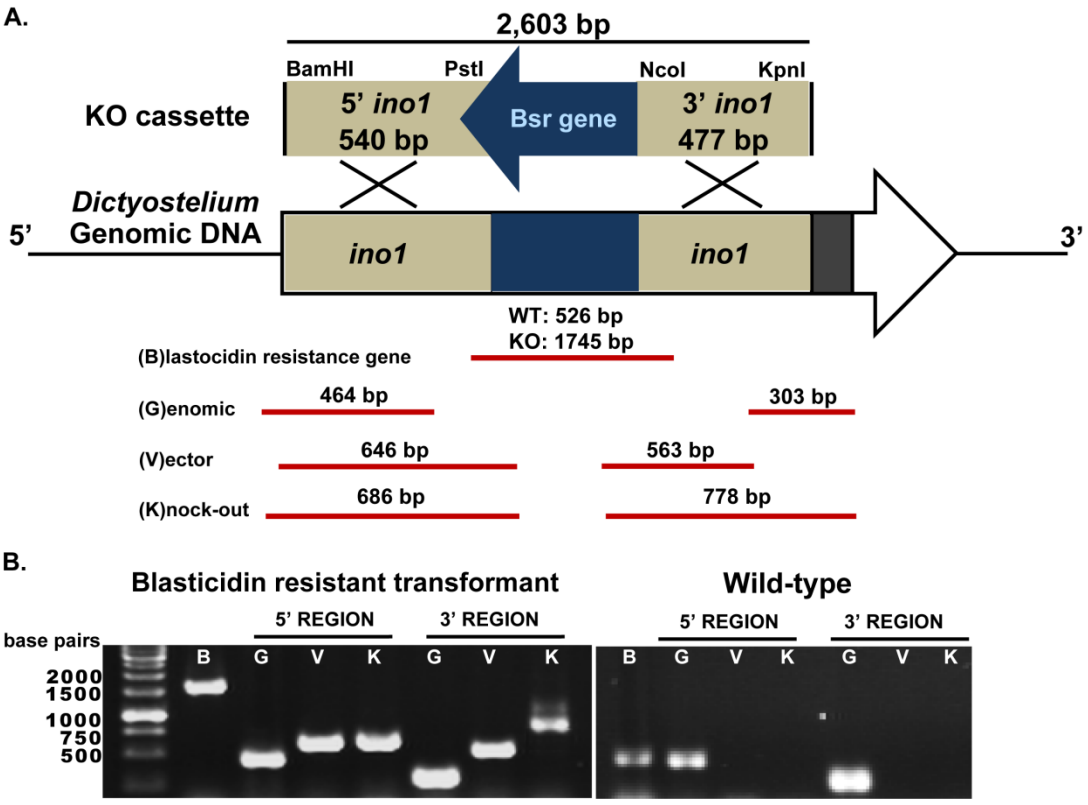

Figure 4.3 PCR screening analysis of the *ino1*$^-$ cells. Potential *ino1*$^-$ mutants resistant to blasticidin were screened using PCR to identify successful homologous integration events on both 5' and 3' sites of the *ino1* gene. (A) A schematic representation of the strategy used to generate and screen an *ino1* knock-out mutant. PCR screening analysis was used to confirm cell transformants that were resistant to blasticidin. The schematic shows blasticidin (BSR), genomic (G) and vector (V) controls as well as the diagnostic knock-out band (KO), together with the indicated DNA sizes in base pairs (bp) for both 5' (N-terminal) and 3' (C-terminal) regions. (B) The PCR analysis of the transformed cells resistant to blasticidin and wild-type control to confirm the homologous recombination event on both 5' and 3' regions of the *ino1* gene.

Identification of the homologous integration of the *ino1* knock-out cassette into the 5' and 3' regions of the *ino1* gene was indicative of the successful deletion of the central part of the gene. The identified positive colony was then serially diluted in media supplemented with 500 µM inositol to derive an isogenic cell line.

4.2.2 Loss of *ino1* gene transcription

Following the identification of the *ino1* knock-out cell line, a reverse transcription PCR (RT-PCR) analysis was used to confirm the loss of gene transcription in these cells (Figure 4.4). cDNA was synthesised from *ino1*$^-$ cells and analysed for the absence of *ino1* gene transcription. In this test, the primers for the PCR reaction were designed to anneal to the DNA region that was deleted in the knock-out cassette. The control reaction was performed using the same PCR conditions for the wild-type *Dictyostelium* strain that was used as a parent to create the *ino1* knock-out cell line. The DNA fragment visible on an agarose gel as a 302 base pair band was indicative of expression of the *ino1* gene. Mitochondrial large subunit rRNA (*rnlA* or *lg7*) PCR product was used as an expression control (559 base pairs), as previously published (Sugden et al., 2010). The absence of the band from cDNA derived from the knock-out cell line was indicative of the loss of gene transcription resulting from successful ablation of the *ino1* gene. This process confirmed that the isolated *ino1*$^-$ colony was isogenic, since a non-homologous transformant would contain the wild-type *ino1* gene fragment.

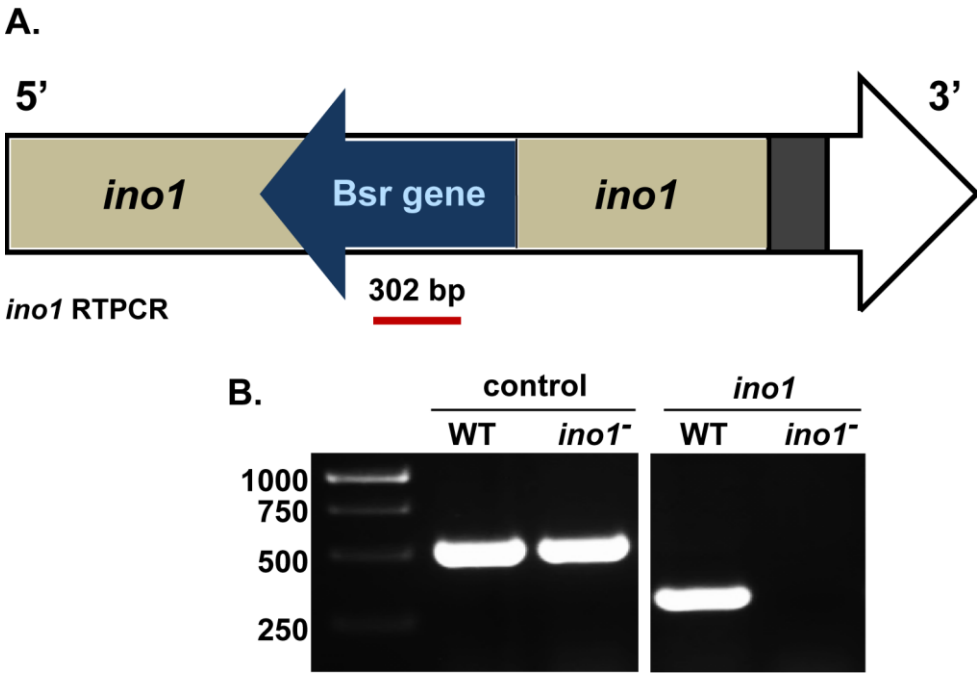

Figure 4.4 RT-PCR analysis of *ino1* gene transcription in the wild-type and the *ino1*⁻ cells. *Ino1*⁻ cells that showed resistance to blasticidin and were confirmed to integrate the knock-out cassette at 5' and 3' sites of the *ino1* gene were analysed for gene expression using RT-PCR. (A) A schematic to show the position where the primers to screen *ino1* loss of transcription anneal. (B) The RT-PCR analysis on the wild-type and *ino1*⁻ cells. RNA was extracted from both cell lines and converted to cDNA using reverse transcriptase. PCR was performed with *ino1* primers located within the deleted region of the *ino1* gene, which were only able to anneal to DNA of the wild-type to allow for amplification of a DNA fragment of 302 base pairs. *Ig7* gene (control) primers were used as a control to give a DNA product of 559 base pairs.

4.3 Creating *ino1* genetic rescue

4.3.1 Expressing the *Dictyostelium ino1* gene in the *ino1*⁻ mutant

To allow for a verification of the *ino1*⁻ phenotype, an *ino1*⁻ mutant cell line was created that expressed the *Dictyostelium ino1* gene fused to an RFP gene at the C-terminus under control of an actin 15 constitutive promoter (*ino1*⁻*::dino1*-RFP) (Figure 4.5). The *Dictyostelium ino1 (dino1)* gene was amplified using PCR with sequence-specific primers, and cloned into a plasmid containing mRFPmars (389-2, sourced from Dr Annette Müller-Taubenberger). The presence of the correct *ino1-RFP* sequence was verified by DNA sequencing using sequence-specific primers. The *ino1-RFP* containing plasmid was electroporated into *ino1*⁻ cells, and an isogenic cell

line was selected by a growth on a bacterial plate. *Ino1-RFP* gene expression was confirmed by RT-PCR, and the presence of the Ino1-RFP protein was confirmed by Western Blot analysis (Figure 4.5 A, B). Live-cell imaging revealed a cytosolic distribution of the Ino1-RFP protein (Figure 4.5 C). The *ino1*$^{-}$ mutant expressing *ino1-RFP* was used in all the rescue experiments described in this thesis.

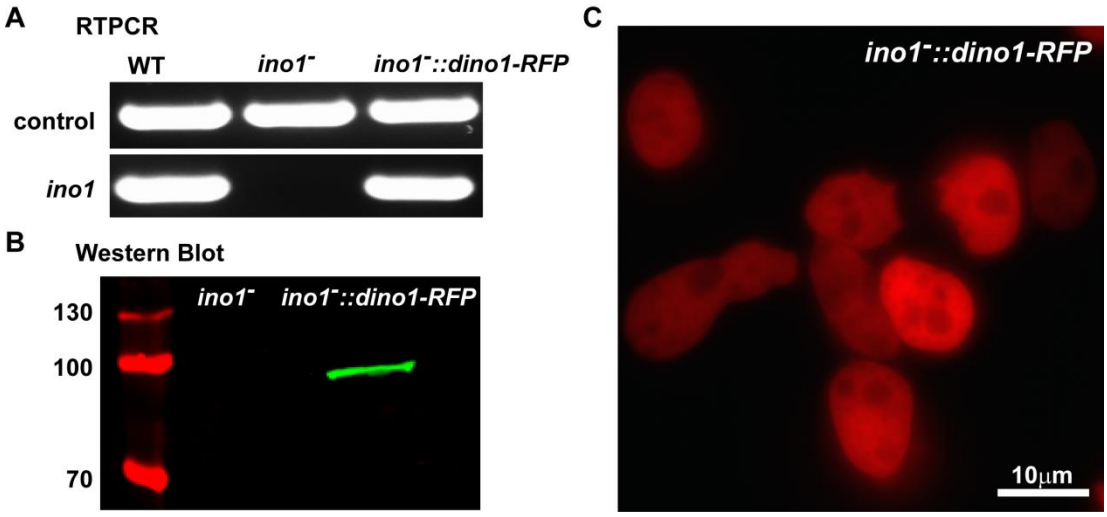

Figure 4.5 Overexpressing the *Dictyostelium ino1* gene tagged with RFP in the *ino1*$^{-}$ mutant. *Ino1*$^{-}$ cells were transformed with a plasmid containing *dino1-RFP* gene expressed from an actin15 promoter, and analysed for gene expression, and production and localisation of the Ino1-RFP protein. (A) RT-PCR analysis of the wild type Ax2, *ino1*$^{-}$, and *ino1*$^{-}$*::dino1-RFP* rescue cells, where RNA was extracted from the cells and converted to cDNA using reverse transcriptase. PCR was performed with d*ino1* primers located within the deleted region of the *ino1* gene, and were only able to anneal to DNA of the wild-type *Dictyostelium* and *ino1*$^{-}$ rescue strains to allow for the amplification of a DNA fragment of 302 base pairs. *Ig7* gene (control) primers were used as a control to give a DNA product of 559 base pairs. (B) Western Blot analysis for the presence of Ino1-RFP protein (approx. 85kDa) using anti-RFP antibody. (C) *Dictyostelium* Ino1-RFP protein shows cytosolic localization by live-cell imaging with a fluorescence microscopy.

To examine the functionality of the Ino1 protein fused to a marker at the N-terminus, the *Dictyostelium ino1 (dino1)* gene was amplified by PCR using sequence specific primers and cloned into a GFP-containing plasmid (pTX-GFP (Levi et al., 2000)). The presence of the correct GFP-*ino1* sequence was verified by DNA sequencing using sequence-specific primers. The GFP-*ino1* containing plasmid was electroporated into *ino1*$^{-}$ cells, and an isogenic cell line was selected by a growth on bacteria. Live cell imaging showed a cytosolic localisation of the GFP-Ino1 protein (Figure 4.6). The

ino1⁻::GFP-dino1 mutant was able to grow and develop in the absence of inositol (data not quantified).

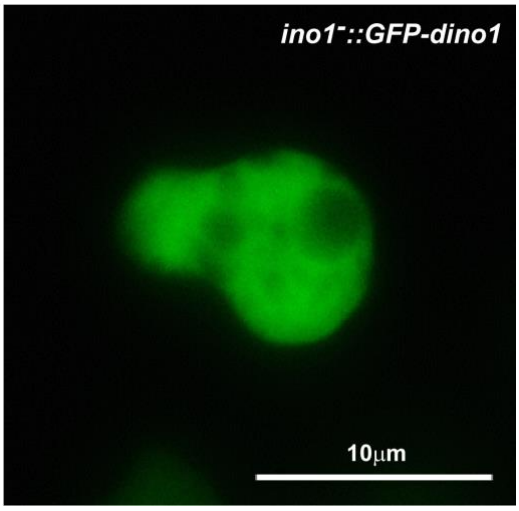

Figure 4.6 Localisation of GFP-dIno1 in *ino1⁻* cells. *Ino1⁻* cells were transformed with a plasmid containing *GFP-dino1* gene expressed from an actin15 promoter, and analysed for the localisation of the GFP-Ino1 protein. GFP-Ino1 protein shows cytosolic localization in live cells by fluorescence microscopy.

4.3.2 Expressing the human *ino1* gene in the *Dictyostelium ino1⁻* mutant

Based on a high degree of evolutionary conservation of the *Dictyostelium* and human Ino1 proteins (see chapter 3), the human *ino1* (*hino1*) gene was expressed in *Dictyostelium ino1⁻* cells to test for functional complementation. DNA encoding the human *ino1* gene optimised to *Dictyostelium* codon bias was synthesised with restriction sites to enable cloning into an N-terminal GFP fusion vector pDM317 (Veltman et al., 2009) (*ino1⁻::GFP-hino1*) and a C-terminal mRFPmars fusion vector 389-2 sourced from Dr Annette Müller-Taubenberger (*ino1⁻::hino1-RFP*). Live-cell imaging revealed a cytosolic localisation of both of the tagged human Ino1 proteins (Figure 4.7). Tagging the human Ino1 protein at the N-terminus enabled *ino1⁻* cells to grow in the absence of exogenous inositol; however, the slow growth of the overexpressing cells did not allow for growth quantification. Tagging the human Ino1 protein at the C-terminus did not rescue inositol auxotrophy of the *ino1⁻* cells. Slow growth of these strains did not allow for further experimental analysis.

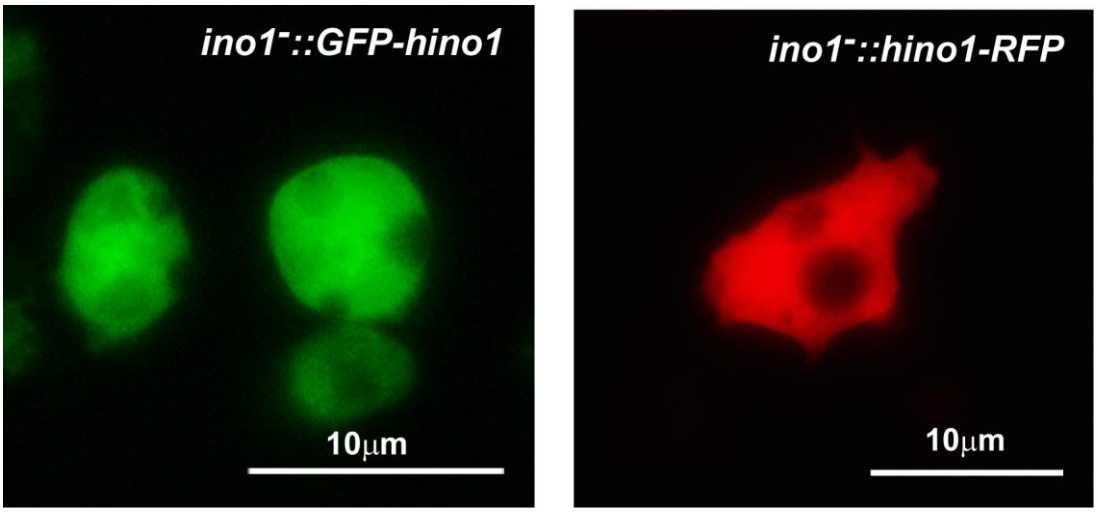

Figure 4.7 Localisation of the human GFP-Ino1 and Ino1-RFP proteins in *ino1*⁻ cells. *Ino1*⁻ cells were transformed with a plasmid containing either *GFP-hino1* or *hino1-RFP* gene expressed from an actin15 promoter, and analysed for the localisation of the human Ino1 protein. Both GFP-Ino1 and Ino1-RFP showed cytosolic localization by fluorescence microscopy.

4.4 Growth of the *ino1*⁻ mutant

Since Ino1 catalyses the first rate-limiting step in inositol production, the loss of the Ino1 protein would result in inositol depletion in the *ino1*⁻ cells, with a potential impact on cell growth. Growth rate of the wild-type and *ino1*⁻ mutant was assessed by incubating cells in growth medium supplemented with various concentrations of inositol at a starting density of $1x10^5$ cells/ml, and were then counted daily until wild-type cells reached the stationary phase ($1.88 x10^7$ cells/ml) (Figure 4.8 A). Concentrations from 0 µM to 500 µM of inositol were used in this experiment. Wild-type cells went through the logarithmic, exponential and stationary phases within 192 hours without the need for exogenous inositol supplementation. In contrast, *ino1*⁻ cells were unable to grow in the absence of inositol supplementation. After 72 hours of inositol removal, the number of *ino1*⁻ cells was seven-fold lower in comparison to the inositol-supplemented (500 µM) control and started to decrease over time, suggesting that the internalised inositol reserves were being depleted. Growth of the *ino1*⁻ mutant was restored by adding 150 µM inositol to the growth media. There was no difference observed in the growth of the *ino1*⁻ cells supplemented with 300 µM or 500 µM inositol, suggesting inositol saturation at 300 µM. Addition of inositol enabled the growth of the

ino1⁻ mutant in the liquid media; however, growth was not restored to the wild-type level even at higher inositol concentrations (Figure 4.8 A). Cell density of the wild-type cells grown in the liquid media was significantly higher than that of the *ino1*⁻ cells, even with inositol supplementation. Doubling times were calculated for cultures growing in the logarithmic phase. Wild-type cells doubled every 18 hours while *ino1*⁻ cells every 25 hours (when grown in the media with 300 µM inositol) or every 23 hours (when grown in the media with 500 µM inositol) indicating that the *ino1*⁻ mutant supplemented with inositol exhibits a slower growth rate (approximately one third) compared to the wild-type under the tested conditions (Figure 4.8 A).

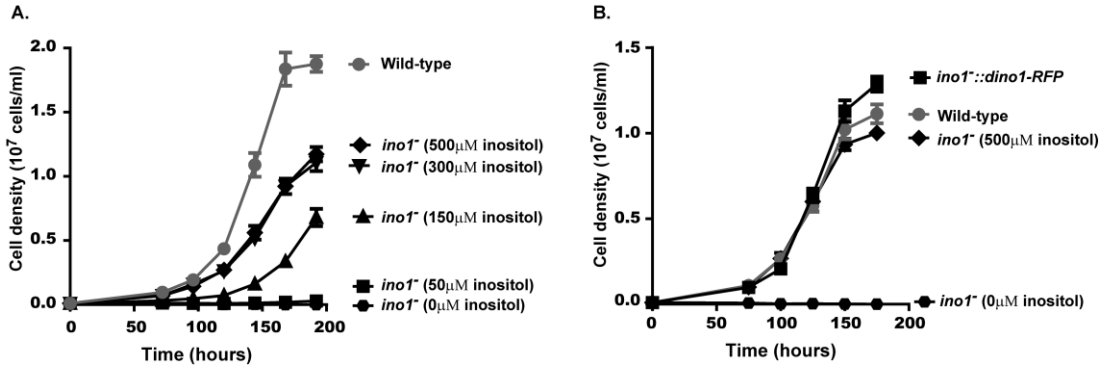

Time (hours)	wild type vs. *ino1⁻* inositol concentration (µM)				
	0	50	150	300	500
0	ns	ns	ns	ns	ns
72	ns	ns	ns	ns	ns
96	**	**	*	ns	ns
120	***	***	***	**	*
144	***	***	***	***	***
168	***	***	***	***	***
192	***	***	***	***	***

ns P >0.05 *P <0.05 **P <0.01 ***P <0.001

Time (hours)	wild type vs. *ino1⁻*+ inositol		
	0µM	500µM	*ino1⁻::dino1-RFP*
0	ns	ns	ns
72	ns	ns	ns
96	**	ns	ns
120	***	ns	ns
144	***	ns	ns
168	***	ns	ns
192	***	ns	ns

ns P >0.05 *P <0.05 **P <0.01 ***P <0.001

Figure 4.8 Growth of the *ino1⁻* mutant in liquid medium. Wild-type and *ino1⁻* cells were grown in shaking suspension +/- inositol as indicated. *Ino1⁻* cells were unable to grow without inositol below the tested concentration of 150 µM. Ino1-RFP expression restored the growth of *ino1⁻* cells under no inositol conditions. Difference in cell density between wild-type and *ino1⁻* cells (grown in the presence of 500 µM inositol) was observed to be variable (as shown in panel A and B), which might have arisen from the biological variability between different batches of the wild-type cells used. (A) Wild-type and *ino1⁻* cells were counted every 24 hours for 192 hours, starting from an initial cell density of $1x10^5$ cells/ml. (B) Wild-type, *ino1⁻*, and *ino1⁻::dino1-RFP* cells were counted every 24 hours for 192 hours starting from an initial cell density of $1x10^5$ cells/ml. Statistical analysis was performed using 2-way ANOVA with Bonferroni post-test and comparison were to the wild-type control, the significance values are presented in the tables below the graphs. (A) n= 3 technical repeats; 1 biological replicate, (B) n = 3 technical repeats; 1 biological replicate.

Another growth experiment was conducted to test for the ability of Ino1-RFP to restore the growth of *ino1⁻* cells in media without inositol. Here,

cell density and growth rate between wild-type and *ino1*⁻ cells was observed to be similar (21 hours doubling time for wild-type and *ino1*⁻ +500 µM inositol) (Figure 4.8 B). The difference in the cell density of the wild-type cultures presented in the graphs in figure 4.8 panel A and B might have arisen from the biological variability between different batches of the wild-type cells used for these experiments. Overexpressing *Dictyostelium ino1-RFP* rescued the growth of *ino1*⁻ cells in liquid culture without the addition of exogenous inositol (Figure 4.8 B). Additionally, the doubling time for the *ino1*⁻ cells expressing *dino1-RFP* decreased to 15 hours compared to 21 hours for the wild-type control, suggesting that overproduction of Ino1 protein in the *ino1*⁻ cells increases their growth rate. These data suggest that *ino1*⁻ mutant is an inositol auxotroph.

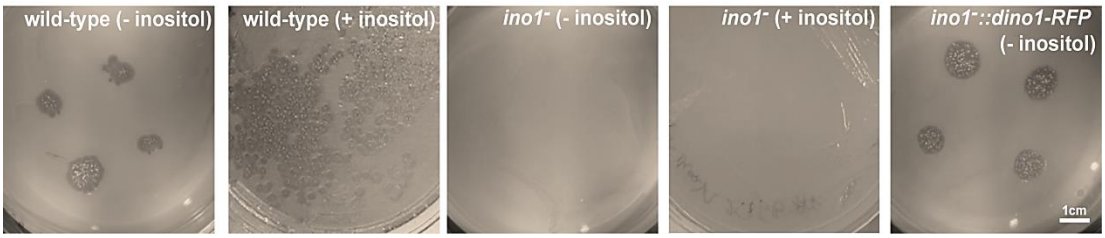

Figure 4.9 Growth of *ino1*⁻ cells on bacteria. Wild-type and *ino1*⁻ cells were plated onto agar plates seeded with live bacteria (*Raoultella planticola*), except for the plates marked "+ inositol" where inositol (500 µM) was added to heat-killed *R.planticola,* and inoculated for 7 days at 22°C. Wild-type cells formed plaques indicative of the ability to grown by consuming bacteria, whereas *ino1*⁻ cells did not form plaques regardless of inositol supplementation. Overexpressing *dino1* tagged with RFP in the *ino1*⁻ cells rescued the inability of those cells to grow on bacteria without inositol supplementation. Size bar represents 1 cm.

During the selection for the *ino1* knock-out isogenic cell lines, the *ino1*⁻ mutant was plated onto nutrient agar plates containing live bacteria (*Raoultella planticola*). Under these conditions, wild-type *Dictyostelium* Ax2 cells are able to grow by consumption of bacteria (phagocytosis) (Cardelli, 2001). Bacterial consumption is visible as formation of plaques of cleared bacteria (Figure 4.9). As these plaques enlarge, the bacteria are depleted in the centre of the plaque and the cells in this area begin to starve and undergo the developmental process to produce fruiting bodies. During the clonal selection, the *ino1*⁻ cells were not able to grow and no plaques were seen to be formed (Figure 4.9). This loss was not corrected by adding inositol (500 µM/plate) to the growth medium (both in the agar and mixed with heat-

killed bacteria). Overexpressing *dino1-RFP* in the *ino1*$^{-}$ cells restored the growth on bacterial plates in the absence of inositol, suggesting a requirement for Ino1 protein to complete phagocytosis.

Since the *ino1*$^{-}$ cells were unable to grow on agar plates seeded with bacteria, the mutant cells were analysed for their ability to phagocytose in liquid culture. For this purpose, a bacteria clearing assay was performed where wild-type and *ino1*$^{-}$ cells were incubated in shaking suspension in the presence of heat-killed *R.planticola* as a food source (Figure 4.10). For this experiment, *ino1*$^{-}$ cells were in the absence of inositol for a total of 25 hours (including 7 hours of the assay duration). Consumption of bacteria was determined by measuring the loss of light absorbance over time.

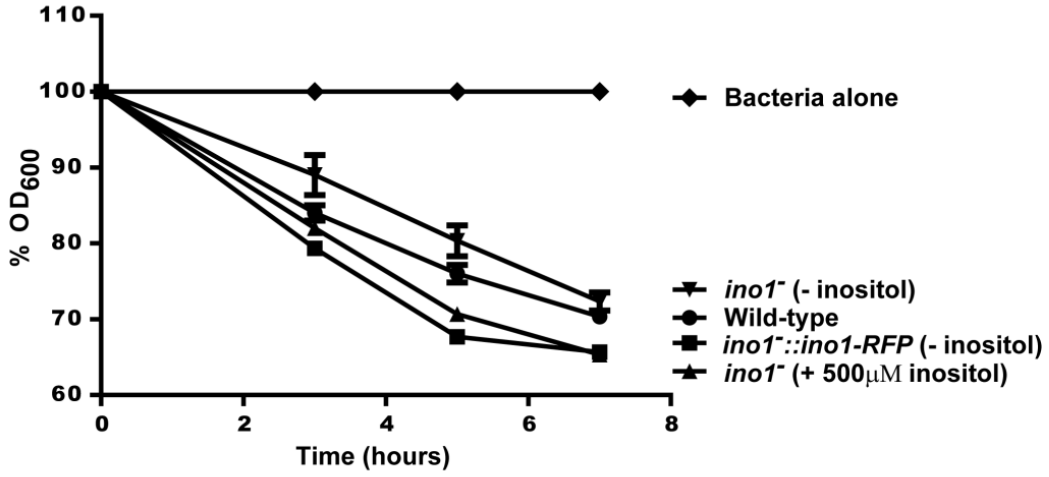

Figure 4.10 *Ino1*$^{-}$ ability to phagocytose in shaking suspension. Wild-type, *ino1*$^{-}$, and *ino1*$^{-}$*::dino1-RFP* cells were inoculated with heat-killed bacteria *(R.planticola)* in the presence or absence of inositol and optical density was measured over a period of 7 hours. No significant differences were observed between the wild-type (control) and *ino1*$^{-}$ strains in the ability to clear away bacteria from the suspension. n = 3 technical repeats; 1 biological replicate

The wild-type cells cleared away 30% of bacteria, while the *ino1*$^{-}$ cells grown without inositol cleared away 28% of bacteria over 7 hours (Figure 4.10). Also, the *ino1*$^{-}$ cells overexpressing Ino1 or incubated with inositol (500 μM) cleared away 34% and 35% of bacteria, respectively. The optical density was also measured after 24 hours from the time when the cells were incubated with bacteria (Table 4.1). By that time, the wild-type cells cleared away 57% of bacteria, while the *ino1*$^{-}$ cells grown in absence of inositol or in the presence of inositol (500 μM) cleared away 61%, and 66% of bacteria,

respectively; the *ino1*$^-$ cells overexpressing *ino1-RFP* cleared away 73% of bacteria. The *ino1*$^-$ mutant thus showed no significant difference in the ability to phagocytose when compared to wild-type.

	Time (hours)				
	0	3	5	7	24
Bacteria alone	100	100	100	100	96
Wild-type	100	84	76	70	43
***ino1*$^-$ (- inositol)**	100	89	80	72	39
***ino1*$^-$ (+ 500 µM inositol)**	100	82	71	65	34
ino1*$^-$*::dino1-RFP	100	79	68	66	27

Table 4.1 Percentage of bacteria consumed over time by wild-type and *ino1*$^-$ strains. *Dictyostelium ino1*$^-$ cells are able to phagocytose bacteria at the same rate as the wild-type strain. Statistical analysis between wild-type and *ino1*$^-$ strains was performed using two-tailed student's *t*-test and compared to wild-type control. No significant difference was found. n = 3 technical repeats; 1 biological replicate

4.5 Development

When starved of nutrients, *Dictyostelium* cells aggregate to form fruiting bodies over a period of 24 hours. To investigate the effect of *ino1* ablation on this developmental process, the wild-type and the *ino1*$^-$ cells were starved on nitrocellulose membranes over a 24-hour period to induce development. In the wild-type cells, these conditions lead to the development of fruiting bodies containing a basal disk, stalk, and a round spore head (sorus) (Figure 4.11 A,B) (Schaap and Wang, 1986). In the *ino1*$^-$ mutant, the development into fruiting bodies was dependent upon inositol treatment prior to setting up the development assay. *Ino1*$^-$ cells were able to form fruiting bodies when the cells had been grown in the presence of exogenous inositol (500 µM) prior to the transfer onto nitrocellulose membranes. *Ino1*$^-$ cells were arrested in development when the cells were grown in the absence of exogenous inositol for a period of 24 hours before their transfer onto nitrocellulose membranes, although the cells were able to aggregate (Figure 4.11 B). This analysis shows a requirement of inositol to complete development in *Dictyostelium.* Overexpressing *ino1-RFP* (*ino1*$^-$*::dino1-RFP*) restored fruiting body formation in the *ino1*$^-$ cells grown in the absence of inositol which indicates that the developmental defect was due to the loss of *ino1* gene.

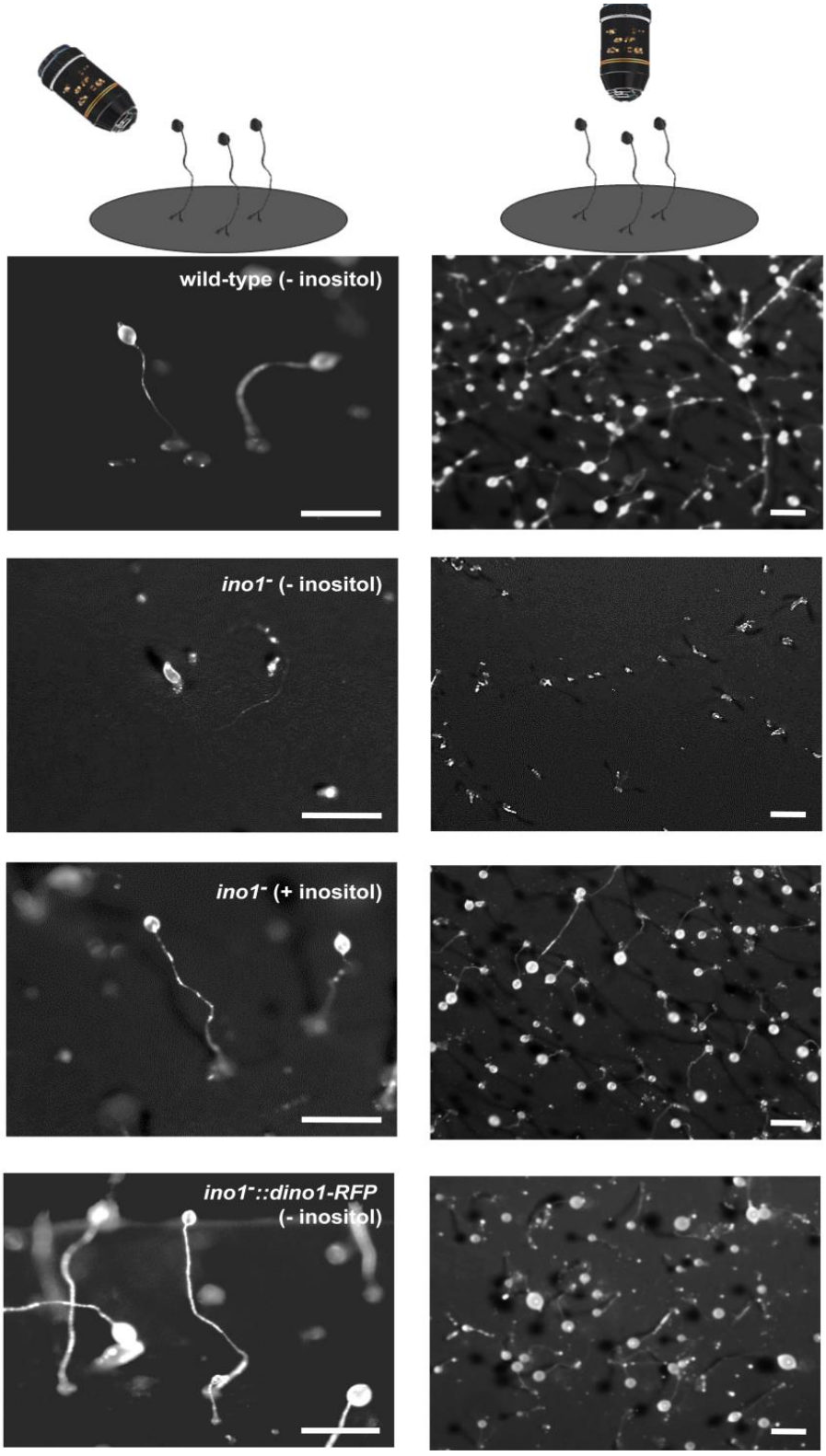

Figure 4.11 The effect of *ino1* ablation on *Dictyostelium* development. Wild-type and *ino1*$^{-}$ mutant cells were developed on nitrocellulose membranes over 24-hour period. The *ino1*$^{-}$ cells were grown in the presence (500 µM) or absence of inositol prior to the development assay. The wild-type cells formed mature fruiting bodies over 24 hours, while the *ino1*$^{-}$ cells required the presence of inositol prior to the development assay to be able to complete differentiation into fruiting bodies. Overexpression of *ino1-RFP* rescued the impaired developmental phenotype of the *ino1*$^{-}$ cells. Representative of 3 independent technical repeats. Size bars represent 0.5 mm.

4.6 Discussion

To investigate the role of the Ino1 protein in *Dictyostelium,* a cell line was created with 19% of the *ino1* gene removed using the homologous recombination method. The loss of *ino1* expression was confirmed by reverse transcription PCR. The created *ino1*$^-$ mutant was grown in the presence of inositol in the liquid media (500 µM) to avoid a potential lethality resulting from a lack of inositol, as previously demonstrated (Culbertson and Henry, 1975; Fischbach et al., 2006). Various expression constructs were also created to complement for the loss of *ino1* in *Dictyostelium.*

Dictyostelium Ino1 expressed with a GFP tag at the N-terminus or an RFP tag at the C-terminus restored the growth of the *ino1*$^-$ mutant without exogenous inositol supplementation. Human Ino1 expressed with a GFP tag at the N-terminus in the *ino1*$^-$ mutant resulted in very slow growth in medium without added inositol. The growth was reduced to a level that would not allow quantification. Human Ino1 with an RFP at the C-terminus was not able to restore the ability of these cells to grow without inositol supplementation, even though expression was observed in the *ino1*$^-$ cells by live cell imaging. Studies to examine the chemical properties of the Ino1 protein purified from human foetal liver showed that the highest activity of the enzyme was observed at a temperature of 40°C (Chhetri et al., 2012). cDNA coding for the Ino1 derived from a post-mortem human prefrontal cortex was previously shown to be functional in yeast, complementing the inositol auxotrophy (Ju et al., 2004). Enzyme activity of the purified human Ino1 measured by Ju et al. (2004) was reported to be optimal at 37°C (~65 U/mg), reaching ~29 U/mg at 30°C and ~17U/mg at 20°C. In this study, yeast cells expressing human Ino1 protein were grown at a temperature of 30°C. It is thus possible that the 22°C temperature at which the *Dictyostelium ino1*$^-$ strain was grown was not permissive for human Ino1 enzyme activity, thus resulting in an insufficient level of inositol production to rescue the inositol auxotrophy of the *ino1*$^-$ mutant. Since the optimal temperature for the growth of *Dictyostelium* is 21-23°C, and growth is significantly repressed above 25°C, this hypothesis could not be tested *in vivo* in the axenic strains used in this project.

Dictyostelium and human Ino1 proteins tagged at the N- and C-termini had a cytosolic localisation by fluorescence microscopy. In agreement with this finding, Ino1 protein was previously reported to be present in the cytosol in a soluble form in unicellular and multicellular eukaryotes (Lackey et al., 2003). However, despite the wide acceptance that inositol phosphate biosynthesis is restricted to the cytosol, there is evidence to suggest that Ino1 can also be localised to membrane-bound organelles, including mitochondria, the endoplasmic reticulum, and the nucleus, opening interesting avenues to exploration (Kerr and Corbett, 2010; Lackey et al., 2003).

Growth assays were performed using the wild-type and *ino1*$^-$ cells inoculated in liquid media, where *ino1*$^-$ mutant was unable to grow without exogenous inositol supplementation (≥ 150 µM). *Dictyostelium ino1*$^-$ mutants were previously shown to be unable to grow without inositol supplementation in liquid media (Fischbach et al., 2006). Cells utilise pinocytosis to take up nutrients when cultured in liquid medium (Clarke and Kayman, 1987). Low inositol levels may affect nutrient uptake via a disruption of inositol phosphate and phosphoinositide cycle in cells (Bohdanowicz and Grinstein, 2013; Rupper et al., 2001; van Haastert and van Dijken, 1997). Previous studies have shown, however, that pinocytosis was not affected in *Dictyostelium* cells with a disrupted *ino1* gene that were starved of inositol (Fischbach et al., 2006). This result suggests that fluid internalisation is not disrupted by the absence of inositol.

In contrast to the growth in liquid media, *ino1*$^-$ cells were unable to grow with bacteria on agar plates, even with added inositol. However, the cells were able to clear away the bacteria when inoculated in liquid (the growth rate was not measured). The bacteria were heat-killed before inositol was added to ensure that inositol would not be metabolised by the bacteria. *Dictyostelium* inositol-auxotrophic mutants have been previously shown to be unable to grow on bacterial lawns or in suspensions of bacteria, and a disruption of phagocytosis has been reported in *Dictyostelium* mutants with an inactivated *ino1* gene (Fischbach et al., 2006). However, contradictory to the findings presented in this thesis, the internalisation of bacteria was severely reduced during inositol starvation, and the ability to phagocytose

was completely lost by the *ino1* mutant cells after 24 hours without inositol (Fischbach et al., 2006). This discrepancy can result from a difference in methods used. Fischbach et al. used FITC-labelled bacteria, while the assay described in this thesis involved the use of freshly heat-killed bacteria. FITC-labelled bacteria are particles that had to be phagocytosed by cells. Indeed, *ino1*$^{-}$ cells were shown to be defective in phagocytosis but not pinocytosis (Fischbach et al., 2006). Additionally, the pinocytosis rate of cells cultured on bacteria has been shown to be negligible (Clarke and Kayman, 1987). The nutrients released from the freshly killed bacteria and dissolved in the liquid would therefore not require phagocytosis, because pinocytosis would be sufficient for cells to take up the nutrient-containing liquid. *Ino1*$^{-}$ cells may thus be able to internalise smaller particles dissolved in liquid by endocytosis or pinocytosis but be unable to do this when grown on a solid substrate. These results suggest that the processes of phagocytosis, endocytosis and pinocytosis have different dependencies on inositol-derived compounds. Phagocytosis and particle digestion occurs over a number of steps that include the particle binding to the cell surface, followed by an engulfment of the particle by pseudopod extension, and finally the fission and fusion reactions to form phagolysosomes (Cardelli, 2001). Phosphoinositides are essential in these processes in a number of cell types, including *Dictyostelium* (Botelho et al., 2000).

During starvation, *Dictyostelium* cells aggregate and initiate multicellular development to undergo a change in morphology and produce spore-bearing fruiting bodies. Inositol metabolites are required for cell signalling and membrane reorganisation especially, during the initial stages of development (cell aggregation) (Cai and Devreotes, 2011). *Ino1*$^{-}$ cells grown in the absence of inositol prior to development initiation were not able to form fruiting bodies, and inositol was sufficient to rescue this phenotype. Also, overexpressing Ino1-RFP in the *ino1*$^{-}$ cells restored this developmental phenotype. These data suggests that development of *Dictyostelium* requires the presence of inositol.

4.7 Summary

This chapter described generation of the *ino1*$^-$ mutant and a genetic rescue with *Dictyostelium* and human Ino1 proteins. Both human and *Dictyostelium* Ino1 proteins were shown to localise to the cytosol. The *ino1*$^-$ mutant exhibited inositol auxotrophy and an inositol requirement for development. Exogenous inositol (500 µM) allowed for growth of these cells in liquid medium, and for completion of multicellular development, but was not able to rescue the inability of *ino1*$^-$ cells to phagocytose bacteria on agar plates.

Chapter 5
Effects of inositol depletion and Ino1 loss on cell function

Chapter V

Effects of inositol depletion and Ino1 loss on cell function

5.1 Introduction

The studies described in the previous chapter showed that loss of Ino1 in *Dictyostelium* cells leads to inositol auxotrophy, highlighting the importance of inositol in cell growth and development, and reproducing the “inositol-less death” phenotype (Culbertson and Henry, 1975; Fischbach et al., 2006). Inositol has been shown to be important for a vast number of cellular functions, including cell adhesion, cytokinesis, autophagy, and cell movement (Criollo et al., 2007; Europe-Finner et al., 1989; Fischbach et al., 2006; Logan and Mandato, 2006; Mayer and Tomlinson, 1983; Sarkar and Rubinsztein; Sarkar et al., 2005; Schiebler et al., 2015; Steger et al., 2003; Vicencio et al., 2009; Yorek et al., 1993; Zhang et al., 2012). Indeed, a genome-wide screen for non-lethal mutations causing inositol auxotrophy in *S.cerevisiae* found 419 genes (Villa-García et al., 2011), whereas the presence of inositol repressed the expression of 32 genes and choline repressed the expression of 93 genes (Jesch et al., 2005). Thus, inositol depletion can have a variety of cellular responses that could arise due to alteration of signalling pathways.

Analysis of an inositol auxotrophic strain of *Dictyostelium* during inositol starvation revealed a decrease in inositol, a change in phosphoinositide levels, and the build-up of a glycolysis metabolite, 2,3-bisphosphoglycerate (Fischbach et al., 2006). Inositol depletion may also disturb the turnover of inositol phosphate to phosphoinositide, which can have an impact on vital processes like nutrient consumption (Azab et al., 2007). Phosphoinositides are synthesised in the endoplasmic reticulum and transported to other membranes within the cell, either by vesicular transport or via transfer proteins (De Camilli et al., 1996). Phosphoinositides are critically involved in a range of cellular functions, including phospholipid

synthesis, the UPR (unfolded protein response), protein secretion, signalling events in cellular compartments, motility, and intracellular membrane trafficking (Balla, 2001; Brill et al., 2011b; Cremona and De Camilli, 2001; Peracino et al., 2010; Sbrissa et al., 2007; Walter and Ron, 2011). Since inositol is a precursor to a family of phosphoinositides, its removal is predicted to have an impact on *Dictyostelium* cell physiology and metabolism, as was previously demonstrated in yeast (Gaspar et al., 2006; Villa-García et al., 2011). For example, phosphoinositide 4,5 bisphosphate (PIP2), which is associated predominantly with intracellular membranes, plays a role in cell substrate adhesion and cytokinesis (Brill et al., 2011b; Logan and Mandato, 2006). PIP2 and PIP3 also activate a variety of effector proteins by targeting them to specific membrane locations, where they activate signal transduction pathways, and have important roles in cell movement during development (Dormann et al., 2004; Dowler et al., 2000; Nichols et al., 2015; Stephens et al., 2008).

Inositol is synthesised *de novo* in cells by the Ino1 enzyme, and thus the loss of the protein, which leads to inositol auxotrophy, can have a potential effect on cell physiology and metabolism. The current understanding of the role of Ino1 is based on its catalytic activity as an isomerase that converts glucose 6-phosphate to inositol 3-phosphate (Kofman and Belmaker, 1993), and few studies have differentiated between a loss of the Ino1 enzyme and inositol depletion. These aspects of inositol biology have not been examined in *Dictyostelium*. This chapter describes an investigation of the physiological and metabolic effects of inositol depletion and the loss of Ino1 protein in *Dictyostelium*.

5.2 Intracellular inositol levels during inositol starvation

Loss of Ino1 is predicted to block the *de novo* biosynthesis of inositol, and is therefore likely to affect intracellular inositol levels. To test this prediction, inositol levels were measured in the *ino1*$^{-}$ mutant during inositol supplementation and starvation. Inositol levels were quantified by NMR in the *ino1*$^{-}$ and wild-type cells, in the presence or absence of exogenous inositol

(Dr S. Claus and C. Le Roy, University of Reading) (Figure 5.1). Wild-type cells grown without inositol supplementation contained 1.5 ± 0.1 µM inositol, which increased significantly to 3.4 ± 0.1 µM following supplementation with inositol (500 µM, $p < 0.0001$), and returned to the baseline level of 1.5 ± 0.1 µM after 12-hour inositol removal. *Ino1*$^-$ cells grown with inositol supplementation had an inositol level of 1.8 ± 0.1 µM, which was slightly higher than the 1.6 ± 0.1 µM present in wild-type cells grown without exogenous inositol (control); the value for *ino1*$^-$ cells significantly decreased to 0.8 ± 0.1 µM following the removal of exogenous inositol for 12 hours ($p = 0.0013$). The reduced inositol level was maintained at 24-hour post inositol removal at 1.2 ± 0.1 µM, and returned to 2.0 ± 0.1 µM following the re-introduction of inositol. These data show that, in *ino1*$^-$ cells, inositol was depleted following withdrawal of exogenous supply. Additionally, wild-type *Dictyostelium* cells were demonstrated to take up inositol from extracellular sources even when inositol is already produced by these cells.

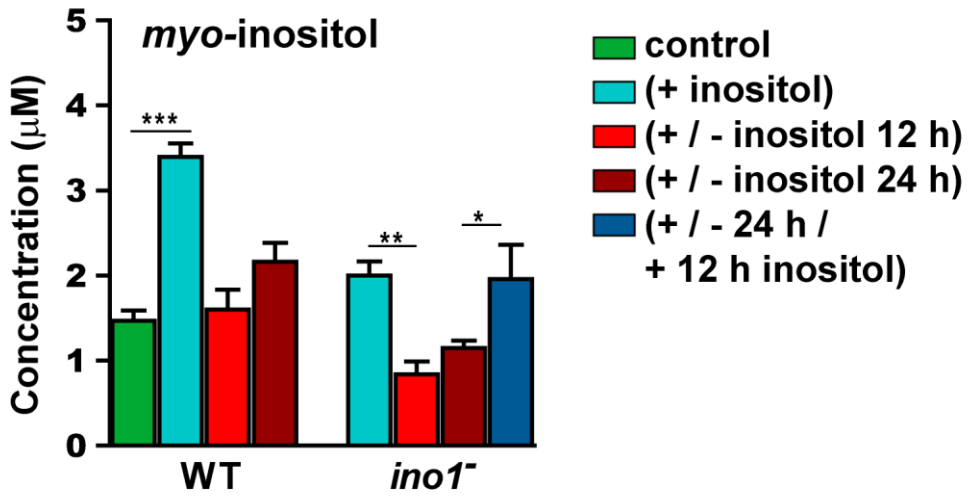

Figure 5.1 The effect of inositol depletion on intracellular inositol concentration. To analyse inositol levels in wild-type and *ino1*$^-$ cells, the cells were grown in the presence of inositol (500 µM, denoted '+'), the absence of inositol (12h or 24h; denoted '+/-') or in inositol added (500 µM for 12h) after a 24-hour depletion period (denoted '+/-/+'). Inositol levels were measured by NMR. The level of inositol was reduced following inositol depletion for 12 or 24 hours in the *ino1*$^-$ mutant, and restored to basal levels following reintroduction for 12 hours. Statistical analysis was carried out between two groups using unpaired two-tailed student's *t*-test; *$p < 0;05$, **$p < 0.01$, ***$p < 0.001$; n = 4 independent technical repeats. The work presented here was done in collaboration with Dr S P Claus and C. Le Roy, University of Reading.

5.3 Cell viability and adhesion

Dictyostelium cell viability is often assessed by counting plaques formed on bacterial lawns. However, this method could not be used since *ino1*$^-$ cells were unable to grow on bacteria. As an alternative approach to determine cell viability during inositol depletion, experiments were performed where the cells were stained with vital dyes. Two dyes were used to analyse cell viability: fluorescein diacetate (FDA) and propidium iodide (PI). In these experiments, live cells convert the non-fluorescent FDA into a fluorescent compound (fluorescein), providing an indication of viability. In an alternative approach, PI is added to cells, and enters dying cells that have damaged membranes, and stains the cell nucleus with a red fluorescent signal, which is a sign of cell death. However, both of these approaches were unsuccessful, since FDA was not converted to fluorescein by all the live cells, and PI did not appear to stain all the dead cells. Therefore, no direct measure of loss of cell viability as a result of deletion of Ino1 was possible.

Loss of cell adhesion has been previously linked to inositol depletion (Fischbach et al., 2006; Zhu et al., 2015). To monitor this effect in *Dictyostelium*, the number of cells that remained attached to culture plates following the removal of exogenous inositol was assessed over a period of 72 hours (Figure 5.2). In the presence of 500 µM inositol, *ino1*$^-$ cells proliferated and remained adherent (Figure 5.2). However, the removal of exogenous inositol caused a decrease in cell density to 88.5% after 24 hours and to 33.5% after 72 hours (compared to *ino1*$^-$ + inositol condition). *Ino1*$^-$ cells expressing *ino1-RFP* initially grew to a significantly higher density than the *ino1*$^-$ mutant cultured in the presence of exogenous inositol. However, after 46 hours, cell density started to decrease, reaching a number similar to that of *ino1*$^-$ cells grown in the presence of inositol. These experiments showed that initially the number of adherent *ino1*$^-$ cells increased, and then after 24 hours of inositol depletion rapidly started to decrease, suggesting that the absence of inositol triggered a loss in substrate adhesion. The 24-hour time point was used for analysing the effects of inositol starvation on the *ino1*$^-$ cells in subsequent experiments.

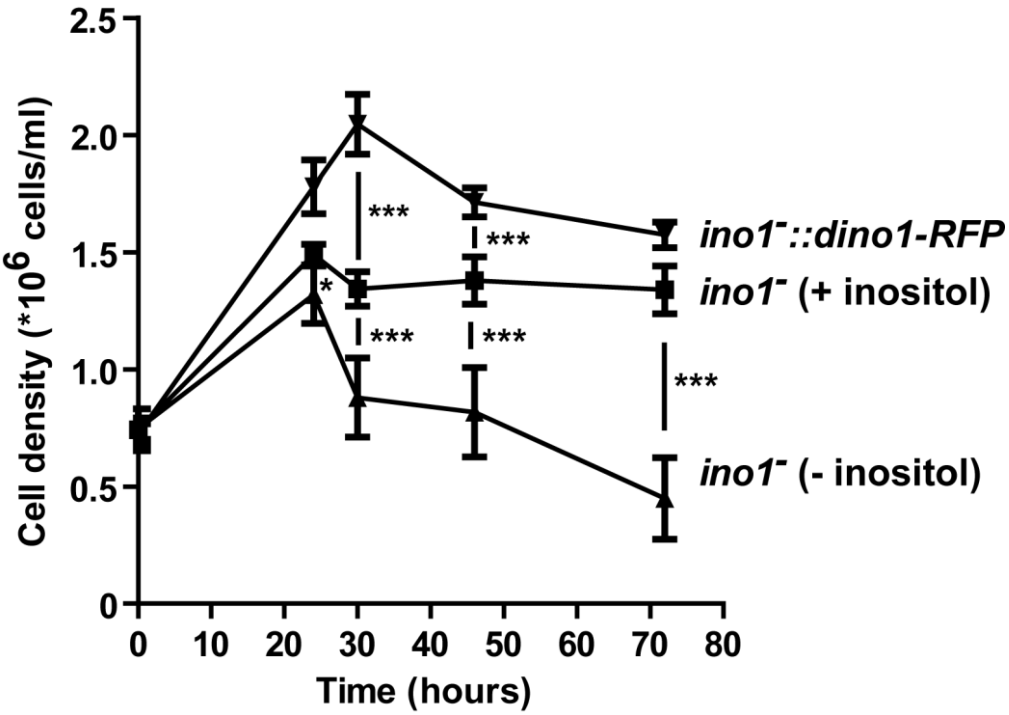

Figure 5.2 The effect of inositol depletion on cell-substrate adhesion in *ino1*⁻ cells. Cell adhesion was monitored in wild-type and *ino1*⁻ cells, and in *ino1*⁻ cells expressing *ino1-RFP*, in the presence (500 µM) and absence of inositol for at least 24 hours. The medium was gently removed and the cells detached from the surface of the dish by pipetting. The detached cells were counted to obtain cell density. *Ino1*⁻ cells grown in the absence of inositol started to lose substrate adhesion after 24 hours following inositol removal. Supplementation of growth media with 500 µM inositol or *ino1-RFP* overexpression resulted in cells remaining adherent to the dishes. Statistical significance was determined for each individual time point in separate test by an unpaired two-tailed student's *t*-test; **p* < 0.05, ****p* < 0.001, *ino1*⁻*::dino1-RFP* was compared to *ino1*⁻ (+inositol) and to *ino1*⁻ (+inositol) to *ino1*⁻ (-inositol); n = 3 technical repeats; 1 biological replicate.

5.4 Cytokinesis

Dictyostelium cells grow by nutrient consumption followed by cell division, where during the process of cytokinesis the nuclei and cytoplasm of a dividing cell are separated into two daughter cells (Robinson et al., 2002). Since *ino1*⁻ cells grew at a slower rate than the wild-type cells, the effect of inositol depletion on cytokinesis was examined. In this experiment, cells were grown in shaking suspension with or without inositol (500 µM). Wild-type or *ino1*⁻ cells were stained with DAPI to visualise and count the number of nuclei per cell (Figure 5.3) (Pakes et al., 2012). In these experiments, the majority of wild-type cells (90%) had one or two nuclei per cell, with 10% of cells having ≥3 nuclei. The *ino1*⁻ cells, however, showed a significant increase (*p* <

0.001) in the nuclei number following inositol depletion compared to the wild-type strain. In the absence of inositol, 24.7% of the *ino1*⁻ cells accumulated ≥3 nuclei, compared to 7.7% for the wild-type cells. This effect was rescued by growing cells in the presence of 500 µM inositol (9.7% of the *ino1*⁻ cells accumulated ≥3 nuclei) or by overexpressing *ino1-RFP* in these cells (10% of the *ino1*⁻*::dino1-RFP* cells accumulated ≥3 nuclei) (Figure 5.3 B). These data suggest that inositol depletion leads to a reduction in cytokinesis.

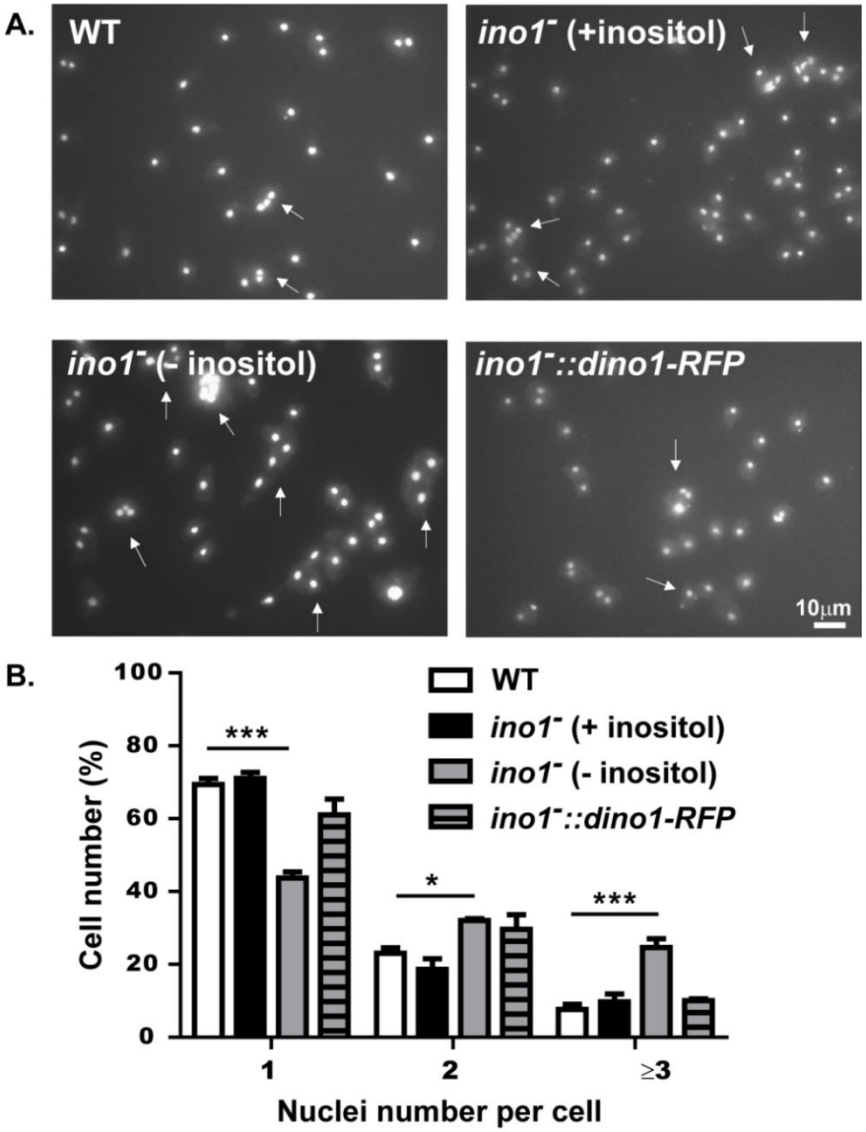

Figure 5.3 Inositol depletion leads to a cytokinesis defect. Wild-type and *ino1*⁻ mutant cells were grown in liquid medium +/- exogenous inositol (500 µM). The *ino1*⁻ cells were kept in the medium without inositol for 24 hours prior to image acquisition. Cells were fixed with methanol and stained with DAPI. (A) Stained cell nuclei were visualised in the wild-type, the *ino1*⁻, and *ino1*⁻*::dino1-RFP* cells and (B) quantified in the presence or absence (24 hours) of inositol treatment using the ImageJ software. Error bars represent SEM. Statistical significance was determined by 2-way ANOVA with Bonferroni post-test, *$p < 0.05$, ***$p <$ 0.001 and difference presented to wild-type control; n ≥ 250 cells analysed per condition from 3 independent technical repeats, 1 biological replicate.

5.5 Autophagy

Autophagy is a biological process that leads to the degradation and recycling of cellular material (Mesquita et al., 2013). During autophagy, cellular components are engulfed inside autophagosomes, which then fuse with lysosomes to degrade the engulfed cell material. Stress conditions, including nutrient depletion, can trigger autophagy (Kosta et al., 2004). For this reason, the effect of inositol depletion on the number of autophagosomes being formed in the *ino1*$^-$ cells was assessed.

In *Dictyostelium*, the formation of autophagosomes can be visualised by the incorporation of fluorescently-tagged autophagy-related protein 8 (Atg8) into autophagosomal membranes (Otto et al., 2003). In the following experiment, wild-type and *ino1*$^-$ cells were grown in the presence of exogenous inositol (500 µM) or in the absence of inositol (24 hours in the case of the *ino1*$^-$ mutant). Live images were acquired using a fluorescence microscopy, and the number of autophagosomes per cell was quantified (Figure 5.4).

Autophagosome number per cell was similar between the *ino1*$^-$ cells (1.4 autophagosomes per cell) and wild-type cells (1.1 autophagosomes per cell) when both strains were grown in the presence of inositol (500 µM) and to the wild-type cells grown in the absence of inositol (2.0 autophagosomes per cell) (Figure 5.4 A,B). Inositol starvation led to a nearly four–fold increase in the autophagosome number per cell in the *ino1*$^-$ cells (7.0 autophagosomes per cell) as compared to the wild-type (2.0 autophagosomes per cell) when both strains were grown for 24 hours in the absence of inositol, while the cell size of both strains remained comparable (average cell area: *ino1*$^-$ = 123 µm^2; wild-type = 147 µm^2) (Figure 5.3 B,C). These data suggest that *ino1*$^-$ cells lacking inositol exhibit an autophagic response.

Interestingly, the growth of both wild-type and the *ino1*$^-$ cells in medium containing added inositol (500 µM) led to a decrease in cell area (average cell area: *ino1*$^-$ without inositol = 123 µm^2, and with inositol = 92

μm^2; wild-type without inositol = 147 μm^2, and with inositol = 107 μm^2) (Figure 5.4 C). No significant difference was found in the cell area between the wild-type and the *ino1*$^-$ cells.

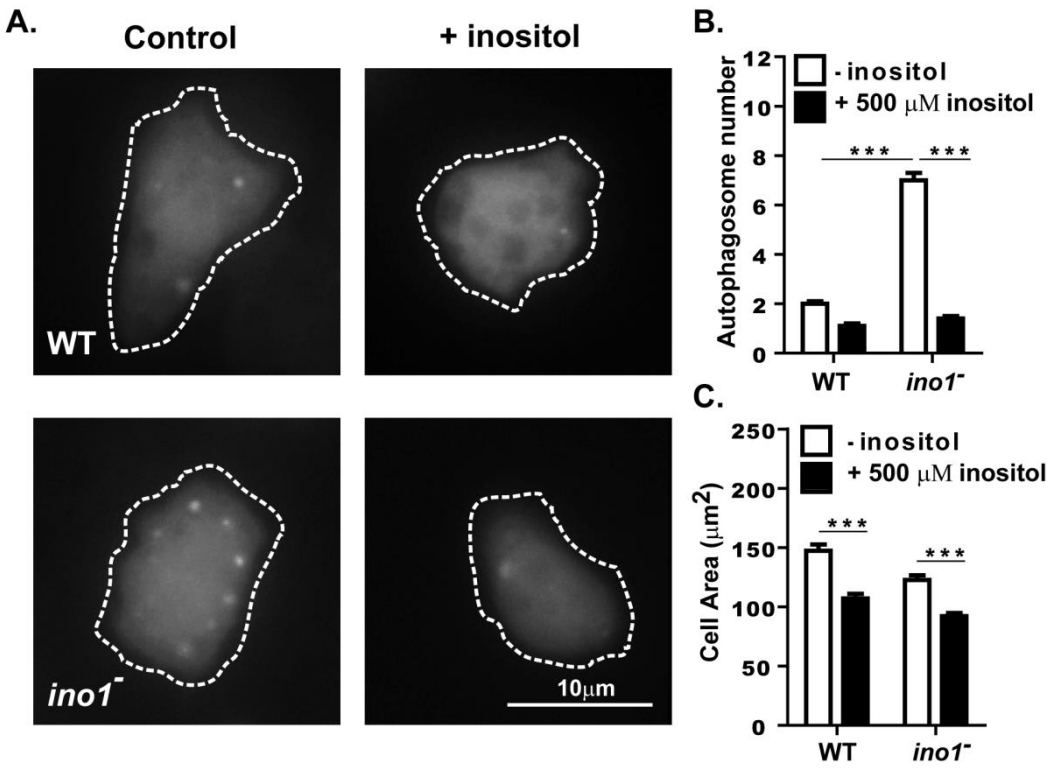

Figure 5.4 The effect of inositol depletion on the accumulation of autophagosomes. Wild-type and *ino1*$^-$ cells were grown in liquid medium +/- exogenous inositol (500 µM). The medium was changed to LowFlo medium (Formedium) for approximately 16 hours to minimise the background fluorescence. The *ino1*$^-$ cells were kept in the medium without inositol for 24 hours prior to image acquisition. (A) Autophagosomes were visualised in the wild-type and the *ino1*$^-$ cells expressing atg8-GFP and (B) quantified in the presence or absence (24 hours) of inositol treatment using the ImageJ software. (C) Cell size was quantified by measuring the surface area with the ImageJ software. Error bars represent SEM. Statistical significance was determined by a two-tailed student's *t*-test; ***$p < 0.001$; n ≥ 117 cells analysed per condition from 3 independent technical repeats, 1 biological replicate.

5.6 Chemotaxis towards cAMP

Cell migration and adhesion play important roles in *Dictyostelium* development, where cells initiate aggregation and form multicellular fruiting bodies when the food is depleted (Loomis, 2014). Chemotaxis is the oriented movement of cells in response to a chemical gradient. During the early stages of development, *Dictyostelium* cells release a chemoattractant, cAMP,

that is sensed by neighbouring cells, prompting these cells to initiate movement along the gradient towards the source of the chemical (Schaap and Wang, 1986). Since cell adhesion and development were impaired in the *ino1*$^{-}$ mutant deprived of inositol, the ability of these cells to chemotax was assessed.

Chemotaxis towards cAMP was measured in a Dunn Chamber (Zicha et al., 1991). Aggregation-competent cells were subjected to a cAMP (5 µM) gradient in a Dunn chamber over a 12-minute period, and cell movement was analysed with Image Pro 6.3 software to determine the velocity (µm/min), aspect (roundness) and persistence (Figure 5.5 & Table 5.1). Aspect refers to a ratio between X and Y axes of a cell; an aspect of 1 indicates a perfectly round cell and an aspect greater than 1 indicates an elongated (polarised) cell. Persistence of a cell is the ratio of the distance between the start and endpoints and the total length of the track for the cell, and indicates directionality of the movement, 1 being straight. Under these conditions, the wild-type chemotaxing cells had a constant velocity (8.73 µm/min), an average aspect of 2.96 and persistence of 0.917, indicating that these cells moved in a straight line towards the cAMP source (Figure 5.5 & Table 5.1). The *ino1*$^{-}$ mutant cells grown in the presence of inositol (500 µM) were also able to move with a similar velocity (6.79 µm/min). In contrast, *ino1*$^{-}$ cells grown in the absence of inositol showed decreased velocity (4.42 µm/min, $p < 0.001$) compared to wild-type cells (Figure 5.5 & Table 5.1). In addition, analysis of the aspect of *ino1*$^{-}$ and wild-type cells suggested that *ino1*$^{-}$ cells were significantly more round. These experiments showed that the addition of exogenous inositol corrected the reduced velocity of the *ino1*$^{-}$ cells; however, the less polarised cell shape was not rescued by exogenous inositol.

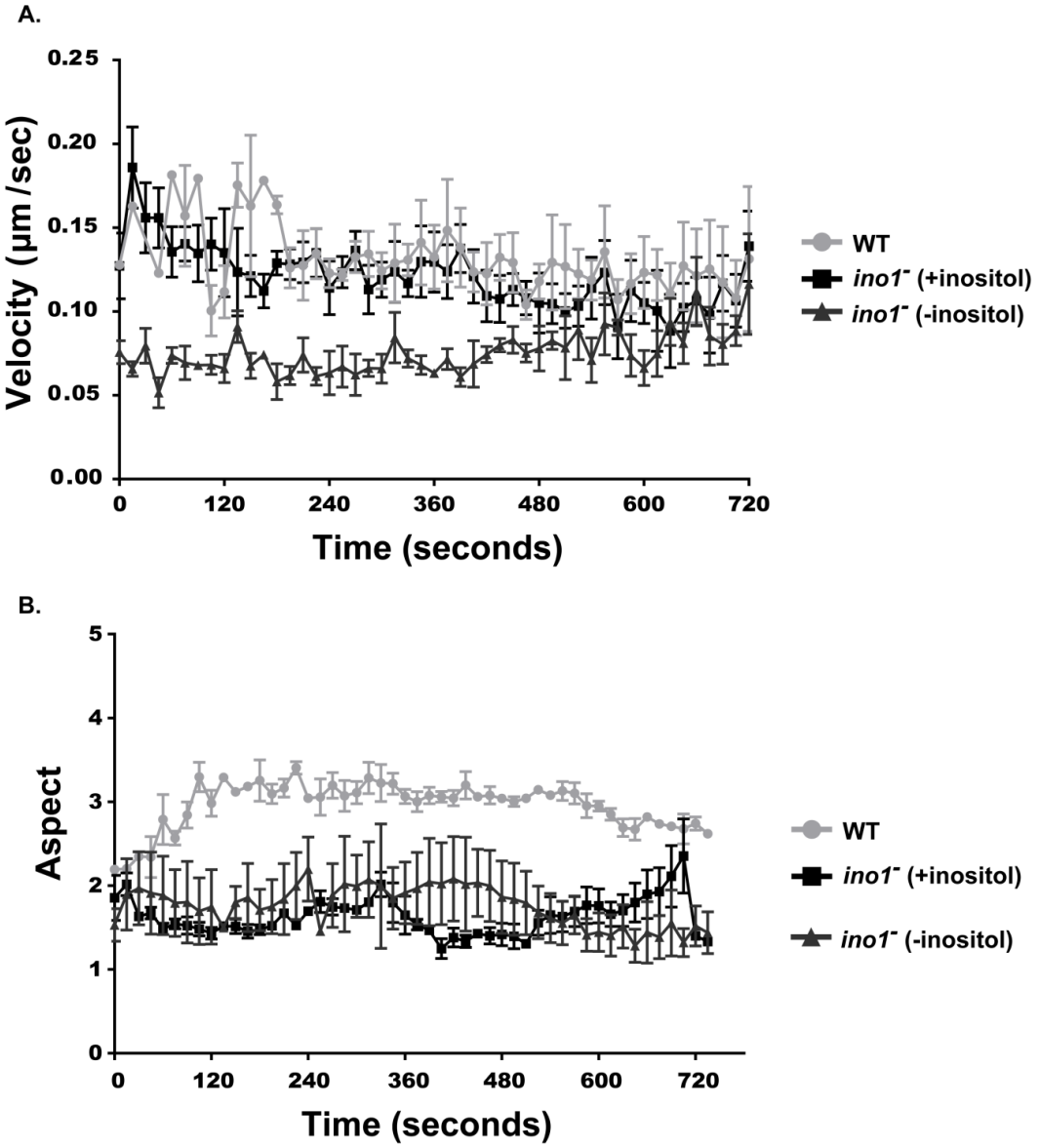

Figure 5.5 The effect of inositol depletion and Ino1 loss on chemotaxis. The movement of aggregation-competent *ino1*$^{-}$ cells, grown in medium with inositol (500 µM), or without inositol for 24 hours, towards cAMP (5 µM) in a Dunn chamber was recorded by time-lapse imaging over a 12-minute period (1 image taken every 15 seconds). Image Pro 6.3 software was used to capture the recording and to analyse cell movement. (A) Plots showing the velocity of the wild-type and *ino1*$^{-}$ strains. (B) Analysis of the aspect (roundness) of the wild-type and *ino1*$^{-}$ cells. n ≥ 20 cells analysed per condition from 3 independent technical repeats, 1 biological replicate.

Strain	Velocity (µm/min)	Aspect	Persistence
WT (Ax2)	8.73	2.96	0.917
***ino1*⁻ (+inositol)**	6.79	1.63 (***)	1.177
***ino1*⁻ (-inositol)**	4.42 (*** / +)	1.76 (*** / ++)	1.809 (*)

Table 5.1 Average velocity, aspect and persistence of *ino1*⁻ cells during chemotaxis towards cAMP. Aggregation-competent *ino1*⁻ cells were grown with or without inositol (500 µM) for 24 hours, and their movement towards cAMP (5 µM) in a Dunn chamber was recorded using time-lapse imaging over a 12 minute period (1 image taken every 15 seconds). Image Pro 6.3 software was used to capture the recording and to analyse cell movement. Velocity shows the distance travelled by cells over time. Aspect refers to the roundness of cells (1 = perfectly round). Persistence is a measure of distance travelled by a cell over the total distance to travel towards the chemoattractant (1 mm bridge distance in a Dunn chamber). Statistical significance was determined by an unpaired two-tailed student's *t*-test; *****$p < 0.05$, *******$p < 0.001$ for the comparison between wild-type and *ino1*⁻ cells; $^{+}p < 0.05$, $^{++}p < 0.01$ for the comparison between *ino1*⁻ cells +/-inositol; n = 9 cells quantified per condition from 3 independent technical repeats, 1 biological replicate.

5.7 Metabolic profile of the *ino1*⁻ mutant

Inositol plays a key role in a range of cellular processes and is a necessary constituent of a number of signalling chemicals (Deranieh and Greenberg, 2009). Thus, a reduction in the production of inositol would likely have a broad impact on cell metabolism. To investigate the potential metabolic changes caused by loss of Ino1, the metabolic profile of the wild-type (Ax2) and *ino1*⁻ mutant cells was obtained (collaboration with Dr S.P. Claus and C. Le Roy, The University of Reading). In these experiments, *ino1*⁻ and wild-type cells were grown in the presence or absence of inositol (500 µM) for 12 or 24 hours to monitor changes caused by reduced inositol availability. In addition, following inositol removal (24 hours), inositol was re-introduced (500 µM, 12 hours) to the growth medium, in order to assess any changes caused by inositol rescue.

The metabolic consequences of inositol depletion were assessed by comparing the metabolic profiles of wild-type and *ino1*⁻ cells under different inositol treatment conditions (Figure 5.6). Both ablation of *ino1* and inositol

treatment induced specific metabolic changes. Principal component analysis (PCA) of metabolic profiles indicated that the greatest metabolic change between the wild-type and *ino1*$^{-}$ cells was independent of exogenous inositol supplementation. *Ino1* ablation accounted for 53% and inositol treatment for 12% of the total variance as observed in PCA (Figure 5.6 A). Ino1 loss resulted in an increase in amino acids and compounds related to amino acid breakdown (alanine, aspartate, isoleucine, lysine, methionine, GABA, putrescine), in energy-related metabolites (fumarate, lactate), in adenosine phosphorylated derivatives (5'-AMP, 3'-AMP, ATP, cAMP), and in sn-glycero-3-phosphocholine (GPC) (Figure 5.6 B). Inositol treatment resulted in an increase in the amino acids phenylalanine, leucine, methionine, and tyrosine (Figure 5.6 C). Metabolic profile analysis thus suggested a vital role of the Ino1 protein in metabolic regulation in *Dictyostelium*, with only minor changes in metabolite levels associated with inositol depletion.

The distribution of data points (circles denoting wild-type and triangles denoting *ino1*$^{-}$ mutant) along the X-Y axes on the PC plot shown in figure 5.8A informs about the similarity between these cell lines under the different treatment conditions (the closer the data points are along a given axis, the more similar the metabolic profile is under the given conditions). Inositol treatment did not have a major metabolic impact on wild-type cells since treating wild-type cells (control) with inositol (+inositol) did not increase the metabolic distance between these two conditions (Figure 5.6 A). Interestingly, re-introduction of inositol for 12 hours after a 24-hour inositol depletion period made the metabolic profile of the *ino1*$^{-}$ cells under the +/-/+inositol condition more similar to the metabolic profile of the wild-type (control) than the metabolic profile of the *ino1*$^{-}$ cells grown with inositol supplementation (+inositol) (Figure 5.6 A).

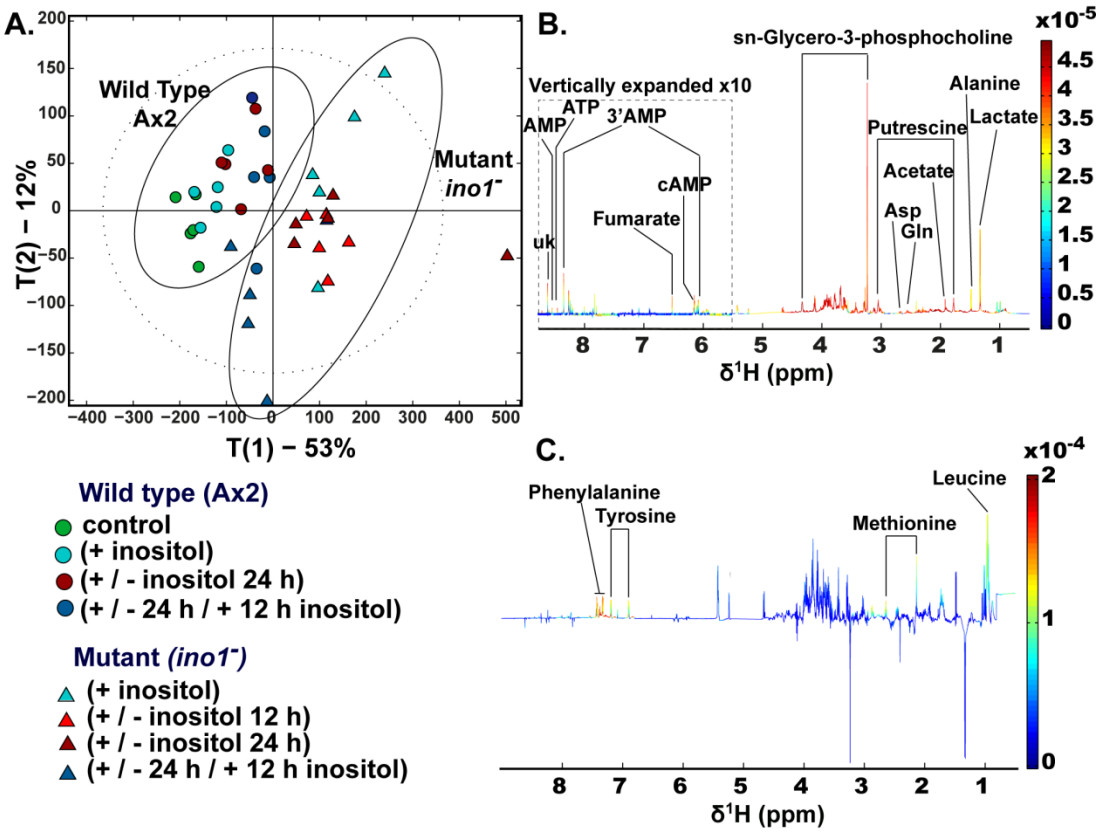

Figure 5.6 Comparison of the metabolic profiles of wild-type and *ino1*⁻ mutant cells during inositol depletion. To monitor the metabolic profiles of the wild-type and *ino1*⁻ mutant, the cells were grown in the presence of inositol (500 µM, denoted +inositol), the absence of inositol (for 12 or 24h denoted +/-), or in inositol added after 24h depletion period (500 µM for 12h denoted +/-/+ 12h). Control, shown in green, refers to the wild-type cells grown without inositol. Metabolic analysis was performed with Nuclear Magnetic Resonance (NMR). (A) Metabolic variations existing between cell type and inositol exposure were assessed by principal component analysis (PCA) generated from the ^{1}H-NMR spectra of the *Dictyostelium* metabolic fingerprints. The main source of variation (53%) was driven by the mutation while inositol depletion accounted for approximately 12% of the metabolic variation in this dataset. (B) Loadings plot associated with PC1 (red peaks pointing upwards are positively associated with PC1 while those pointing downwards are negatively associated with PC1). (C) Loadings plot associated with PC2. The work presented here was done in collaboration with Dr S.P. Claus and Caroline Le Roy, University of Reading. n = 4 independent technical repeats, 1 biological replicate; samples were prepared with 2 x 10^{7} cells per condition

Since Ino1 absence resulted in a major change in the metabolic profile of *Dictyostelium* cells, the specific metabolic fluctuations were analysed using orthogonal projections to latent structures discriminant analysis (O-PLS DA) to provide a statistical method for multivariate data. O-PLS removes variation from X (descriptor variables) that is not correlated to Y (property variables). Initially, the *ino1*⁻ (+inositol) metabolic profile was compared against the wild-type metabolic profile using analysis that took mutation as a predictor of the

difference. As seen in plot A, the scores associated with the metabolic profiles of the wild-type and *ino1*$^-$ cells group separately, indicating that the *ino1* ablation caused a significant change in the *Dictyostelium* metabolic profile (R^2Y = 0.89, Q^2Y = 0.88 and *p* value for 500 random permutations = 0.002) (Figure 5.7). No effect on the metabolic profile was seen due to the selection antibiotic (blasticidin) for the *ino1*$^-$ cells (O-PLS model parameters: R^2Y = 0.18 and Q^2Y = 0). Analysing the levels of the individual metabolites (Figures 5.7 B & 5.8) confirmed that Ino1 loss was associated with a significant increase in the amino acids alanine, aspartate, glycine, GABA, isoleucine, lysine, and methionine, in metabolites associated with the regulation of cell cycle and DNA metabolism, including guanosine, ATP, deoxy-ADP, 5'AMP, 3'AMP, UTP, β-alanine (a biomarker of the degradation of pyrimidines) (Di Meo et al., 2015) and sn-glycero-3-phosphocholine (GPC). Also, the levels of putrescine, lactate, acetate, fumarate and succinate were significantly increased.

The impact of inositol depletion on the metabolic profile of the *ino1*$^-$ mutant was also analysed. *Ino1*$^-$ cells grown in the presence of inositol and starved of inositol for up to 24 hours were compared for metabolic differences (Figures 5.7 C,D). The scores generated by this O-PLS DA model, where inositol depletion was used as a predictor of the difference, were seen to group separately on the plot presented in Figure 5.7 C, indicating that inositol depletion had an impact on the metabolic profile of the *ino1*$^-$ mutant (R^2Y= 0.67, Q^2Y=0.51 and *p* value for 500 permutations = 0.002). However, inositol depletion had less of an impact compared to Ino1 loss on *Dictyostelium* metabolic profile, since the distance between the scores representing *ino1*$^-$ +/-inositol groups (Figure 5.7 C) is smaller than between the scores representing wild-type and *ino1*$^-$ groups (Figure 5.7 A).

Finally, the effect of a re-introduction of inositol after a 24-hour starvation period was assessed in the *ino1*$^-$ mutant (Figure 5.7 E,F). The O-PLS DA analysis was performed where the metabolic effect of the absence of inositol for up to 24 hours was compared against the effect of inositol re-supplementation. The score grouping on the plot in Figure 5.7 E indicates

that inositol re-introduction greatly altered the metabolic profile of the *ino1*$^-$ cells (R2Y = 0.90, Q2Y = 0.86 and *p* value for 500 permutations = 0.002). This mirrors the findings presented in Figure 5.6 A, where inositol re-supply shifted the *ino1*$^-$ metabolic profile to resemble that of the wild-type. Since inositol supplementation after a period of starvation, rather than constant growth in inositol supplemented medium, caused the *ino1*$^-$ metabolic profile to be closer to that of the wild-type, this result suggests that inositol acted as a switch to re-set the metabolic state of the *ino1*$^-$ cells.

In contrast to the loss of Ino1, inositol depletion caused limited changes to the *Dictyostelium* metabolic profile. Comparing *ino1*$^-$ cells grown in the presence or absence of inositol, it was seen that inositol supplementation led to an increase of inositol, glycogen, glucose and lipids, and a decrease in succinate and lactate (Figure 5.7 D); comparing inositol depletion to inositol re-introduction, it was seen that inositol depletion caused an increase in amino acids tyrosine, phenylalanine and isoleucine, and the compounds sn-glycero-3-phosphocholine, maltose, acetate, formate, lactate and putrescine (Figure 5.7 F). Supervised analysis to evaluate the general impact of inositol depletion on individual metabolites was conducted (Figure 5.8), and suggested that inositol depletion resulted in changes in some amino acids (increases in alanine, GABA, glycine, valine, and a decrease in phenylalanine), an increase in lactate, fumarate, and succinate, and a decrease in 3'AMP, guanosine and glycogen (Figure 5.8). Although it was observed that the *ino1*$^-$ mutant was already in a catabolic state, the addition of inositol lessened this phenotype, since markers of anabolism (glycogen and lipids) were higher in cells supplemented with inositol, while those not supplemented were associated with markers of catabolism (lactate and succinate). Overall, the metabolic profile analysis suggests that the absence of Ino1 rather than inositol depletion triggered broad metabolic changes, while inositol supplementation lessened the impact of these changes.

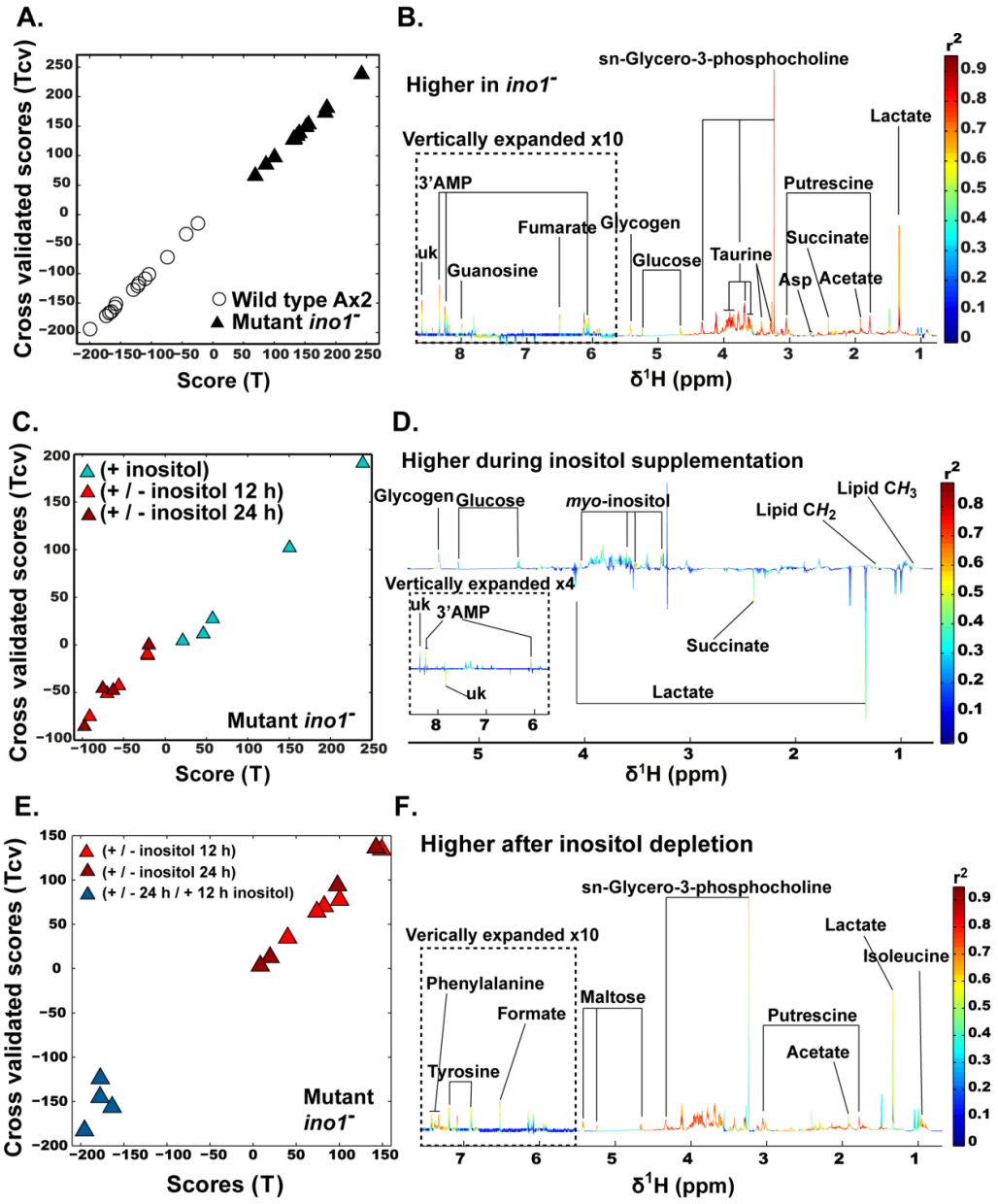

Figure 5.7 Comparative analysis of the metabolic profile of the *ino1*⁻ mutant under different inositol treatment conditions. Extended analysis of the metabolic profile was performed using NMR. (A,B) Metabolic changes induced by *ino1* ablation to determine the specific impact of the mutation on cell metabolism. (A) Plot of the scores against the cross validated scores generated by the O-PLS DA (R^2Y = 0.89, Q^2Y = 0.88 and *p* value for 500 random permutations =0.002) using the ^{1}H-NMR spectra of the wild-type and *ino1*⁻ cells (except +/-/+inositol condition) as a matrix of independent variables and mutation as a predictor. (B) Loadings plot associated with O-PLS DA model. Peaks in red indicate increased metabolite levels in response to the mutation. (C,D) Metabolic changes induced by inositol treatment in the *ino1*⁻ mutant. (C) Plot of the scores against the cross validated scores generated by the O-PLS DA (R^2Y = 0.67, Q^2Y = 0.51 and *p* value for 500 permutations = 0.002) using the ^{1}H-NMR spectra of the *ino1*⁻ cells (-12h & -24h inositol vs +inositol) as a matrix of independent variables and depletion of inositol as a predictor. (D) Loadings plot associated with the O-PLS DA model. Peaks in red indicate increased metabolite levels in response to inositol presence. (E,F) Re-introduction of inositol post-deprivation induces a metabolic shift. (E) Plot of the scores against the cross validated scores generated by the O-PLS DA (R^2Y = 0.90, Q^2Y = 0.86 and *p* value for 500 permutations = 0.002) using the ^{1}H-NMR spectra of the *ino1*⁻ cells (-12h and -24h inositol vs

+/-/+inositol) as a matrix of independent variables and inositol re-introduction as a predictor. (F) Loadings plot associated with the O-PLS DA model. Peaks in red indicate increased metabolite levels in response to the depletion of inositol. The work presented here was done in collaboration with Dr S.P. Claus and C. Le Roy, University of Reading. n = 4 independent technical repeats, 1 biological replicate; samples were prepared with 2 x 10^7 cells per condition.

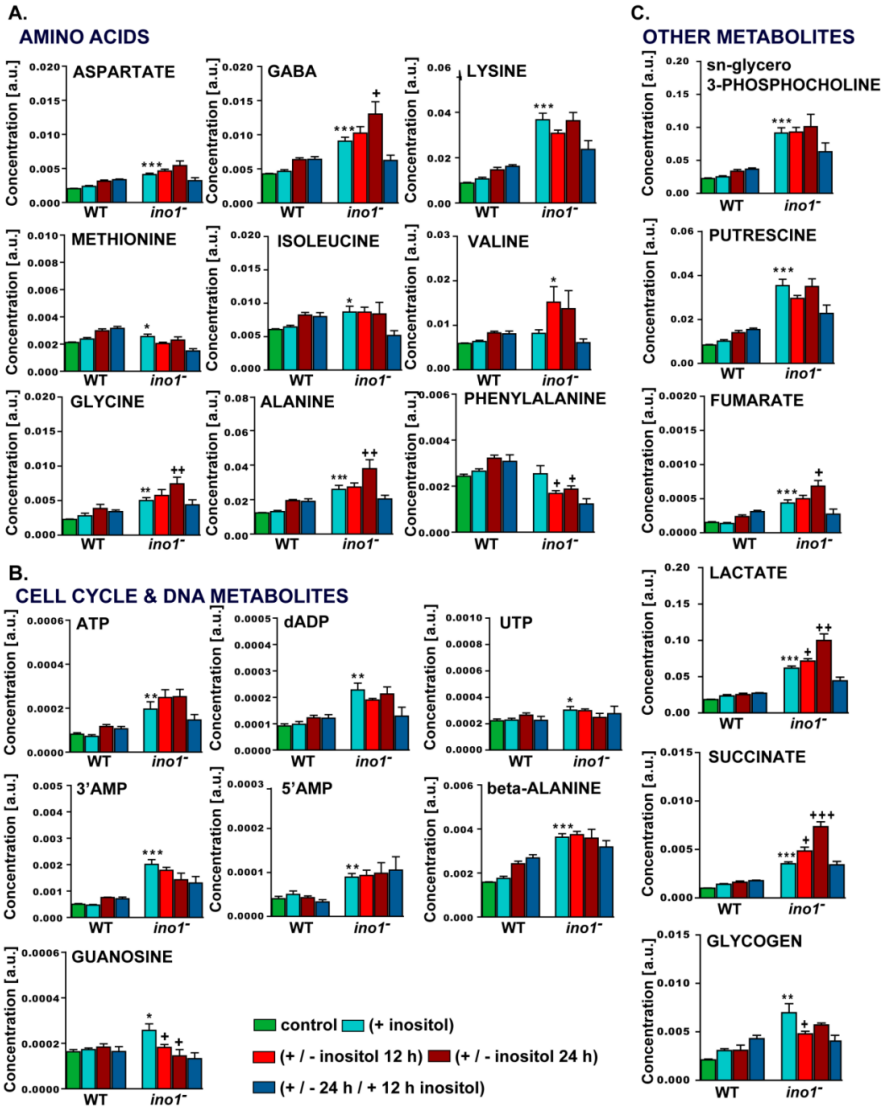

Figure 5.8 Levels of metabolites in the wild-type and *ino1*$^-$ cells grown under different inositol conditions. Metabolite levels were measured by NMR, quantified using MATLAB, and plotted using GraphPad Prism 5.02. The changes observed in wild-type and *ino1*$^-$ cells were measured for (A) amino acids, (B) cell cycle- and DNA-related metabolites, and (C) other metabolites. Control, shown in green, refers to the wild-type cells grown without inositol. Statistical analysis was carried out between wild-type (Ax2) (+inositol) and *ino1*$^-$ (+inositol) by unpaired two-tailed student's *t*-test to illustrate the significance of changes due to the loss of Ino1 protein, shown as "*", ***p* < 0;05, ****p* < 0;01, *****p* < 0;001; A separate unpaired two-tailed student's *t*- test was used to compare *ino1*$^-$ (+inositol) and *ino1*$^-$ (-inositol 12h and 24h), shown as "$^+$", $^+p < 0.05$, $^{++}p < 0.01$, $^{+++}p < 0.001$. The work presented here was done in collaboration with Dr S.P. Claus and Caroline Le Roy, University of Reading. n = 4 independent technical repeats, 1 biological replicate; samples were prepared with 2 x 10^7 cells per condition.

5.8 Phosphoinositide levels during inositol depletion

Inositol is a precursor to a family of membrane phospholipids (Seelan et al., 2009b). Thus, the inositol depletion phenotype described here enabled an analysis of the effect of reduced inositol levels on phosphoinositide levels (in collaboration with Dr J. Clark and Dr P. Hawkins, Babraham Institute, Cambridge). Two types of phospholipids are present in *Dictyostelium*, diacyl phospholipids containing two acyl linkages to the glycerol backbone, and the recently reported ether/acyl phospholipids containing a glycerol backbone linked to a fatty alcohol at position 1 (Clark et al., 2014) (Figure 5.9 A). Both types of phospholipids form separate pools of glycerophospholipids, synthesised from glucose, as exemplified by the pathway for the diacyl-linked species (Figure 5.9 B). Phosphatidic acid (PA) and CDP-DAG are precursors of phosphatidylserine (PS), phosphatidylethanolamine (PE), and phosphatidylcholine (PC), or phosphatidylinositol (PI) when combined with inositol. There are different forms of PIs, depending on the phosphorylation state of these molecules: phosphatidylinositol monophosphate (PIP), phosphatidylinositol bisphosphate (PIP2) and phosphatidylinositol trisphosphate (PIP3) (Figure 5.9 B). Diacyl and ether phospholipid species was quantified by mass spectrometry in the wild-type and *ino1*$^{-}$ cells that had been grown in the presence or absence of inositol (500 µM) (Figure 5.9 C-F). Separation of distinct phospholipid species was limited to those of different molecular weights. Phosphatidic acid (PA), a phospholipid precursor that comprises a glycerol backbone and two fatty acid tails, was examined first. Both diacyl-linked and ether-linked PA levels decreased during early inositol depletion (12 hours) in the *ino1*$^{-}$ cells (Figure 5.9 C,D). Phosphoinositol (PI) (formed by the addition of the inositol head group to PA) decreased following inositol depletion (in the *ino1*$^{-}$ mutant), with a greater reduction in diacyl- than ether-linked PI. A similar effect was seen for the diacyl-linked phosphatidylinositol monophosphate (PIP). Surprisingly, inositol depletion resulted in a reduction in diacyl-linked phosphoinositol bisphosphate (PIP2), but not in ether-linked PIP2. For phosphoinositol trisphosphate (PIP3), only ether-linked PIP3 was detectable, and was reduced compared to wild-type cells, independent of exogenous inositol supply. The reintroduction of inositol

for 12 hours after a 24-hour starvation period restored the level of the majority of ether-linked and diacyl-linked phospholipids. These data suggest that the pool of diacyl-linked phospholipids is more sensitive to inositol depletion than ether-linked species, and that cellular ether-linked PIP2 levels are maintained during these conditions.

Since a decrease in inositol levels attenuated the production of phosphoinositides, and caused a transient reduction of PA, seen at 12 hours of inositol starvation, changes in other glycerophospholipids were also examined. No change in phosphatidylserine (PS) was seen in the wild-type cells grown in the presence or absence of inositol (500 µM); however, *ino1*$^{-}$ cells depleted of inositol for 24 hours showed a non-significant increase in PS that was further elevated following inositol replenishment for both ether-linked and diacyl-linked species (Figure 5.9 E,F). Phosphatidylethanolamine and phosphatidylcholine did not change in the wild-type or *ino1*$^{-}$ cells under any experimental condition (Figure 5.9 E,F).

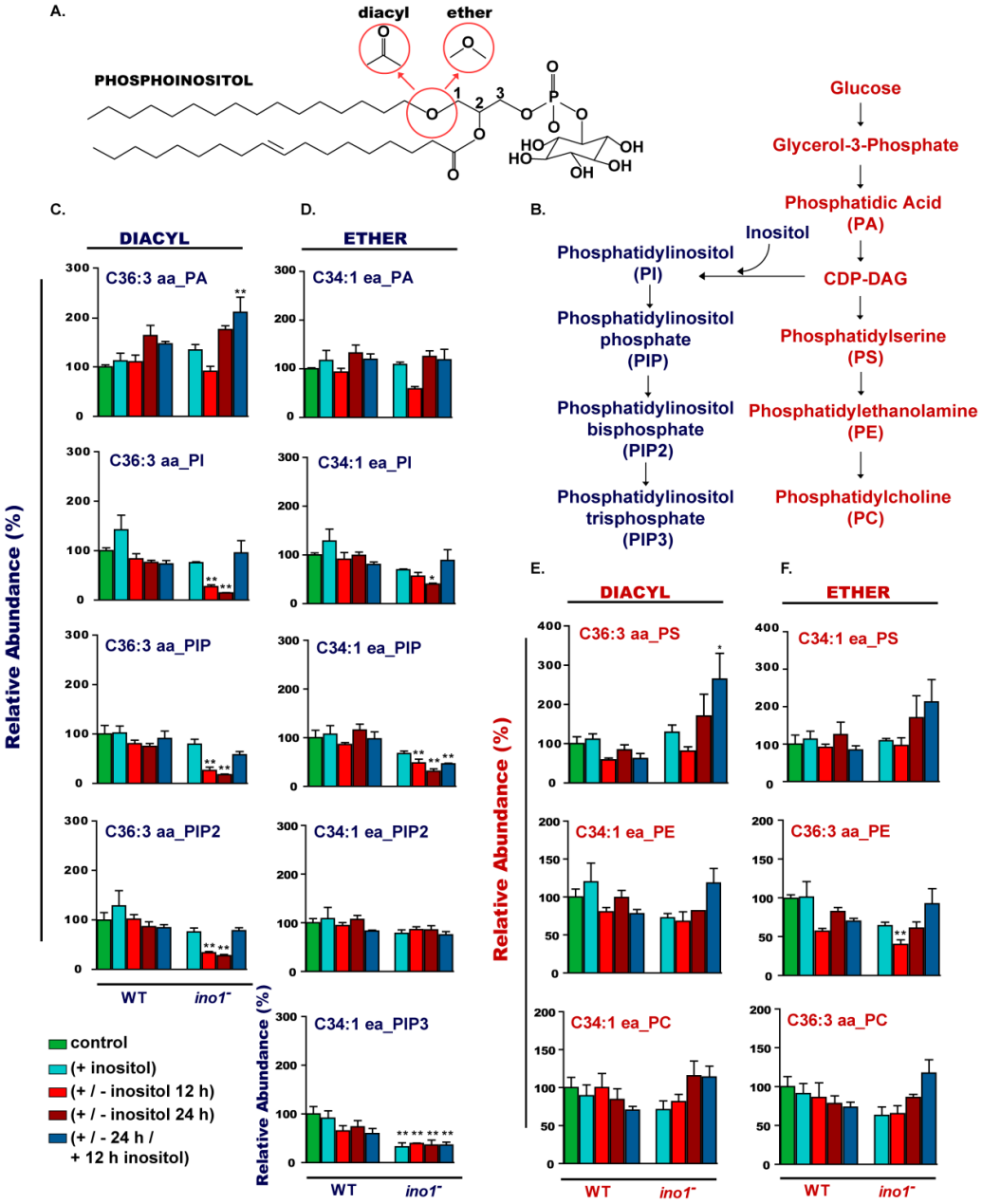

Figure 5.9 Inositol depletion affects the level of phosphatidylinositol and its phosphate derivatives. Wild-type and *ino1*⁻ cells were grown in the presence of inositol (500 µM, denoted '+'), the absence of inositol (12 or 24h; denoted '+/-'), or in inositol added after 24h depletion period (500 µM for 12h; denoted '+/-/+'). (A) The structure of inositol phosphate showing diacyl or ether/acyl fatty acid linkages to a glycerol backbone. (B) Metabolic pathway depicting phospholipid production from phosphatidic acid (PA) with diacyl-linked species used as an example. The levels of ether/acyl (C34:1ea) or diacyl (C36:3aa) phospholipids measured in the *ino1*⁻ cells are shown as a percentage relative to phospholipid levels present in the wild-type strain grown in the absence of inositol. (C-D) Inositol depletion reduced the level of diacyl-linked PI, PIP, and PIP2 (PIP3 was undetectable), and the levels of ether-linked PI, PIP, and PIP3, in the *ino1*⁻ cells. (E-F) Inositol starvation increased the PS level, while the level of PE and PC remained unchanged in the *ino1*⁻ cells. Error bars represent SEM. Statistical analysis was carried out between wild-type (Ax2) (+inositol) and *ino1*⁻(+inositol) by unpaired two-tailed student's *t*-test; **p* < 0;05, ***p* < 0.01, ****p* < 0.001; n = 3 independent technical repeats, 1 biological replicate; samples were prepared with 1.7 x 10^6 cells per condition. The work presented here was done in collaboration with Dr J. Clark and Dr P. Hawkins, Babraham Institute, Cambridge.

5.9 Discussion

In this chapter, the effects of starvation of inositol and the loss of Ino1 on cell function were investigated. The data presented showed that during inositol depletion *Dictyostelium* cells still maintained inositol, albeit at a significantly reduced level (inositol level decreased from 2.0 µM to 0.84 µM after 12-hour inositol starvation). The addition of exogenous inositol for 12 hours after 24-hour depletion restored the level of inositol in the *ino1*$^-$ cells (1.96 µM) to the basal concentration (2 µM). This result suggested that *Dictyostelium* cells were able to take up inositol from extracellular sources to replenish the intracellular pool, and thus inositol availability was not a major contributing factor to the phenotypic consequences of inositol starvation. Interestingly, wild-type *Dictyostelium* cells cultured in the presence of exogenous inositol (500 µM) had an increased level of intracellular inositol (3.4 µM with inositol supplementation vs 1.5 µM without inositol supplementation). This finding is consistent with the growth phenotype in liquid medium reported in chapter 4, where the wild-type cells grown in the presence of inositol reached a higher cell density compared to the cells without inositol supplementation. These findings suggest that even though axenic *Dictyostelium* wild-type cells had inositol levels sufficient for vital cell functions, the exposure to exogenous inositol prompts these cells to take up more inositol from the growth media.

Due to a vital role of inositol in cell function, cell-substrate adhesion was monitored in the *ino1*$^-$ cells in the absence of inositol. *Ino1*$^-$ cells exhibited reduced cell substrate adhesion in the absence of inositol. Overexpressing *ino1-RFP* in the *ino1*$^-$ mutant or provision of exogenous inositol rescued the reduction in adhesion. Moreover, *ino1-RFP* overexpression in the *ino1*$^-$ cells resulted in a higher number of cells that remained attached to a substratum in the first 46 hours of the experiment. Inositol is a precursor for phosphatidylinositol 4,5-bisphosphate (PIP2), which as a regulator of actin polymerisation and depolymerisation is critical for cell motility, adhesion and cytokinesis (Echard, 2012). Cytokinesis is the final step of the cell division process, ensuring the partitioning of the nuclear and

cytoplasmic contents into independent daughter cells (D'Avino et al., 2005). It consists of three sequentially occurring phases: an assembly of the cytokinetic apparatus, furrow progression, and fission (abscission) of the daughter cells (Logan and Mandato, 2006). Recent studies showed that elevating PIP2 at the cleavage furrow is essential for its stability (Logan and Mandato, 2006). Removing inositol from *Dictyostelium ino1*$^{-}$ cells for 24 hours caused over a twofold increase in the percentage of cells having ≥ 3 nuclei and a threefold reduction in substrate adhesion. Since inositol is a precursor for PIP2, its depletion could cause impaired cytokinesis, possibly through an inability of the cleavage furrow to close. Inositol has been previously shown to play a role in cell-substrate attachment dynamics (Fischbach et al., 2006; Zhu et al., 2015). Inositol depletion thus can impair cytokinesis, likely via a PIP2 reduction and a decreased substrate attachment.

Autophagy plays a major role in the maintenance of cell viability during nutrient starvation conditions (Mizushima et al., 2002), and recent studies have shown a link between inositol depletion and autophagy. Depleting inositol caused a change in the level of phospholipids and inositol-containing secondary messengers, like inositol-1,4,5 trisphosphate (InsP3), thus altering intracellular signalling (Takeda et al., 2014). Lower levels of InsP3 were shown to stimulate autophagy (Vicencio et al., 2009), whereas enhancing InsP3 levels inhibits autophagy that is induced by nutrient depletion (Criollo et al., 2007). Additionally, the bipolar disorder drugs carbamazepine, VPA, and lithium, which were proposed to act via inositol depletion (Berridge et al., 1989; Williams et al., 2002), were shown to induce autophagy, both *in vitro* and *in vivo* (Sarkar et al., 2005; Chiu and Chuang, 2011; Toker and Agam, 2014; Toker et al., 2014; Motoi et al., 2014). Schielber et al., (2015) also reported that carbamazepine (50 µM) leads to the death of mycobacteria after 24 hours via an autophagy process, triggered by inositol depletion alone. Since inositol-starved *Dictyostelium ino1*$^{-}$ cells exhibited impaired growth and a development phenotype, and unbalanced growth has been previously suggested in these cells as a result of inositol depletion (see chapter 4 Discussion), the potential upregulation of autophagy was investigated in these cells. For this purpose, Atg8 protein tagged with GFP

was overexpressed in both the *ino1*$^-$ mutant and wild-type cells. Post-translationally modified Atg8 is present on the autophagosome membranes, where the protein stays conjugated to phosphatidylethanolamine (Mizushima et al., 2002). The presence of GFP-Atg8 on the autophagosome membranes was used as a marker allowing for the quantification of the number of autophagosomes. *Ino1*$^-$ cells had nearly four–fold more autophagosomes per cell after 24 hours of inositol starvation compared to the either the wild-type or *ino1*$^-$ cells grown in the presence of exogenous inositol (500 µM). An increased number of autophagosomes suggests an upregulation of autophagy in the *ino1*$^-$ cells during inositol depletion. This is supported by the metabolic profile of the *ino1*$^-$ mutant, where the accumulation of amino acids and their breakdown products, favouring a catabolic state, was observed.

Autophagosomes require fusion with endosomes, and later with lysosomes, to allow for the degradation of their components (Kirisako et al., 1999; Mizushima et al., 2002). Thus, alternatively, the accumulation of autophagosomes in the *ino1*$^-$ mutant could also be due to endosome dysfunction (preventing fusion of autophagosomes with late endosomes and lysosomes), membrane imbalance (resulting from a reduction of phosphatidylinositol and phosphatidylethanolamine), or an impaired acidification of lysosomes, which is essential for their fusion with autophagosomes (Yamamoto et al., 1998). Indeed, perturbation of endosome function in yeast led to an accumulation of autophagosomes that were not able to fuse with lysosomes (Fujita et al., 2003; Nara et al., 2002) and a yeast mutant with defective vacuole fusion events had a higher number of autophagosomes in the cytoplasm compared to the wild-type cells (Kirisako et al., 1999). The increased number of autophagosomes in the *Dictyostelium ino1*$^-$ mutant during inositol depleting conditions needs to be investigated further to confirm whether autophagy is upregulated or the clearance of autophagosomes forming at the basal rate is reduced because of defective fusion. However, an unbalanced cell growth and an increase in the protein degradation products in these cells as a result of inositol starvation support an increased autophagic response in these cells. It is perhaps not surprising that inositol starvation would trigger autophagy, since this process is

responsible for the majority of starvation-induced proteolysis in cells (Mortimore and Poso, 1987). To investigate a defect related to autophagosome accumulation in the *ino1*$^-$ cells, a difference in the rate of autophagosome formation can be monitored in the wild-type and *ino1*$^-$ cells during inositol depletion over a few-hour time period.

Cell migration plays an essential role for *Dictyostelium* to initiate development when nutrients are depleted (King and Insall, 2009). In the experiments described in this chapter, the effect of inositol depletion was examined in the *ino1*$^-$ cells chemotaxing up a cAMP gradient in a Dunn chamber. Regardless of inositol supplementation, the *ino1*$^-$ cells were able to migrate towards the cAMP source. However, inositol depletion significantly reduced the velocity of the *ino1*$^-$ cells, while Ino1 loss resulted in a significantly less polarised cell shape compared to wild-type. Cytoskeleton re-organisation involving changes in actin polymerisation is an important aspect of cell migration, and regulation of cell substrate adhesion can influence the speed and directionality of moving cells (King and Insall, 2009; Stephens et al., 2008). It is possible that impaired cell substrate adhesion in the *ino1*$^-$ mutant caused a reduction in velocity. Similarly, a reduction in speed during chemotaxis and random cell movement was observed in a *Dictyostelium* sextuple *pi3k*$^-$ mutant that does not produce PIP3. This result suggests that reduced levels of PIP3 in the *ino1*$^-$ cells may have caused a decrease in the speed of moving cells. This idea is strengthened by the finding that the *ino1*$^-$ cells had lowered PIP3 levels compared to the wild-type cells, regardless of inositol supplementation, even though the intracellular inositol level was comparable to that observed in the wild-type cells. It additionally suggests that the Ino1 protein may be involved in regulating PIP3 levels. It is also interesting to observe that the *ino1*$^-$ cells supplied with inositol had reduced cell polarity, which suggests a requirement for Ino1 protein in re-arrangement of cell shape during cell movement. Phosphatidylinositol 3-kinase (PI3K) is responsible for PIP3 production, and since the PI3K inhibitor LY294002 has been shown to affect the frequency of pseudopod generation (Andrew and Insall, 2007), the reduced levels of PIP3 and altered cell polarity of the *ino1*$^-$

mutant could also suggest a possible impairment in the stability of protrusion formation in the migrating *ino1*$^{-}$ cells.

Ino1 loss was shown to significantly impact *Dictyostelium* metabolism. To better understand the metabolic role of Ino1 in cells, the metabolic profiles of wild-type and *ino1*$^{-}$ mutant cells subjected to different inositol conditions were analysed. The greatest change in metabolic profile was observed between the cells with and without the Ino1 protein. The differences between the metabolic profiles of the wild-type *Dictyostelium* and the *ino1*$^{-}$ mutant were not rescued by the addition of inositol, suggesting that the observed metabolic shift was not due to inositol levels *per se*, but rather an absence of the Ino1 protein. Surprisingly, *ino1*$^{-}$ cells exposed to inositol depletion and then rescued by exogenous inositol showed a similar metabolic profile to that of the wild-type cells grown without inositol. Individual metabolite analysis showed that Ino1 loss was associated with an increase in certain amino acids, in metabolites regulating cell cycle and DNA function, and an osmolyte *sn*-glycero-3-phosphocholine (GPC), suggesting that the lack of inositol was compensated for by the production of another osmolyte. The level of putrescine was significantly increased, indicative of an inhibition of cell proliferation (Kumar et al. 2014). Also, higher levels of lactate were observed, suggestive of an increase in the NADH to H+/NAD+ ratio and stimulation of the lactate dehydrogenase activity. An increase in NADH to H+/NAD+ ratio (linked to catabolic reactions) would also inhibit the citrate synthase and slow down the Krebs cycle, resulting in an accumulation of some intermediates, like acetate (derived from the spontaneous hydrolysis of oxaloacetate), fumarate, and succinate. Inositol treatment was seen to have little impact on *ino1*$^{-}$ cells compared to wild-type. Overall, these data indicate that the *ino1*$^{-}$ cells were in a catabolic state and support the potential triggering of autophagy in the *ino1*$^{-}$ mutant during inositol starvation. This is further strengthened by research showing that inositol depletion and amino acid deprivation led to an autophagic response (Criollo et al., 2007; Sarkar and Rubinsztein, 2006; Sarkar et al., 2005; Vicencio et al., 2009). Autophagy is regulated by three signalling systems in cells: a Tor-kinase complex, an Atg1-phosphoprotein kinase complex, and a phosphatidylinositol 3-kinase (PI3K)

complex (Glick et al., 2010). Inositol depletion was shown to lead to autophagy via an mTOR independent mechanism (Sarkar and Rubinsztein, 2006; Criollo et al., 2007), while amino acid deprivation was reported to cause autophagy via mTOR/raptor signalling through activation of class 3 phosphatidylinositol 3OH-kinase. Therefore, the potential autophagy observed in the *ino1*$^{-}$ mutant could be a result of varied responses to a global scale nutrient deprivation.

Inositol depletion however still reduced the level of phosphoinositides, and caused an increase in the level of phosphatidic acid and phosphatidylserine. Similar to our findings, Yamagami et al. (2015) reported that inositol depletion caused changes in lipid composition in yeast, including a decrease in phosphatidylinositol and an increase in phosphatidylserine. Inositol depletion also restored vesicle transport in yeast phospholipid flippase mutants (Yamagami et al., 2015). Phospholipid flippases play a role in maintaining phospholipid distribution at the plasma membrane and are implicated in the formation of transport vesicles (Yamagami et al., 2015). Mutations in phospholipid flippases cause defects in growth and endocytic recycling in yeast cells (Takeda et al., 2015). The restoration of the function of the endocytic recycling pathway and promotion of vesicle production was mediated by an increased cellular level of phosphatidylserine, which was proposed to actively recruit proteins for vesicle production or by inducing a curvature in the cytoplasmic membrane that facilitated vesicle formation (Takeda et al., 2014). Phosphatidylserine levels, which increased after 24 hours of inositol starvation in *Dictyostelium ino1*$^{-}$ mutant cells, can facilitate endocytosis.

The effect of *ino1* deletion and inositol rescue on the level of phosphoinositides was also examined. *Dictyostelium* cells use two distinct types of glycerophospholipids: one type of phospholipid contains fatty acid tails linked to a glycerol backbone with a double acyl (diacyl) linkage, and the second type comprises a fatty alcohol (ether) at the *sn-1* position and an acyl at the *sn-2* position (Clark et al., 2014). Both of these types of phospholipids were reduced by inositol depletion, with an enhanced reduction of diacyl species. Specifically, inositol depletion led to a rapid reduction in PI and PIP

(ether and diacyl species), and diacyl PIP2, but unexpectedly had little effect on ether PIP2. Only ether-linked PIP3 could be monitored in samples, and this was heavily reduced under all conditions, independent of exogenous inositol. Since ether-linked phosphoinositides account for over 95% of *Dictyostelium* inositol phospholipids (Clark et al., 2014), the enhanced reduction in diacyl phosphoinositides may be a reflection of their lower abundance. Alternatively, diacyl compounds may comprise a more labile pool of signalling molecules than ether phosphoinositides.

Cellular levels of ether PIP2 were maintained during inositol starvation. The maintenance of PIP2 levels during inositol depletion was a surprising finding, although other phosphoinositides (PI, PIP, PIP3) were significantly depleted. This suggests a critical role for PIP2 in cell function, a view that is supported by recent studies that demonstrated an essential role for PIP2 in cytokinesis (Mitsuhiro et al., 2012), vesicle formation and transport (Klopfenstein et al., 2002), and *Dictyostelium* cell movement during chemotaxis. Knock-out of PIP5 kinase (PikI) that produces PIP2 caused a 90% reduction in PIP2 level, and resulted in a highly disorientated movement of the *pikI*$^{-}$ mutant in cAMP gradients (Fets et al., 2014). These findings have relevance to phosphoinositide metabolism in the brain, as a recent study suggests that phosphoinositides, and specifically PIP2, play an important role in membrane traffic at the synapse (Cremona and De Camilli, 2001). PIP2 was implicated in neurotransmitter secretion, nucleation of clathrin coats, and the formation of a cytoskeletal scaffold to promote endocytosis at the synapse area, where PIP2 dephosphorylation accompanies the release of newly formed vesicles (Cremona and De Camilli, 2001). The pivotal role of PIP2 in these processes and in *Dictyostelium* cell growth and development could therefore explain the requirement for cells to maintain the levels of this essential molecule. This assertion is strengthened by the finding that the protein complexes involved in exocytosis and endocytosis at the synapse are highly conserved throughout evolution, and are similar to protein complexes that take part in exocytosis and endocytosis in all eukaryotic cells (Cremona and De Camilli, 2001).

5.10 Summary

Overall, the data presented in this chapter show that the depletion of inositol leads to a dramatic change in cell physiology, potentially leading to an autophagic response, a reduction in cell division, and a loss of substrate adhesion that could be a contributing factor in the velocity reduction of chemotaxing *ino1*$^{-}$ mutant cells. Inositol depletion also led to a decrease in the level of inositol phospholipids, and yet the level of PIP2 was maintained by cells, indicating an important role of this phospholipid. Removal of Ino1 protein accounted for a significant change in the *Dictyostelium* metabolic profile when compared to inositol depletion. The Ino1 protein may also be involved in maintaining PIP3 levels, and its loss caused a reduction in the polarised cell shape during chemotaxis.

Chapter 6
Cellular roles of Ino1

Chapter VI

Cellular roles of Ino1

6.1 Introduction

The established role for the Ino1 enzyme is *de novo* inositol production (Dean-Johnson and Henry, 1989). In the previous chapters however, Ino1 was shown to be involved in cell growth, shape and metabolic regulation, regardless of inositol provision. To investigate a role for Ino1 in regulating these processes independent of its catalytic activity, the induction of *Ino1* transcription and the effects of Ino1 mutations on cell growth and development were examined.

Ino1 transcription has been extensively researched, showing that the transcription of the gene was tightly regulated by the presence of inositol, choline, and Ino1 protein itself, as well as cellular events like the unfolded protein response (Brickner and Walter, 2004; Donahue et al., 2010; Felberbaum et al., 2012; Ford et al., 2007; Grigat et al., 2012; Kerr and Corbett, 2010; Konarzewska et al., 2012; Loewy and Henry, 1984; Shetty and Lopes, 2010). Structure and enzyme activity studies showed that the Ino1 protein exists as a homotetramer in yeast and as a homotrimer in mammals (Klig and Henry, 1984; Majumder et al., 1997; Seelan et al., 2004). Each Ino1 monomer has three major domains: a catalytic domain that binds the substrate glucose-6-phosphate, an NAD-binding domain, and a central domain that consists of the N- and C-termini that functions to stabilise the two other domains (Jin et al., 2004; Stein and Geiger, 2002). For Ino1 to complete its catalytic cycle, the active site folds to completely encapsulate the substrate in an example of induced fit.

There is little experimental evidence relating to the role of Ino1 post-translational modification. However, a recent study suggests that Ino1 activity is regulated by phosphorylation, where by mass spectrometry analysis five

phosphosites were identified in yeast Ino1 protein (Deranieh et al., 2013). Phosphorylation of rat Ino1 extracted from brain was also demonstrated via phosphospecific ProQ-Diamond staining and Western blot analysis (Parthasarathy et al., 2013). Three of the identified phosphosites in yeast (S184, S296, S374) were conserved in the human Ino1 (S177, S279, S357). Phosphorylation was also shown to regulate an activity of human and yeast Ino1 (Deranieh et al., 2013). Phosphodeficient (S296A) and phosphomimetic (SS296D) mutations in Ino1 from yeast (and a corresponding S279 site in human Ino1) decreased the enzymatic activity, suggesting that the position of serine at this site was critical for Ino1 enzymatic activity. Similarly, phosphomimetic mutations S184D and S374D caused a decrease in Ino1 activity showing that the phosphorylation of these two sites was inhibitory. Additionally, the double mutation S184A/S374A caused an increase in Ino1 activity to enhance growth rate in yeast (Deranieh et al., 2013).

Ino1 activity is also affected by therapeutically relevant drugs, where the mood stabilising drugs, valproic acid and lithium, were shown to lower intracellular inositol and inositol trisphosphate levels (Eickholt et al., 2005; Ju and Greenberg, 2003; Vaden et al., 2001; Williams et al., 2002). In yeast and *Dictyostelium*, the resulting inositol depletion caused an increase in expression of *ino1*, which is regulated in response to inositol. In yeast, valproic acid and lithium also increased the expression of a regulatory gene, *ino2*, which controls the inositol and phospholipid biosynthetic pathways (Vaden et al., 2001). Additionally, valproic acid was shown to inhibit the activity of the Ino1 enzyme *in vivo,* but not *in vitro,* in yeast and in mouse frontal cortex extracts, suggesting an indirect mechanism of action of this drug on Ino1 (Ju et al., 2004; Shaltiel et al., 2004).

To decipher the regulatory roles of proteins in cells, it is useful to investigate their binding partners and the processes these proteins are involved in. Few studies have identified Ino1 interacting proteins. However, Ino1 interactors isolated from yeast and human studies included proteins involved in the regulation of DNA transcription and translation, nucleic acid-, phospholipid-, nitrogen- and carbohydrate metabolism, intracellular protein

transport, endocytosis, membrane growth and polarity, electron transport chain function, and ubiquitination (Schlecht et al., 2012; Tarassov et al., 2008; Wan et al., 2015).

In this chapter, initial experiments that sought to develop an assay for monitoring *ino1* expression were investigated. In addition, mutations in the catalytic core and phosphorylation sites of the enzyme as well as the effects of inositol depleting drugs on the development of the *ino1* mutants were examined. Finally, potential Ino1 binding partners in *Dictyostelium* were identified by a proteomics approach following isolation by protein-protein interactions using total cell lysates.

6.2 Monitoring *ino1* gene transcription

To monitor *ino1* transcription in response to changing inositol levels, a plasmid construct was created that enabled the β-galactosidase gene to be expressed under the control of the *ino1* promoter (Figure 6.1). Primers for PCR amplification were designed to amplify 0.35, 0.7 and 1.0 kb of the promoter sequence upstream of the *ino1* start codon (Figure 6.1 A) and the resultant PCR products were cloned and sequenced. Due to the high AT content of this region (Figure 6.1 B), sequence analysis revealed that all sequenced clones contained mismatches to the available *ino1* sequence (DDB_G0285505). The nucleic acid sequence that contained the highest number of matched bases, further referred to as the *ino1* promoter, was cloned into the pDdGal vector (Harwood and Drury, 1990), replacing the actin15 promoter to drive the expression of the β-galactosidase gene in *Dictyostelium ino1*$^-$ cells (Figure 6.1 C-E). The β-galactosidase enzyme activity was detected in the lysates prepared from *ino1*$^-$ cells transformed with reporter vectors by an Enzyme Assay System from Promega. Cell lysate was prepared from adherent cells using reporter lysis buffer. β-galactosidase activity was assayed with a buffer that contained the substrate ONPG (o-nitrophenyl-β-D-galactopyranoside) (Figure 6.1 F). *Ino1*$^-$ cells expressing β-galactosidase vectors were deprived of inositol for 16 hours prior to the assay. The production of the yellow colour was visible in the *Ino1*$^-$ cells

transformed with the pDdGal vector only (Act15-*lacZ*) and quantified by absorbance reading at ʎ420 (Figure 6.1 F). Cell lysate from the *ino1*$^{-}$ control not expressing β- galactosidase did not produce a visible colour change and the absorbance reading at ʎ420 was similar to the blank control. These data suggested that the assay was functioning and that the β-galactosidase enzyme was active in the *ino1*$^{-}$ cells. However, vector containing the 0.7kb sequence upstream of the *ino1* gene (*ino1-lacZ*) did not express the β-galactosidase enzyme at a detectable level under the tested conditions as no change was observed for the β-galactosidase activity in the *ino1*$^{-}$ cells transformed with this construct. This was suggestive of the cloned *ino1* promoter fragment to be non-functional, which may be a result of the mutations in the promoter sequence or, alternatively, the 700bp of the *ino1* promoter fragment was not sufficient to drive gene expression. Due to time restrictions these assays were not developed further.

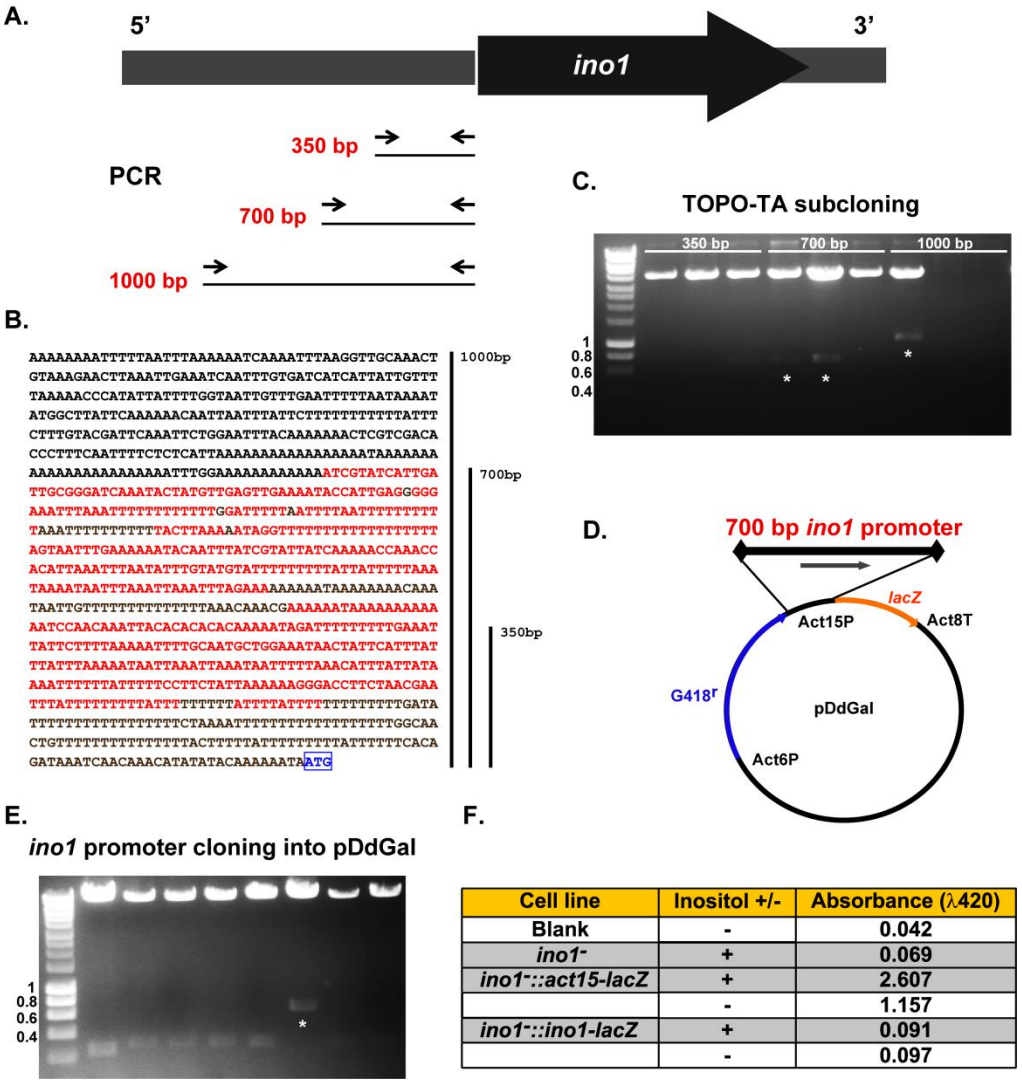

Cell line	Inositol +/-	Absorbance (λ420)
Blank	-	0.042
ino1⁻	+	0.069
ino1⁻*::act15-lacZ*	+	2.607
	-	1.157
ino1⁻*::ino1-lacZ*	+	0.091
	-	0.097

Figure 6.1 Monitoring Ino1 levels via *ino1* transcription in response to inositol. An *Ino1-lacZ* reporter construct was created to express β-galactosidase in *ino1*⁻ cells to measure the level of gene transcription driven by the *ino1* promoter in response to inositol treatment. (A) 0.35, 0.7 and 1.0 kb of the nucleic acid sequence upstream of the *ino1* start codon was amplified by PCR using sequence specific primers. PCR products were then subcloned into a TOPO-TA vector for DNA vector amplification in bacteria. (B) Diagram showing 1000 base pairs of the AT-rich DNA sequence upstream of the *ino1* start codon. The sizes of the regions amplified by PCR to clone into the pDdGal vector are marked to the right of the sequence. DNA sequence marked in red was confirmed by sequencing to be complementary to the 0.7kb promoter fragment subsequently cloned into the pDdGal vector. The *ino1* start codon is shown in blue font and highlighted by a blue box. (C) A test digest was performed to select the clone with the correct size PCR product (marked by an asterisk), followed by gene sequencing to confirm the correct sequence. (D) The 0.7kb *ino1* promoter fragment was cloned into a pDdGal vector to replace the Act15 promoter. The completed vector contained the *lacZ* gene coding for the β-galactosidase enzyme transcribed from the putative *ino1* promoter (700 bp upstream of the *ino1* start codon). (E) The correct cloned vector was selected by restriction digest analysis with the enzymes that were used to create the construct. The fragment of the correct size (700 bp) is marked by an asterisk. (F) β-galactosidase enzyme activity was assayed using a colourimetric method, where the rate of conversion of a colourless substrate into a coloured product was quantified by absorbance measurement. Molecular weight marker sizes are shown in kilo base pairs.

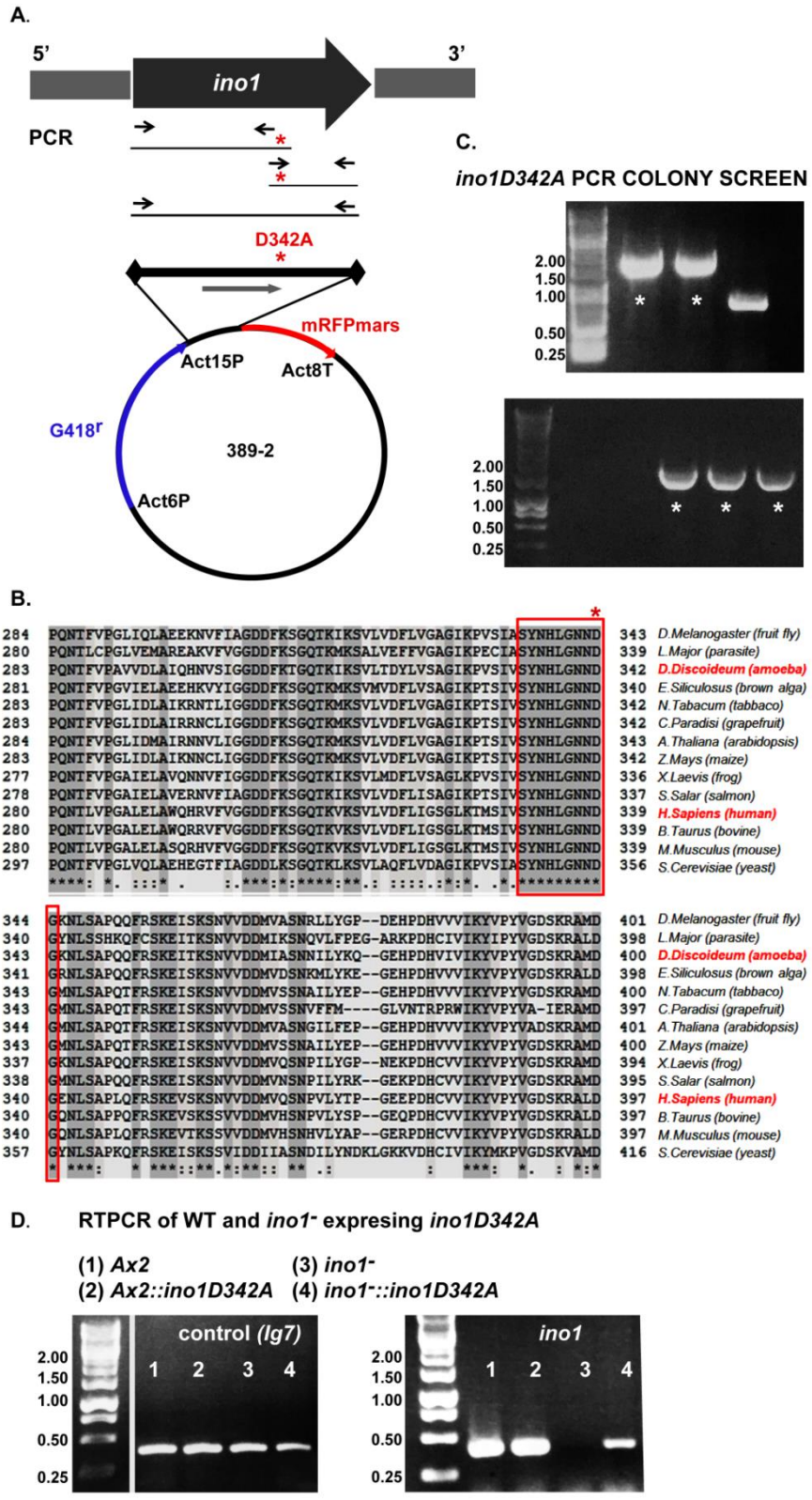

Figure 6.2 Creating a catalytically-inactive Ino1. (A) Cloning of the *ino1-D342A* construct into the 389-2 vector containing mRFPmars to be expressed as a C-terminal tag. *Ino1* sequence was amplified with sequence-specific primers in two separate PCR steps, where two fragments of the *ino1* gene were amplified first to introduce a point mutation at the amino acid position D342 (GAT to GCA), followed by a PCR amplification with a mixture of the two DNA fragments as a template to obtain a full length mutated *ino1*. (B) Multiple sequence alignment of a portion of the Ino1 proteins from various species to show amino acids conserved around the catalytic domain region. The highly conserved amino acid signature

belonging to the putative catalytic site (Majumder et al., 2003) is highlighted in a red box. The mutated aspartic acid residue is marked with a red asterisk. (C) 389-2 vector ligated with *ino1D342A* sequence was transformed into bacteria and the independent clones were screened using a PCR approach with sequence-specific primers. The clones containing DNA that showed the band of a correct size during DNA gel electrophoresis (1.67kb, marked with an asterisk) were sequenced to confirm the presence of the introduced mutation. (D) Ax2 and *ino1*$^{-}$ cells were transformed with the *ino1D342A* construct. The expression of the *ino1* gene was confirmed with RTPCR on the colonies resistant to the selection antibiotic (G418). Molecular weight marker sizes are shown as kilo base pairs.

6.3 Investigating a catalytically inactive Ino1 mutation

To examine a possible non-catalytic function for Ino1, a mutated *Dictyostelium* Ino1 protein was expressed that was likely to have disrupted catalytic activity (Figure 6.2). For these experiments, a construct was created to express *Dictyostelium* Ino1 with a point mutation, D342A tagged with a C-terminal RFP in the 389-2 vector (courtesy of Dr Annette Müller-Taubenberger) (Figure 6.2 A-C). The construct was created by the overlap extension PCR method using sequence-specific primers (Figure 6.2 A). The presence of the D342A mutation in the *ino1* gene was confirmed by DNA sequencing. The expression of Ino1-D342A in wild-type and *ino1*$^{-}$ cells was verified by RTPCR (Figure 6.2 D).

Ino1-D342A did not rescue the inability of *ino1*$^{-}$ cells to grow without inositol supplementation, both on bacterial lawns or in liquid suspension, suggesting that the mutated protein was catalytically inactive (Figure 6.3 A & B). Expression of Ino1-D342A in wild-type cells did not hinder the growth of these cells on bacterial lawns (Figure 6.3 A). However, Ino1-D342A significantly decreased the growth of wild-type cells in liquid media compared to an untransformed control; grown without inositol, the doubling time of wild-type control was 23 hours, wild-type expressing Ino1-D342A 43 hours. Inositol supplementation (500 µM) reduced the doubling time of wild-type expressing Ino1-D342A to 27 hours but did not rescue the growth of these cells to the level of the wild-type control (Figure 6.3 B). Cell density of wild-type cells expressing Ino1-D342A was lower than the wild-type control, regardless of inositol supplementation. Also, addition of 500 µM exogenous inositol partially rescued the growth defect of the *ino1*$^{-}$ mutant expressing Ino1-D342A (doubling time of 26 hours). Furthermore, *ino1*$^{-}$ cells grown in the

presence of 500 µM inositol had higher cell density than wild-type cells expressing the mutated Ino1-D342A protein.

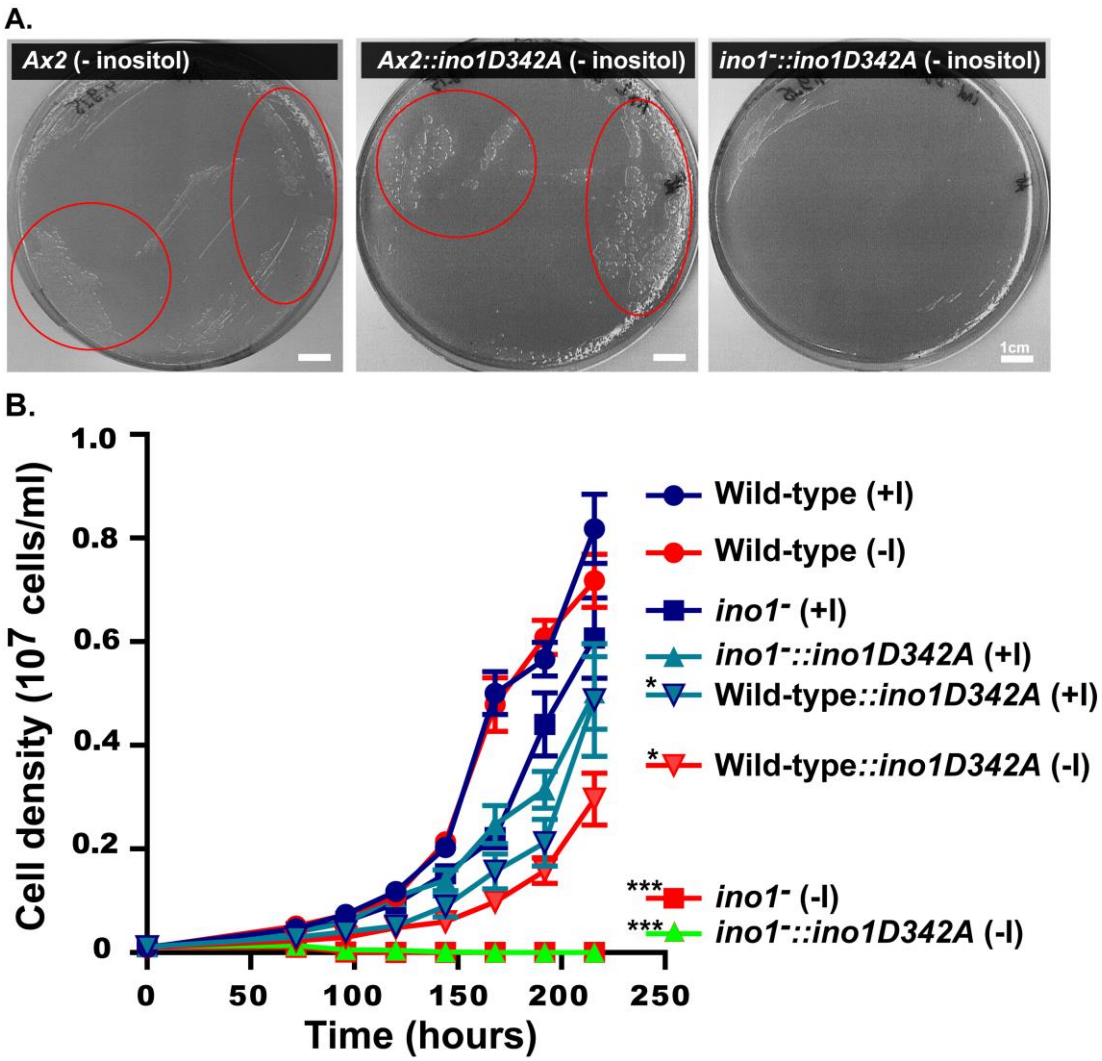

Figure 6.3 Growth of *Dictyostelium* cells expressing catalytically-inactive Ino1. Ino1-RFP protein with a point mutation (aspartic acid to alanine substitution, *ino1D342A*) in a highly conserved region of the catalytic domain was expressed in wild-type and *ino1*$^-$ cells. (A) Grown in the absence of exogenous inositol, wild-type (Ax2) cells transformed with *ino1D342A* were able to grow on bacterial lawn similar to the untransformed control (growth zones are marked in red), while *ino1*$^-$ cells were unable to grow. (B) In wild-type cells, overexpression of the mutated Ino1 protein caused a significant decrease in the growth compared to untransformed wild-type cells, even with the addition of 500 µM inositol to the growth media. *Ino1*$^-$ cells were not able to grow without extracellular inositol supply and the overexpression of the Ino1-D342A did not rescue this growth phenotype, indicating that the protein was catalytically inactive. Addition of 500 µM inositol to the growth medium partially rescued the inositol auxotrophy phenotype of *ino1*$^-$ cells and *ino1*$^-$ cells expressing *ino1-D342A*. (+I): +500µM inositol; (-I): no inositol added. Error bars represent SEM. Statistical analysis was carried out in separate tests for each individual condition compared to wild-type (-I) by unpaired two-tailed *t*-test, *$p < 0.05$, ***$p < 0.001$; n = 3 technical repeats; 1 biological replicate.

6.4 Investigating the effect of Ino1 phosphomutations

A multiple sequence alignment confirmed that *Dictyostelium* Ino1 contained serine residues at positions cognate to the yeast and human Ino1 phosphosites at S179, S282, S360 (Figure 6.4 A). To gain more information about a potential role of Ino1 phosphorylation in *Dictyostelium* growth, cell lines expressing *ino1* with single point mutations corresponding to the putative Ino1 phosphorylation sites were created. In order to introduce single point mutations in Ino1 S179, S282, and S360, three plasmids were created using pTXGFP vector as a backbone (Levi et al., 2000) (Figure 6.4B). Mutations (S179A, TCC to GCC; S282A, TCA to GCA; S360A, TCA to GCA) were introduced by overlap extension PCR with sequence-specific primers (Figure 6.4 B). The presence of the full length (1.67kb) *ino1* gene was shown by restriction digest analysis (Figure 6.4 C). The correct *ino1* sequences containing each substitution were confirmed by DNA sequencing and the expression of *ino1* in *ino1*$^{-}$ cells was verified by RTPCR (Figure 6.4 D). *Ino1*$^{-}$ cells expressing Ino1 with S179A, S280A, or S360A mutations were able to grow in the absence of inositol supplementation (not quantified). These results suggest that phosphorylation of Ino1 at these sites is not necessary for catalytic activity of the protein.

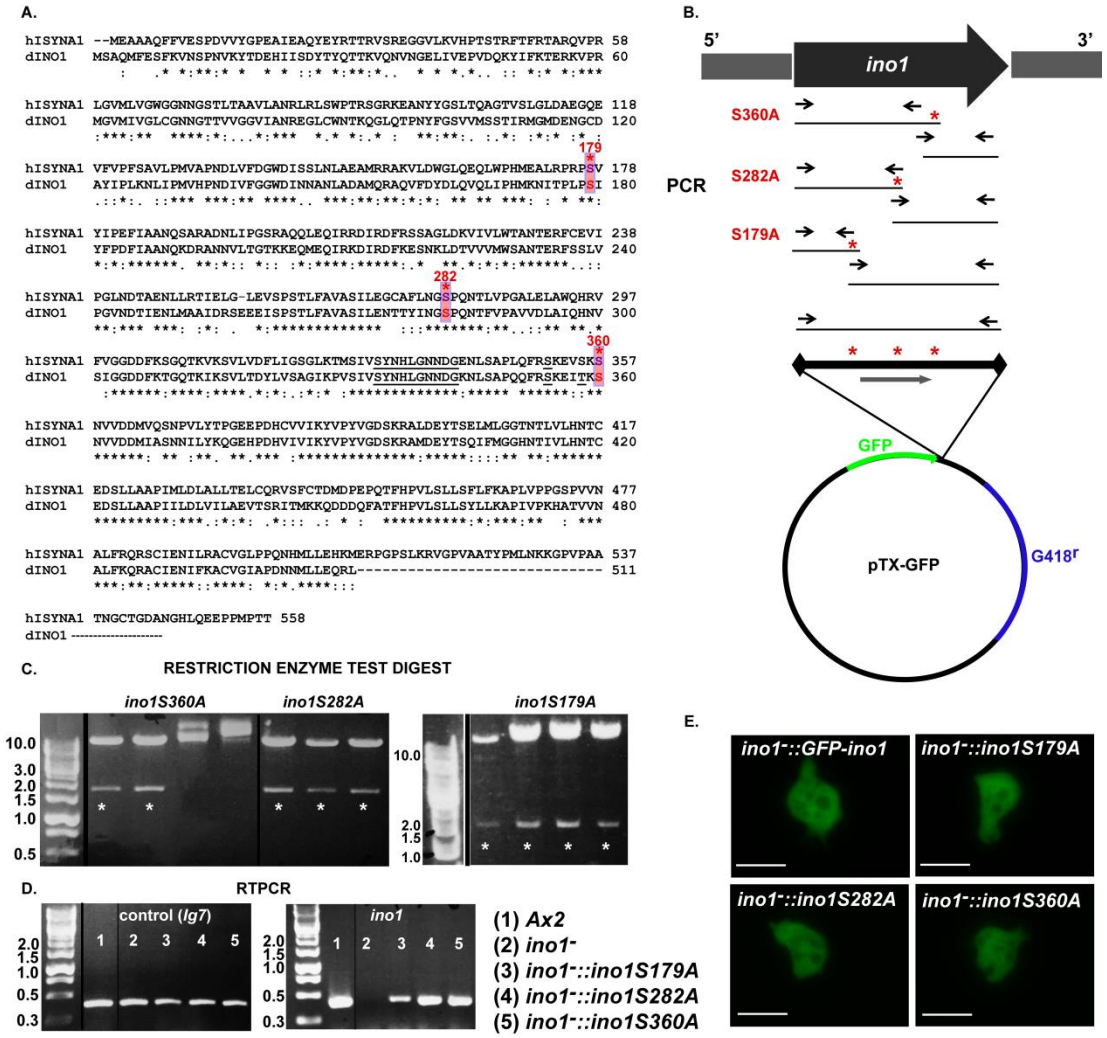

Figure 6.4 Creating Ino1 phosphomutations. (A) Multiple sequence alignment of the human (hISYNA1) and *Dictyostelium* (dINO1) Ino1 proteins. Black asterisks indicate identical amino acids while red asterisks indicate the putative phosphorylation sites. These three serine residues (S179, S282, S360) in the *Dictyostelium* protein sequence were substituted with alanine. (B) Cloning of the *ino1-S179A, ino1-S282A,* and *ino1-S360A* constructs into the pTXGFP vector containing GFP to be expressed as an N-terminal tag. To introduce each mutation separately, *ino1* sequence was amplified with sequence-specific primers in two separate PCR steps, where the two fragments of the *ino1* gene were first amplified to introduce a point mutation at the amino acid positions S179 (TCC to GCC), S282 (TCA to GCA), or S360 (TCA to GCA), followed by a PCR reaction with a mixture of the two DNA amplicons as a template to obtain the full length *ino1*. (C) pTXGFP vector containing *ino1S179A, ino1S282A, or ino1S360A* sequence was transformed into bacteria and independent clones were screened by restriction digest with the enzymes used to clone the *ino1* gene into pTXGFP. The clones containing a band of the correct size by DNA gel electrophoresis (1.67kb, marked with an asterisk) were confirmed to contain the introduced mutation by DNA sequencing. (D) *Ino1*$^{-}$ cells were transformed with *ino1S179A, ino1S282A, or ino1S360A* plasmids. The expression of *ino1* was confirmed RTPCR on the colonies resistant to the selection antibiotic (G418). (E) Fluorescence images of live *ino1*$^{-}$ cells expressing Ino1 with different phosphomutations. Ino1 proteins with a single mutation at the three individual phosphosites localised to the cytosol, like the native Ino1 protein tagged with GFP (*Ino1*$^{-}$*::GFP-Ino1*). Molecular weight marker sizes are shown as kilo base pairs. Size bar represents 10 µm.

6.5 The effect of inositol-depleting drugs on development of *ino1* mutants

Dictyostelium development, where cells aggregate to form fruiting bodies, was shown to be sensitive to inositol-depleting drugs (Eickholt et al., 2005; Williams et al., 1999, 2002). Since Ino1 is responsible for the production of inositol in cells, the effect of the inositol-depleting drugs VPA and lithium was investigated during development of cells that either lacked or overproduced Ino1 protein (Figure 6.5). In these experiments, wild-type *Dictyostelium* cells (Ax2 strain) formed mature fruiting bodies, containing a basal disk, stalk, and round spore head, over a period of 24 hours (Schaap and Wang, 1986), while *ino1*$^-$ cells required prior supplementation with exogenous inositol (500 µM) to complete this developmental process. Overexpressing *ino1-RFP* in *ino1*$^-$ cells rescued the inability of these cells to develop without inositol supplementation. These results were consistent with the observation that inositol depletion blocks *Dictyostelium* development.

Analysis of the effect of inositol-depleting drugs on the development of wild-type cells showed that VPA (1 mM) treatment led to a complete block in development (Figure 6.5). Removing or overproducing the Ino1 protein in *Dictyostelium* did not increase resistance to VPA (1 mM). However, decreasing the concentration of VPA (0.5 mM) reduced the inhibitory effect of the drug, so that wild-type and *ino1*$^-$ cells were able to form fruiting bodies within 24 hours. Treatment of wild-type cells with LiCl (10 mM) also caused a block in development, resulting in no fruiting bodies forming (Figure 6.5). Removing or overproducing Ino1 protein did not rescue *Dictyostelium* sensitivity to lithium at concentration (10 mM). Although *ino1* ablation or overproduction of the Ino1 protein did not give rise to major morphological changes in development, the *ino1*$^-$ cells were not able to develop without prior inositol supplementation, suggesting that the catalytic role of Ino1 in inositol biosynthesis is essential for multicellular development. These results also suggest that Ino1 protein is not a direct target of VPA and lithium, since altering Ino1 protein levels would be predicted to alter sensitivity to these drugs if it were the direct target.

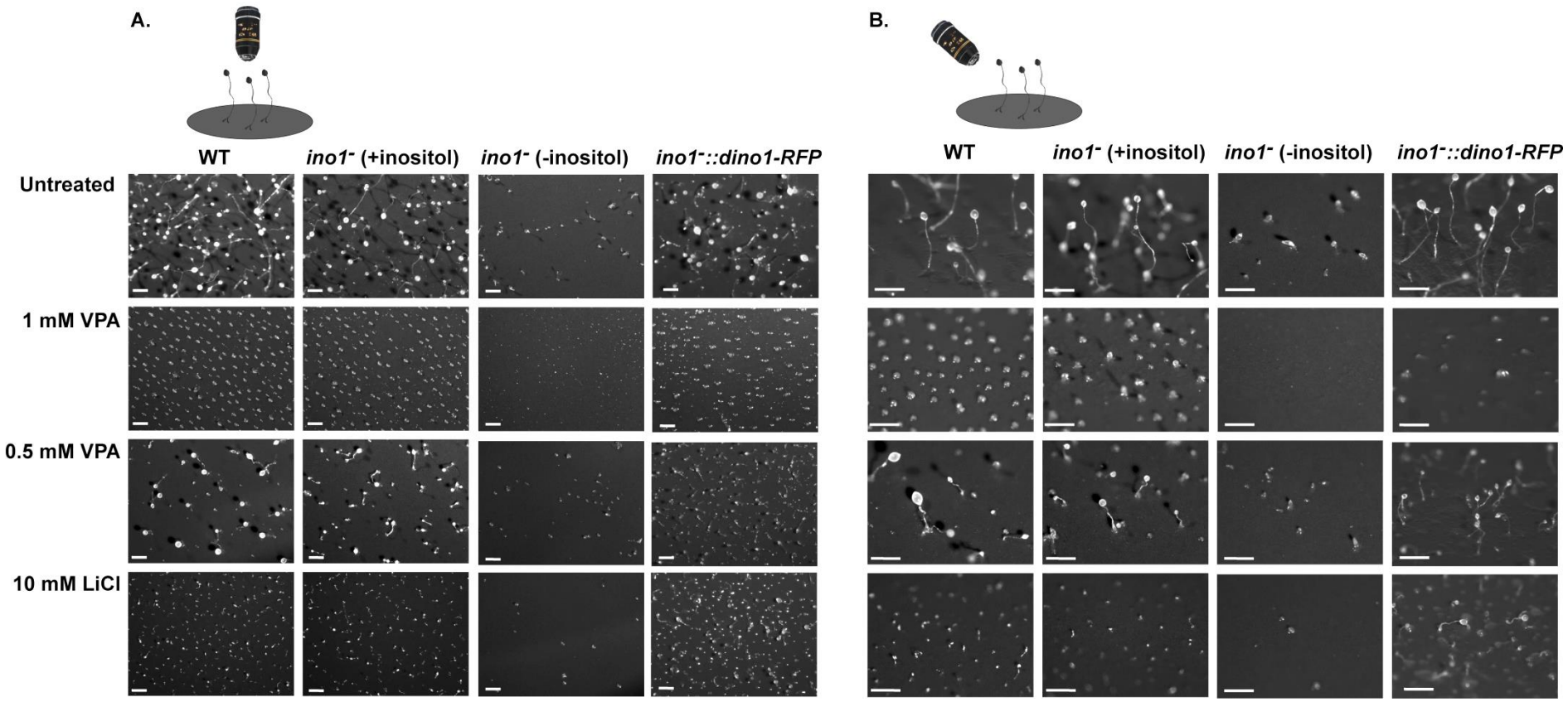

Figure 6.5 Development of the *ino1*⁻ mutants. *Dictyostelium* wild-type (Ax2) and *ino1*⁻ cells were developed on nitrocellulose filters over a period of 24 hours. Cells were treated with VPA (0.5 mM or 1 mM) or lithium (10 mM) at the start of the 24-hour development assay period. *Ino1*⁻ cells were grown in the presence of 500 µM inositol or without inositol for 24 hours prior to the development assay. Schematic images of the microscope lens over the filter with fruiting bodies represent the angle of the camera used to record development from (A) an aerial and (B) side angle view. Representative of 3 independent technical repeats. Size bars represent 0.5 mm.

6.6 Ino1 binding partners

6.6.1 Proteomics

Immunoprecipitation was employed to identify potential Ino1 binding partners. Lysates were obtained from wild-type and *ino1*$^{-}$ cells overexpressing Ino1-RFP, and RFP was immunoprecipitated using agarose beads coated with an anti-RFP antibody, followed by SDS-PAGE separation and mass spectrometry analysis (Figure 6.6 A). This method relied on immobilising Ino1 and its binding partners on anti-RFP coated beads via an RFP tag present on the Ino1 protein (Figure 6.6 B). Protein complexes were visualised by Coomassie stain and western blot (Figure 6.6 A). A band of the expected size for the monomeric Ino1-RFP protein (~84 kDa) was visible by Coomassie stain and western blot with anti-RFP antibody, confirming that the protein was present in the cell lines used for these experiments. A number of higher molecular weight bands were also seen in the Coomassie-stained gels (Figure 6.6 C); sixteen unique protein bands visible only in the Ino1-RFP bound fraction and absent from the equivalent control RFP sample were excised, along with the corresponding region from the control (*ino1*$^{-}$ expressing RFP or wild-type cells) and analysed by mass spectrometry (S. Lilla and Prof R. Insall, Beatson Institute,Glasgow) to identify interacting proteins (Figure 6.6 C).

6.6.2 Intracellular protein-protein interaction

The mass spectrometry analysis identified ~300 interactors in three independent experiments, of which 104 potential binding partners were selected based on two criteria, namely a minimum threshold of peptide hits of 2 and an absence from the control sample (Table 6.1). Potential binding partners were then divided into six major functional groups: actin-related, immunity and stress, metabolism, nucleic acid-related (translation, transcription, regulation of gene expression and DNA recombination), protein-related (catabolism, modification and transport, signal transduction, ATP hydrolysis and proton transport (Supplementary Material, Table S2).

Due to the large number of potential binding partners, further analysis focused on three proteins: GpmA, a phosphoglycerate mutase, the product of which, 2,3-bisphospho-D-glycerate, was found to accumulate in *ino1*$^{-}$ cells starved of inositol (Fischbach et al., 2006); PefB, a penta-EF-hand containing protein linked to neurodegenerative and lysosomal diseases (Vergarajauregui et al., 2009; Vito et al., 1996); SecG, a putative Arf-guanine-nucleotide exchange factor (GEF) involved in development and substrate adhesion (Garcia et al., 2013; Shina et al., 2010); and Q54IX5, an uncharacterised protein, which was present in all three independent immunoprecipitation experiments (Figure 6.7). Expression constructs were made for all three proteins initially with a FLAG epitope in *ino1*$^{-}$ cells and co-immunoprecipitation was performed with cell lysates incubated with anti-RFP coated agarose beads (Figure 6.7 A&B). The bound protein fractions were analysed for the presence of a FLAG-tagged protein by western blot analysis where FLAG -GpmA was shown to bind weakly, and FLAG-Q54IX5 was shown to bind strongly to Ino1-RFP; FLAG-SecG and FLAG-PefB could not be detected (Figure 6.7 B). Furthermore, the Q54IX5-Ino1 interaction was confirmed using the reverse co-immunoprecipitation. Extracts from *ino1*$^{-}$ cells co-expressing Ino1-RFP and GFP-Q54IX5 were incubated with anti-GFP-coated agarose beads and the co-precipitation of Ino1-RFP was detected by western blot analysis with anti-RFP antibody (Figure 6.7 C). Fluorescence microscopy of live cells showed that GFP-Q54IX5 protein localises to the cytosol, similar to the Ino1-RFP protein (Figure 6.7 D).

The outcome of these experiments was the identification of a variety of actin and metabolism-associated proteins as potential Ino1 binding partners. The binding of Q54IX5, a SEL1 domain-containing protein with an unknown function, was confirmed by the reverse-immunoprecipitation approach. The weak interaction between FLAG-GpmA and Ino1-RFP detected in the initial experiment could not be confirmed by reverse immunoprecipitation using GFP-gpmA protein. SecG protein could not be resolved on the SDS-PAGE gel, possibly due to the large size of the protein.

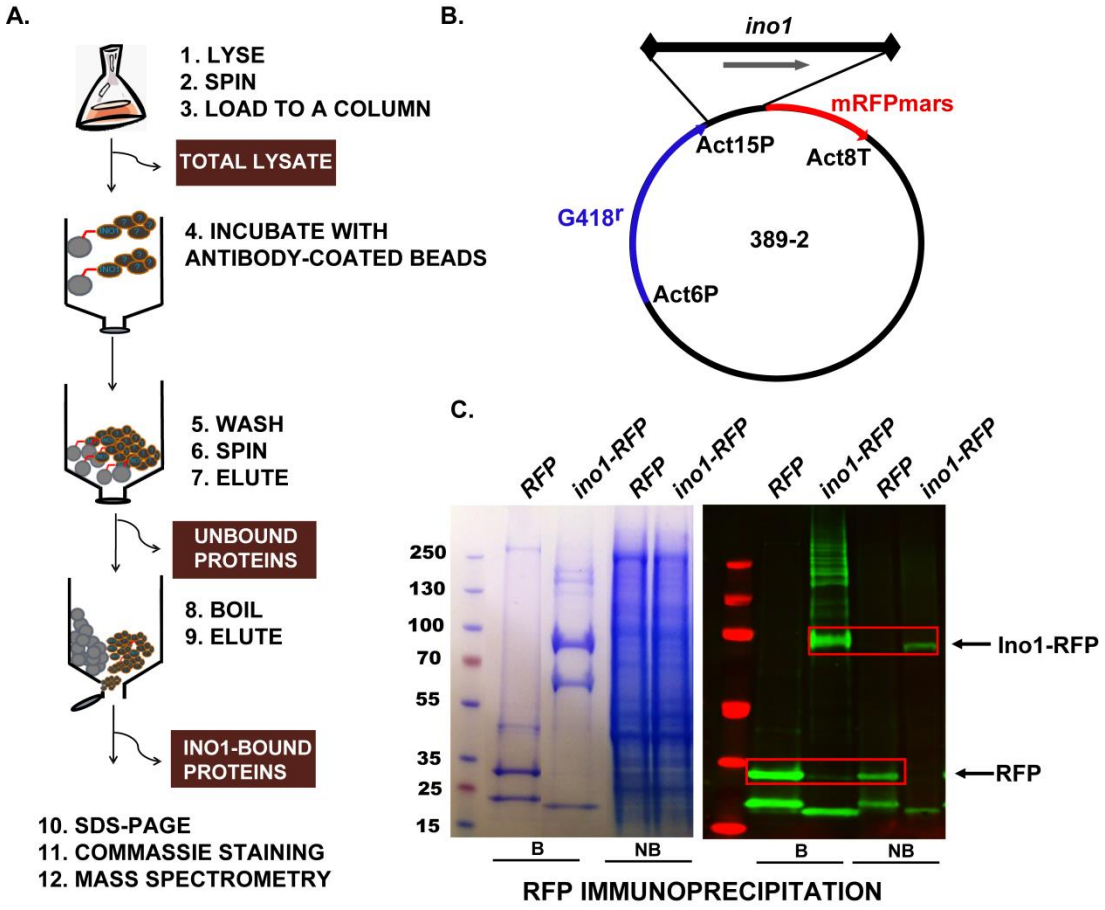

Figure 6.6 Immunoprecipitation of the Ino1 protein. Ino1-RFP protein was immunoprecipitated using anti-RFP coated beads. Extracts from *ino1*$^{-}$ cells expressing *ino1-RFP* or RFP only (control) were used to identify specific binding partners. (A) Schematic representation of the immunoprecipitation procedure. *Dictyostelium ino1*$^{-}$ cells expressing Ino1-RFP were lysed and incubated with anti-RFP coated beads to bind Ino1-RFP and any interacting proteins to the beads. Unbound proteins (NB) were eluted. The beads were then washed, boiled to dissociate immunocomplexes, and the Ino1-bound complexes eluted. The eluates were subject to SDS-PAGE and Coomassie staining. The bands specific to the *ino1-RFP* immunoprecipitate were analysed using mass spectrometry. (B) Schematic of the plasmid construct transformed into *ino1*$^{-}$ cells to express *ino1-RFP.* (C) Coomassie stain and western blot of one of the three immunoprecipitation repeats that was used to identify putative Ino1-interacting proteins. Left: the purified Ino1 complexes were separated on an SDS-PAGE gel and visualised with Coomassie stain. Right: Western blot analysis to confirm the presence of a full-length Ino1-RFP protein in the lysates using an anti-RFP monoclonal antibody. (B) bound; (NB) non-bound.

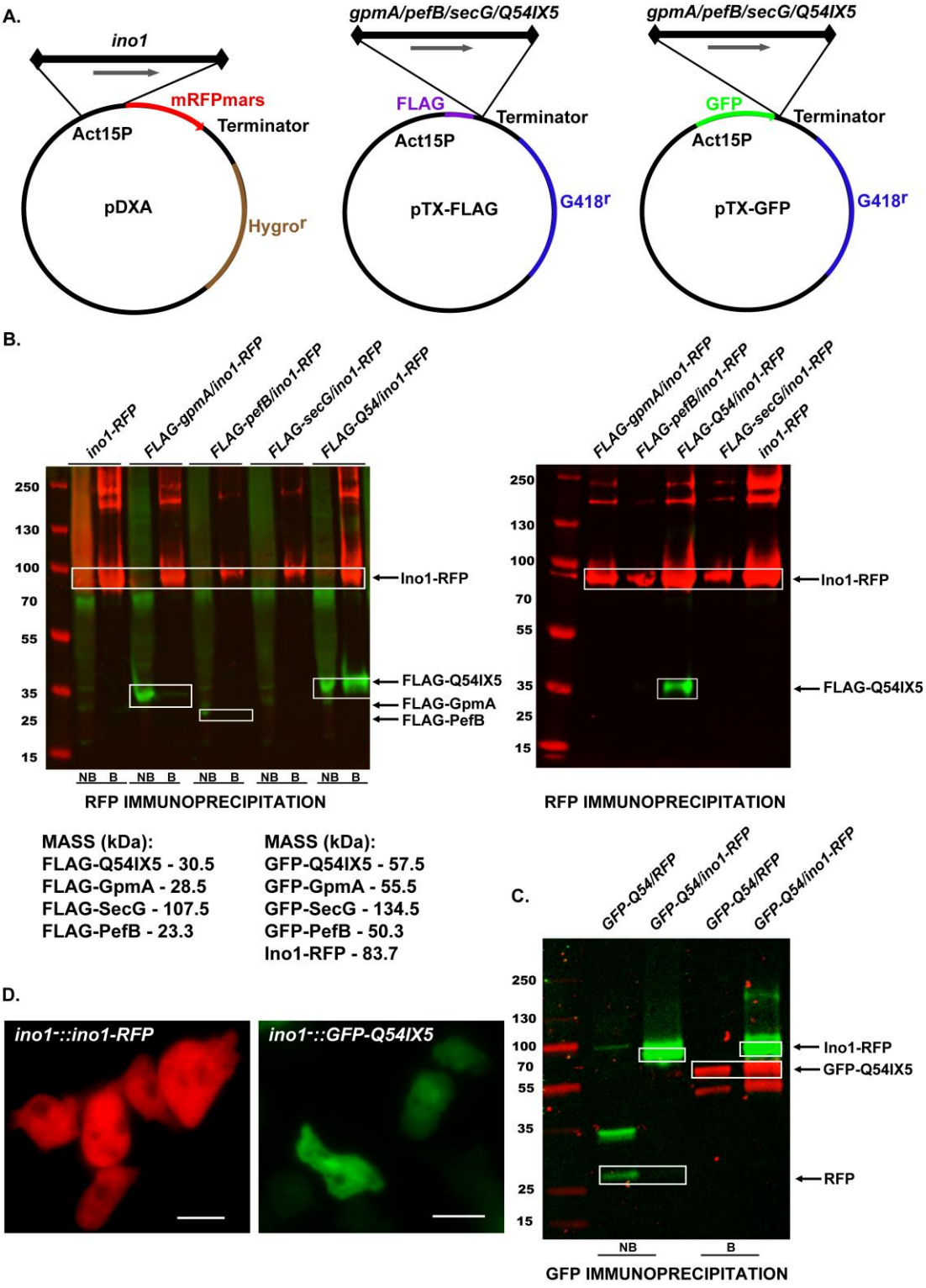

Figure 6.7 Ino1 protein interaction analysis. (A) Schematic showing vectors transformed into *Dictyostelium ino1*$^{-}$ cells to co-express Ino1-RFP along with its putative interacting protein, with either a FLAG or GFP tag. Hygromycin (50 µg/ml) and neomycin (G418) (20 µg/ml) were used for a double selection to isolate these cell lines. (B) FLAG-tagged GpmA, PefB, SecG and Q54IX5 proteins co-expressed in *ino1*$^{-}$ cells with Ino1-RFP were investigated by co-immunoprecipitation using anti-RFP-coated beads, followed by western blot analysis with anti-RFP and anti-FLAG antibodies. Left: first repeat of the immunoprecipitation; gel electrophoresis showed the presence of FLAG-GpmA, FLAG-PefB

and FLAG-Q54IX5 proteins (FLAG-SecG protein was not detected) in the eluate that was not bound to the antibody-coated beads. A weak band representing FLAG-GpmA in the bound fraction (Ino1-RFP bound proteins) was not confirmed in the second repeat of the immunoprecipitation. FLAG-PefB was also not seen in the bound fraction. FLAG-Q54IX5 was present in both repeats of the immunoprecipitation. The strong band detected for FLAG-Q54IX5 suggested a strong interaction with Ino1-RFP protein. (C) The Ino1-Q54IX5 interaction was confirmed by immunoprecipitation of GFP-Q54IX5 with anti-GFP-coated beads from *ino1*$^-$ cells co-expressing Ino1-RFP, followed by western blot analysis with anti-RFP and anti-GFP antibodies. GFP-Q54IX5 protein co-immunoprecipitated Ino1-RFP but not RFP, suggesting that the interaction was specific to Ino1. (D) Live cell imaging revealed cytosolic localisation of the GFP-Q54IX5 protein. Similarly, Ino1-RFP protein was also detected in the cytosol. Size bars represent 10 µm.

6.7 Discussion

In the previous chapters, the *ino1*$^-$ mutant cells were shown to be dependent on a supply of exogenous inositol in order to grow and develop. However, only the presence of the Ino1 protein, and not inositol supplementation, led to a full restoration of the growth rate, and rescued the inability of the *ino1*$^-$ mutant to consume bacteria (Chapter IV). The loss of the Ino1 protein, as opposed to inositol deprivation, also caused major metabolic changes in *Dictyostelium* (Chapter V), suggesting that Ino1 protein itself was important in regulating cell function.

To gain more insight into a cellular role for Ino1, the level of Ino1 production in response to inositol treatment was investigated by measuring the expression of the *lacZ* gene, which encodes the β-galactosidase enzyme, from the inositol-sensitive *ino1* promoter. The expression of *ino1* is regulated by the presence of intracellular inositol, since in yeast a decrease in inositol level activates *ino1* transcription (Culbertson et al., 1976; Ford et al., 2007; Shetty and Lopes, 2010). In *Dictyostelium ino1*$^-$ cells, lowered intracellular inositol levels are predicted to activate transcription of the lacZ gene when placed under control of the *ino1* promoter. β-galactosidase activity was thus monitored by measuring colour change in *ino1*$^-$ cells expressing the *ino1-lacZ* construct using colourimetry. 700 bp upstream of the *ino1* start codon were cloned into a vector containing the *lacZ* gene, since the identity of the *ino1* promoter is not known in *Dictyostelium.* However, this AT-rich upstream sequence, the presumptive *ino1* promoter region, proved to be problematic for the generation of a mutation-free construct because of Taq polymerase

errors or replication within bacteria; a clone with the highest homology to the sequence from the annotated *Dictyostelium* genome of this region was used in this experiment. β-galactosidase enzymatic activity was detected in the positive control samples, *ino1*$^{-}$ cells constitutively expressing the *lacZ* gene from an actin15 promoter, but was undetectable in the *ino1*$^{-}$ cells expressing *lacZ* gene under control of the putative *ino1* promoter. This result indicated that the *ino1* promoter was not functional in these cells, presumably resulting either from the nucleotide mismatches in the cloned *ino1* promoter sequence from the published sequence, or because the region cloned was too small. This approach requires further optimisation and was not taken forward in this project due to time constraints.

To study the non-catalytic role of Ino1, a point mutation was introduced at the core catalytic site of the protein. The aspartic acid present within the *Dictyostelium* Ino1 catalytic region at position 342 is highly conserved in the Ino1 proteins from various biological species (Majumder et al., 2003) (Figure 6.2 B), and thus mutation of this residue was expected to disturb catalytic function of the Ino1 protein. The aspartic acid was replaced with alanine, as it is small, non-polar, hydrophobic and relatively non-reactive, and thus was unlikely to cause protein missfolding or unwanted reactiveness with other molecules. On the other hand, since aspartic acid is polar and negatively charged (often found in protein active sites (Betts and Russell, 2003)), a substitution with alanine would be predicted to significantly compromise the interactions of the Ino1 protein that contribute to its catalytic activity. Since the introduced D342A mutation is in the catalytic site of the inositol biosynthetic enzyme, it is predicted to disrupt inositol production. *Ino1*$^{-}$ cells producing Ino1-D342A would therefore be predicted to still require exogenous inositol to grow. Expression of Ino1-D342A in *Dictyostelium ino1*$^{-}$ cells did not rescue the inositol auxotrophy resulting from *ino1* loss, suggesting that Ino1 with this mutation could not catalyse inositol biosynthesis and hence, *ino1*$^{-}$ cells producing Ino1-D342A protein were unable to grow in the absence of exogenous inositol. Overexpression of the mutated protein in wild-type cells reduced their growth, independently of exogenous inositol provision even though the cells were able to proliferate.

Ino1 protein exists as a homotetramer or a trimer in other organisms (Majumder et al., 1997). This, it is possible that, by similarity, assembly of oligomers in *Dictyostelium* from the endogenous pool of catalytically functional Ino1 monomers and a population of heterologously overexpressed, catalytically non-functional, Ino1 monomers would yield oligomers that were catalytically inactive or had a reduced ability to produce inositol, hence, leading to a decrease in cell growth. However, the addition of exogenous inositol in the media did not fully restore the growth rate of wild-type cells expressing Ino1-D342A to the level observed in untransformed wild-type cells, potentially suggesting a role for Ino1 in other cellular functions. Alternatively, the inactivated protein may bind to an deplete the Ino1 substrate, glucose 6-phosphate, thereby reducing growth rate.

Published data relating to an *in vivo* regulation of Ino1 showed that the protein is phosphorylated in yeast at S184, S296, and S374 and these sites are also conserved in humans (Deranieh et al., 2013) and rat (Parthasarathy et al., 2013). By homology alignment, these phosphorylation sites are also predicted in *Dictyostelium.* Analysis of phosphodeficient and phosphomimetic site-mutants in yeast indicated that the three conserved sites in yeast (S184, S296, and S374) and human (S177, S279, and S357) affected Ino1 activity (Deranieh et al., 2013). Phosphodeficient and phosphomimetic Ino1 mutations in the amino acid residue S296 in yeast Ino1 (corresponding to S279 in human Ino1) were shown to decrease Ino1 activity and cell growth. However, phosphomimetic but not phosphodeficient mutations of S184 and S374 in yeast (corresponding to S177 and S357 in human Ino1) decreased Ino1 activity. These findings indicate that, in yeast, phosphorylation at S296 (human S279) is crucial for the protein function while phosphorylation of Ino1 at S184 and S374 (human S177 and S357) is inhibitory (Deranieh et al., 2013). *Dictyostelium* Ino1 phosphodeficient mutations (S179A, S282A, and S360A) still rescued the growth defect of *ino1*$^{-}$ cells in the absence of inositol, indicating that the absence of phosphorylation at these serines did not block Ino1 activity. Since it was shown that phosphorylation of yeast and human Ino1 had an inhibitory growth effect, it is possible that creating phosphomimetic mutations at S179, S282 and S360 in *Dictyostelium* Ino1

protein would also decrease Ino1 activity. Furthermore, as an experimental follow-up, the effect of generating double or triple Ino1 phosphomutations may further define the role of these amino acids. Similarly, double mutation in the yeast Ino1 at S184A/S374A caused an increase in the protein activity, gave a growth advantage, and partially rescued sensitivity to VPA in yeast cells (Deranieh et al., 2013), and these effects could be examined in *Dictyostelium.*

When starved of nutrients, *Dictyostelium* cells initiate a developmental program, where single cells aggregate to form a multicellular organism (Krichevsky and Wright, 1963). During development, a subset of cells release a chemical, cAMP, that is sensed by surrounding cells to activate signalling pathways within these cells, allowing for their migration and aggregation (Loomis, 2014). *Dictyostelium* cell migration and differentiation involves cell-substrate adhesion and constant reorganisation of cell-shape, and thus many proteins involved in development are involved in regulation of cytoskeletal activity, such as Rac/Cdc42 GTPases, talin, myosin II or the polymorphic adhesion proteins TgrB1 and TgrC2 (Devreotes and Horwitz, 2015; Dumontier et al., 2000; Hirose et al., 2015; Park et al., 2004; Tarantola et al., 2014; Wang et al., 2014; Zhu et al., 2015). For example, a myosin II light chain gene disruption leads to abnormal development where 50% of cell aggregates are arrested at the mound stage and the other 50% form aberrant fruiting bodies with short, thickened stalks (Chen et al., 1995). As shown in the previous chapter, *ino1* disruption caused cell-adhesion and chemotaxis defects, and therefore it was useful to analyse development of the *ino1*$^-$ mutants. Additionally, as the inositol-depleting drugs VPA and lithium block *Dictyostelium* development (Williams et al., 2002), investigating the effect of these drugs on development of the cells lacking or overproducing Ino1 could provide insight into the roles of Ino1 in these cells and the specific targets of these drugs. Developmental analysis of the *ino1*$^-$ mutants showed no change in the formation or morphology of the fruiting body in the cells lacking or overproducing Ino1 (provided that the former was cultured in the inositol-supplemented media). Also, no difference was seen between the 1 mM VPA- or 10 mM lithium-treated *ino1* mutant cells relative to the wild-type control,

suggesting that neither of these drugs directly target Ino1 in these cells. This finding is corroborated by previous studies where VPA was shown to inhibit inositol biosynthetic activity of Ino1 *in vivo* but not *in vitro* (Deranieh et al., 2013; Ju and Greenberg, 2003; Shaltiel et al., 2004). The indirect inhibition of Ino1 by VPA suggests that there is another protein or a complex of proteins that mediate the action of this drug *in vivo*.

To investigate a potential non-catalytic role of Ino1 in *Dictyostelium*, co-immunoprecipitation to identify putative binding partners of the protein was performed. Anti-RFP agarose beads were used to immobilise Ino1-RFP and any potential interacting proteins. The isolated complexes were then separated on by SDS-PAGE, visualised with Coomassie blue stain and analysed by mass spectrometry. Coomassie blue was chosen for the stain as it has high sensitivity, gives more homogeneity, and does not interfere with mass spectrometry (Gauci et al., 2013; Neuhoff et al., 1988). Data for 90 potential Ino1 interactors was gathered over three independent experiments. These proteins were related to the processes of cytoskeletal organisation, mitochondrial respiration, proton transport, DNA and protein regulation, metabolism, including fatty acid, glycolysis, and purine metabolism. These cellular processes were previously linked to proteins reported to be Ino1 interactors in *Saccharomyces cerevisiae* (yeast) (Boettner et al., 2011; Szappanos et al., 2011; Tarassov et al., 2008) and in humans (Emdal et al., 2015; Low et al., 2014; Wan et al., 2015). Components of the peripheral V1 complex of vacuolar ATPase were also identified in the mass spectrometry analysis. These complexes are responsible for acidifying intracellular compartments in eukaryotic cells (Balakrishna et al., 2015). In yeast, the V-ATPase complex is dysregulated following *ino1* deletion and inositol depletion (Deranieh et al., 2015). Thus the roles for putative Ino1 interactors are consistent with those found in other organisms.

Four proteins of interest were chosen for further interaction studies to confirm their interaction with Ino1. These include GpmA, a phosphoglycerate mutase linked to inositol auxotrophy in yeast via dysregulation of glycolysis (Shi et al., 2005), and related to 2,3 bisphosphoglycerate (2,3 BPG) that was

previously shown to be elevated in a *Dictyostelium ino1*$^{-}$ mutant (Fischbach et al., 2006). FLAG-GpmA was shown to bind Ino1-RFP though the interaction may reflect weak *in vivo* binding within a complex and further experiments are needed to verify this.

A second putative Ino1 interactor that was investigated was PefB, a calcium-binding protein similar to the apoptosis-linked gene 2 (ALG-2) protein implicated in Alzheimer's disease progression (Lacanà et al., 1997; Vito et al., 1996) and an interactor of mucolipin-1 linked to a recessive lysosomal storage disease (Vergarajauregui et al., 2009). A protein of the predicted size (23.3 kDa) was present in cell extracts, suggesting correct expression of the gene. However, a specific Ino1-PefB interaction could not be detected as no band was seen in the bound fraction, suggesting that PefB protein did not interact with Ino1 in these experiments.

The third protein of interest was SecG, an ankyrin repeat-, PH- and SEC7-domain containing protein belonging to the cytohesin family of proteins. This protein is involved in chemotaxis towards cAMP during development and substrate adhesion in *Dictyostelium* (Garcia et al., 2013; Shina et al., 2010). This protein was of interest since in the previous chapters, the Ino1 protein was shown to be required for cell movement during chemotaxis towards cAMP and cell-substrate adhesion. SecG is needed for coordination of F-actin organization during development (Garcia et al., 2013) and cell-substrate adhesion (though not cell-cell adhesion) (Shina et al., 2010). The expression of FLAG-SecG however did not enable the detection of tagged SecG in either non-bound or bound fractions. It is possible that the protein was expressed at a low level or it was degraded since a small number of very faint low molecular weight bands were detected with anti-FLAG antibodies in the western blots, suggesting that protein degradation occurred. However, similar bands were present in all the samples, and thus it is likely that this degradation is not SecG-specific. During early development proteolytic activity is reduced (Fong and Rutherford, 1978), and therefore, a further optimisation approach to decrease the possible degradation of SecG

and enhance its detection would be to pulse *Dictyostelium* cells with cAMP for 5 hours in order to initiate development prior to cell lysis.

Finally, another protein of interest in the Ino1 interaction studies was Q54IX5, an uncharacterised protein with three Sel1-like domains and a tetratricopeptide repeat (TPR). The interaction of Q54IX5 with Ino1 was confirmed by co-immunoprecipitation of FLAG-Q54IX5 with Ino1-RFP. Further analysis by performing a reverse immunoprecipitation indicated that Ino-RFP strongly interacted with GFP-Q54IX5 protein. Q54IX5 is predicted to belong to the SEL1 subfamily and it contains the tetratricopeptide repeat (TPR) structural motif. TPRs often form scaffolds to mediate protein-protein interactions during the assembly of multiprotein complexes (Blatch and Lässle, 1999). It is therefore possible that the Ino1 interaction with Q54IX5 facilitates Ino1 binding to other proteins.

Two potential roles for Ino1-Q54IX5 interaction can be proposed here. Firstly, a Ino1-Q54IX5 interaction may be involved in the regulation of the Unfolded Protein Response (UPR), a cellular stress response that is conserved between mammals, yeast and worms (Walter and Ron, 2011). UPR is activated in response to an accumulation of unfolded or misfolded proteins in the endoplasmic reticulum (Walter and Ron, 2011). The human SEL1L protein (found to be 37% identical to Q54IX5 via a BLAST search) is an important protein involved in homeostatic pathways where it participates in a ubiquitin-dependent degradation of misfolded endoplasmic reticulum proteins (Cattaneo et al., 2014). UPR is required for sustained high-level *ino1* expression in wild-type *S. cerevisiae* (Chang et al., 2002). *Ino1* transcription is regulated by intracellular inositol and choline levels, where the decrease in both molecules activates *ino1* transcriptional regulators that bind to UAS_{INO} promoter element to de-repress *ino1* transcription (Shetty and Lopes, 2010). The UPR effect on *ino1* transcription is, however, not via an UAS_{INO1} promoter element, and is also independent of inositol depletion or changes in lipid metabolism (Chang et al., 2002). In the view of these facts, there is a possibility that Q54IX5 protein may interact with Ino1 to facilitate *ino1* expression independent of inositol levels in cells. Since Q54IX5 contains a

number of TPR motifs, which facilitate the formation of protein-protein complexes (Blatch and Lässle, 1999), this interaction might allow for Ino1 binding to other proteins, and potentially those involved in UPR. To strengthen this assumption, a number of proteins identified by the immunoprecipitation experiments were related to protein ubiquitination and UPR (Supplementary material, Table S2). Moreover, VPA has been proposed to regulate UPR, and the downregulation of SEL1L protein in glioma stem cells sensitised these cells to cytotoxic effects of VPA (Cattaneo et al., 2014), which has a potential therapeutic role. The role of Ino1 in its own gene upregulation, independent of inositol, remains to be investigated.

A second possible role for an Ino1-Q54IX5 interaction is the regulation of processes like the immune response or phagocytosis in an inositol-independent manner. This hypothesis is based on the similarities between *ino1*$^{-}$ and *Dd5P4*$^{-}$ mutants (Loovers et al., 2007). The *Dictyostelium* Dd5P4 gene encodes a type II inositol 5-phosphatase that when deleted in *Dictyostelium* causes a similar phenotype to the *ino1*$^{-}$ mutant described in this work, namely, slower growth in axenic media and strongly reduced growth on bacteria (shown to be due to an inefficiency in closing the phagocytic cup and forming a phagosome) (Loovers et al., 2002, 2007). The human homologue of Dd5P4, OCRL1, was shown to functionally replace *Dictyostelium* Dd5P4 (Loovers et al., 2007). When expressed in *Dictyostelium Dd5P4*$^{-}$ cells, OCRL1 was shown to interact with a SEL1-like repeat protein, allowing for its binding to phosphatidylinositol 3-phosphate to partially rescue the impaired growth phenotype of *Dd5P4*$^{-}$ cells (Loovers et al., 2007). Additionally, during *Legionella pneumophila* infection, OCRL1 was shown in *Dictyostelium* to localise to the replicative vacuole to suppress the infection by binding to a SEL1-like domain-containing protein involved in the vacuole formation (Weber et al., 2009). Transcriptional regulation of *ino1* and phagocytosis-related roles of Ino1-Q54IX5 interaction remain to be examined in future studies.

Finally, the immunoprecipitation approach described here for Ino1-RFP identified multiple high molecular weight bands in a ladder-like pattern. This pattern suggests the presence of ubiquitin-conjugates (S.Lilla, personal

observation) as a result of Ino1 protein ubiquitination or sumoylation. Small ubiquitin-related modifiers (SUMOs) are ubiquitin-like polypeptides that are covalently conjugated to cellular proteins as part of the post-translational modifications that participate in diverse cellular processes, including transcriptional regulation, maintenance of genome integrity, and autophagy (Johnson, 2004). SUMO attachment to protein is reversible and controlled by enzymes involved in ubiquitin pathways. Additionally, a number of proteins conjugated with SUMOs can be recognized by SUMO-targeted ubiquitin ligases (STUbLs), and thus marked for a degradation by the proteasome (Hemelaar et al., 2004; Schwartz and Hochstrasser, 2003). Several SUMO pathway enzymes were previously found to be required for growth under inositol depletion conditions (Felberbaum et al., 2012), corroborating the idea that Ino1 may be ubiquitinated/sumoylated.

6.8 Summary

Studies to identify novel roles of Ino1 in regulating cellular function involved introducing single point mutations in the Ino1 protein and co-immunoprecipitation to identify Ino1 binding partners. Using an immunoprecipitation approach, a number of potential Ino1 binding partners was identified, including proteins related to cytoskeletal organisation, mitochondrial respiration chain, proton transport, DNA and protein regulation, and metabolism. The interactions of Ino1 with GpmA, a phosphoglycerate mutase and Q54IX5, which belongs to the SEL1 subfamily and contains a tetratricopeptide repeat (TPR), were confirmed. Although the Ino1-Q54IX5 interaction is still to be investigated, it is proposed that Q54IX5 functions in mediating protein-protein interaction involving Ino1, potentially during the assembly of a multiprotein complex.

Chapter 7
Conclusions

Chapter VII

Conclusions

7.1 Background

Inositol and inositol-containing compounds are vital cellular components, thus it is often difficult to investigate the effects of inositol depletion without inducing cell death. Previous studies reported in organisms such as the yeast *S.cerevisiae, A.thaliana,* and *Dictyostelium*, have shown a loss of viability associated with inositol depletion, termed “inositol-less death”. Inositol depletion has been also linked to an imbalance in the synthesis of cellular components leading to an “unbalanced cell growth” (Culbertson et al., 1976; Donahue et al., 2010; Fischbach et al., 2006; Ohnishi et al., 2014; Ridgway and Douglas, 1958). Inositol is involved in a number of cellular events that maintain cell homeostasis and function, including cell movement, cytokinesis, protein modification and degradation, and autophagy (Brill et al., 2011a; Criollo et al., 2007; Deranieh and Greenberg, 2009; Deranieh et al., 2015; Di Daniel et al., 2006; Europe-Finner et al., 1989; Guérin et al., 2009; Jesch et al., 2005; Kim et al., 2013; Kotaria et al., 2013; Michell et al., 1992; Straub et al., 2006; Toker and Agam, 2014; Vicencio et al., 2009; Williams et al., 2002; Yamagami et al., 2015; Zhang et al., 2012). Additionally, inositol, along with choline, is an important osmolyte (Villarreal and Kültz, 2015) that plays a role in stress response.

Inositol dysregulation has been reported in a variety of human health disorders. A number of structurally different bipolar disorder treatments, carbamazepine, valproic acid (VPA), and lithium, that act via an inositol depletion mechanism (Williams et al., 2002), have been shown to induce autophagy *in vitro* and *in vivo* (Motoi et al., 2014; Toker et al., 2014). Similarly, carbamazepine initiated an autophagic response and reduced intracellular inositol and phosphoinositide levels in an animal model organism and in *Dictyostelium* (Schiebler et al., 2015). Also, altered inositol levels have

been reported in the brains of patients suffering from bipolar disorder (Shimon et al., 1997), major depressive disorder (Coupland et al., 2005), and schizophrenia (Shimon et al., 1998). Following this, inositol has been proposed as a therapy in the treatment of bipolar disorder (Chengappa et al., 2000), depression, and panic disorders (Palatnik et al., 2001). Additionally, Ino1 protein levels have been reported to be elevated in post-mortem brains of Alzheimer's patients (Shimohama et al., 1998), although in other studies pathologically lowered inositol levels and mitochondrial dysfunction have been demonstrated in mouse neurons (Trushina et al., 2012). The roles of inositol in the various cellular processes mentioned here and their linked diseases are not yet clearly defined. This project aimed at investigating the mechanisms of inositol regulation in *Dictyostelium* cells.

7.2 The effects of inositol depletion on *Dictyostelium ino1*$^-$ cells (Figure 7.1)

7.2.1 Reduction in the inositol level and inositol auxotrophy

To examine the role of inositol depletion on cell function and metabolism, the Ino1 enzyme, essential for the *de novo* production of inositol, was genetically ablated. The concentration of inositol was measured in the *ino1*$^-$ cells exposed to inositol depleting conditions, showing that the levels of inositol decreased rapidly in the *ino1*$^-$ mutant by 35% - 60% within 12 to 24 hours of inositol starvation. This finding confirms the necessary role for Ino1 in producing inositol. Ablation of *ino1* produced an inositol auxotrophic phenotype and defective development, which was rescued by treatment with exogenous inositol.

7.2.2 Decrease in the level of phosphoinositides

Reduced inositol also caused a general decrease in the level of phosphoinositides in cells. Understanding the role of inositol-dependent loss of phosphoinositides in *Dictyostelium* is complicated by the presence of novel chemical species. *Dictyostelium* has been reported to contain two types of phosphoinositides, varying by the glycerol-fatty acid linkages that comprise

diacyl (acyl/acyl) containing or an ether (ether/acyl) containing phosphoinositides (Clark et al., 2014). Inositol reduction caused a rapid decrease in PI and PIP (both diacyl and ether species) and diacyl PIP2, however, the level of ether PIP2 was not changed, highlighting the importance of this phospholipid for cell function. The ether species of phospholipids are more abundant and comprise over 95% of *Dictyostelium* inositol phospholipids (Clark et al., 2014). As a result, diacyl phospholipids might be broken down more rapidly, or alternatively, these compounds may provide more labile signalling molecules compared to ether phospholipids.

7.2.3 Reduction in actin-dependent cell functions

Inositol depletion also reduced cytokinesis, cell substrate adhesion, and velocity during chemotaxis in the *ino1*$^{-}$ mutant. These cellular functions are dependent on actin dynamics, where PIP2 plays an important role (Wu et al., 2014). PIP2 participates in signalling pathways that regulate actin polymerisation and depolymerisation in substrate attachment (Wu et al., 2014), and is critical for proper scission of the cleavage furrow in cell division (Logan and Mandato, 2006). Since cell motility and migration requires a controlled attachment and detachment from the substrate, the reduction in cell velocity observed in the *ino1*$^{-}$ mutant may result from an impaired cell-substrate adhesion. Activation of small GTP-binding proteins regulates actin structures in cells, and the generation of contractile forces during cell migration, with PIP2 levels being central to these processes (Wu et al., 2014). PIP2 promotes the initiation of new actin filaments and enables the elongation of the existing ones (Insall and Weiner, 2001). Therefore, a decreased level of the diacyl PIP2 observed during inositol depletion may lead to a reduction of cytokinesis, cell-substrate adhesion and the speed of cell movement. Interestingly, ether PIP2 levels were not changed by the removal of inositol supplementation. Thus, diacyl PIP2 may be preferentially used in the regulation of cell function during cell attachment, division and motility events.

7.2.4 Autophagosome accumulation

During inositol starvation, *ino1*$^{-}$ cells were shown to accumulate over three-fold more autophagosomes than wild-type or *ino1*$^{-}$ cells grown in the presence of inositol. Autophagosomes are produced during autophagy to clear away non-functional cellular components, for example misfolded proteins or damaged organelles during stress responses like nutrient starvation (Glick et al., 2010). The phosphoinositides PIP, PIP2, and PIP3, and their effectors, play an important role in various aspects of autophagy, including the control of autophagosome biogenesis, maturation, and intracellular transport (Dall'Armi et al., 2013). For example, the local production of PIP on the isolation membrane (one of the initial steps of autophagosome formation) promotes the membrane negative curvature and controls autophagosome size (Dall'Armi et al., 2013). PIP2 controls late stages of autophagy, specifically the maturation and turnover of autophagosomes, where it promotes membrane trafficking and fusion events, as well as compartment acidification (Dove et al., 2009). Also, the conversion of PIP2 to PIP3 is the initial trigger that activates mTOR complex 1 (mTORC1) and suppresses autophagy (Zoncu et al., 2011). Thus, the decreased level of phosphoinositides resulting from inositol depletion may lead to an accumulation of not fully formed autophagosomes.

7.2.5 Increased catabolism supports an induction of autophagy

Inositol depletion accounted for a minor change in the metabolic profile of *Dictyostelium ino1*$^{-}$ cells, leading to an increase in amino acids and products of the Kreb's cycle, which is suggestive of enhanced catabolism. Amino acid deficiency has been shown to activate autophagy by direct inhibition of various components of the signalling pathways downstream from growth factors (Beugnet et al., 2003; Lynch, 2001; Nobukuni et al., 2005). As a result, inositol depletion can potentially initiate a stress response due to nutrient deprivation over 24 hours, and thus trigger an autophagic response, possibly leading to cell death.

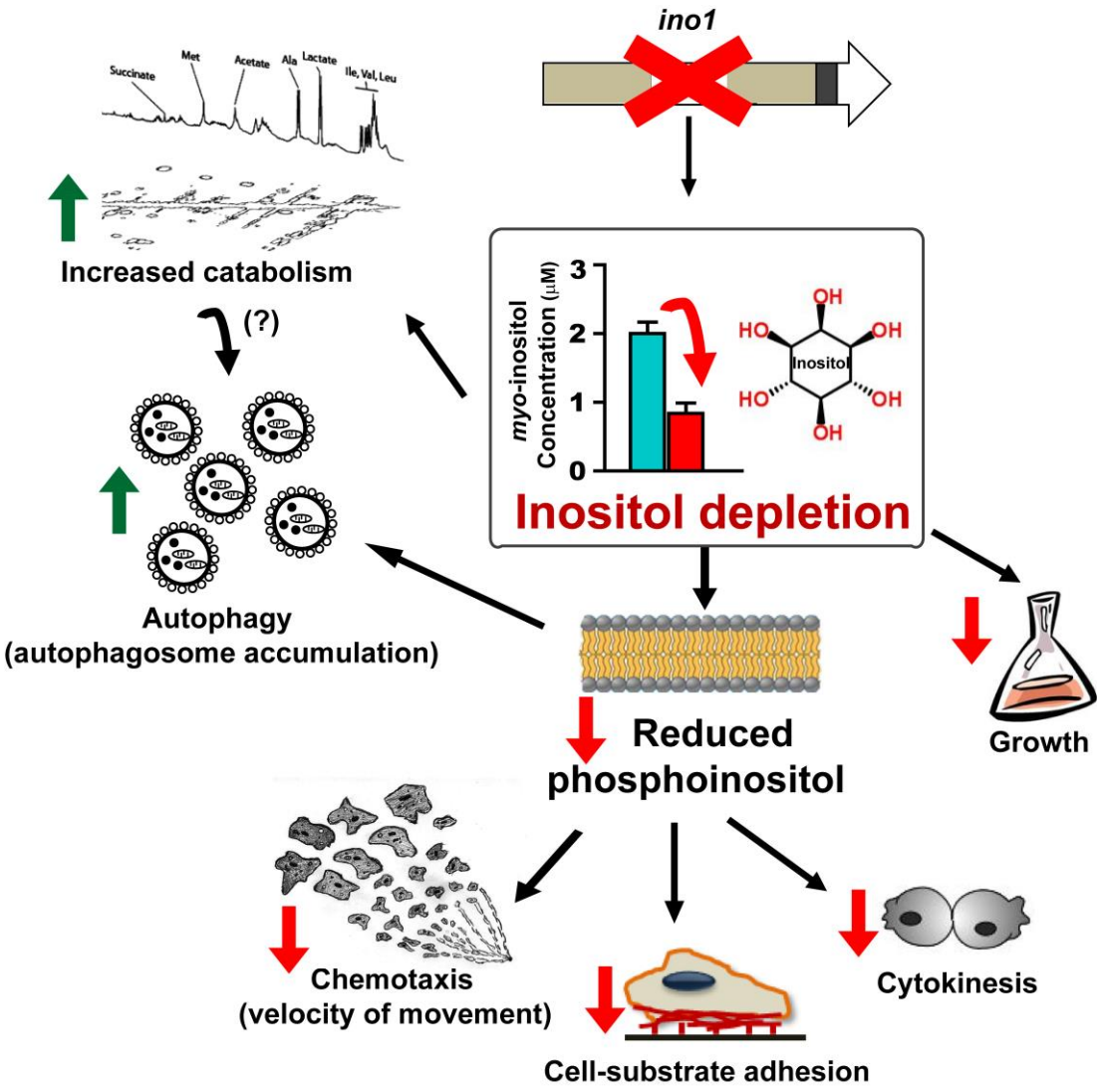

Figure 7.1 The effects of inositol depletion on *Dictyostelium ino1*⁻ cells. Inositol levels were reduced in the *ino1*⁻ cells in the absence of exogenous inositol, and were rescued by the addition of inositol. A number of cellular functions were assessed to investigate this relationship. Inositol depletion caused an inability of cells to grow in liquid media and a decrease in phosphoinositol production, which in turn reduced cell velocity during chemotaxis, cell-substrate attachment, cytokinesis, and likely caused an impairment of cellular membrane synthesis. Reduced inositol levels also led to increased catabolism in cells, marked by an increase in amino acid levels and compounds related to energy metabolism in cells. *Ino1*⁻ cells starved of inositol were shown to accumulate autophagosomes, possibly as a result of increased autophagy linked to a metabolic imbalance caused by the nutrient starvation.

These findings thus confirm an important role for inositol in maintaining optimal growth conditions in cells and give a validation for the unbalanced growth of inositol auxotrophs. Furthermore, these studies suggest a number of phenotypic, but no major metabolic changes, in the cells that are exposed to inositol depleting conditions (Figure 7.1).

7.3 The effects of the Ino1 loss on *Dictyostelium ino1*$^-$ cells (Figure 7.2)

7.3.1 Impaired cell growth and phagocytosis

Ino1 loss led to inositol depletion in the absence of exogenous inositol, but additionally some changes that were not rescued by inositol supplementation. Inositol levels in the *ino1*$^-$ cells grown in the presence of exogenous inositol were equivalent to the level of inositol in the wild-type cells. Hence, the behavioural changes observed in the *ino1*$^-$ mutant in the presence of inositol may be due to a loss of the Ino1 protein. Since the inositol auxotrophy of the *ino1*$^-$ mutant was only partially rescued by exogenous inositol supplied in saturating conditions (300µM and 500µM), this suggests a potential role for Ino1 protein outside of inositol biosynthesis to promote cell growth. Additionally, Ino1 may be involved in mediating efficient phagocytosis, since inositol supplementation in the *ino1*$^-$ cells grown on agar plates seeded with bacteria did not rescue the inability of these cells to phagocytose.

7.3.2 Reduced cell polarity and decreased PIP3 levels

Ino1$^-$ cells showed reduced polarity during chemotaxis, regardless of the presence of exogenous inositol, thus suggesting that Ino1 protein is involved in signalling leading to cell polarisation during chemotaxis or the localised production (spatial distribution) of inositol is important in this process. Interestingly, ether PIP3 levels were severely reduced in the *ino1*$^-$ mutant (diacyl PIP3 levels were too low to allow for quantification), even in the conditions where inositol was present, suggesting that the absence of the Ino1 protein had an inositol-independent effect on the regulation of PIP3 levels. Signalling via PIP3 is required for cell polarisation during cell movement (Hoeller and Kay, 2007), and since PIP3 levels were reduced in the *ino1*$^-$ mutant, the data supports a notion of Ino1 regulating these processes independent of inositol biosynthesis. These findings thus suggest that the loss of the Ino1 protein may lead to a decrease in PIP3 production, which reduces the effective chemotaxis in the *ino1*$^-$ cells.

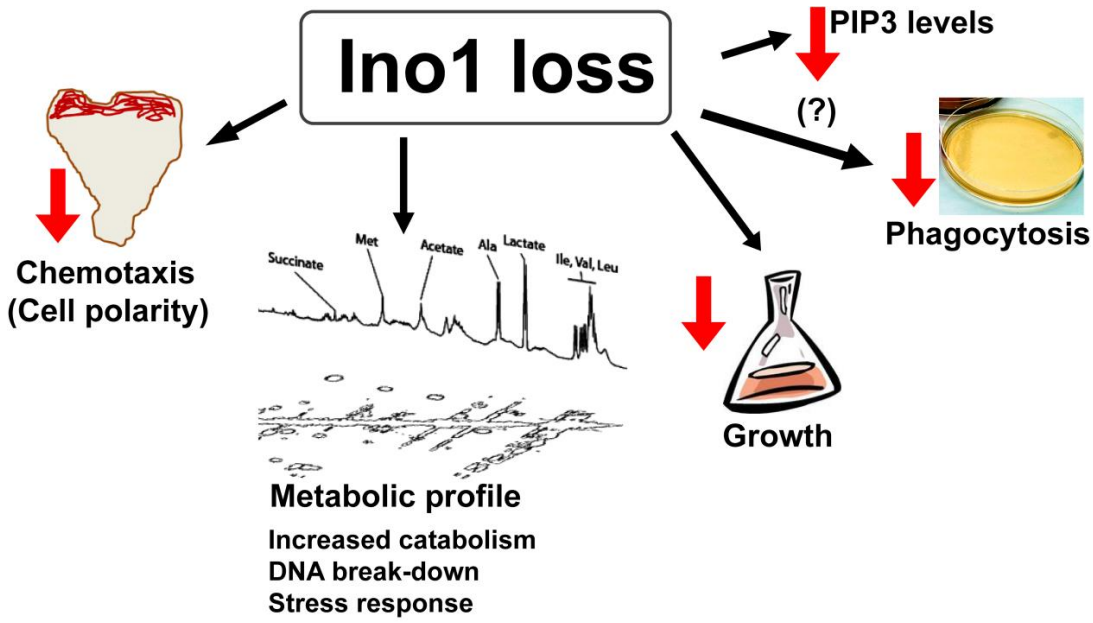

Figure 7.2 The effects of the Ino1 loss. Ino1 loss caused a number of cellular effects that were not rescued by the addition of exogenous inositol. This includes a major change in the metabolic profile of *Dictyostelium,* specifically observed by an increase in the level of some amino acids, break-down products of nucleic acids, energy-related metabolites, and stress-related molecules. Ino1 loss also caused a reduction in cell polarity, possibly due to a decrease in PIP3 production. *Ino1*$^{-}$ cells, even when grown in the presence of inositol, were not able to phagocytose; the growth in liquid media was also not fully restored, suggesting that Ino1 protein may be also involved in these biological processes.

7.3.3 Major changes in the metabolic profile

The general differences in the metabolic profile of *Dictyostelium ino1*$^{-}$ mutant were due to the loss of the Ino1 protein rather than inositol treatment. Although inositol depletion accounted for a minor variation in the metabolic profile of the *ino1*$^{-}$ mutant, the removal of the Ino1 protein led to a wide metabolic change in these cells. Metabolic profile analysis showed that the Ino1 loss caused an increase in amino acids and a build-up of molecules related to energy metabolism (fumarate, lactate, acetate and succinate that are linked to the Kreb's cycle), likely via the loss of inositol synthesis in these cells. Additionally, Ino1 absence resulted in an increase in metabolites related to nucleotide degradation (β-alanine) and stress response (glycerophosphocholine), independently of inositol provision. These metabolic changes represent differences in protein, energy, and DNA regulation, which have major effects on cellular function, and suggest an

important role for the Ino1 protein in metabolic regulation, independent of inositol levels.

7.4 Relationship between inositol depletion and Ino1 loss

It is likely that the molecular and metabolic effects of Ino1 presence and inositol depletion are interrelated. Decreased intracellular inositol levels have been shown to activate *ino1* expression in a number of organisms, including yeast (Shetty et al., 2013; Vaden et al., 2001), *Dictyostelium* (Williams et al., 2002), and mice (Shamir et al., 2003); therefore, inositol depletion is potentially elevating Ino1 levels. Many studies concerning inositol depletion have predominately relied on using inositol-depleting drugs that are prescribed as bipolar disorder treatments and act via multiple targets (Ju and Greenberg, 2003; Shaltiel et al., 2004; Terbach and Williams, 2009). Hence, results reported by these studies are likely to be complicated by secondary effects.

The results presented in this thesis suggest that short-term inositol depletion does not cause large scale metabolic changes in *Dictyostelium*. Additionally, under normal circumstances, reduced inositol levels increase *ino1* transcription, thus acting to reverse this deficit (Williams et al., 2002), and protecting cells against the effects of inositol imbalance. In contrast, a dysregulation of this responsive mode, where Ino1 protein is absent (*ino1*$^-$ mutant), is likely to cause greater metabolic effects with possibly enhanced phenotypic changes. Indeed, antisense silencing of the *Dictyostelium ino1* expression (Fischbach et al., 2006) resulted in less severe phenotypic effects compared to those observed in the *ino1* knock-out.

7.5 Ino1 protein binding partners

Protein interaction studies were conducted to examine a potential role for Ino1 in cell signalling, independent of its ability to synthesise inositol. Immunoprecipitation experiments showed that Ino1 interacts with a protein, Q54IX5, with an unidentified function that contains SEL1-like domain and

tetratricopeptide repeats, which are typically present in proteins that assemble multi-protein complexes. Ino1 was also shown to weakly bind to 2,3-bisphosphoglycerate-dependent phosphoglycerate mutase (GpmA), which catalyses the interconversion of 2-phosphoglycerate and 3-phosphoglycerate. 2,3-BPG is a product of the glycolysis branch, and has been shown *in vitro* to be a competitive inhibitor of inositol-polyphosphate 5-phosphatases (Rana et al., 1986), and is elevated in the *Dictyostelium ino1*$^-$ mutant (Fischbach et al., 2006).

7.6 Mutation in the Ino1 catalytic domain

To investigate a potential non-catalytic role for Ino1 in cell function, an Ino1-D342A protein was expressed in the *ino1*$^-$ and wild-type cells, and the growth of these cells was assessed. The mutation was introduced to replace an amino acid in a conserved catalytic region with one that would likely disrupt the catalytic activity of the Ino1 enzyme. Indeed, the presence of the Ino1-D342A protein did not rescue the inositol auxotrophy resulting from Ino1 loss, confirming that this protein did not catalyse inositol biosynthesis. Furthermore, the mutated protein reduced cell growth in both *ino1*$^-$ and wild-type strains, independently of exogenous inositol supplementation. This dominant negative effect in wild-type cells may be due to depletion of the Ino1 substrate glucose 6-phosphate, with resulting effects on cell energy and metabolism, an inactivation of a potential Ino1 multimeric protein complex, or by other mechanisms.

7.7 Ino1 as a target for VPA

Several studies have suggested VPA may function through an inhibition of Ino1 (Agam et al., 2002; Deranieh et al., 2013; Ju et al., 2004; Shaltiel et al., 2004). The human Ino1 protein is inhibited *in vivo* but not *in vitro* by the inositol-depleting drug VPA (0.6 mM), when the protein was expressed in yeast cells lacking the endogenous Ino1 (Ju et al., 2004). The activity of Ino1 in these cells was decreased by 35%, and the level of inositol reduced by 25%, following VPA treatment (Ju et al., 2004). VPA and lithium

were also previously shown to inhibit *Dictyostelium* development related to inositol depletion (Williams et al., 2002). The VPA-sensitivity of *Dictyostelium* cells lacking or overexpressing Ino1 however did not differ to the VPA-sensitivity observed in the wild-type cells, suggesting that VPA does not directly target Ino1 to cause inositol depletion.

7.8 Implications of our findings for disease

The research presented in this thesis shows an importance of inositol for a number of cellular functions, including cell attachment and autophagy, which have been previously linked to neurodegenerative diseases and neuropsychiatric disorders (Corvin, 2010; Lionaki et al., 2015; Nilsson et al., 2013; O'Dushlaine et al., 2011; Sarkar et al., 2005). Genome-wide association studies have identified significant association between the cell adhesion molecule (CAM) pathway and susceptibility to schizophrenia and bipolar disorder (Corvin, 2010), suggesting a potential role of cell adhesion in pathology of these neuropsychiatric disorders. Different signalling molecules regulate cell adhesion, among them, phosphatidylinositol-4,5-bisphosphate (PIP2) modulates diverse biological processes, including actin cytoskeletal dynamics required for cell adhesion. In this thesis, inositol depletion was shown to cause the loss of cell substrate adhesion in the *ino1*$^{-}$ mutant, which has been suggested to be a result of the dysregulation of PIP2 in these cells. Phospholipids and inositol phosphates have also been linked to autophagy in various model organisms (Criollo et al., 2007; Knorr et al., 2014; Nagata et al., 2010; Parys et al., 2012; Sarkar et al., 2005). Dysregulation of the inositol signalling pathway therefore links to cellular processes previously implicated in human disease, and suggests that molecules like PIP2 may be important regulators of these processes in the context of a disease.

Analysing metabolite changes in patient tissues is informative for research into the molecular basis of human diseases (Bracken et al., 2011). For example, magnetic resonance spectroscopy has previously reported abnormalities in the brain *myo*-inositol concentrations of bipolar patients (Davanzo et al., 2001; Silverstone et al., 2005). The metabolomic study

presented in this thesis reports specific metabolite changes during inositol depletion and Ino1 loss, including increased levels of amino acids, products of DNA break-down, stress response molecules, and energy-related compounds, which may aid discovery of the details of metabolic dysregulation during inositol imbalance in cells.

Additionally, this study shows that the Ino1 protein has a greater impact on the metabolic regulation in *Dictyostelium* cells than inositol depletion, and the loss of this protein causes cellular changes that are not rescued by exogenous inositol supplementation. Ino1 protein levels are also higher in the brains of Alzheimer's disease patients (Shimohama et al., 1998), and patients with family history of a major psychiatric disorder (Shamir et al., 2007). Thus, identifying the roles of Ino1 protein is beneficial to advance research to understand the molecular mechanisms underlying the neurological disorders associated with an inositol imbalance.

7.9 Summary

The aim of this study was to examine the effects of inositol depletion on cell function and metabolism in *Dictyostelium discoideum* by removal of a highly conserved inositol biosynthetic enzyme, Ino1. The results show that Ino1 loss and inositol depletion cause discrete cellular, molecular and metabolic changes. Inositol depletion alters cell physiology, likely leading to an autophagic response, causing a loss in cell-substrate adhesion, reduction in cell division, and a rapid decrease in phospholipids. Inositol depletion does not however cause a large change in the *Dictyostelium* metabolic profile. In contrast, the data presented here suggest that the Ino1 protein plays an important role in cell growth, cell morphology and metabolic regulation, regardless of inositol provision. Ino1 is shown to bind to a putative macromolecular complex linker protein, Q54IX5, suggesting further roles for Ino1. The findings presented in this thesis are likely informative for research into human diseases where inositol involvement has been suggested, and thus may be beneficial for the future development of specific therapies that are more effective and better tolerated than those currently available.

Supplementary Material

Table S1 The list of oligonucleotides used for cloning and screening procedures

Reference	Primer sequence (5’ – 3’)	Notes
ino1 knock-out 3' pLPBLP Forward	AAAAGGATCCTGTCAGCACAAATGTTTGAATC	Clone
ino1 knock-out 3’ pLPBLP Reverse	AAAACTGCAGAGATGGATGGGAGTGGAGTG	Clone
ino1 knock-out 5' pLPBLP Forward	ATACCATGGTCCAGCTGTCGTTGATTTAGCC	Clone
ino1 knock-out 5' pLPBLP Reverse	ATAGGTACCCTGGATGGAAAGTAGCAAATTGATC	Clone
ino1 knock-out RTPCR Forward	GCTGCAAATCAAAAGGATCGTGCC	Screen
ino1 knock-out RTPCR Reverse	AAGGTGTTTTGTGGTGAACCATTGATG	Screen
ino1 knock-out Blast Forward	AGCTGATGCCATGCAACGTGCTC	Screen
ino1 knock-out Blast Reverse	ACTGACGAGATAATCAGTGAGGACAG	Screen
ino1 knock-out Genomic Control Forward	GGCCTTTTCACAGATAAATCAACAAACA	Screen
ino1 knock-out Genomic Control Reverse	GGCCCAACCACCGAAAACAATATCG	Screen
ino1 knock-out Genomic Control Forward	ATAGCTGAAGTTACTAGTCGTATCAC	Screen
ino1 knock-out Vector Control Reverse	GGCCGAGCTAGAAACTTGATAAGAAAGAAAT	Screen
ino1 knock-out Genomic Control Reverse	TGGAGAACGATTGTATTGTGACC	Screen
Blastocidin cassette pLPBLP Forward	AAAAAGATAAAGCTGACCCGAAAG	screen
Blastocidin cassette pLPBLP Reverse	TCAAATAATAATTAACCAACCCAAG	screen
Ino1-RFP (389-2) Forward	TATGGATCCTAATCTTTGTTCTAATAACATG	Clone
Ino1-RFP (389-2) Reverse	GAGCGAATTCATGTCAGCACAAATGTTTGAATC	Clone
mRFPmars Reverse (389-2)	GACCGTTAACTGAACCTTCCA	Screen
D342Adino1 Forward	TAGGTAATAACGCAGGTAAGAATCTCTCTGCTC	Clone
D342Adino1 Reverse	AATGATTGTATGAAACGATTGAAACTGGTTTAATACC	Clone
Ig7_Forward	ACCTACAAGTCGATCAGAGAC	RTPCR control screen
Ig7_Reverse	CACCTCAGTCCTCTCGTAC	RTPCR control screen
hINO1dCB EcoRI Forward	GAATTCATGGAAGCAGCAGCAC	Clone
hINO1dCB Forward	AGGTGCATTAGAATTAGCTTGGC	Clone
hINO1dCB BglII Forward	AGATCTATGGAAGCAGCAGCAC	Clone
hINO1dCB SpeI Reverse	ACTAGTTCAAGTAGTTGGCATTGGTGGT	Clone
hINO1dCB_SacI Forward	GAGCTCATGGAAGCAGCAGCACA	Clone
pefBFLAG Forward	AGATCTATGTACGGATACGGAT	Clone
pefBFLAG Reverse	ACTAGTTTAAACTAAAGCAATGAT	Clone
Q54FLAG Forward	AGATCTATGGAAAATTTAAAATTATT	Clone
Q54FLAG Reverse	ACTAGTTTATTTTTTTAATAAATTTAATTTAG	Clone

secGFLAG Forward	AGATCTATGGGATCAACATCAAATTC	Clone
secGFLAG Reverse	ACTAGTTTAAGATAATGCAGAAGTTTG	Clone
secGMFLAG Forward	GATATGGTAGACCTACTCATTCG	Clone
secGMFLAG Reverse	CGAATGAGTAGGTCTACCATATC	Clone
gpmAFLAG Forward	AGATCTATGGTTTATAAATTAGT	Clone
gpmAFLAG Reverse	ACTAGTTTATTTAGCTTTACCTTGATTGGC	Clone
gpmASacI_FLAG Forward	ATAGAGCTCATGGTTTATAAATTAGTTTTAATTAG	Clone
gpmAXhoI_FLAG Reverse	ATACTCGAGTTATTTAGCTTTACCTTGATTGG	Clone
dINO1_S179A_Forward	CACTCCCAGCCATCTATTTCCCA	Clone
dINO1_S179A_Reverse	TGGGAAATAGATGGCTGGGAGTG	Clone
dINO1_S282A_Forward	CACATACATCAATGGTGCACCACA	Clone
dINO1_S282A_Reverse	TGTGGTGCACCATTGATGTATGTG	Clone
dINO1_S360A_Forward	TTACCAAAGCAAATGTTGTCGATGA	Clone
dINO1_S360A_Reverse	TCATCGACAACATTTGCTTTGGTAA	Clone
dINO1_S354A_Forward	CAATTCCGTGCCAAAGAAATTACC	Clone
dINO1_S354A_Reverse	GGTAATTTCTTTGGCACGGAATTG	Clone
secG_screen Forward	GAGGTTGCACATTTCCTTTTGACTC	Screen
secG_screen Reverse	CCGAATGACCATTGTAGGCTGC	Screen
seC_screenFCT	CTTTGGTTCAAGCAAATCATGCC	Screen
Q54IX5_screen_Forward	GGTATATTACAATGTGATCTC	Screen
dino1_BglIIF (pDM317)	ATAAGATCTATGTCAGCACAAATGTTTG	Clone
dino1_SpeIRSC (pDM317)	ATAACTAGTTTATAATCTTTGTTCTAATAACATG	Clone
dino1_SpeIRNSC (pDM317)	ATAACTAGTTAATCTTTGTTCTAATAACATG	Clone
dino1 pDXA-3H-Hyg	CTTATTTCTTAAAACAAATA	Clone
dino1Bgal_BglIII_R	ATAAGATCTTATTTTTTGTATATATG	ino1 promoter cloning
1K_dino1Bgal_XbaI_F	ATATCTAGAGGGAAATGCAATGCCATTCGGTG	ino1 promoter cloning
0.35K_dino1Bgal_XbaI_F	ATATCTAGACCAACAAATTACACACACACAAAAATAG	ino1 promoter cloning
0.7K_dino1Bgal_XbaI_F	ATATCTAGAATCGTATCATTGATTGCG	ino1 promoter cloning

Table S2 The list of putative Ino1 interacting proteins

Actin-related					
Biological Process	Name	Function	UniProt ID	INO1	Ctrl
❖ **Cytoskeleton organisation** ❖ **Actomyosin contractile ring contraction**	Cortexillin-1 (ctxA)	When linked to F-actin the actin filaments form preferentially anti-parallel bundles that associate into meshworks. Plays a major role in cytokinesis. Negatively regulates cortical localization of rapgap1.	Q54HG2	6	0
❖ **Cytokinesis**	Cortexillin-1 (ctxB)		Q550R2	10	0
❖ **Cell-substrate adhesion**	Talin A (talA)	Involved in the control of cell motility and chemotaxis, phosphatidylinositol-3,4,5-trisphosphate binding.	P0CE94	6	0
❖ **Cell motility**	Talin B (talB)	Required for multicellular morphogenesis. Substrate of pkgB and/or pkbA.	Q54K81	7	0
❖ **Chemotaxis**	SecG	Ankyrin repeat, PH and SEC7 domain containing protein that has ARF guanyl-nucleotide exchange factor activity.	Q54KA7	2	0
❖ **Phototaxis**	Hisactophilin-1 (hatA)	May act as an intracellular pH sensor that links chemotactic signals to responses in the microfilament system of the cells by nucleating actin polymerization or stabilizing the filaments.	P13231	3	0
❖ **Phagocytosis**	Act1	Major actin (cluster)	P07830	32	43
❖ **Response to other organisms**	Act25	Putative actin-25	Q54HF0	9	0
❖ **Development**	Myosin IA heavy chain (myoA)	Motor protein, possibly involved in a wide range of motile processes, such as cell movement across a surface, and extension and retraction of pseudopodia or lamellipodia.	P22467	2	0

Immune Response

Biological Process	Name	Function	UniProt ID	INO1	Ctrl
❖ **Fatty-acid beta oxidation**	MfeA	Peroxisomal multifunctional enzyme A. Enzyme acting on the peroxisomal beta-oxidation pathway for fatty acids. Protects the cells from the increase of the harmful xenobiotic fatty acids incorporated from their diets and optimizes cellular lipid composition for proper development.	Q9NKW1	5	0
❖ **Apoptosis**	DDB_0187993	Cysteine-type endopeptidase activator with activity involved in apoptotic process.	Q54IS1	2	0
❖ **Stress response**	Prdx5	Oxidoreductase activity.	Q54N76	3	0
	Ddj1	Heat shock protein.	Q54VQ1	13	0
	HspK	Small heat shock protein.	Q86H60	3	0

Metabolism

Biological Process	Name	Function	UniProt ID	INO1	Ctrl
❖ **Carbohydrate metabolism**	Gtr2	Uncharacterised.	Q75JH8	8	0
❖ **Cellular aldehyde metabolism**	DDB_0187034	Glutamine-fructose-6-phosphate transaminase.	Q54LK1	2	0
❖ **Electron transport**	Tal	Transaldolase, important for the balance of metabolites in the pentose-phosphate pathway. This protein is involved in the second step of the subpathway that synthesizes D-glyceraldehyde 3-phosphate and beta-D-fructose 6-phosphate from D-ribose 5-phosphate and D-xylulose 5-phosphate (non-oxidative stage).	Q54UP4	2	0

❖ **Glycolysis** ❖ **Tricarboxylic acid cycle** ❖ **Lipid homeostasis** ❖ **Malonyl-CoA biosynthesis**	DDB_G0276821	Putative aldehyde dehydrogenase family 7 member A1 homolog. Aldehyde dehydrogenase (NAD) activity.	P83401	4	0
	Nad7	NADH-ubiquinone oxidoreductase 49 kDa subunit. Core subunit of the mitochondrial membrane respiratory chain NADH dehydrogenase (Complex I).	Q23883	3	0
	Cyb5B	Cytochrome b5 B, heme and electron binding.	Q86L22	2	0
	Pyk	Pyruvate kinase, involved in step 5 of the subpathway that synthesizes pyruvate from D-glyceraldehyde 3-phosphate.	Q54RF5	6	0
	PdhX	Pyruvate dehydrogenase complex subunit homolog. The pyruvate dehydrogenase complex catalyzes the overall conversion of pyruvate to acetyl-CoA and CO2. It contains multiple copies of three enzymatic components: pyruvate dehydrogenase (E1), dihydrolipoamide acetyltransferase (E2) and lipoamide dehydrogenase (E3).	Q86AD5	3	0
	GpmA (PGAM)	Catalyzes the interconversion of 2-phosphoglycerate and 3-phosphoglycerate.	Q54NE6	2	0
	Ogdh	2-oxoglutarate dehydrogenase, mitochondrial. The 2-oxoglutarate dehydrogenase complex catalyzes the overall conversion of 2-oxoglutarate to succinyl-CoA and CO2.	Q54JE4	5	0
	DDB_G0276065	Acyl-coenzyme A oxidase.	Q75JL8	3	0
	AccA	Acetyl-CoA carboxylase, catalyzes the rate-limiting reaction in the biogenesis of long-chain fatty acids. Carries out three functions: biotin carboxyl carrier protein, biotin carboxylase and carboxyltransferase.	Q54J08	8	0
	Glud2	Glutamate dehydrogenase 2. Glutamate dehydrogenase (NAD+) activity and catabolic process to 2-oxoglutarate.	Q54VI3	12	0
	VatA	V-type proton ATPase catalytic subunit A of the peripheral V1 complex of vacuolar ATPase. V-ATPase vacuolar ATPase is responsible for acidifying a variety of intracellular compartments in	P54647	11	0

		eukaryotic cells.			
	VatB	V-type proton ATPase subunit B. Vacuolar ATPase is responsible for acidifying a variety of intracellular compartments in eukaryotic cells. The B subunit is non-catalytic but combines with other subunits to form the catalytic complex.	Q76NU1	22	0

DNA-related					
Biological Process	Name	Function	UniProt ID	INO1	Ctrl
❖ **Nucleotide biosynthesis**	Rvb2	RuvB-like helicase 2	Q54UW5	3	0
❖ **DNA recombination**	Eif3I	Eukaryotic translation initiation factor 3 subunit I. Component of the eukaryotic translation initiation factor 3 (eIF-3) complex, which is involved in protein synthesis and, together with other initiation factors, stimulates binding of mRNA and methionyl-tRNAi to the 40S ribosome.	Q54MT0	3	0
❖ **DNA translation initiation**	LysS	Lysine--tRNA ligase	Q54TY4	4	0
❖ **Regulation of gene expression**	ThyA	Probable thymidylate synthase thy1. Catalyzes the formation of dTMP and tetrahydrofolate from dUMP and methylenetetrahydrofolate.	P15808	3	0
❖ **Transcription**	Eif3m	Eukaryotic translation initiation factor 3 subunit M	Q54KZ8	3	0
❖ **Lysyl-tRNA aminoacylation**	PurA	Adenylosuccinate synthetase that plays an important role in the de novo pathway and in the salvage pathway of purine nucleotide biosynthesis. Catalyzes the first committed step in the biosynthesis of AMP from IMP.	P21900	2	0
❖ **Ribosome biogenesis**	GuaA	GMP synthase [glutamine-hydrolyzing].	P32073	5	0

❖ **rRNA processing**	Pyd1	Dihydropyrimidine dehydrogenase [NADP+]. Catalyzes the reduction of uracil and thymine.	Q55FT1	3	0
	Pyr56	Uridine 5'-monophosphate synthase. Involved in step 1 and 2 of the subpathway that synthesizes UMP from orotate.	P09556	6	0
	UdkC	Uridine-cytidine kinase C. Catalyzes the conversion of uridine into uridine monophosphate and cytidine into cytidine monophosphate in the pyrimidine salvage pathway.	Q54R62	2	0
	Uap56	ATP-dependent RNA helicase activity	Q55CR6	4	0
	Nop56	Nucleolar protein 56. Required for 60S ribosomal subunit biogenesis.	Q54MT2	3	0
	Nop10	H/ACA ribonucleoprotein complex subunit 3. Required for ribosome biogenesis. Part of the H/ACA small nucleolar ribonucleoprotein (H/ACA snoRNP) complex, which catalyzes pseudouridylation of rRNA	Q54J26	2	0
	Polr2e	DNA-directed RNA polymerases I, II, and III subunit rpabc1. DNA-dependent RNA polymerase catalyzes the transcription of DNA into RNA using the four ribonucleoside triphosphates as substrates.	Q54EH2	3	0
	Gtf2b	Transcription initiation factor IIB. General factor that plays a major role in the activation of eukaryotic genes transcribed by RNA polymerase II.	Q54FD6	2	0
	Rpl19	60S ribosomal protein L19. Ribosomal protein that binds calmodulin.	P14329	6	0
	Rps2	40S ribosomal protein S2	P27685	4	0
	Rpl13	60S ribosomal protein L13. Structural constituent of ribosome.	Q54E20	3	0
	DDB_0218525	Structural constituent of ribosome.	Q54QM2	2	0
	Cnrl	Putative countin receptor Cnr9. Histone methyltransferase activity (H3-K36 specific).	Q55D68	3	0

Protein-related					
Biological Process	Name	Function	UniProt ID	INO1	Ctrl
❖ **Amino acid biosynthesis** ❖ **Protein folding** ❖ **Protein transport** ❖ **Proteolysis and sorocarp development** ❖ **Posttranslational protein targeting to membrane**	DDB_G0272318	Importin subunit alpha-B. Functions in nuclear protein import via a substrate-importin alpha-beta transport complex that passes though the nuclear pore complexes (NPC). Binds specifically and directly to substrates containing either a simple or bipartite NLS motif.	Q76P29	3	0
	EmpB	Transmembrane emp24 domain-containing protein B. Budding of coatomer-coated and other species of coated vesicles.	Q54BN0	4	0
	PefB	Penta-EF hand domain-containing protein 2, calcium-dependent cysteine-type endopeptidase activity.	Q95YL4	2	0
	Tcp1	T-complex protein 1 subunit alpha. Molecular chaperone; assists the folding of proteins upon ATP hydrolysis. Known to play a role, in vitro, in the folding of actin and tubulin.	Q55BM4	3	0
	CysB	Cystathionine beta-synthase involved in the first step of the subpathway that synthesizes L-cysteine from L-homocysteine and L-serine.	P46794	7	0
	Nfs1	Probable cysteine desulfurase, mitochondrial. Catalyzes the removal of elemental sulfur from cysteine to produce alanine. It supplies the inorganic sulfur for iron-sulfur (Fe-S) clusters.	Q54X04	3	0
	DDB_G0287543	Endoplasmic reticulum transmembrane protein YET-like. May play a role in anterograde transport of membrane proteins from the endoplasmic reticulum to the Golgi.	Q54K74	4	0
	CrtA	Calreticulin. Molecular calcium-binding chaperone promoting folding, oligomeric assembly and quality control in the ER via the calreticulin/calnexin cycle. This lectin may interact	Q23858	6	0

		transiently with almost all of the monoglucosylated glycoproteins that are synthesized in the ER.			
	Ascc3	Activating signal cointegrator 1 complex subunit 3.	Q54G57	4	0
	Ost1	Dolichyl-diphosphooligosaccharide--protein glycosyltransferase subunit 1. Essential subunit of the N-oligosaccharyl transferase (OST) complex which catalyzes the transfer of a high mannose oligosaccharide from a lipid-linked oligosaccharide donor to an asparagine residue within an Asn-X-Ser/Thr consensus motif in nascent polypeptide chains.	Q54C27	3	0
	MppA2	Mitochondrial-processing peptidase subunit alpha-2. Acts cooperatively with the beta subunit of the mitochondrial processing protease/peptidase. Alpha subunit participates in substrate recognition while beta subunit is the catalytic subunit.	Q54F93	6	0
	DDB_G0291650	Probable importin-5 homolog. Functions in nuclear protein import as nuclear transport receptor. Serves as receptor for nuclear localization signals (NLS) in cargo substrates.	Q54EW3	5	0
	Ap1b1	AP-1 complex subunit beta. Subunit of clathrin-associated adaptor protein complex 1 that plays a role in protein sorting in the trans-Golgi network (TGN) and endosomes. The AP complexes mediate the recruitment of clathrin to membranes and the recognition of sorting signals within the cytosolic tails of transmembrane cargo molecules. Also involved in early steps of phagocytosis and macropinocytosis.	Q54X82	3	0
	Apm1		Q54HS9	4	0
	Spcs3	Signal peptidase complex subunit 3. Component of the microsomal signal peptidase complex which removes signal peptides from nascent proteins as they are translocated into the lumen of the endoplasmic reticulum.	B0G180	2	0
	OatA	Probable ornithine aminotransferase involved in the first step of the subpathway that synthesizes L-glutamate 5-semialdehyde	Q54JP5	2	0

		from L-ornithine.			
	PsmC3	26S protease regulatory subunit 6A homolog. The 26S protease is involved in the ATP-dependent degradation of ubiquitinated proteins. The regulatory (or ATPase) complex confers ATP dependency and substrate specificity to the 26S complex.	Q54PN7	7	0
	Lap	Cytosol aminopeptidase. Presumably involved in the processing and regular turnover of intracellular proteins. Catalyzes the removal of unsubstituted N-terminal amino acids from various peptides.	Q5V9F0	3	0
	PsmD8	Probable 26S proteasome non-ATPase regulatory subunit 8 involved in ATP-dependent degradation of ubiquitinated proteins.	P02889	2	0
	PsmD7	26S proteasome non-ATPase regulatory subunit 7. Acts as a regulatory subunit of the 26S proteasome which is involved in the ATP-dependent degradation of ubiquitinated proteins.	Q54WI8	3	0
	UbqB	Ubiquitin-60S ribosomal protein L40	P14794	11	0
	UbqC	Ubiquitin-40S ribosomal protein S27a (cluster)	P14797	10	6
	Uba1	Ubiquitin-like modifier-activating enzyme 1. Activates ubiquitin by first adenylating with ATP its C-terminal glycine residue and thereafter linking this residue to the side chain of a cysteine residue in E1, yielding a ubiquitin-E1 thioester and free AMP.	Q55C16	3	0
	PsmC2	26S protease regulatory subunit 7. The 26S protease is involved in the ATP-dependent degradation of ubiquitinated proteins. The regulatory (or ATPase) complex confers ATP dependency and substrate specificity to the 26S complex.	Q86JA1	4	0
	PsmB5	Proteasome subunit beta type-5 that is part of the multicatalytic proteinase complex that has an ATP-dependent proteolytic activity. Cleaves peptide bonds with very broad specificity.	Q54BC8	3	0

	PsmB7	Proteasome subunit beta type-7 that is part of the multicatalytic proteinase complex that has an ATP-dependent proteolytic activity. Cleaves peptide bonds with very broad specificity.	Q54QR2	2	0
	DDB_0190095	Ubiquitinyl hydrolase 1. Thiol-dependent hydrolysis of ester, thioester, amide, peptide and isopeptide bonds formed by the C-terminal Gly of ubiquitin (a 76-residue protein attached to proteins as an intracellular targeting signal).	Q55EJ1	2	0
	PsmB6	Proteasome subunit beta type-6 that is part of the multicatalytic proteinase complex that has an ATP-dependent proteolytic activity. Cleaves peptide bonds with very broad specificity.	Q55GJ6	2	0
	UbqA	Polyubiquitin-A.	P0CG76	12	0
	PsmD4	26S proteasome non-ATPase regulatory subunit 4. Binds and presumably selects ubiquitin-conjugates for destruction.	Q553E0	2	0

Uncharacterised

Name	Function	UniProt ID	INO1	Ctrl
DDB_G0290597	Zinc ion binding.	Q54FT8	3	0
DDB_G0288947	Uncharacterised	Q54I73	7	0
DDB0187985	Uncharacterised	Q54IS9	6	0
DDB_0187949	Putative uncharacterized protein	Q54IX5	7	0
zipA	Zipper-like domain-containing protein	Q54L07	2	0
DDB_0185982	Putative uncharacterized protein	Q54PQ6	2	0

DDB_0205144	Putative uncharacterized protein	Q54SZ1	2	0
DDB_0205702	Hydrolase acitivity	Q54X02	3	0
DDB_0203302	Putative uncharacterized protein	Q555X7	2	0
DDB_0167407	Putative uncharacterized protein	Q86I47	2	0
DDB_G0268034	Rab GDP-dissociation inhibitor activity.	Q55FM7	3	0

Table S2 The list of putative Ino1 interactors. Co-immunoprecipitation was conducted using *ino1*$^{-}$ cells expressing *ino1-RFP* with anti-RFP coated beads; *ino1*$^{-}$ cells expressing RFP only (two independent repeats) or Ax2 cells expressing RFP only (one repeat) were used as a control (crt). Mass spectrometry was used to analyse unique bands from the Ino1 pull down data. The MS/MS protein data was analysed using Scaffold 3 software with the analysis parameters set to a minimum peptide threshold of 2. Presented here are 104 putative Ino1 interactors identified by this approach and absent in the control.

Sequence of the human *ino1* gene codon optimised for expression in *Dictyostelium discoideum*

ATGGAAGCAGCAGCACAATTTTTTGTAGAATCACCAGATGTAGTTTATGGTCCAGAAGCTATTGAAGCACAATATGAATATAGAACAACAAGAGTTTCAAGAGAAGGTGGTGTTTT
AAAAGTACATCCAACATCAACTAGATTTACATTTAGAACTGCTAGACAAGTTCCAAGATTAGGTGTTATGTTAGTAGGTTGGGGTGGTAATAATGGTTCAACATTAACTGCAGCTG
TTTTAGCAAATAGATTAAGATTATCATGGCCAACAAGATCAGGTAGAAAAGAAGCAAATTATTATGGTTCATTAACACAAGCTGGTACTGTTTCATTAGGTTTAGATGCAGAAGGT
CAAGAAGTTTTTGTACCATTTTCAGCAGTTTTACCAATGGTAGCTCCAAATGATTTAGTTTTTGATGGTTGGGATATTTCATCATTAAATTTAGCAGAAGCTATGAGAAGAGCTAA
AGTTTTAGATTGGGGTTTACAAGAACAATTATGGCCACATATGGAAGCATTAAGACCAAGACCATCAGTTTATATTCCAGAATTTATTGCAGCTAATCAATCAGCAAGAGCTGATA
ATTTAATTCCAGGTTCAAGAGCACAACAATTAGAACAAATTAGAAGAGATATTAGAGATTTTAGATCATCAGCTGGTTTAGATAAAGTTATTGTATTATGGACAGCAAATACTGAA
AGATTTTGTGAAGTTATTCCAGGTTTAAATGATACAGCTGAAAATTTGTTAAGAACTATTGAATTAGGTTTAGAAGTTTCACCATCAACATTATTTGCAGTAGCTTCAATTTTAGA
AGGTTGTGCATTTTTAAATGGTTCACCACAAAATACTTTAGTTCCAGGTGCATTAGAATTAGCTTGGCAACATAGAGTTTTTGTAGGTGGTGATGATTTTAAATCAGGTCAAACAA
AAGTTAAATCAGTTTTAGTTGATTTCTTAATTGGTTCAGGTTTAAAAACTATGAGTATTGTTTCATATAATCATTTAGGTAATAATGATGGTGAAAATTTATCAGCACCATTACAA
TTTAGATCAAAAGAAGTTTCAAAATCAAATGTTGTAGATGATATGGTTCAATCAAATCAAGTATTATATACACCAGGTGAAGAACCAGATCATTGTGTTGTAATTAAATATGTTCC
ATATGTAGGTGATGGTAAAAGAGCATTAGATGAATATACATCAGAATTAATGTTAGGTGGTACAAATACTTTAGTTTTACATAATACTTGTGAAGATTCATTATTAGCAGCTCCAA
TTATGTTAGATTTAGCATTATTAACAGAATTATGTCAAAGAGTTTCATTTTGTACAGATATGGACCCAGAACCACAAACTTTTCATCCAGTTTTATCATTATTATCATTTTTATTT
AAAGCTCCATTAGTACCAAGAGGTTCACCAGTTGTAAATGCATTATTTAGACAAAGATCATGTATTGAAAATATTTTAAGAGCATGTGTTGGTTTACCACCACAAAATCATATGTT
ATTAGAACATAAAATGGAAAGACCAGGTCCATCATTAAAAAGAGTTGGTCCAGTAGCAGCTACATATCCAATGTTAAATAAAAAAGGTCCAGTTCCAGCAGCTACTAATGGTTGTA
CAGGTGATGCTAATGGTCATTTACAAGAAGAACCACCAATGCCAACTACT

References

Abreu, E.F.M., Aragão, F.J.L., 2007. Isolation and characterization of a myo-inositol-1-phosphate synthase gene from yellow passion fruit (Passiflora edulis f. flavicarpa) expressed during seed development and environmental stress. Ann. Bot. 99, 285–92. doi:10.1093/aob/mcl256

Adley, K.E., Keim, M., Williams, R.S.B., 2006. Pharmacogenetics: defining the genetic basis of drug action and inositol trisphosphate analysis. Methods Mol. Biol. 346, 517–34. doi:10.1385/1-59745-144-4:517

Agam, G., Shamir, A., Shaltiel, G., Greenberg, M.L., 2002. Myo-inositol-1-phosphate (MIP) synthase: a possible new target for antibipolar drugs. Bipolar Disord. 4 Suppl 1, 15–20.

Andrew, N., Insall, R.H., 2007. Chemotaxis in shallow gradients is mediated independently of PtdIns 3-kinase by biased choices between random protrusions. Nat. Cell Biol. 9, 193–200. doi:10.1038/ncb1536

Annesley, S.J., Fisher, P.R., 2009. Dictyostelium discoideum--a model for many reasons. Mol. Cell. Biochem. 329, 73–91. doi:10.1007/s11010-009-0111-8

Azab, A.N., He, Q., Ju, S., Li, G., Greenberg, M.L., 2007. Glycogen synthase kinase-3 is required for optimal de novo synthesis of inositol. Mol. Microbiol. 63, 1248–58. doi:10.1111/j.1365-2958.2007.05591.x

Bachhawat, N., Mande, S.C., 1999. Identification of the INO1 gene of Mycobacterium tuberculosis H37Rv reveals a novel class of inositol-1-phosphate synthase enzyme. J. Mol. Biol. 291, 531–6. doi:10.1006/jmbi.1999.2980

Balakrishna, A.M., Manimekalai, M.S.S., Grüber, G., 2015. Protein-protein interactions within the ensemble, eukaryotic V-ATPase, and its concerted interactions with cellular machineries. Prog. Biophys. Mol. Biol. 119, 84–93. doi:10.1016/j.pbiomolbio.2015.05.003

Balla, T., 2001. Pharmacology of phosphoinositides, regulators of multiple cellular functions. Curr. Pharm. Des. 7, 475–507.

Bamburg, J.R., Bernstein, B.W., 2010. Roles of ADF/cofilin in actin polymerization and beyond. F1000 Biol. Rep. 2, 62. doi:10.3410/B2-62

Baum, A.E., Akula, N., Cabanero, M., Cardona, I., Corona, W., Klemens, B.,

Schulze, T.G., Cichon, S., Rietschel, M., Nöthen, M.M., Georgi, A., Schumacher, J., Schwarz, M., Abou Jamra, R., Höfels, S., Propping, P., Satagopan, J., Detera-Wadleigh, S.D., Hardy, J., McMahon, F.J., 2008. A genome-wide association study implicates diacylglycerol kinase eta (DGKH) and several other genes in the etiology of bipolar disorder. Mol. Psychiatry 13, 197–207. doi:10.1038/sj.mp.4002012

Belmaker, R.H., Shapiro, J., Vainer, E., Nemanov, L., Ebstein, R.P., Agam, G., 2002. Reduced inositol content in lymphocyte-derived cell lines from bipolar patients. Bipolar Disord. 4, 67–9.

Bennett, M., Onnebo, S.M.N., Azevedo, C., Saiardi, a, 2006. Inositol pyrophosphates: metabolism and signaling. Cell. Mol. Life Sci. 63, 552–64. doi:10.1007/s00018-005-5446-z

Berridge, M.J., Downes, C.P., Hanley, M.R., 1989. Neural and developmental actions of lithium: a unifying hypothesis. Cell 59, 411–9.

Betts, M.J., Russell, R.B., 2003. Amino Acid Properties and Consequences of Subsitiutions [WWW Document]. Bioinforma. Genet. John Wiley Sons, Ltd. URL https://biokamikazi.files.wordpress.com/2013/06/aminoacid_and_substitutions.pdf (accessed 12.26.15).

Beugnet, A., Tee, A.R., Taylor, P.M., Proud, C.G., 2003. Regulation of targets of mTOR (mammalian target of rapamycin) signalling by intracellular amino acid availability. Biochem. J. 372, 555–66. doi:10.1042/BJ20021266

Blatch, G.L., Lässle, M., 1999. The tetratricopeptide repeat: a structural motif mediating protein-protein interactions. Bioessays 21, 932–9. doi:10.1002/(SICI)1521-1878(199911)21:11<932::AID-BIES5>3.0.CO;2-N

Boeckeler, K., Adley, K., Xu, X., Jenkins, A., Jin, T., Williams, R.S.B., 2006. The neuroprotective agent, valproic acid, regulates the mitogen-activated protein kinase pathway through modulation of protein kinase A signalling in Dictyostelium discoideum. Eur. J. Cell Biol. 85, 1047–57. doi:10.1016/j.ejcb.2006.04.013

Bohdanowicz, M., Grinstein, S., 2013. Role of phospholipids in endocytosis, phagocytosis, and macropinocytosis. Physiol. Rev. 93, 69–106. doi:10.1152/physrev.00002.2012

Botelho, R.J., Teruel, M., Dierckman, R., Anderson, R., Wells, A., York, J.D., Meyer, T., Grinstein, S., 2000. Localized biphasic changes in phosphatidylinositol-4,5-bisphosphate at sites of phagocytosis. J. Cell Biol. 151, 1353–68.

Bracken, B.K., Jensen, J.E., Prescot, A.P., Cohen, B.M., Renshaw, P.F., Ongür, D., 2011. Brain metabolite concentrations across cortical regions in healthy adults. Brain Res. 1369, 89–94. doi:10.1016/j.brainres.2010.11.036

Brickner, J.H., Walter, P., 2004. Gene recruitment of the activated INO1 locus to the nuclear membrane. PLoS Biol. 2, e342. doi:10.1371/journal.pbio.0020342

Brill, J. a, Wong, R., Wilde, A., 2011a. Phosphoinositide function in cytokinesis. Curr. Biol. 21, R930–4. doi:10.1016/j.cub.2011.10.001

Brill, J. a, Wong, R., Wilde, A., 2011b. Phosphoinositide function in cytokinesis. Curr. Biol. 21, R930–4. doi:10.1016/j.cub.2011.10.001

Burton, A., Hu, X., Saiardi, A., 2009. Are inositol pyrophosphates signalling molecules? J. Cell. Physiol. 220, 8–15. doi:10.1002/jcp.21763

Cai, H., Devreotes, P.N., 2011. Moving in the right direction: how eukaryotic cells migrate along chemical gradients. Semin. Cell Dev. Biol. 22, 834–41. doi:10.1016/j.semcdb.2011.07.020

Cardelli, J., 2001. Phagocytosis and macropinocytosis in Dictyostelium: phosphoinositide-based processes, biochemically distinct. Traffic 2, 311–20.

Chang, Y.-Y., Neufeld, T.P., 2010. Autophagy takes flight in Drosophila. FEBS Lett. 584, 1342–9. doi:10.1016/j.febslet.2010.01.006

Charest, P.G., Shen, Z., Lakoduk, A., Sasaki, A.T., Briggs, S.P., Firtel, R.A., 2010. A Ras signaling complex controls the RasC-TORC2 pathway and directed cell migration. Dev. Cell 18, 737–49. doi:10.1016/j.devcel.2010.03.017

Chen, T.L., Kowalczyk, P.A., Ho, G., Chisholm, R.L., 1995. Targeted disruption of the Dictyostelium myosin essential light chain gene produces cells defective in cytokinesis and morphogenesis. J. Cell Sci. 108 (Pt 1, 3207–18.

Chen, Y., Klionsky, D.J., 2011. The regulation of autophagy - unanswered questions. J. Cell Sci. 124, 161–70. doi:10.1242/jcs.064576

Chengappa, K.N., Levine, J., Gershon, S., Mallinger, A.G., Hardan, A., Vagnucci, A., Pollock, B., Luther, J., Buttenfield, J., Verfaille, S., Kupfer, D.J., 2000. Inositol as an add-on treatment for bipolar depression. Bipolar Disord. 2, 47–55.

Chhetri, D.R., Gupta, S., Mukherjee, A.K., Adhikari, J., 2012. L-myo-inositol-1-phosphate synthase expressed in developing organ: isolation and characterisation of the enzyme from human fetal liver. Appl. Biochem. Biotechnol. 167, 2269–82. doi:10.1007/s12010-012-9767-8

Chisholm, R.L., Firtel, R.A., 2004. Insights into morphogenesis from a simple developmental system. Nat. Rev. Mol. Cell Biol. 5, 531–41. doi:10.1038/nrm1427

Cho, S.-J., Yun, S.-M., Jo, C., Lee, D.-H., Choi, K.J., Song, J.C., Park, S.I., Kim, Y.-J., Koh, Y.H., 2015. SUMO1 promotes Aβ production via the modulation of autophagy. Autophagy 11, 100–12. doi:10.4161/15548627.2014.984283

Clark, J., Kay, R.R., Kielkowska, A., Niewczas, I., Fets, L., Oxley, D., Stephens, L.R., Hawkins, P.T., 2014. Dictyostelium uses ether-linked inositol phospholipids for intracellular signalling. EMBO J. 33, 2188–200. doi:10.15252/embj.201488677

Clarke, M., Kayman, S.C., 1987. The axenic mutations and endocytosis in Dictyostelium. Methods Cell Biol. 28, 157–76.

Clements, R.S., Darnell, B., 1980. Myo-inositol content of common foods: development of a high-myo-inositol diet. Am. J. Clin. Nutr. 33, 1954–67.

Coady, M.J., Wallendorff, B., Gagnon, D.G., Lapointe, J.-Y., 2002. Identification of a novel Na+/myo-inositol cotransporter. J. Biol. Chem. 277, 35219–24. doi:10.1074/jbc.M204321200

Cocco, L., Manzoli, L., Barnabei, O., Martelli, A.M., 2004. Significance of subnuclear localization of key players of inositol lipid cycle. Adv. Enzyme Regul. 44, 51–60. doi:10.1016/j.advenzreg.2003.11.009

Cocorocchio, M., Ives, R., Clapham, D., Andrews, P.L.R., Williams, R.S.B., 2015. Bitter tastant responses in the amoeba Dictyostelium correlate

with rat and human taste assays. ALTEX. doi:10.14573/altex.1509011

Cohen, H., Kotler, M., Kaplan, Z., Matar, M.A., Kofman, O., Belmaker, R.H., 1997. Inositol has behavioral effects with adaptation after chronic administration. J. Neural Transm. 104, 299–305.

Corvera, S., D'Arrigo, A., Stenmark, H., 1999. Phosphoinositides in membrane traffic. Curr. Opin. Cell Biol. 11, 460–5. doi:10.1016/S0955-0674(99)80066-0

Corvin, A.P., 2010. Neuronal cell adhesion genes: Key players in risk for schizophrenia, bipolar disorder and other neurodevelopmental brain disorders? Cell Adh. Migr. 4, 511–514. doi:10.4161/cam.4.4.12460

Coupland, N.J., Ogilvie, C.J., Hegadoren, K.M., Seres, P., Hanstock, C.C., Allen, P.S., 2005. Decreased prefrontal Myo-inositol in major depressive disorder. Biol. Psychiatry 57, 1526–34. doi:10.1016/j.biopsych.2005.02.027

Cremona, O., De Camilli, P., 2001. Phosphoinositides in membrane traffic at the synapse. J. Cell Sci. 114, 1041–52.

Criollo, A., Maiuri, M.C., Tasdemir, E., Vitale, I., Fiebig, A.A., Andrews, D., Molgó, J., Díaz, J., Lavandero, S., Harper, F., Pierron, G., di Stefano, D., Rizzuto, R., Szabadkai, G., Kroemer, G., 2007. Regulation of autophagy by the inositol trisphosphate receptor. Cell Death Differ. 14, 1029–39. doi:10.1038/sj.cdd.4402099

Croze, M.L., Géloën, A., Soulage, C.O., 2015. Abnormalities in myo-inositol metabolism associated with type 2 diabetes in mice fed a high-fat diet: benefits of a dietary myo-inositol supplementation. Br. J. Nutr. 113, 1862–75. doi:10.1017/S000711451500121X

Croze, M.L., Soulage, C.O., 2013. Potential role and therapeutic interests of myo-inositol in metabolic diseases. Biochimie 95, 1811–27. doi:10.1016/j.biochi.2013.05.011

Croze, M.L., Vella, R.E., Pillon, N.J., Soula, H. a, Hadji, L., Guichardant, M., Soulage, C.O., 2013. Chronic treatment with myo-inositol reduces white adipose tissue accretion and improves insulin sensitivity in female mice. J. Nutr. Biochem. 24, 457–66. doi:10.1016/j.jnutbio.2012.01.008

Culbertson, M.R., Donahue, T.F., Henry, S. a, 1976. Control of inositol

biosynthesis in Saccharomyces cerevisiae: properties of a repressible enzyme system in extracts of wild-type (Ino+) cells. J. Bacteriol. 126, 232–42.

Culbertson, M.R., Henry, S.A., 1975. Inositol-requiring mutants of Saccharomyces cerevisiae. Genetics 80, 23–40.

D'Avino, P.P., Savoian, M.S., Glover, D.M., 2005. Cleavage furrow formation and ingression during animal cytokinesis: a microtubule legacy. J. Cell Sci. 118, 1549–58. doi:10.1242/jcs.02335

Dall'Armi, C., Devereaux, K.A., Di Paolo, G., 2013. The role of lipids in the control of autophagy. Curr. Biol. 23, R33–45. doi:10.1016/j.cub.2012.10.041

Davanzo, P., Thomas, M.A., Yue, K., Oshiro, T., Belin, T., Strober, M., McCracken, J., 2001. Decreased anterior cingulate myo-inositol/creatine spectroscopy resonance with lithium treatment in children with bipolar disorder. Neuropsychopharmacology 24, 359–69. doi:10.1016/S0893-133X(00)00207-4

De Camilli, P., Emr, S.D., McPherson, P.S., Novick, P., 1996. Phosphoinositides as regulators in membrane traffic. Science 271, 1533–9.

De Lozanne, A., Spudich, J.A., 1987. Disruption of the Dictyostelium myosin heavy chain gene by homologous recombination. Science 236, 1086–91.

Dean-Johnson, M., Henry, S.A., 1989. Biosynthesis of inositol in yeast. Primary structure of myo-inositol-1-phosphate synthase (EC 5.5.1.4) and functional analysis of its structural gene, the INO1 locus. J. Biol. Chem. 264, 1274–83.

Denton, D., Nicolson, S., Kumar, S., 2012. Cell death by autophagy: facts and apparent artefacts. Cell Death Differ. 19, 87–95. doi:10.1038/cdd.2011.146

Deranieh, R.M., Greenberg, M.L., 2009. Cellular consequences of inositol depletion. Biochem. Soc. Trans. 37, 1099–103. doi:10.1042/BST0371099

Deranieh, R.M., He, Q., Caruso, J.A., Greenberg, M.L., 2013. Phosphorylation regulates myo-inositol-3-phosphate synthase: A novel

regulatory mechanism of inositol biosynthesis. J. Biol. Chem. 288, 26822–33. doi:10.1074/jbc.M113.479121

Deranieh, R.M., Shi, Y., Tarsio, M., Chen, Y., McCaffery, J.M., Kane, P.M., Greenberg, M.L., 2015. Perturbation of the vacuolar-ATPase: A novel consequence of inositol depletion. J. Biol. Chem. 290, 27460–72. doi:10.1074/jbc.M115.683706

Devreotes, P., Horwitz, A.R., 2015. Signaling Networks that Regulate Cell Migration. Cold Spring Harb. Perspect. Biol. 7, a005959. doi:10.1101/cshperspect.a005959

Di Daniel, E., Cheng, L., Maycox, P.R., Mudge, A.W., 2006. The common inositol-reversible effect of mood stabilizers on neurons does not involve GSK3 inhibition, myo-inositol-1-phosphate synthase or the sodium-dependent myo-inositol transporters. Mol. Cell. Neurosci. 32, 27–36. doi:10.1016/j.mcn.2006.01.015

Di Meo, I., Lamperti, C., Tiranti, V., 2015. Mitochondrial diseases caused by toxic compound accumulation: from etiopathology to therapeutic approaches. EMBO Mol. Med. 7, 1257–66. doi:10.15252/emmm.201505040

Donahue, J.L., Alford, S.R., Torabinejad, J., Kerwin, R.E., Nourbakhsh, A., Ray, W.K., Hernick, M., Huang, X., Lyons, B.M., Hein, P.P., Gillaspy, G.E., 2010. The Arabidopsis thaliana Myo-inositol 1-phosphate synthase1 gene is required for Myo-inositol synthesis and suppression of cell death. Plant Cell 22, 888–903. doi:10.1105/tpc.109.071779

Dormann, D., Weijer, G., Dowler, S., Weijer, C.J., 2004. In vivo analysis of 3-phosphoinositide dynamics during Dictyostelium phagocytosis and chemotaxis. J. Cell Sci. 117, 6497–509. doi:10.1242/jcs.01579

Dove, S.K., Dong, K., Kobayashi, T., Williams, F.K., Michell, R.H., 2009. Phosphatidylinositol 3,5-bisphosphate and Fab1p/PIKfyve underPPIn endo-lysosome function. Biochem. J. 419, 1–13. doi:10.1042/BJ20081950

Dowler, S., Montalvo, L., Cantrell, D., Morrice, N., Alessi, D.R., 2000. Phosphoinositide 3-kinase-dependent phosphorylation of the dual adaptor for phosphotyrosine and 3-phosphoinositides by the Src family of tyrosine kinase. Biochem. J. 349, 605–10.

Dumontier, M., Höcht, P., Mintert, U., Faix, J., 2000. Rac1 GTPases control

filopodia formation, cell motility, endocytosis, cytokinesis and development in Dictyostelium. J. Cell Sci. 113 (Pt 1, 2253–65.

Echard, A., 2012. Phosphoinositides and cytokinesis: the “PIP” of the iceberg. Cytoskeleton (Hoboken). 69, 893–912. doi:10.1002/cm.21067

Eichinger, L., Pachebat, J.A., Glöckner, G., Rajandream, M.-A., Sucgang, R., Berriman, M., Song, J., Olsen, R., Szafranski, K., Xu, Q., Tunggal, B., Kummerfeld, S., Madera, M., Konfortov, B.A., Rivero, F., Bankier, A.T., Lehmann, R., Hamlin, N., Davies, R., Gaudet, P., Fey, P., Pilcher, K., Chen, G., Saunders, D., Sodergren, E., Davis, P., Kerhornou, A., Nie, X., Hall, N., Anjard, C., Hemphill, L., Bason, N., Farbrother, P., Desany, B., Just, E., Morio, T., Rost, R., Churcher, C., Cooper, J., Haydock, S., van Driessche, N., Cronin, A., Goodhead, I., Muzny, D., Mourier, T., Pain, A., Lu, M., Harper, D., Lindsay, R., Hauser, H., James, K., Quiles, M., Madan Babu, M., Saito, T., Buchrieser, C., Wardroper, A., Felder, M., Thangavelu, M., Johnson, D., Knights, A., Loulseged, H., Mungall, K., Oliver, K., Price, C., Quail, M.A., Urushihara, H., Hernandez, J., Rabbinowitsch, E., Steffen, D., Sanders, M., Ma, J., Kohara, Y., Sharp, S., Simmonds, M., Spiegler, S., Tivey, A., Sugano, S., White, B., Walker, D., Woodward, J., Winckler, T., Tanaka, Y., Shaulsky, G., Schleicher, M., Weinstock, G., Rosenthal, A., Cox, E.C., Chisholm, R.L., Gibbs, R., Loomis, W.F., Platzer, M., Kay, R.R., Williams, J., Dear, P.H., Noegel, A.A., Barrell, B., Kuspa, A., 2005. The genome of the social amoeba Dictyostelium discoideum. Nature 435, 43–57. doi:10.1038/nature03481

Eickholt, B.J., Towers, G.J., Ryves, W.J., Eikel, D., Adley, K., Ylinen, L.M.J., Chadborn, N.H., Harwood, A.J., Nau, H., Williams, R.S.B., 2005. Effects of Valproic Acid Derivatives on Inositol Trisphosphate Depletion , Teratogenicity , Glycogen Synthase Kinase-3 ␣ Inhibition , and Viral Replication : A Screening Approach for New Bipolar Disorder Drugs Derived from the Valproic Acid Core Structure 67, 1426–1433. doi:10.1124/mol.104.009308.of

Escalante, R., Vicente, J.J., 2000. Dictyostelium discoideum: a model system for differentiation and patterning. Int. J. Dev. Biol. 44, 819–35.

Europe-Finner, G.N., Gammon, B., Wood, C.A., Newell, P.C., 1989. Inositol tris- and polyphosphate formation during chemotaxis of Dictyostelium. J. Cell Sci. 93 (Pt 4), 585–92.

Faix, J., Kreppel, L., Shaulsky, G., Schleicher, M., Kimmel, A.R., 2004. A rapid and efficient method to generate multiple gene disruptions in Dictyostelium discoideum using a single selectable marker and the Cre-loxP system. Nucleic Acids Res. 32, e143. doi:10.1093/nar/gnh136

Felberbaum, R., Wilson, N.R., Cheng, D., Peng, J., Hochstrasser, M., 2012. Desumoylation of the endoplasmic reticulum membrane VAP family protein Scs2 by Ulp1 and SUMO regulation of the inositol synthesis pathway. Mol. Cell. Biol. 32, 64–75. doi:10.1128/MCB.05878-11

Fenili, D., Brown, M., Rappaport, R., McLaurin, J., 2007. Properties of scyllo-inositol as a therapeutic treatment of AD-like pathology. J. Mol. Med. (Berl). 85, 603–11. doi:10.1007/s00109-007-0156-7

Fischbach, A., Adelt, S., Müller, A., Vogel, G., 2006. Disruption of inositol biosynthesis through targeted mutagenesis in Dictyostelium discoideum: generation and characterization of inositol-auxotrophic mutants. Biochem. J. 397, 509–18. doi:10.1042/BJ20060277

Fong, D., Rutherford, C.L., 1978. Protease activity during cell differentiation of the cellular slime mold Dictyostelium discoideum. J. Bacteriol. 134, 521–7.

Ford, J., Odeyale, O., Eskandar, A., Kouba, N., Shen, C.-H., 2007. A SWI/SNF- and INO80-dependent nucleosome movement at the INO1 promoter. Biochem. Biophys. Res. Commun. 361, 974–9. doi:10.1016/j.bbrc.2007.07.109

Francione, L.M., Annesley, S.J., Carilla-Latorre, S., Escalante, R., Fisher, P.R., 2011. The Dictyostelium model for mitochondrial disease. Semin. Cell Dev. Biol. 22, 120–30. doi:10.1016/j.semcdb.2010.11.004

Fujita, H., Yamanaka, M., Imamura, K., Tanaka, Y., Nara, A., Yoshimori, T., Yokota, S., Himeno, M., 2003. A dominant negative form of the AAA ATPase SKD1/VPS4 impairs membrane trafficking out of endosomal/lysosomal compartments: class E vps phenotype in mammalian cells. J. Cell Sci. 116, 401–14.

Garcia, R., Nguyen, L., Brazill, D., 2013. Dictyostelium discoideum SecG interprets cAMP-mediated chemotactic signals to influence actin organization. Cytoskeleton (Hoboken). 70, 269–80. doi:10.1002/cm.21107

Gaspar, M.L., Aregullin, M.A., Jesch, S.A., Henry, S.A., 2006. Inositol induces a profound alteration in the pattern and rate of synthesis and turnover of membrane lipids in Saccharomyces cerevisiae. J. Biol. Chem. 281, 22773–85. doi:10.1074/jbc.M603548200

Gauci, V.J., Padula, M.P., Coorssen, J.R., 2013. Coomassie blue staining for

high sensitivity gel-based proteomics. J. Proteomics 90, 96–106. doi:10.1016/j.jprot.2013.01.027

Geer, L.Y., Domrachev, M., Lipman, D.J., Bryant, S.H., 2002. CDART: protein homology by domain architecture. Genome Res. 12, 1619–23. doi:10.1101/gr.278202

GhoshDastidar, K., Chatterjee, A., Chatterjee, A., Majumder, A.L., 2006. Evolutionary divergence of L-myo-inositol 1-phosphate synthase: significance of a “core catalytic structure”. Subcell. Biochem. 39, 315–40.

Giusti, C., Tresse, E., Luciani, M.-F., Golstein, P., 2009. Autophagic cell death: Analysis in Dictyostelium. Biochim. Biophys. Acta - Mol. Cell Res. 1793, 1422–1431. doi:10.1016/j.bbamcr.2008.12.005

Glick, D., Barth, S., Macleod, K.F., 2010. Autophagy: cellular and molecular mechanisms. J. Pathol. 221, 3–12. doi:10.1002/path.2697

Grigat, M., Jäschke, Y., Kliewe, F., Pfeifer, M., Walz, S., Schüller, H.-J., 2012. Multiple histone deacetylases are recruited by corepressor Sin3 and contribute to gene repression mediated by Opi1 regulator of phospholipid biosynthesis in the yeast Saccharomyces cerevisiae. Mol. Genet. Genomics 287, 461–72. doi:10.1007/s00438-012-0692-x

Guérin, R., Beauregard, P.B., Leroux, A., Rokeach, L. a, 2009. Calnexin regulates apoptosis induced by inositol starvation in fission yeast. PLoS One 4, e6244. doi:10.1371/journal.pone.0006244

Harwood, A.J., Drury, L., 1990. New vectors for expression of the E.coli lacZ gene in Dictyostelium. Nucleic Acids Res. 18, 4292.

Hemelaar, J., Borodovsky, A., Kessler, B.M., Reverter, D., Cook, J., Kolli, N., Gan-Erdene, T., Wilkinson, K.D., Gill, G., Lima, C.D., Ploegh, H.L., Ovaa, H., 2004. Specific and covalent targeting of conjugating and deconjugating enzymes of ubiquitin-like proteins. Mol. Cell. Biol. 24, 84–95.

Henley, J.M., Craig, T.J., Wilkinson, K.A., 2014. Neuronal SUMOylation: mechanisms, physiology, and roles in neuronal dysfunction. Physiol. Rev. 94, 1249–85. doi:10.1152/physrev.00008.2014

Henry, S. a, Atkinson, K.D., Kolat, a I., Culbertson, M.R., 1977. Growth and metabolism of inositol-starved Saccharomyces cerevisiae. J. Bacteriol.

130, 472–84.

Hibi, M., Nagasaki, A., Takahashi, M., Yamagishi, A., Uyeda, T.Q.P., 2004. Dictyostelium discoideum talin A is crucial for myosin II-independent and adhesion-dependent cytokinesis. J. Muscle Res. Cell Motil. 25, 127–40.

Hillis, D.M., Bull, J.J., 1993. An Empirical Test of Bootstrapping as a Method for Assessing Confidence in Phylogenetic Analysis. Syst. Biol. 42, 182–192. doi:10.1093/sysbio/42.2.182

Hirose, S., Santhanam, B., Katoh-Kurosawa, M., Shaulsky, G., Kuspa, A., 2015. Allorecognition, via TgrB1 and TgrC1, mediates the transition from unicellularity to multicellularity in the social amoeba Dictyostelium discoideum. Development 142, 3561–70. doi:10.1242/dev.123281

Hirsch, J.P., Henry, S.A., 1986. Expression of the Saccharomyces cerevisiae inositol-1-phosphate synthase (INO1) gene is regulated by factors that affect phospholipid synthesis. Mol. Cell. Biol. 6, 3320–8.

Hoeller, O., Kay, R.R., 2007. Chemotaxis in the absence of PIP3 gradients. Curr. Biol. 17, 813–7. doi:10.1016/j.cub.2007.04.004

Huang, Y.E., Iijima, M., Parent, C.A., Funamoto, S., Firtel, R.A., Devreotes, P., 2003. Receptor-mediated regulation of PI3Ks confines PI(3,4,5)P3 to the leading edge of chemotaxing cells. Mol. Biol. Cell 14, 1913–22. doi:10.1091/mbc.E02-10-0703

Insall, R., Kuspa, A., Lilly, P.J., Shaulsky, G., Levin, L.R., Loomis, W.F., Devreotes, P., 1994. CRAC, a cytosolic protein containing a pleckstrin homology domain, is required for receptor and G protein-mediated activation of adenylyl cyclase in Dictyostelium. J. Cell Biol. 126, 1537–45.

Insall, R.H., Weiner, O.D., 2001. PIP3, PIP2, and cell movement--similar messages, different meanings? Dev. Cell 1, 743–7.

Jesch, S.A., Zhao, X., Wells, M.T., Henry, S.A., 2005. Genome-wide analysis reveals inositol, not choline, as the major effector of Ino2p-Ino4p and unfolded protein response target gene expression in yeast. J. Biol. Chem. 280, 9106–18. doi:10.1074/jbc.M411770200

Jin, X., Foley, K.M., Geiger, J.H., 2004. The structure of the 1L-myo-inositol-1-phosphate synthase-NAD+-2-deoxy-D-glucitol 6-(E)-

vinylhomophosphonate complex demands a revision of the enzyme mechanism. J. Biol. Chem. 279, 13889–95. doi:10.1074/jbc.M308986200

Johnson, E.S., 2004. Protein modification by SUMO. Annu. Rev. Biochem. 73, 355–82. doi:10.1146/annurev.biochem.73.011303.074118

Ju, S., Greenberg, M.L., 2003. Valproate disrupts regulation of inositol responsive genes and alters regulation of phospholipid biosynthesis. Mol. Microbiol. 49, 1595–603.

Ju, S., Shaltiel, G., Shamir, A., Agam, G., Greenberg, M.L., 2004. Human 1-D-myo-inositol-3-phosphate synthase is functional in yeast. J. Biol. Chem. 279, 21759–65. doi:10.1074/jbc.M312078200

Kaiser, L.G., Schuff, N., Cashdollar, N., Weiner, M.W., 2005. Scyllo-inositol in normal aging human brain: 1H magnetic resonance spectroscopy study at 4 Tesla. NMR Biomed. 18, 51–5. doi:10.1002/nbm.927

Kamimura, Y., Xiong, Y., Iglesias, P.A., Hoeller, O., Bolourani, P., Devreotes, P.N., 2008. PIP3-independent activation of TorC2 and PKB at the cell's leading edge mediates chemotaxis. Curr. Biol. 18, 1034–43. doi:10.1016/j.cub.2008.06.068

Kelley, L.A., Mezulis, S., Yates, C.M., Wass, M.N., Sternberg, M.J.E., 2015. The Phyre2 web portal for protein modeling, prediction and analysis. Nat. Protoc. 10, 845–858. doi:10.1038/nprot.2015.053

Kennington, A.S., Hill, C.R., Craig, J., Bogardus, C., Raz, I., Ortmeyer, H.K., Hansen, B.C., Romero, G., Larner, J., 1990. Low urinary chiro-inositol excretion in non-insulin-dependent diabetes mellitus. N. Engl. J. Med. 323, 373–8. doi:10.1056/NEJM199008093230603

Kerr, S.C., Corbett, A.H., 2010. Should INO stay or should INO Go: a DNA "zip code" mediates gene retention at the nuclear pore. Mol. Cell 40, 3–5. doi:10.1016/j.molcel.2010.09.017

Kerscher, O., 2007. SUMO junction-what's your function? New insights through SUMO-interacting motifs. EMBO Rep. 8, 550–5. doi:10.1038/sj.embor.7400980

Ketter, T.A., Miller, S., Dell'Osso, B., Wang, P.W., 2016. Treatment of bipolar disorder: Review of evidence regarding quetiapine and lithium. J. Affect.

Disord. 191, 256–273. doi:10.1016/j.jad.2015.11.002

Kim, Y.J., Hernandez, M.-L.G., Balla, T., 2013. Inositol lipid regulation of lipid transfer in specialized membrane domains. Trends Cell Biol. 23, 270–8. doi:10.1016/j.tcb.2013.01.009

King, J., Keim, M., Teo, R., Weening, K.E., Kapur, M., McQuillan, K., Ryves, J., Rogers, B., Dalton, E., Williams, R.S.B., Harwood, A.J., 2010. Genetic control of lithium sensitivity and regulation of inositol biosynthetic genes. PLoS One 5, e11151. doi:10.1371/journal.pone.0011151

King, J.S., Insall, R.H., 2009. Chemotaxis: finding the way forward with Dictyostelium. Trends Cell Biol. 19, 523–30. doi:10.1016/j.tcb.2009.07.004

King, J.S., Insall, R.H., 2008. Chemotaxis: TorC before you Akt... Curr. Biol. 18, R864–6. doi:10.1016/j.cub.2008.07.051

King, J.S., Teo, R., Ryves, J., Reddy, J. V, Peters, O., Orabi, B., Hoeller, O., Williams, R.S.B., Harwood, A.J., 2009. The mood stabiliser lithium suppresses PIP3 signalling in Dictyostelium and human cells. Dis. Model. Mech. 2, 306–12. doi:10.1242/dmm.001271

Kirisako, T., Baba, M., Ishihara, N., Miyazawa, K., Ohsumi, M., Yoshimori, T., Noda, T., Ohsumi, Y., 1999. Formation process of autophagosome is traced with Apg8/Aut7p in yeast. J. Cell Biol. 147, 435–46.

Klig, L.S., Henry, S. a, 1984. Isolation of the yeast INO1 gene: located on an autonomously replicating plasmid, the gene is fully regulated. Proc. Natl. Acad. Sci. U. S. A. 81, 3816–20.

Knecht, D.A., Loomis, W.F., 1987. Antisense RNA inactivation of myosin heavy chain gene expression in Dictyostelium discoideum. Science 236, 1081–6.

Knorr, R.L., Nakatogawa, H., Ohsumi, Y., Lipowsky, R., Baumgart, T., Dimova, R., 2014. Membrane morphology is actively transformed by covalent binding of the protein Atg8 to PE-lipids. PLoS One 9, e115357. doi:10.1371/journal.pone.0115357

Kölsch, V., Charest, P.G., Firtel, R.A., 2008. The regulation of cell motility and chemotaxis by phospholipid signaling. J. Cell Sci. 121, 551–9.

doi:10.1242/jcs.023333

Konarzewska, P., Esposito, M., Shen, C.-H., 2012. INO1 induction requires chromatin remodelers Ino80p and Snf2p but not the histone acetylases. Biochem. Biophys. Res. Commun. 418, 483–8. doi:10.1016/j.bbrc.2012.01.044

Kosta, A., Roisin-Bouffay, C., Luciani, M.-F., Otto, G.P., Kessin, R.H., Golstein, P., 2004. Autophagy gene disruption reveals a non-vacuolar cell death pathway in Dictyostelium. J. Biol. Chem. 279, 48404–9. doi:10.1074/jbc.M408924200

Kotaria, N., Kiladze, M., Zhvania, M.G., Japaridze, N.J., Bikashvili, T., Solomonia, R.O., Bolkvadze, T., 2013. The protective effect of myo-inositol on hippocamal cell loss and structural alterations in neurons and synapses triggered by kainic acid-induced status epilepticus. Cell. Mol. Neurobiol. 33, 659–71. doi:10.1007/s10571-013-9930-y

Kovács, A.L., Reith, A., Seglen, P.O., 1982. Accumulation of autophagosomes after inhibition of hepatocytic protein degradation by vinblastine, leupeptin or a lysosomotropic amine. Exp. Cell Res. 137, 191–201.

Krauss, M., Haucke, V., 2007. Phosphoinositide-metabolizing enzymes at the interface between membrane traffic and cell signalling. EMBO Rep. 8, 241–6. doi:10.1038/sj.embor.7400919

Krichevsky, M.I., Wright, B.E., 1963. Environmental control of the course of development in Dictyostelium discoideum. J. Gen. Microbiol. 32, 195–207. doi:10.1099/00221287-32-2-195

Kurnasov, O. V, Luk, H.-J.D., Roberts, M.F., Stec, B., 2013. Structure of the inositol-1-phosphate cytidylyltransferase from Thermotoga maritima. Acta Crystallogr. D. Biol. Crystallogr. 69, 1808–17. doi:10.1107/S0907444913015278

Kuspa, A., Loomis, W.F., 1994. REMI-RFLP Mapping in the Dictyostelium Genome. Genetics 138, 665–674.

Lacanà, E., Ganjei, J.K., Vito, P., D'Adamio, L., 1997. Dissociation of apoptosis and activation of IL-1beta-converting enzyme/Ced-3 proteases by ALG-2 and the truncated Alzheimer's gene ALG-3. J. Immunol. 158, 5129–35.

Lackey, K.H., Pope, P.M., Johnson, M.D., 2003. Expression of 1L-myoinositol-1-phosphate synthase in organelles. Plant Physiol. 132, 2240–7.

Lester, H.E., Gross, S.R., 1959. Efficient method for selection of auxotrophic mutants of Neurospora. Science 129, 572.

Levi, S., Polyakov, M., Egelhoff, T.T., 2000. Green fluorescent protein and epitope tag fusion vectors for Dictyostelium discoideum. Plasmid 44, 231–8. doi:10.1006/plas.2000.1487

Lilly, P.J., Devreotes, P.N., 1995. Chemoattractant and GTP gamma S-mediated stimulation of adenylyl cyclase in Dictyostelium requires translocation of CRAC to membranes. J. Cell Biol. 129, 1659–65.

Lionaki, E., Markaki, M., Palikaras, K., Tavernarakis, N., 2015. Mitochondria, autophagy and age-associated neurodegenerative diseases: New insights into a complex interplay. Biochim. Biophys. Acta 1847, 1412–23. doi:10.1016/j.bbabio.2015.04.010

Loewy, B.S., Henry, S. a, 1984. The INO2 and INO4 loci of Saccharomyces cerevisiae are pleiotropic regulatory genes. Mol. Cell. Biol. 4, 2479–85.

Logan, M.R., Mandato, C.A., 2006. Regulation of the actin cytoskeleton by PIP2 in cytokinesis. Biol. Cell 98, 377–88. doi:10.1042/BC20050081

Lohia, A., Hait, N.C., Majumder, A.L., 1999. L-myo-Inositol 1-phosphate synthase from Entamoeba histolytica. Mol. Biochem. Parasitol. 98, 67–79.

Loomis, W.F., 2014. Cell signaling during development of Dictyostelium. Dev. Biol. 391, 1–16. doi:10.1016/j.ydbio.2014.04.001

Loovers, H.M., Kortholt, A., de Groote, H., Whitty, L., Nussbaum, R.L., van Haastert, P.J.M., 2007. Regulation of phagocytosis in Dictyostelium by the inositol 5-phosphatase OCRL homolog Dd5P4. Traffic 8, 618–28. doi:10.1111/j.1600-0854.2007.00546.x

Luciani, M.-F., Giusti, C., Harms, B., Oshima, Y., Kikuchi, H., Kubohara, Y., Golstein, P., 2011. Atg1 allows second-signaled autophagic cell death in Dictyostelium. Autophagy 7, 501–8.

Ludtmann, M.H.R., Boeckeler, K., Williams, R.S.B., 2011. Molecular pharmacology in a simple model system: implicating MAP kinase and phosphoinositide signalling in bipolar disorder. Semin. Cell Dev. Biol. 22, 105–13. doi:10.1016/j.semcdb.2010.11.002

Ludtmann, M.H.R., Otto, G.P., Schilde, C., Chen, Z.-H., Allan, C.Y., Brace, S., Beesley, P.W., Kimmel, A.R., Fisher, P., Killick, R., Williams, R.S.B., 2014. An ancestral non-proteolytic role for presenilin proteins in multicellular development of the social amoeba Dictyostelium discoideum. J. Cell Sci. 127, 1576–84. doi:10.1242/jcs.140939

Lynch, C.J., 2001. Role of leucine in the regulation of mTOR by amino acids: revelations from structure-activity studies. J. Nutr. 131, 861S–865S.

Maeba, R., Hara, H., Ishikawa, H., Hayashi, S., Yoshimura, N., Kusano, J., Takeoka, Y., Yasuda, D., Okazaki, T., Kinoshita, M., Teramoto, T., 2008. Myo-inositol treatment increases serum plasmalogens and decreases small dense LDL, particularly in hyperlipidemic subjects with metabolic syndrome. J. Nutr. Sci. Vitaminol. (Tokyo). 54, 196–202.

Maeda, Y., 2005. Regulation of growth and differentiation in Dictyostelium. Int. Rev. Cytol. 244, 287–332. doi:10.1016/S0074-7696(05)44007-3

Majumder, A.L., Chatterjee, A., Ghosh Dastidar, K., Majee, M., 2003. Diversification and evolution of L-myo-inositol 1-phosphate synthase. FEBS Lett. 553, 3–10. doi:10.1016/S0014-5793(03)00974-8

Majumder, A.L., Johnson, M.D., Henry, S.A., 1997. 1L-myo-inositol-1-phosphate synthase. Biochim. Biophys. Acta 1348, 245–56.

Manji, H.K., Bersudsky, Y., Chen, G., Belmaker, R.H., Potter, W.Z., 1996. Modulation of protein kinase C isozymes and substrates by lithium: the role of myo-inositol. Neuropsychopharmacology 15, 370–81. doi:10.1016/0893-133X(95)00243-7

Manstein, D.J., Titus, M. a, De Lozanne, a, Spudich, J. a, 1989. Gene replacement in Dictyostelium: generation of myosin null mutants. EMBO J. 8, 923–32.

Marchler-Bauer, A., Derbyshire, M.K., Gonzales, N.R., Lu, S., Chitsaz, F., Geer, L.Y., Geer, R.C., He, J., Gwadz, M., Hurwitz, D.I., Lanczycki, C.J., Lu, F., Marchler, G.H., Song, J.S., Thanki, N., Wang, Z., Yamashita, R.A., Zhang, D., Zheng, C., Bryant, S.H., 2014. CDD: NCBI's conserved domain database. Nucleic Acids Res. 43, D222–6.

doi:10.1093/nar/gku1221

Marchler-Bauer, A., Panchenko, A.R., Shoemaker, B.A., Thiessen, P.A., Geer, L.Y., Bryant, S.H., 2002. CDD: a database of conserved domain alignments with links to domain three-dimensional structure. Nucleic Acids Res. 30, 281–3.

Martin, K.L., Smith, T.K., 2006. The glycosylphosphatidylinositol (GPI) biosynthetic pathway of bloodstream-form Trypanosoma brucei is dependent on the de novo synthesis of inositol. Mol. Microbiol. 61, 89–105. doi:10.1111/j.1365-2958.2006.05216.x

Mayer, J.H., Tomlinson, D.R., 1983. Prevention of defects of axonal transport and nerve conduction velocity by oral administration of myo-inositol or an aldose reductase inhibitor in streptozotocin-diabetic rats. Diabetologia 25, 433–8.

McLaurin, J., Franklin, T., Chakrabartty, A., Fraser, P.E., 1998. Phosphatidylinositol and inositol involvement in Alzheimer amyloid-beta fibril growth and arrest. J. Mol. Biol. 278, 183–94. doi:10.1006/jmbi.1998.1677

McLaurin, J., Golomb, R., Jurewicz, A., Antel, J.P., Fraser, P.E., 2000. Inositol stereoisomers stabilize an oligomeric aggregate of Alzheimer amyloid beta peptide and inhibit abeta -induced toxicity. J. Biol. Chem. 275, 18495–502. doi:10.1074/jbc.M906994199

McMains, V.C., Myre, M., Kreppel, L., Kimmel, A.R., 2010. Dictyostelium possesses highly diverged presenilin/gamma-secretase that regulates growth and cell-fate specification and can accurately process human APP: a system for functional studies of the presenilin/gamma-secretase complex. Dis. Model. Mech. 3, 581–94. doi:10.1242/dmm.004457

Meng, P.H., Raynaud, C., Tcherkez, G., Blanchet, S., Massoud, K., Domenichini, S., Henry, Y., Soubigou-Taconnat, L., Lelarge-Trouverie, C., Saindrenan, P., Renou, J.P., Bergounioux, C., 2009. Crosstalks between myo-inositol metabolism, programmed cell death and basal immunity in Arabidopsis. PLoS One 4, e7364. doi:10.1371/journal.pone.0007364

Mesquita, A., Calvo-Garrido, J., Carilla-Latorre, S., Escalante, R., 2013. Monitoring autophagy in Dictyostelium. Methods Mol. Biol. 983, 461–70. doi:10.1007/978-1-62703-302-2_26

Michell, R.H., Conroy, L.A., Finney, M., French, P.J., Bunce, C.M., Anderson, K., Baxter, M.A., Brown, G., Gordon, J., Jenkinson, E.J., 1992. Inositol lipids and phosphates in the proliferation and differentiation of lymphocytes and myeloid cells. Ciba Found. Symp. 164, 2–11; discussion 12–6.

Mizushima, N., Ohsumi, Y., Yoshimori, T., 2002. Autophagosome Formation in Mammalian Cells Tracing of autophagosome formation with mammalian Apg proteins Initial step of autophagosome formation. Cell 429, 421–429. doi:10.1247/csf.27.421

Montagnes, D., Roberts, E., Lukeš, J., Lowe, C., 2012. The rise of model protozoa. Trends Microbiol. 20, 184–91. doi:10.1016/j.tim.2012.01.007

Moore, G.J., Bebchuk, J.M., Parrish, J.K., Faulk, M.W., Arfken, C.L., Strahl-Bevacqua, J., Manji, H.K., 1999. Temporal dissociation between lithium-induced changes in frontal lobe myo-inositol and clinical response in manic-depressive illness. Am. J. Psychiatry 156, 1902–8.

Motoi, Y., Shimada, K., Ishiguro, K., Hattori, N., 2014. Lithium and Autophagy. ACS Chem. Neurosci. 5, 434–442. doi:10.1021/cn500056q

Murphy, A., Shamshirsaz, A., Markovic, D., Ostlund, R., Koos, B., 2015. Urinary Excretion of Myo-Inositol and D-Chiro-Inositol in Early Pregnancy Is Enhanced in Gravidas With Gestational Diabetes Mellitus. Reprod. Sci. 23, 365–71. doi:10.1177/1933719115602767

Nagasaki, A., de Hostos, E.L., Uyeda, T.Q.P., 2002. Genetic and morphological evidence for two parallel pathways of cell-cycle-coupled cytokinesis in Dictyostelium. J. Cell Sci. 115, 2241–2251.

Nagata, E., Saiardi, A., Tsukamoto, H., Satoh, T., Itoh, Y., Itoh, J., Shibata, M., Takizawa, S., Takagi, S., 2010. Inositol hexakisphosphate kinases promote autophagy. Int. J. Biochem. Cell Biol. 42, 2065–71. doi:10.1016/j.biocel.2010.09.013

Nara, A., Mizushima, N., Yamamoto, A., Kabeya, Y., Ohsumi, Y., Yoshimori, T., 2002. SKD1 AAA ATPase-dependent endosomal transport is involved in autolysosome formation. Cell Struct. Funct. 27, 29–37.

Neuhoff, V., Arold, N., Taube, D., Ehrhardt, W., 1988. Improved staining of proteins in polyacrylamide gels including isoelectric focusing gels with clear background at nanogram sensitivity using Coomassie Brilliant Blue G-250 and R-250. Electrophoresis 9, 255–62.

doi:10.1002/elps.1150090603

Nichols, J.M., Veltman, D., Kay, R.R., 2015. Chemotaxis of a model organism: progress with Dictyostelium. Curr. Opin. Cell Biol. 36, 7–12. doi:10.1016/j.ceb.2015.06.005

Nierenberg, A.A., Ostacher, M.J., Calabrese, J.R., Ketter, T.A., Marangell, L.B., Miklowitz, D.J., Miyahara, S., Bauer, M.S., Thase, M.E., Wisniewski, S.R., Sachs, G.S., 2006. Treatment-resistant bipolar depression: a STEP-BD equipoise randomized effectiveness trial of antidepressant augmentation with lamotrigine, inositol, or risperidone. Am. J. Psychiatry 163, 210–6. doi:10.1176/appi.ajp.163.2.210

Nilsson, P., Loganathan, K., Sekiguchi, M., Matsuba, Y., Hui, K., Tsubuki, S., Tanaka, M., Iwata, N., Saito, T., Saido, T.C., 2013. Aβ secretion and plaque formation depend on autophagy. Cell Rep. 5, 61–9. doi:10.1016/j.celrep.2013.08.042

Nobukuni, T., Joaquin, M., Roccio, M., Dann, S.G., Kim, S.Y., Gulati, P., Byfield, M.P., Backer, J.M., Natt, F., Bos, J.L., Zwartkruis, F.J.T., Thomas, G., 2005. Amino acids mediate mTOR/raptor signaling through activation of class 3 phosphatidylinositol 3OH-kinase. Proc. Natl. Acad. Sci. U. S. A. 102, 14238–43. doi:10.1073/pnas.0506925102

Norman, R.A., McAlister, M.S.B., Murray-Rust, J., Movahedzadeh, F., Stoker, N.G., McDonald, N.Q., 2002. Crystal structure of inositol 1-phosphate synthase from Mycobacterium tuberculosis, a key enzyme in phosphatidylinositol synthesis. Structure 10, 393–402.

O'Dushlaine, C., Kenny, E., Heron, E., Donohoe, G., Gill, M., Morris, D., Corvin, a, 2011. Molecular pathways involved in neuronal cell adhesion and membrane scaffolding contribute to schizophrenia and bipolar disorder susceptibility. Mol. Psychiatry 16, 286–92. doi:10.1038/mp.2010.7

Octtaviani, E., Effler, J.C., Robinson, D.N., 2006. Enlazin, a natural fusion of two classes of canonical cytoskeletal proteins, contributes to cytokinesis dynamics. Mol. Biol. Cell 17, 5275–86. doi:10.1091/mbc.E06-08-0767

Ohnishi, T., Murata, T., Watanabe, A., Hida, A., Ohba, H., Iwayama, Y., Mishima, K., Gondo, Y., Yoshikawa, T., 2014. Defective craniofacial development and brain function in a mouse model for depletion of intracellular inositol synthesis. J. Biol. Chem. 289, 10785–96. doi:10.1074/jbc.M113.536706

Otto, G.P., Wu, M.Y., Kazgan, N., Anderson, O.R., Kessin, R.H., 2004. Dictyostelium macroautophagy mutants vary in the severity of their developmental defects. J. Biol. Chem. 279, 15621–9. doi:10.1074/jbc.M311139200

Otto, G.P., Wu, M.Y., Kazgan, N., Anderson, O.R., Kessin, R.H., 2003. Macroautophagy is required for multicellular development of the social amoeba Dictyostelium discoideum. J. Biol. Chem. 278, 17636–45. doi:10.1074/jbc.M212467200

Pakes, N.K., Veltman, D.M., Rivero, F., Nasir, J., Insall, R., Williams, R.S.B., 2012. The Rac GEF ZizB regulates development, cell motility and cytokinesis in Dictyostelium. J. Cell Sci. 125, 2457–65. doi:10.1242/jcs.100966

Palatnik, A., Frolov, K., Fux, M., Benjamin, J., 2001. Double-blind, controlled, crossover trial of inositol versus fluvoxamine for the treatment of panic disorder. J. Clin. Psychopharmacol. 21, 335–9.

Park, D., Jeong, S., Lee, S., Park, S., Kim, J.I., Yim, J., 2000. Molecular characterization of Drosophila melanogaster myo-inositol-1-phosphate synthase. Biochim. Biophys. Acta 1494, 277–81.

Park, K.C., Rivero, F., Meili, R., Lee, S., Apone, F., Firtel, R.A., 2004. Rac regulation of chemotaxis and morphogenesis in Dictyostelium. EMBO J. 23, 4177–89. doi:10.1038/sj.emboj.7600368

Parthasarathy, L.K., Seelan, R.S., Wilson, M. a, Vadnal, R.E., Parthasarathy, R.N., 2003. Regional changes in rat brain inositol monophosphatase 1 (IMPase 1) activity with chronic lithium treatment. Prog. Neuropsychopharmacol. Biol. Psychiatry 27, 55–60.

Parthasarathy, R.N., Lakshmanan, J., Thangavel, M., Seelan, R.S., Stagner, J.I., Janckila, a J., Vadnal, R.E., Casanova, M.F., Parthasarathy, L.K., 2013. Rat brain myo-inositol 3-phosphate synthase is a phosphoprotein. Mol. Cell. Biochem. 378, 83–9. doi:10.1007/s11010-013-1597-7

Parys, J.B., Decuypere, J., Bultynck, G., 2012. Role of the inositol 1,4,5-trisphosphate receptor/Ca2+-release channel in autophagy. Cell Commun. Signal. 10.

Peracino, B., Balest, A., Bozzaro, S., 2010. Phosphoinositides differentially regulate bacterial uptake and Nramp1-induced resistance to Legionella infection in Dictyostelium. J. Cell Sci. 123, 4039–51.

doi:10.1242/jcs.072124

Pollitt, A.Y., Insall, R.H., 2009. WASP and SCAR/WAVE proteins: the drivers of actin assembly. J. Cell Sci. 122, 2575–8. doi:10.1242/jcs.023879

Rana, R.S., Sekar, M.C., Hokin, L.E., MacDonald, M.J., 1986. A possible role for glucose metabolites in the regulation of inositol-1,4,5-trisphosphate 5-phosphomonoesterase activity in pancreatic islets. J. Biol. Chem. 261, 5237–40.

RayChaudhuri, A., Hait, N.C., Dasgupta, S., Bhaduri, T.J., Deb, R., Majumder, A.L., 1997. L-myo-Inositol 1-Phosphate Synthase from Plant Sources (Characteristics of the Chloroplastic and Cytosolic Enzymes). Plant Physiol. 115, 727–736.

Reidick, C., El Magraoui, F., Meyer, H.E., Stenmark, H., Platta, H.W., 2014. Regulation of the Tumor-Suppressor Function of the Class III Phosphatidylinositol 3-Kinase Complex by Ubiquitin and SUMO. Cancers (Basel). 7, 1–29. doi:10.3390/cancers7010001

Ridgway, G.J., Douglas, H.C., 1958. Unbalanced growth of yeast due to inositol deficiency. J. Bacteriol. 76, 163–6.

Robery, S., Mukanowa, J., Percie du Sert, N., Andrews, P.L.R., Williams, R.S.B., 2011. Investigating the effect of emetic compounds on chemotaxis in Dictyostelium identifies a non-sentient model for bitter and hot tastant research. PLoS One 6, e24439. doi:10.1371/journal.pone.0024439

Robery, S., Tyson, R., Dinh, C., Kuspa, A., Noegel, A.A., Bretschneider, T., Andrews, P.L.R., Williams, R.S.B., 2013. A novel human receptor involved in bitter tastant detection identified using Dictyostelium discoideum. J. Cell Sci. 126, 5465–76. doi:10.1242/jcs.136440

Robinson, D.N., Girard, K.D., Octtaviani, E., Reichl, E.M., 2002. Dictyostelium cytokinesis: from molecules to mechanics. J. Muscle Res. Cell Motil. 23, 719–27.

Rupper, a C., Rodriguez-Paris, J.M., Grove, B.D., Cardelli, J. a, 2001. p110-related PI 3-kinases regulate phagosome-phagosome fusion and phagosomal pH through a PKB/Akt dependent pathway in Dictyostelium. J. Cell Sci. 114, 1283–95.

Santamaria, A., Di Benedetto, A., Petrella, E., Pintaudi, B., Corrado, F., D'Anna, R., Neri, I., Facchinetti, F., 2015. Myo-inositol may prevent gestational diabetes onset in overweight women: a randomized, controlled trial. J. Matern. Fetal. Neonatal Med. 1–4. doi:10.3109/14767058.2015.1121478

Sarge, K.D., Park-Sarge, O.-K., 2009. Sumoylation and human disease pathogenesis. Trends Biochem. Sci. 34, 200–5. doi:10.1016/j.tibs.2009.01.004

Sarkar, S., Floto, R.A., Berger, Z., Imarisio, S., Cordenier, A., Pasco, M., Cook, L.J., Rubinsztein, D.C., 2005. Lithium induces autophagy by inhibiting inositol monophosphatase. J. Cell Biol. 170, 1101–11. doi:10.1083/jcb.200504035

Sarkar, S., Rubinsztein, D.C.,. Inositol and IP3 levels regulate autophagy: biology and therapeutic speculations. Autophagy 2, 132–4.

Sasaki, A.T., Chun, C., Takeda, K., Firtel, R.A., 2004. Localized Ras signaling at the leading edge regulates PI3K, cell polarity, and directional cell movement. J. Cell Biol. 167, 505–18. doi:10.1083/jcb.200406177

Sbrissa, D., Ikonomov, O.C., Fu, Z., Ijuin, T., Gruenberg, J., Takenawa, T., Shisheva, A., 2007. Core protein machinery for mammalian phosphatidylinositol 3,5-bisphosphate synthesis and turnover that regulates the progression of endosomal transport. Novel Sac phosphatase joins the ArPIKfyve-PIKfyve complex. J. Biol. Chem. 282, 23878–91. doi:10.1074/jbc.M611678200

Schaap, P., Wang, M., 1986. Interactions between adenosine and oscillatory cAMP signaling regulate size and pattern in Dictyostelium. Cell 45, 137–144. doi:10.1016/0092-8674(86)90545-3

Schiebler, M., Brown, K., Hegyi, K., Newton, S.M., Renna, M., Hepburn, L., Klapholz, C., Coulter, S., Obregón-Henao, A., Henao Tamayo, M., Basaraba, R., Kampmann, B., Henry, K.M., Burgon, J., Renshaw, S.A., Fleming, A., Kay, R.R., Anderson, K.E., Hawkins, P.T., Ordway, D.J., Rubinsztein, D.C., Floto, R.A., 2015. Functional drug screening reveals anticonvulsants as enhancers of mTOR-independent autophagic killing of Mycobacterium tuberculosis through inositol depletion. EMBO Mol. Med. 7, 127–39. doi:10.15252/emmm.201404137

Schlecht, U., Miranda, M., Suresh, S., Davis, R.W., St Onge, R.P., 2012. Multiplex assay for condition-dependent changes in protein-protein

interactions. Proc. Natl. Acad. Sci. U. S. A. 109, 9213–8. doi:10.1073/pnas.1204952109

Schwartz, D.C., Hochstrasser, M., 2003. A superfamily of protein tags: ubiquitin, SUMO and related modifiers. Trends Biochem. Sci. 28, 321–8. doi:10.1016/S0968-0004(03)00113-0

Scioscia, M., Kunjara, S., Gumaa, K., McLean, P., Rodeck, C.H., Rademacher, T.W., 2007. Urinary excretion of inositol phosphoglycan P-type in gestational diabetes mellitus. Diabet. Med. 24, 1300–4. doi:10.1111/j.1464-5491.2007.02267.x

Seelan, R.S., Lakshmanan, J., Casanova, M.F., Parthasarathy, R.N., 2009a. Identification of myo-inositol-3-phosphate synthase isoforms: characterization, expression, and putative role of a 16-kDa gamma(c) isoform. J. Biol. Chem. 284, 9443–57. doi:10.1074/jbc.M900206200

Seelan, R.S., Lakshmanan, J., Casanova, M.F., Parthasarathy, R.N., 2009b. Identification of myo -Inositol-3-phosphate Synthase Isoforms 284, 9443–9457. doi:10.1074/jbc.M900206200

Seelan, R.S., Parthasarathy, L.K., Parthasarathy, R.N., 2004. E2F1 regulation of the human myo-inositol 1-phosphate synthase (ISYNA1) gene promoter. Arch. Biochem. Biophys. 431, 95–106. doi:10.1016/j.abb.2004.08.002

Serretti, A., Drago, A., De Ronchi, D., 2009. Lithium pharmacodynamics and pharmacogenetics: focus on inositol mono phosphatase (IMPase), inositol poliphosphatase (IPPase) and glycogen sinthase kinase 3 beta (GSK-3 beta). Curr. Med. Chem. 16, 1917–48.

Shaldubina, A., Stahl, Z., Furszpan, M., Regenold, W.T., Shapiro, J., Belmaker, R.H., Bersudsky, Y., 2006. Inositol deficiency diet and lithium effects. Bipolar Disord. 8, 152–9. doi:10.1111/j.1399-5618.2006.00290.x

Shaltiel, G., Shamir, A., Shapiro, J., Ding, D., Dalton, E., Bialer, M., Harwood, A.J., Belmaker, R.H., Greenberg, M.L., Agam, G., 2004. Valproate decreases inositol biosynthesis. Biol. Psychiatry 56, 868–74. doi:10.1016/j.biopsych.2004.08.027

Shamir, A., Shaltiel, G., Greenberg, M.L., Belmaker, R.H., Agam, G., 2003. The effect of lithium on expression of genes for inositol biosynthetic enzymes in mouse hippocampus; a comparison with the yeast model. Brain Res. Mol. Brain Res. 115, 104–10.

Shamir, A., Shaltiel, G., Mark, S., Bersudsky, Y., Belmaker, R.H., Agam, G., 2007. Human MIP synthase splice variants in bipolar disorder. Bipolar Disord. 9, 766–71. doi:10.1111/j.1399-5618.2007.00440.x

Shen, X., Xiao, H., Ranallo, R., Wu, W.-H., Wu, C., 2003. Modulation of ATP-dependent chromatin-remodeling complexes by inositol polyphosphates. Science 299, 112–4. doi:10.1126/science.1078068

Shetty, A., Lopes, J.M., 2010. Derepression of INO1 transcription requires cooperation between the Ino2p-Ino4p heterodimer and Cbf1p and recruitment of the ISW2 chromatin-remodeling complex. Eukaryot. Cell 9, 1845–55. doi:10.1128/EC.00144-10

Shetty, A., Swaminathan, A., Lopes, J.M., 2013. Transcription regulation of a yeast gene from a downstream location. J. Mol. Biol. 425, 457–65. doi:10.1016/j.jmb.2012.11.018

Shi, Y., Vaden, D.L., Ju, S., Ding, D., Geiger, J.H., Greenberg, M.L., 2005. Genetic perturbation of glycolysis results in inhibition of de novo inositol biosynthesis. J. Biol. Chem. 280, 41805–10. doi:10.1074/jbc.M505181200

Shimohama, S., Tanino, H., Sumida, Y., Tsuda, J., Fujimoto, S., 1998. Alteration of myo-inositol monophosphatase in Alzheimer's disease brains. Neurosci. Lett. 245, 159–62.

Shimon, H., Agam, G., Belmaker, R.H., Hyde, T.M., Kleinman, J.E., 1997. Reduced frontal cortex inositol levels in postmortem brain of suicide victims and patients with bipolar disorder. Am. J. Psychiatry 154, 1148–50.

Shimon, H., Sobolev, Y., Davidson, M., Haroutunian, V., Belmaker, R.H., Agam, G., 1998. Inositol levels are decreased in postmortem brain of schizophrenic patients. Biol. Psychiatry 44, 428–32.

Shina, M.C., Müller, R., Blau-Wasser, R., Glöckner, G., Schleicher, M., Eichinger, L., Noegel, A.A., Kolanus, W., 2010. A cytohesin homolog in Dictyostelium amoebae. PLoS One 5, e9378. doi:10.1371/journal.pone.0009378

Silverstone, P.H., McGrath, B.M., Kim, H., 2005. Bipolar disorder and myo-inositol: a review of the magnetic resonance spectroscopy findings. Bipolar Disord. 7, 1–10. doi:10.1111/j.1399-5618.2004.00174.x

Steger, D.J., Haswell, E.S., Miller, A.L., Wente, S.R., O'Shea, E.K., 2003. Regulation of chromatin remodeling by inositol polyphosphates. Science 299, 114–6. doi:10.1126/science.1078062

Stein, A.J., Geiger, J.H., 2002. The crystal structure and mechanism of 1-L-myo-inositol- 1-phosphate synthase. J. Biol. Chem. 277, 9484–91. doi:10.1074/jbc.M109371200

Stephens, L., Milne, L., Hawkins, P., 2008. Moving towards a better understanding of chemotaxis. Curr. Biol. 18, R485–94. doi:10.1016/j.cub.2008.04.048

Straub, S. V, Bonev, A.D., Wilkerson, M.K., Nelson, M.T., 2006. Dynamic inositol trisphosphate-mediated calcium signals within astrocytic endfeet underlie vasodilation of cerebral arterioles. J. Gen. Physiol. 128, 659–69. doi:10.1085/jgp.200609650

Sugden, C., Ross, S., Bloomfield, G., Ivens, A., Skelton, J., Mueller-Taubenberger, A., Williams, J.G., 2010. Two novel Src homology 2 domain proteins interact to regulate dictyostelium gene expression during growth and early development. J. Biol. Chem. 285, 22927–35. doi:10.1074/jbc.M110.139733

Takeda, M., Yamagami, K., Tanaka, K., 2014. Role of phosphatidylserine in phospholipid flippase-mediated vesicle transport in Saccharomyces cerevisiae. Eukaryot. Cell 13, 363–75. doi:10.1128/EC.00279-13

Tamura, K., Peterson, D., Peterson, N., Stecher, G., Nei, M., Kumar, S., 2011. MEGA5: molecular evolutionary genetics analysis using maximum likelihood, evolutionary distance, and maximum parsimony methods. Mol. Biol. Evol. 28, 2731–9. doi:10.1093/molbev/msr121

Tanaka, S., Nikawa, J., Imai, H., Yamashita, S., Hosaka, K., 1996. Saccharomyces cerevisiae pis. FEBS Lett. 393, 89–92.

Tarantola, M., Bae, A., Fuller, D., Bodenschatz, E., Rappel, W.-J., Loomis, W.F., 2014. Cell substratum adhesion during early development of Dictyostelium discoideum. PLoS One 9, e106574. doi:10.1371/journal.pone.0106574

Tarassov, K., Messier, V., Landry, C.R., Radinovic, S., Serna Molina, M.M., Shames, I., Malitskaya, Y., Vogel, J., Bussey, H., Michnick, S.W., 2008. An in vivo map of the yeast protein interactome. Science 320, 1465–70. doi:10.1126/science.1153878

Teo, R., King, J., Dalton, E., Ryves, J., Williams, R.S.B., Harwood, A.J., 2009. PtdIns(3,4,5)P(3) and inositol depletion as a cellular target of mood stabilizers. Biochem. Soc. Trans. 37, 1110–4. doi:10.1042/BST0371110

Terbach, N., Shah, R., Kelemen, R., Klein, P.S., Gordienko, D., Brown, N. a, Wilkinson, C.J., Williams, R.S.B., 2011. Identifying an uptake mechanism for the antiepileptic and bipolar disorder treatment valproic acid using the simple biomedical model Dictyostelium. J. Cell Sci. 124, 2267–76. doi:10.1242/jcs.084285

Terbach, N., Williams, R.S.B., 2009. Structure-function studies for the panacea, valproic acid. Biochem. Soc. Trans. 37, 1126–32. doi:10.1042/BST0371126

Thakkar, J.K., Raju, M.S., Kennington, A.S., Foil, B., Caro, J.F., 1990. [3H]myoinositol incorporation into phospholipids in liver microsomes from humans with and without type II diabetes. The lack of synthesis of glycosylphosphatidylinositol, precursor of the insulin mediator inositol phosphate glycan. J. Biol. Chem. 265, 5475–81.

Toker, L., Agam, G., 2014. Lithium, Inositol and Mitochondria. ACS Chem. Neurosci. 5, 411–2. doi:10.1021/cn5001149

Toker, L., Bersudsky, Y., Plaschkes, I., Chalifa-Caspi, V., Berry, G.T., Buccafusca, R., Moechars, D., Belmaker, R.H., Agam, G., 2014. Inositol-related gene knockouts mimic lithium's effect on mitochondrial function. Neuropsychopharmacology 39, 319–28. doi:10.1038/npp.2013.194

Topham, M.K., Epand, R.M., 2009. Mammalian diacylglycerol kinases: molecular interactions and biological functions of selected isoforms. Biochim. Biophys. Acta 1790, 416–24. doi:10.1016/j.bbagen.2009.01.010

Trushina, E., Nemutlu, E., Zhang, S., Christensen, T., Camp, J., Mesa, J., Siddiqui, A., Tamura, Y., Sesaki, H., Wengenack, T.M., Dzeja, P.P., Poduslo, J.F., 2012. Defects in mitochondrial dynamics and metabolomic signatures of evolving energetic stress in mouse models of familial Alzheimer's disease. PLoS One 7, e32737. doi:10.1371/journal.pone.0032737

Uyeda, T.Q.P., Nagasaki, A., 2004. Variations on a theme: the many modes of cytokinesis. Curr. Opin. Cell Biol. 16, 55–60. doi:10.1016/j.ceb.2003.11.004

Vaden, D.L., Ding, D., Peterson, B., Greenberg, M.L., 2001. Lithium and valproate decrease inositol mass and increase expression of the yeast INO1 and INO2 genes for inositol biosynthesis. J. Biol. Chem. 276, 15466–71. doi:10.1074/jbc.M004179200

van Haastert, P.J.., van Dijken, P., 1997. Biochemistry and genetics of inositol phosphate metabolism in Dictyostelium. FEBS Lett. 410, 39–43. doi:10.1016/S0014-5793(97)00415-8

Veltman, D.M., Akar, G., Bosgraaf, L., Van Haastert, P.J.M., 2009. A new set of small, extrachromosomal expression vectors for Dictyostelium discoideum. Plasmid 61, 110–8. doi:10.1016/j.plasmid.2008.11.003

Vergarajauregui, S., Martina, J.A., Puertollano, R., 2009. Identification of the penta-EF-hand protein ALG-2 as a Ca2+-dependent interactor of mucolipin-1. J. Biol. Chem. 284, 36357–66. doi:10.1074/jbc.M109.047241

Vicencio, J.M., Ortiz, C., Criollo, A., Jones, A.W.E., Kepp, O., Galluzzi, L., Joza, N., Vitale, I., Morselli, E., Tailler, M., Castedo, M., Maiuri, M.C., Molgó, J., Szabadkai, G., Lavandero, S., Kroemer, G., 2009. The inositol 1,4,5-trisphosphate receptor regulates autophagy through its interaction with Beclin 1. Cell Death Differ. 16, 1006–17. doi:10.1038/cdd.2009.34

Villa-García, M.J., Choi, M.S., Hinz, F.I., Gaspar, M.L., Jesch, S., Henry, S., 2011. Genome-wide screen for inositol auxotrophy in Saccharomyces cerevisiae implicates lipid metabolism in stress response signaling., Molecular genetics and genomics : MGG. doi:10.1007/s00438-010-0592-x

Villarreal, F.D., Kültz, D., 2015. Direct Ionic Regulation of the Activity of Myo-Inositol Biosynthesis Enzymes in Mozambique Tilapia. PLoS One 10, e0123212. doi:10.1371/journal.pone.0123212

Vito, P., Lacanà, E., D'Adamio, L., 1996. Interfering with apoptosis: Ca(2+)-binding protein ALG-2 and Alzheimer's disease gene ALG-3. Science 271, 521–5.

Walter, P., Ron, D., 2011. The unfolded protein response: from stress pathway to homeostatic regulation. Science 334, 1081–6. doi:10.1126/science.1209038

Wan, C., Borgeson, B., Phanse, S., Tu, F., Drew, K., Clark, G., Xiong, X., Kagan, O., Kwan, J., Bezginov, A., Chessman, K., Pal, S., Cromar, G.,

Papoulas, O., Ni, Z., Boutz, D.R., Stoilova, S., Havugimana, P.C., Guo, X., Malty, R.H., Sarov, M., Greenblatt, J., Babu, M., Derry, W.B., R. Tillier, E., Wallingford, J.B., Parkinson, J., Marcotte, E.M., Emili, A., 2015. Panorama of ancient metazoan macromolecular complexes. Nature 525, 339–44. doi:10.1038/nature14877

Wang, C., Chowdhury, S., Driscoll, M., Parent, C.A., Gupta, S.K., Losert, W., 2014. The interplay of cell-cell and cell-substrate adhesion in collective cell migration. J. R. Soc. Interface 11, 20140684. doi:10.1098/rsif.2014.0684

Wang, Y., Dasso, M., 2009. SUMOylation and deSUMOylation at a glance. J. Cell Sci. 122, 4249–52. doi:10.1242/jcs.050542

Williams, R., Ryves, W.J., Dalton, E.C., Eickholt, B., Shaltiel, G., Agam, G., Harwood, a J., 2004. A molecular cell biology of lithium. Biochem. Soc. Trans. 32, 799–802. doi:10.1042/BST0320799

Williams, R.S., Eames, M., Ryves, W.J., Viggars, J., Harwood, a J., 1999. Loss of a prolyl oligopeptidase confers resistance to lithium by elevation of inositol (1,4,5) trisphosphate. EMBO J. 18, 2734–45. doi:10.1093/emboj/18.10.2734

Williams, R.S.B., 2009. Employing multiple models, methods and mechanisms in bipolar disorder research. Biochem. Soc. Trans. 37, 1077–9. doi:10.1042/BST0371077

Williams, R.S.B., 2005. Pharmacogenetics in model systems: defining a common mechanism of action for mood stabilisers. Prog. Neuropsychopharmacol. Biol. Psychiatry 29, 1029–37. doi:10.1016/j.pnpbp.2005.03.020

Williams, R.S.B., Cheng, L., Mudge, A.W., Harwood, A.J., 2002. A common mechanism of action for three mood-stabilizing drugs. Nature 417, 292–5. doi:10.1038/417292a

Witke, W., Nellen, W., Noegel, A., 1987. Homologous recombination in the 6, 4143–4148.

Wong, Y.C., Holzbaur, E.L.F., 2015. Autophagosome dynamics in neurodegeneration at a glance. J. Cell Sci. 128, 1259–67. doi:10.1242/jcs.161216

Wu, C.-Y., Lin, M.-W., Wu, D.-C., Huang, Y.-B., Huang, H.-T., Chen, C.-L., 2014. The role of phosphoinositide-regulated actin reorganization in chemotaxis and cell migration. Br. J. Pharmacol. 171, 5541–54. doi:10.1111/bph.12777

Xu, X., Müller-Taubenberger, A., Adley, K.E., Pawolleck, N., Lee, V.W.Y., Wiedemann, C., Sihra, T.S., Maniak, M., Jin, T., Williams, R.S.B., 2007. Attenuation of phospholipid signaling provides a novel mechanism for the action of valproic acid. Eukaryot. Cell 6, 899–906. doi:10.1128/EC.00104-06

Yamagami, K., Yamamoto, T., Sakai, S., Mioka, T., Sano, T., Igarashi, Y., Tanaka, K., 2015. Inositol depletion restores vesicle transport in yeast phospholipid flippase mutants. PLoS One 10, e0120108. doi:10.1371/journal.pone.0120108

Yamamoto, A., Tagawa, Y., Yoshimori, T., Moriyama, Y., Masaki, R., Tashiro, Y., 1998. Bafilomycin A1 prevents maturation of autophagic vacuoles by inhibiting fusion between autophagosomes and lysosomes in rat hepatoma cell line, H-4-II-E cells. Cell Struct. Funct. 23, 33–42. doi:10.1247/csf.23.33

Yang, Z., Klionsky, D.J., 2010. Eaten alive: a history of macroautophagy. Nat. Cell Biol. 12, 814–22. doi:10.1038/ncb0910-814

Yorek, M.A., Wiese, T.J., Davidson, E.P., Dunlap, J.A., Stefani, M.R., Conner, C.E., Lattimer, S.A., Kamijo, M., Greene, D.A., Sima, A.A., 1993. Reduced motor nerve conduction velocity and Na(+)-K(+)-ATPase activity in rats maintained on L-fucose diet. Reversal by myo-inositol supplementation. Diabetes 42, 1401–6.

Zang, J.H., Cavet, G., Sabry, J.H., Wagner, P., Moores, S.L., Spudich, J.A., 1997. On the role of myosin-II in cytokinesis: division of Dictyostelium cells under adhesive and nonadhesive conditions. Mol. Biol. Cell 8, 2617–29.

Zhang, G., Tian, Y., Hu, K., Zhu, Y., Chater, K.F., Feng, C., Liu, G., Tan, H., 2012. Importance and regulation of inositol biosynthesis during growth and differentiation of Streptomyces. Mol. Microbiol. 83, 1178–94. doi:10.1111/j.1365-2958.2012.08000.x

Zheng, X., Liu, Z., Zhang, Y., Lin, Y., Song, J., Zheng, L., Lin, S., 2015. Relationship Between Myo-Inositol Supplementary and Gestational Diabetes Mellitus: A Meta-Analysis. Medicine (Baltimore). 94, e1604.

doi:10.1097/MD.0000000000001604

Zhu, X., Bouffanais, R., Yue, D.K.P., 2015. Interplay between motility and cell-substratum adhesion in amoeboid cells. Biomicrofluidics 9, 054112. doi:10.1063/1.4931762

Zicha, D., Dunn, G.A., Brown, A.F., 1991. A new direct-viewing chemotaxis chamber. J. Cell Sci. 99 (Pt 4), 769–75.

Zoncu, R., Efeyan, A., Sabatini, D.M., 2011. mTOR: from growth signal integration to cancer, diabetes and ageing. Nat. Rev. Mol. Cell Biol. 12, 21–35. doi:10.1038/nrm3025